ISOLATION AND CHARACTERIZATION OF COMPOUNDS FROM THE BARK OF *Ochreinauclea maingayi* (HOOK. F.) RISDS. (RUBIACEAE) WITH THE AID OF LCMS/MS MOLECULAR NETWORKING AND THEIR ANTICHOLINESTERASE ACTIVITY

NORFAIZAH BINTI OSMAN

FACULTY OF SCIENCES
UNIVERSITI MALAYA
KUALA LUMPUR

2023

ISOLATION AND CHARACTERIZATION OF COMPOUNDS FROM THE BARK OF *Ochreinauclea maingayi* (HOOK. F.) RISDS. (RUBIACEAE) WITH THE AID OF LCMS/MS MOLECULAR NETWORKING AND THEIR ANTICHOLINESTERASE ACTIVITY

NORFAIZAH BINTI OSMAN

THESIS SUBMITTED IN FULFILMENT OF THE REQUIREMENTS FOR THE DEGREE OF DOCTOR OF PHILOSOPHY

DEPARTMENT OF CHEMISTRY
FACULTY OF SCIENCES
UNIVERSITI MALAYA
KUALA LUMPUR

2023

UNIVERSITI MALAYA

ORIGINAL LITERARY WORK DECLARATION

Name of Candidate: **NORFAIZAH BINTI OSMAN**

(Matric No: **SHC140070 / 17055248/3**

Name of Degree: **DOCTOR OF PHILOSOPHY**

Title of Thesis ("this Work"):

ISOLATION AND CHARACTERIZATION OF COMPOUNDS FROM THE BARK OF *Ochreinauclea maingayi* (HOOK. F.) RISDS. (RUBIACEAE) WITH THE AID OF LCMS/MS MOLECULAR NETWORKING AND THEIR ANTICHOLINESTERASE ACTIVITY

Field of Study: **PHYSICAL SCIENCE CHEMISTRY (NATURAL PRODUCT CHEMISTRY)**

I do solemnly and sincerely declare that:

(1) I am the sole author/writer of this Work;
(2) This Work is original;
(3) Any use of any work in which copyright exists was done by way of fair dealing and for permitted purposes and any excerpt or extract from, or reference to or reproduction of any copyright work has been disclosed expressly and sufficiently and the title of the Work and its authorship have been acknowledged in this Work;
(4) I do not have any actual knowledge nor do I ought reasonably to know that the making of this work constitutes an infringement of any copyright work;
(5) I hereby assign all and every rights in the copyright to this Work to the University of Malaya ("UM"), who henceforth shall be owner of the copyright in this Work and that any reproduction or use in any form or by any means whatsoever is prohibited without the written consent of UM having been first had and obtained;
(6) I am fully aware that if in the course of making this work, I have infringed any copyright whether intentionally or otherwise, I may be subject to legal action or any other action as may be determined by UM.

Candidate's Signature Date:

Subscribed and solemnly declared before,

Witness's Signature Date:

Name:

Designation:

ISOLATION AND CHARACTERIZATION OF COMPOUNDS FROM THE BARK OF *Ochreinaulea maingayi* (HOOK.F.) RISDS. (RUBIACEAE) WITH THE AID OF LCMS/MS MOLECULAR NETWORKING AND THEIR ANTICHOLINESTERASE ACTIVITY

ABSTRACT

A phytochemical investigation of the dichloromethane crude extract (DCE) from the bark of *Ochreinauclea maingayi* was performed with the aid of LCMS/MS-based molecular networking (MN) to accelerate the research workflow. MN permits extracting information on related molecules from the DCE based on the similarity of their fragmentation MS/MS spectra. In this study, one new indole alkaloid, dihydrodeglycocdambine **(149)**, together with other twenty-one known compounds, was successfully identified from MN analysis. With the aid of LCMS/MS molecular networking, **149** was successfully isolated and purified from the bark of *O. maingayi* using the chromatography technique, together with sixteen knows compounds; neonaucline**(5)**, naucledine **(6)**, harmane **(7)**, naulafine **(33)**, cadambine **(35)**, *nor*harmane **(124)**, methyl *9H-β*-carboline-4-carboxylate **(150)**, 1,2,3,4 tetranorharmane-1-one **(151)**, cinnamamide **(152)**, benzamide **(153)**, scopoletine **(154)**, 4′-hydroxyacetophenone **(155),** decarboxyportentol acetate **(156)**, scoparone **(157)**, 2'-hydroxy-3'-methoxyacetophenone **(158)** and hexyl *p*-coumarate **(159)**. All structures were elucidated using spectroscopic methods; UV, IR, NMR and LCMS. The DCE of the bark of *O. maingayi* has been tested for butyrylcholinesterase (BChE) inhibitory assay inhibited moderately with more than 54 % with 100 µg/mL. Further evaluation showed that fractions 7 and 9 could inhibit the BChE at more than 80 % at 100 µg/mL. Both fractions yielded three compounds: harmane **(7)**, naucledine **(6)** and dihydrodeglycocadambine **(149)**. Naucledine **(6)** was the most potent BChE inhibitor with an IC_{50} value of 22.08 µM followed by harmane **(7)** and dihydrodeglycocadambine **(149)** (23.96 and 30.32 µM, respectively). According to the kinetic study, BChE was inhibited by **6** in a mixed mode type. A molecular docking (MD)

analysis showed that **6** docked deep into the bottom gorge of BChE, interacted with Ser 198 and His 438 at the catalytic site, and formed hydrogen bonds with Gly 116 in an oxyanion hole.

Keywords: *Ochreinauclea maingayi*, indole alkaloid, molecular networking, anticholinesterase activity, molecular docking.

PENGASINGAN DAN PENCARIAN SEBATIAN DARIPADA KULIT KAYU *Ochreinaulea maingayi* (HOOK.F.) RISDS. (RUBIACEAE) DENGAN BANTUAN RANGKAIAN MOLEKUL LCMS/MS DAN AKTIVITI ANTIKOLINESTERASENYA

ABSTRAK

Penyiasatan fitokimia terhadap ekstrak mentah diklorometana (DCE) daripada kulit kayu *Ochreinauclea maingayi* dilakukan dengan bantuan rangkaian molekul (MN) berasaskan LCMS/MS untuk mempercepatkan aliran kerja penyelidikan. MN membenarkan pengekstrakan maklumat mengenai molekul berkaitan dari DCE berdasarkan persamaan spektrum MS/MS pemecahan mereka. Dalam kajian ini, satu sebatian indol alkaloid baru telah dikenalpasti, dihydrodeglykokadambina **(149),** bersama dua puluh satu sebatian telah berjaya dikenalpasti daripada analisis MN. Dengan bantuan rangkaian molekul (MN), **149** berjaya di asingkan dan di tulenkan daripada kulit *O. maingayi* menggunakan teknik kromatografi bersama enam belas sebatian lain; neonauklina **(5)**, naukledina **(6)**, harmana **(7)**, *nor*harmana **(124)**, naulafina **(33)**, kadambina **(35)**, metil 9*H*-*β*-karbolin-4-karbosilat **(150),** 1,2,3,4 tetranorharmana-1-on **(151)**, sinnamamida **(152)**, benzamida **(153)**, skopoletina **(154)**, 4'-hidroxi asetofenon **(155),** dekarboxiportentol asetat **(156)**, skoparon **(157)**, 2'-hidroxi-3 metoxiasetofenon **(158)** dan hexil *p*-koumarat **(159)**. Semua struktur telah dijelaskan menggunakan kaedah spektroskopi; UV, IR, NMR dan LCMS. DCE kulit *O. maingayi* telah diuji untuk ujian perencatan butirilkholinesterase (BChE) dihalang secara sederhana dengan lebih daripada 54% pada 100µg/mL. Penilaian lanjut menunjukkan bahawa pecahan 7 dan 9 dapat menghalang BChE pada lebih daripada 80% pada 100µg/mL. Kedua-dua pecahan menghasilkan tiga sebatian; harmana **(7)**, naukledina **(6)** dan dihidrodeglykokadambina **(159)**. Naukledina **(6)** ialah perencat BChE yang paling kuat dengan nilai IC_{50} sebanyak 22.08 µM diikuti oleh harmana **(7)** dan dihidrodeglykokadambina **(159)** (23.96 dan 30.32 µM). Menurut kajian kinetik, BChE telah dihalang oleh **(6)** dalam jenis perencatan mod campuran. Analisis dok molekul

(MD) menunjukkan bahawa **(6)** berlabuh jauh ke dalam gaung bawah BChE, berinteraksi dengan Ser 198 dan His 438 pada bahagian katalitik, dan membentuk ikatan hidrogen dengan Gly 116 dalam lubang oksianion.

Kata Kunci: *Ochreinauclea maingayi*, indol alkaloid, rangkaian molekular, aktiviti antikolinesterase, kajian dok molekul.

ACKNOWLEDGEMENTS

First and foremost, I want to thank Almighty Allah S.W.T, Most Gracious and Most Merciful. I want to thank my supervisors, Profesor Dr. Khalijah Awang and Dr. Azeana Zahari, for the time they devoted to providing me with guidance, suggestions, care, and courage throughout the completion of my dissertation. May Allah bless them abundantly.

My sincerest gratitude goes out to the members of Phyto Laboratory, especially; Dr. Liew Sook Yee, Miss Hazrina Hazni, Dr. Nooraimi, Dr. Shelly Gapil, Dr. Haslinda, Dr. Muhamad Aqmal, Mr. Hafiz Husna, Dr. Leong Sow Tein, Mrs. Julia, Mr. Afiq, Dr. Syazreen Nadia, Dr. Devi Rosmy, Ms. Aisyah, Ms. Yallini, Ms. Azirah, Dr. Chong Soon Lim, Mrs. Mahfuzah, Dr. Norsita Tohar, Dr. Wan Nurul Nazneem, Mrs. Hazlina, Dr. Rosalind, Mr. Hisyam and others for their kind help, support and friendship. I wish to acknowledge the herbarium staff, Mr. Rafly, Mr. Din, and Mr. Teo, for their help in collecting the sample, and NMR staff, Ms. Norzalida, Mr. Nordin, and Mr. Fateh.

I extended my appreciation, especially to my parents Mr. Osman and Mrs. Khazanah; my husband, Mr. Zulkhairi; my children, Mr. Zhafif, Ms. Nuha and Ms. Naima, and my siblings, Mr. Abd. Mannan, Mrs. Siti Habsaah, Mr. Abd. Basid, Mrs. Fatehah, Mr. Abd. Muhaimin, Mrs. Rabaah, Mrs. Siti Zulaiha and Mr. Irfan for their supports and prayer throughout my PhD. Without their tremendous understanding, encouragement, and constant prayers, I will not complete my PhD.

TABLE OF CONTENTS

LIST OF FIGURES

LIST OF SCHEMES

LIST OF TABLES

LIST OF SYMBOLS AND ABBREVIATIONS

α	:	Alpha
β	:	Beta
d	:	Doublet
dd	:	Doublet of doublet
dt	:	Doublet of triplet
J	:	Coupling constant
m	:	Multiplet
m/z	:	Mass per charge
q	:	Quartet
t	:	Triplet
δ	:	Chemical shift
λ_{max}	:	Maximum wavelength
Å	:	Armstrong
℃	:	Degree Celsius
Da	:	Dalton
µM	:	Micromolar
µL	:	Microliter
µg/mL	:	Micrograms per millilitre
cm^{-1}	:	Centimetre
G	:	Gram
Hz	:	Hertz
IR	:	Infrared
kg	:	Kilograms
nm	:	Nanometre

MHz	:	Mega Hertz
M	:	Molar
mM	:	Millimolar
mg/mL	:	Milligrams per millilitre
mm	:	Millimetre
M	:	Meter
U/mL	:	Unit per millilitre
UV	:	Ultraviolet
^{1}H NMR	:	Proton Nuclear Magnetic Resonance
^{13}C NMR	:	Carbon thirteen Nuclear Magnetic Resonance
1D NMR	:	One Dimension Nuclear Magnetic Resonance
2D NMR	:	Two-dimension Nuclear Magnetic Resonance
AD	:	Alzheimer's disease
ADI	:	Alzheimer Diseases International
BChE	:	Butyrylcholinesterase
CC	:	Column chromatography
$CDCl_3$	:	Deuterated chloroform
CD_3OD	:	Deuterated methanol
C_5D_5N	:	Deuterated Pyridine-d_5
$CHCl_3$	:	Chloroform
COSY	:	^{1}H-^{1}H Correlation Spectroscopy
DCM	:	Dichloromethane
DCE	:	Dichloromethane crude extract
DEPT	:	Distortionless Enhancement by Polarization Transfer
FDA	:	Food and Drug Administration

LCMS-IT-TOFF	:	Liquid chromatography mass spectrum ion trap time of flight
LC-ESI	:	Liquid Chromatography Electrospray Ionization
HMQC	:	Heteronuclear Multiple Quantum Coherence
HMBC	:	Heteronuclear Multiple Bond Coherence
HSQC	:	Heteronuclear Single Quantum Coherence
NH_3	:	Ammonia
NMR	:	Nuclear Magnetic Resonance
NOESY	:	Nuclear Overhauser Effect Spectroscopy
MC	:	Micro Column Chromatography
MeOH	:	Methanol
MN	:	Molecular Networking
MD	:	Molecular Docking
TLC	:	Thin Layer Chromatography
PTLC	:	Preparative thin layer chromatography

LIST OF APPENDICES

CHAPTER 1: INTRODUCTION

1.1 General

Alzheimer's disease (AD) is neurodegenerative diseases that is increasing globally, especially in developed countries. It was also the leading cause of dementia among the elderly. It was first diagnosed and defined as a clinical pathological syndrome in 1906 by German psychiatrist Dr. Alois Alzheimer's (Yang et al., 2016). Researchers from Alzheimer's Disease International (ADI) reported that this disease is predicted to afflict more than 139 million people globally in 2050, with most victims over 65 years old (Gauthier, 2022). Loss of certain populations of brain cells, which can lead to functional or sensory problems, is a common sign of AD (Pinho et al., 2013). To date, only three medications have been approve for the treatment of AD that range from mild to moderate severity by the Food and Drug Administration (FDA) (Miculas et al., 2023). These medications include galantamine **(1)**, donepezil **(2)**, and rivastigmine **(3)**, as their structure showed in Figure 1.1. Galantamine **(1)** is a natural alkaloid, whilst the other two are synthetic. There is a pressing need to find new candidate drugs for the treatment of AD because the current options are limited. Natural plant products are excellent candidates for consideration as potential leads for the development of AD treatments.

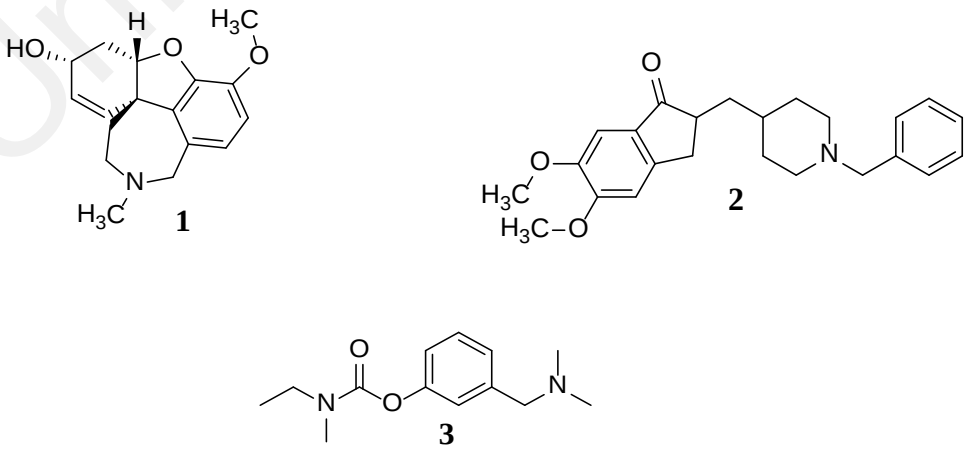

Figure 1.1: Structure of galantamine (1), donepezil (2) and rivastigmine (3).

Malaysia is recognized as one of the world's mega biodiverse regions, ranking 12th by the National Biodiversity Index on the basis of species richness and endemism in four terrestrial vertebrate classes and vascular plants (Tan et al., 2020). It is estimated that Malaysia is home to 15,000 unique species of plants with vascular systems. Peninsular Malaysia is home to approximately 8,300 species, whereas Sabah and Sarawak are home to 12,000 species (Guan & Saw, 2007; Hamidah et al., 2020). It is well known that regional species such as Annonaceae, Meliaceae, Myristicaceae, Myrsinaceae, Piperaceae, Rubiaceae, Rutaceae, Solanaceae, Umbelliferaceae, and Zingibearaceae possess an abundance of valuable chemical substances (Abu Bakar et al., 2018; Rao, 2010).

The Rubiaceae family of plants produces bioactive phytochemicals with great pharmacological potentials, such as those used to treat malaria, hepatitis, dermatitis, oedema, cough, hypertension and diabetes (Karou et al., 2011; Maldonado et al., 2017; Morton, 1992). In the study of primary and secondary metabolite in Rubiaceae family by Martin and Nunez (2015), indole alkaloids have been recognized to be useful chemical markers. Apart from it, anthraquinones, lignoids, triterpene glycosides, iridoids, flavonoids, phenols derivatives and terpenes, were also reported (Martins & Nunez, 2015). Many local species from these families have yet to be extensively examined and investigated.

One of these is the rare genus *Ochreinauclea*, which has only two species: *Ochreinauclea maingayi* (*O. maingayi*) and *Ochreinauclea missionis (O. missionis)*. Traditionally, the endemic plants in India, *O. missionis* is used by native Indians to cure gastritis, arthritis, tumour and fever (Chandrika & Ravishankar, 2009; Naomita & Ravishankar, 2001). However, *O. maingayi* has never been used traditionally, and only one publication on the phytochemical study of *O. maingayi* has been carried out by Mukhtar and coworkers (Mukhtar et al., 2012). They reported a major class of indole

alkaloids together with triterpenoid, *nor*isoprenoid and amide were extracted from the *O. maingayi*. A screening exercise on cholinesterase inhibitor revealed that the bark DCE extract of *O. maingayi* was moderately active. In view of this limited finding, the *O. maingayi* plant will be an interesting subject for further research.

Consequently, we intend to further investigate the compounds that are responsible for BChE activity. To accomplish this, we will employ isolation techniques to identify and characterize the active constituents within *O. maingayi*. Pure compounds are extracted, fractioned, isolated, and elucidated in classic natural product research. This framework consumes a significant amount of solvent and labour. Natural compounds are identified through spectroscopic method experiments and comparisons with compounds discovered by other scientists or researchers, which can be time-consuming, especially when identifying new compounds or skeletons. Recently, bioinformatics tools have become more advanced in enhancing natural product research, enabling natural product chemists to be more efficient in targeting or discovering previously unknown compounds by accelerating the pace of research in this field (Fox Ramos et al., 2019).

Molecular networking (MN), which was developed by the Global Natural Products Social Molecular Network (GNPS), has emerged as a potentially fruitful strategy in the wake of these recent developments. The open access website, GNPS, is a mass spectrometry ecosystem with public reference libraries, public data repositories and live data (Wang et al., 2016). Dorrestein's group developed it in 2012 (Watrous et al., 2012) to analyse metabolite synthesis from a wide range of live microbial colonies; this enabled the mapping of the chemical diversity observed in an untargeted mass spectrometry experiment. Today, GNPS has become a valuable tool for the mass spectrometry community. Hence, this study will employ isolation of compound from the bark of *O. maingayi* together with the aid of MN, a tool that can accelerate the process of natural product research.

1.2 Rubiaceae Family: Classification and General Appearance

Kingdom: Plantae

Division: Magnoliophyta

Class: Magnoliopsida

Order: Rubiales

Family: Rubiaceae

Subfamily: Cinchonoideae
Ixoroideae
Rubioideae

Scheme 1.1: Classification of Rubiaceae family.

The Rubiaceae family (Scheme 1.1) is one of the most prominent angiosperm families, with 13,000 species dispersed among 637 genera (Kuang et al., 2021). It grows all over the world, but most of its species and biomass are found in the tropics and subtropics, especially in humid lowland forests, where it is one of the most species-rich woody plant families (Davis et al., 2009). Coffee, quinine, gambier, ipecac, and kratom are all renowned economic products of the Rubiaceae family (Clarke, 2007b; Eastlack et al., 2020; Simpson, 2010).

The majority of Rubiaceae are tiny trees or shrubs. In addition, there are also in the form of large trees, herbaceous plants, lianas, woody monocausal dwarfs epiphytes, and, on rare occasion, succulent or aquatic lifeforms are found (Davis et al., 2009; Robbrecht, 1988). Simple leaves, interpetiolar stipules, inferior ovaries, and gamopetalous flowers can be used to identify members of the same family. Many Rubiaceae plants have flowers grouped in dense globose crowns (Razafimandimbison & Bremer, 2001).

The subfamilies Rubioideae, Cinchonoideae, Antirheoideae, and Ixoroideae were established by Robbrecht within the family Rubiaceae (Robbrecht, 1988). Since molecular studies have shown Antirheoideae to be polyphyletic with no standardised occurrence of a chemical marker, some authors do not accept it as a subfamily, leading to

the changes that have been made to this family to make it into three subfamilies : Rubioideae, Cinchonoideae, and Ixoroideae (Martins & Nunez, 2015; Razafimandimbison & Bremer, 2001). Scheme 1.2 illustrate the classification of subfamily and tribe of Rubiaceae family.

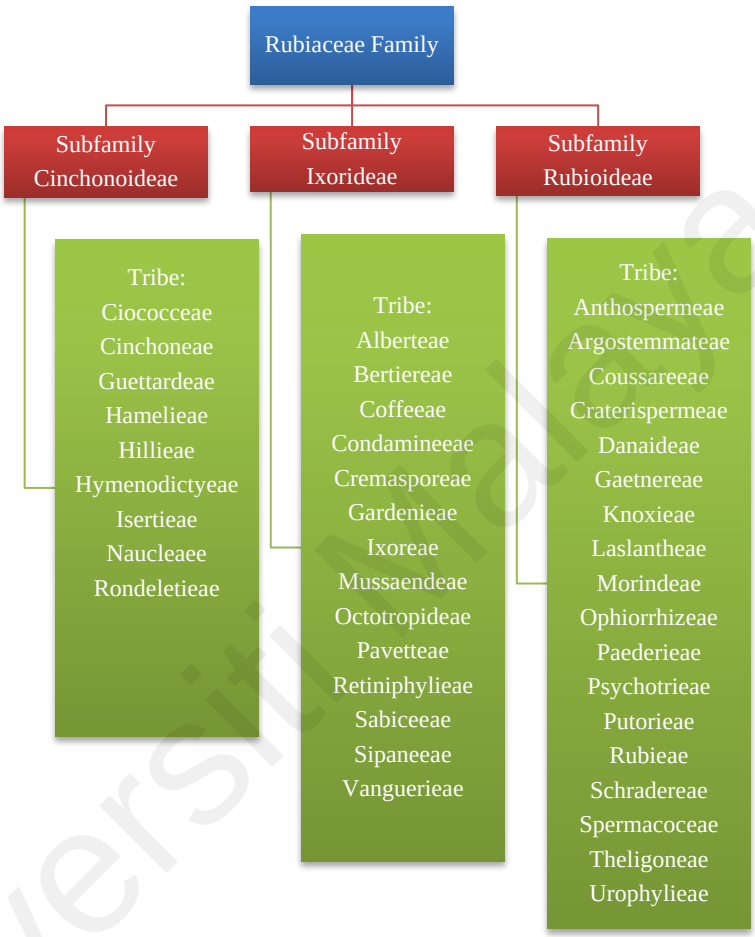

Scheme 1.2: Classification of subfamily and tribe of Rubiaceae family.

Rubiaceae is among the largest tree families in Malaysia, and it is estimated that there are 80 genera with 555 species. A number of plant families, including Kochummenia, Perakanthus, Klossia, and Aleisanthia, are unique to Malaysia (Whitmore & Ng, 1989). The noteworthy timbers of the Rubiaceae family include "laran" (*Neolamarckia cadamba*), "bangkal" (*Orchreinauclea*, *Neonauclea*, *Naucleae*), "mengkudu" (*Morinda*), "meraga" (*Metadina*, *Pertusadina*), "malabera bukit" (*Mussaendopsis beccariana*), "tinjau belukar" (*Porterandia anisophylla*), and "selumar" (*Jackiopsis ornata*) (S. C. Lim, 2004; Whitmore & Ng, 1989).

1.2.1 Classification of Naucleeae Tribes

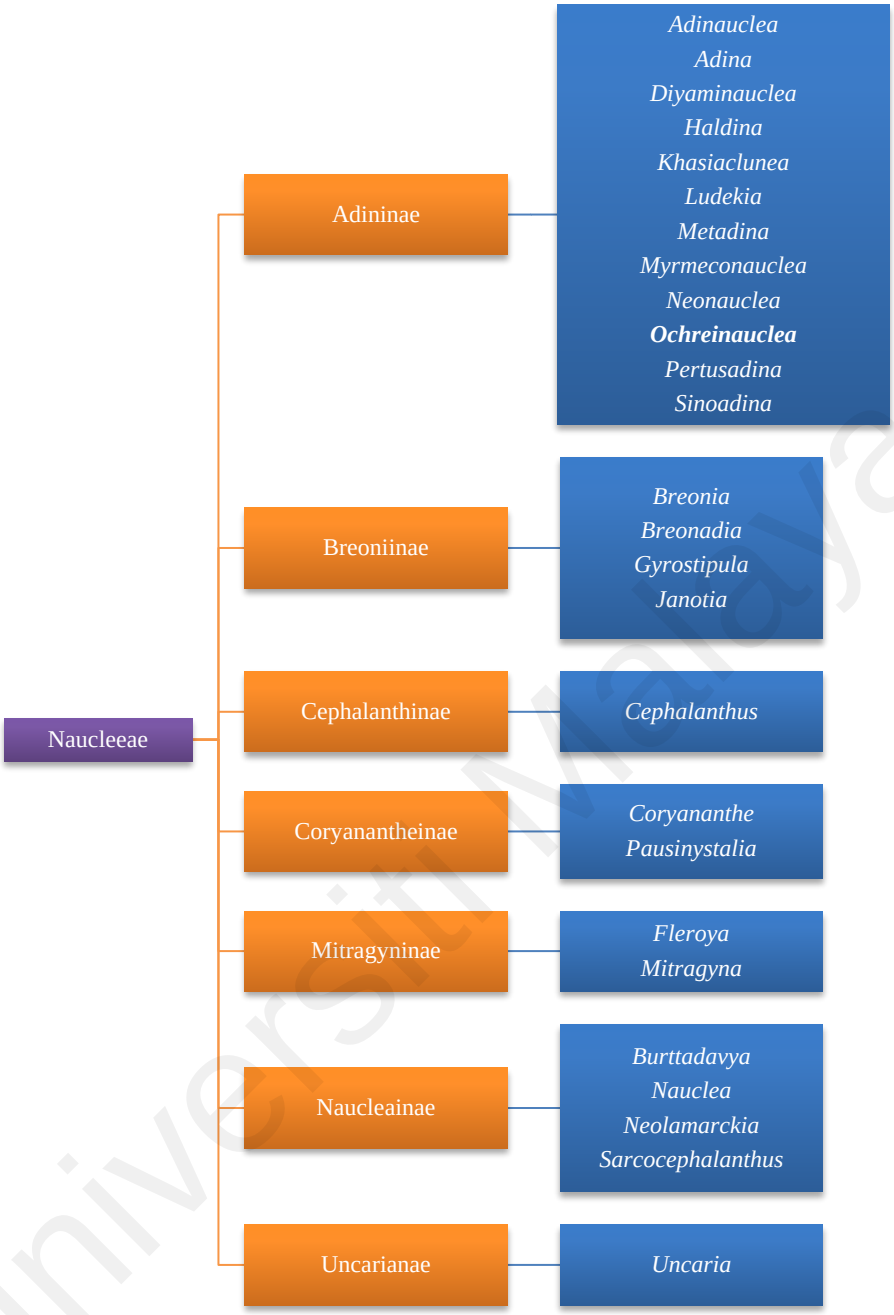

Scheme 1.3: Classification of Naucleeae tribe.

The circumscription of the Naucleeae tribe was developed by Razafimandimbison and Bremer established; it classified the tribe into seven subtribes: Uncariinae Adininae, Cephalanthinae, Breoniinae, Corynantheinae, Naucleinae, Mitragyninae and Uncariinae as depicted in (Razafimandimbison & Bremer, 2002). The Naucleeae tribe comprises twenty-six genera and one hundred and ninety-four species of trees, shrubs, and lianas (Stefan et al., 2014). The tribe is a clearly defined monophyletic group that may be

identified by its spherical inflorescences. Another synapomorphy for the group is epigynous floral nectaries firmly embedded in the hypanthia (El-Sayed & Verpoorte, 2007; Razafimandimbison & Bremer, 2001, 2002).

1.3 Genus: *Ochreinauclea*

The genus *Ochreinauclea* is one of the Rubiaceae family, which consists of two species (Table 1.1) *Ochreinauclea maingayi* and *Ochreinauclea missionis* (Whitmore & Ng, 1989). This plant genus grows into a medium-sized to large tree with pyramidal buds and cone-shaped ends. It has opposite leaves or sometimes groups of three leaves. The blade is chartaceous, narrowly triangular, has a petiole, and lasts for about half a year. The terminal inflorescence is a single flowering head with many subsessile five-merous flowers. Their ovaries connect at the tips, and there are no hairs or interfloral bracts. Their ovary has two chambers, and each chamber has several ovules. The placenta connects the ovules to the septum. The fruit of this plant is partly covered and topped by calyx lobes that don't fall off. Eventually, the fruit breaks up into semi-cocci. The seeds are many and small. They are flat on both sides and have short wings on both sides. (Ridsdale, 1978; Whitmore & Ng, 1989)

Table 1.1: The distribution and uses of *Ochreinauclea species*.

Species	Common Name	Distribution	Uses
O. maingayi	Bangkal Empitat, Limpor, Tepong	Native to Malaysia, Indonesia, and rare in Thailand	Fruit is edible. Timber uses as furniture.(S. C. Lim, 2004)
O. missionis	Jalamdasa	Endemic in India	Bark is used for cure rheumatism, leprosy and ulcer. (Naomita & Ravishankar, 2001) The root and root bark are used to treat rheumatism, dropsy, paralysis, skin diseases, eye diseases, constipation, jaundice, piles, jaundice, fever, hepatitis, and haemophilia. (Chandrika & Ravishankar, 2009)

1.3.1 *Ochreinauclea maingayi* (Hook. f.) Risds.

Ochreinauclea maingayi is a large to medium-sized tree that can reach heights of 25 m and girths of 2 m. The bark is lenticellate and gray brown, but the inner bark is yellow. The inner bark becomes violet when exposed to light. The sapwood is pale yellow. The vegetative terminal bud is conical to pyramidal in shape. The leaves are elliptic to obovate in shape, 10-20 x 5-10 cm in size, glabrous scantily and short-hairy below, and chartaceous to sub coriaceous. The apex is pointy or cuspidate, and the base is acute. The secondary veins 10-14 are paired with drying black above and brown, black below. The stalks are 10-25 mm long, with narrowly triangular stipules overlapping around the terminal bud and each with two prominent lateral keels. Inflorescence stalked solitary head and terminal, globose, 30-35 mm across corollas. Its peduncle is 10-20 mm long with 1-2 nodes bearing small bracts. The flowers have 5-merous and bisexual calyx cups that are joined at the apices with smooth lobes. The corolla is trumpet-shaped and 7-12 mm long, with five ovate lobes that are 2 mm long. The ovary comprises two cells with placentas attached to the middle of the ovary cross wall, while its ovules have many per cell (Whitmore & Ng, 1989). Figure 1.2 indicates the tree (a), bark (b), fruit (c) and (d&e) leaves of *O. maingayi* (Hook. f.) Risds.

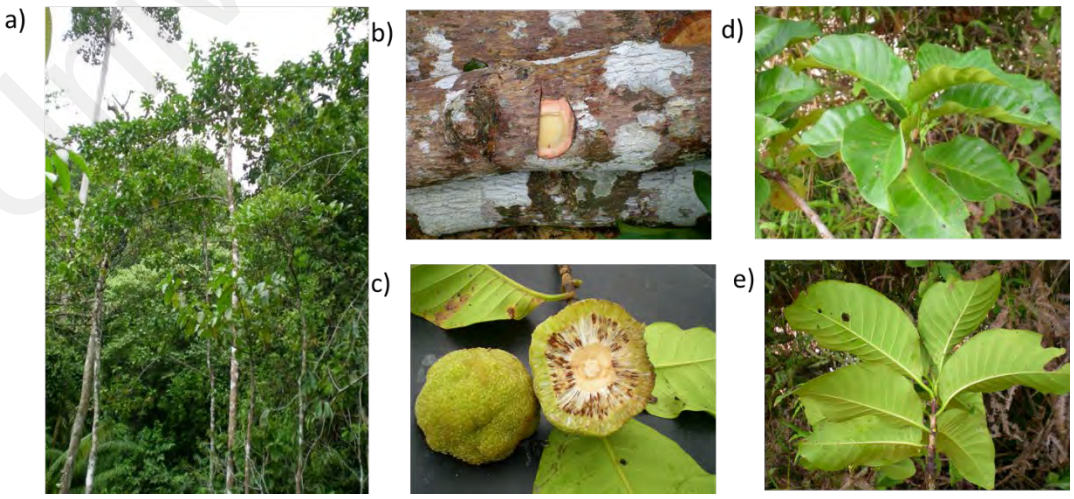

Figure 1.2: a) Tree of *O. maingayi* (Hook. f.) Risds. b) Bark of *O. maingayi* c) Fruit of *O. maingayi* d) & e) Leaves of *O. maingayi* (Source: Herbarium of the Department Chemistry, Universiti Malaya, Kuala Lumpur, serial number KL5595).

1.4 Problem Statements

The isolation of pure natural products (NPs) from complex mixtures is tedious. It requires a multi-step purification process that is time-consuming and resulting in product loss at each stage. It also makes extensive use of chemicals and solvents, which are both expensive and hazardous to the environment. New application strategies are needed to shorten or speed up natural product research workflows. In addition, this study will employ a computational tool (MN) based on LCMS/MS. This new tool will aid in speed up NPs identification.

Cholinesterase inhibitors are a type of medication that is often prescribed to patients in order to alleviate the symptoms of Alzheimer's disease (AD) and other forms of dementia. Because the number of therapeutically accessible cholinesterase inhibitors is limited, researchers are looking for additional effective and less toxic inhibitors, and plants are the most promising source. Due to their intricate nitrogen-containing structures, such as galantamine **(1)**, natural alkaloids are among the most promising candidates for treating AD. A preliminary investigation on dichloromethane crude extract (DCE) of the bark of *O. maingayi* inhibited 54 % of inhibition at 100 µg/mL on butyrylcholinesterase (BChE). The compounds responsible for the activity, however, are unknown. Therefore, in this study, the DCE of the bark of *O. maingayi* will be subjected to bioassay guided of fractionation and isolation to identify the bioactive compounds.

1.5 Objectives

This research work involved the chemical investigation of the bark of the *Ochreinauclea maingayi*, molecular networking (MN) and biological activity. The objectives of this research are outlined as follows:

1. To extract and fractionate the bark of *O. maingayi*.
2. To perform MN analysis to accelerate the natural products research activities.
3. To determine anticholinesterase activity on the fractions and compounds.
4. To isolate and purify the compounds with the chromatography techniques and elucidate the compounds by spectroscopic method.
5. To carry out kinetic and molecular docking studies on the most active compound that actively inhibited the BChE to determine their mode of inhibition (competitive, not competitive, or mixed type) and to investigate the site at which the active compound binds to the enzymes.

CHAPTER 2: LITERATURE REVIEWS

There are limited references in the phytochemical studies for genera *Ochreinauclea* because there are only two species worldwide: *O. missionis* and *O. maingayi*. However, only *O. maingayi*, a Malaysian species, has been studied in terms of phytochemical composition (Mukhtar et al., 2012). In Malaysia, the genera *O. maingayi* are known as "bangkal", and it shares this local name together with species from two other genera; *Neonauclea* and *Nauclea* (S. C. Lim, 2004; Whitmore & Ng, 1989). Since the *O. maingayi* species shares the same local name as the genus *Nauclea* and *Neonauclea*, they also share similarities in chemical constituents. Indole alkaloid is the major compound in these three genera, especially in *Nauclea* species. Table 2.1 shows the isolated indole alkaloid from plants of the genus *Ochreinauclea*, *Nauclea* and *Neonauclea* species with their biological activities (anticholinesterase, vasorelaxant, antimalaria and cytotoxicity activity), whilst the Figure 2.1 illustrated all the chemical structures of indole alkaloids isolated from "bangkal" plants (*Ochreinauclea*, *Nauclea* and *Neonauclea*).

Table 2.1: Indole alkaloids isolated from "bangkal" plants (*Ochreinauclea, Nauclea* and *Neonauclea*) with their biological activities.

Species	Compounds	Resource	Biological activity
Ochreinauclea maingayi (Mukhtar et al., 2012)	Cadamine **(4)** Neonaucline **(5)** Naucledine **(6)** Harmane **(7)**	Malaysia	The vasodilatory effects of compounds **4**, **5**, and **6** were significant. (Mukhtar et al., 2012)
Nauclea officinalis (Liew et al., 2015; Liew et al., 2012; Liu et al., 2022; Liu et al., 2017; Mao et al., 1984; Song et al., 2019; Wang et al., 2022)	Naucleficine **(8)** Nauclefidine **(9)** Nauclefoline **(10)** 1-acetyl-β-carboline **(11)** Naucleidinal **(12)** Angustine **(13)**	China Malaysia	**13**, **14**, and **15** showed potent vasodilator activity with 90 percent or more relaxation at 1×10^{-5} M on an isolated rat aorta (Liew et al., 2012).

Table 2.1, continued.

Species	Compounds	Resource	Biological activity
	Nauclefine **(14)** Naucletine **(15)** Naucline **(16)** Angustidine **(17)** Angustoline **(18)** Harmane **(7)** 3,14-dihydroangustoline **(19)** Strictosamide **(20)** 17-*O*-methyl-19-(*Z*)-naucline (**21)** Naucleofficine III (**22)** Naucleofficine II (**23)** Naucleofficine I (**24)** Naucleofficine D (**25)** Naucleoffieine H (**26)** Naucleoxoside A (**27)** Naucleoxoside B (**28)** (3*S*,19*S*)-3,14-Dihydroangustoline (**29)** (3*S*,19*R*)-3,14-Dihydroangustoline (**30)**		**17**, **14**, **13**, **18** and **7** were potent towards Anticholinesterase activity (Liew et al., 2015). **21** exhibited significant inhibition of nitric oxide production in mouse macrophages RAW 264.7 cells *in vitro* induced by lipopolysaccharide. The IC_{50} value was 3.6 µM (Liu et al., 2017). **26** suppress NO and TNF-overproduction in LPS-induced RAW 264.7 macrophages by blocking the iNOS pathway (Song et al., 2019). IC_{50} values of **14**, **13**, **27**, **28**, **18**, **29** and **30** were comparable to those of dexamethasone for inhibiting nitric oxide (NO) production induced by lipopolysaccharide in mouse macrophage RAW 264.7 cells in vitro (Wang et al., 2022)
Nauclea Subdita (Liew et al., 2014)	Subditine (**31**) Nauclefine **(14)** Angustine **(13)** Angustidine **(17)** Angustoline **(18)**	Malaysia	**31** demonstrates that induction of apoptosis inhibits the proliferation of LNCaP and PC-3 human prostate cancer cells (Liew et al., 2014).

Table 2.1, continued.

Species	Compounds	Resource	Biological activity
Nauclea latifolia (Aggrey et al., 2019; Agomuoh et al., 2013; Brown et al., 1977; Hotellier et al., 1975, 1980; Hotellier et al., 1979; Ngnokam et al., 2003; Shigemori et al., 2003)	Nauclefine (**14**) Naucletine (**15**) Strictosidine (**32**) Naulafine (**33**) 3*α*–dihydrocadambine (**34**) Cadambine (**35**) Naucledinal (**12**) *Epi*-19 naucledinal (**36**) Angustoline (**18**) (3*S*,19*S*)-3,14-dihydroangustoline (**29**) (3*S*,19*R*)-3,14-dihydroangustoline (**30**) Nauclefolinine (**37**) Nauclamides D (**38**) Nauclamides C (**39**) Nauclamides B (**40**) Nauclamides A (**41**) Nauclamides E (**42**) Latifoliamide A (**43**) Latifoliamide B (**44**) Latifoliamide C (**45**) Latifoliamide D (**46**) Latifoliamide E (**47**)	Senegal Nigeria	**38** demonstrated a moderate capacity for promoting LDL uptake (1.26-fold). It dose-dependently increased LDLR protein expression and decreased PCSK9 protein expression from 1 to 50 µM.(Aggrey et al., 2019) **43-47** and **18** exhibited moderate in vitro renin inhibitory activities (Agomuoh et al., 2013).
Nauclea orientalis (Kanchanapoom et al., 2021; Liu et al., 2018; Sichaem et al., 2010; Zhang et al., 2001)	Nauclealines B (**48**) Nauclealines A (**49**) Naucleosides B (**50**) Naucleosides A (**51**) Strictosamide (**20**) Vincosamide (**52**) Angustine (**13**) Naucleaorals A (**53**) Naucleaorals A (**54**) Nauclorienine (**55**)	China Thailand	Compound **54** exhibited significant cytotoxicity to HeLa cells with an IC_{50} of 4.0 µg/mL, whereas compounds **2** and **54** exhibited only moderate cytotoxicity to both cell lines with IC_{50} values of 7.8 and 9.5 µg/mL, respectively**.** (Sichaem et al., 2010)

Table 2.1, continued.

Species	Compounds	Resource	Biological activity
Nauclea orientalis (Kanchanapoom et al., 2021; Liu et al., 2018; Sichaem et al., 2010; Zhang et al., 2001)	Antirhine **(56)** Iso-antirhine **(57)** Alangine **(58)** Naucline **(16)** Neonaucline **(5)** Subditine **(31)** Kanluaengosides C **(59)** Kanluaengosides D **(60)** 10-Hydroxystictosamide **(61)** 10-Hydroxyvincoside lactam **(62)**	China Thailand	Alkaloids **56**, **57**, **58**, **59** exhibited significant inhibitory effects against multiple human cancer cell lines, with IC_{50} values comparable to cisplatin (Liu et al., 2018).
Nauclea parva (Sainsbury & Webb, 1975)	Parvine (nauclefine) **(14)**		
Nauclea diderrichi (Dmitrienko et al., 1974; Murray, 1969)	Naucledine **(6)** Naucleder ine **(63)** Naucleonine **(64)** Naucleonidine **(65)**	Africa	
Neonauclea purpurea (Karaket et al., 2012)	Cadambine **(35)** 3*α*-dihydrocadambine **(34)**	Thailand	**34** exhibited weak in vitro antimalarial activity against the chloroquine-resistant strain K1 of *Plasmodium falciparum*, with IC_{50} values of 6.6. **35** and **34** exhibited no cytotoxicity to monkey (Vero) cells. (Karaket et al., 2012).
Neonauclea schlecteri (Johns et al., 1970)	Gambirine **(66)**		

Table 2.1, continued.

Species	Compounds	Resource	Biological activity
Neonaulea sessilifolia (Itoh et al., 2003)	Neonaucleoside C **(67)** Neonaucleoside B **(68)** Neonaucleoside A **(69)** Strictosidine **(32)** Viscoside **(70)**		

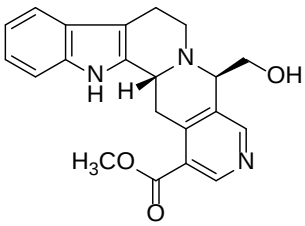

4

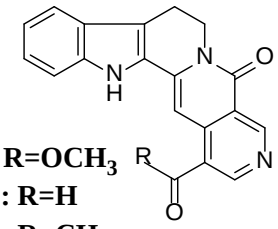

5: R=OCH$_3$
12: R=H
15: R=CH$_3$

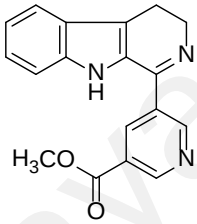

6

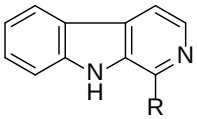

7: R=CH$_3$
11: R=COCH$_3$

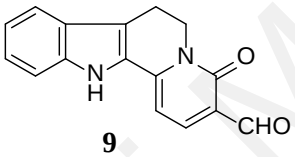

9

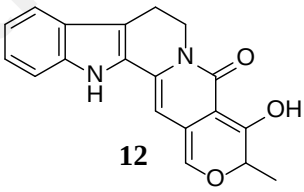

12

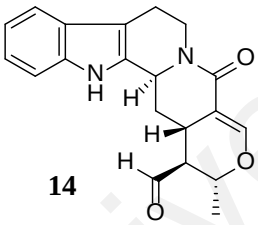

14

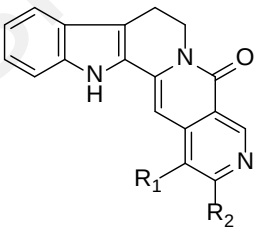

15: R$_1$=CHCH$_2$;R$_2$=H
16: R$_1$=H, R$_2$=H
19: R$_1$=H, R$_2$=CH$_3$
20: R$_1$=COHCH$_3$' R$_2$=H

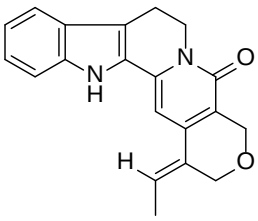

16

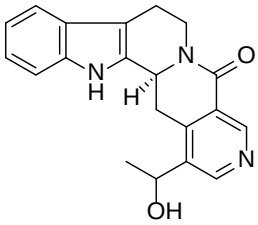

21

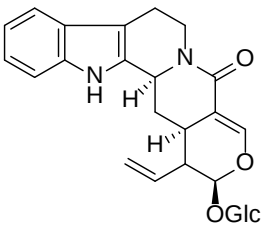

22

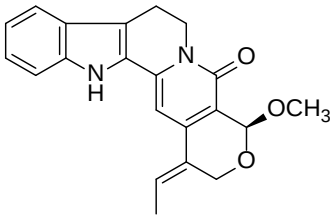

23

Figure 2.1: Structure of indole alkaloids isolated from "bangkal" plants (*Ochreinauclea*, *Nauclea* and *Neonauclea*).

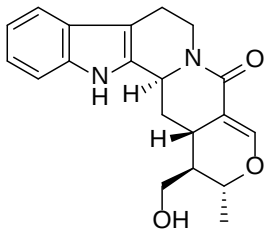

24

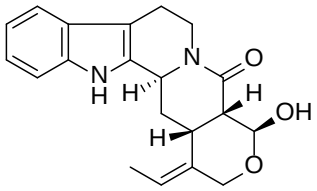

25

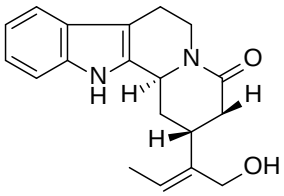

26

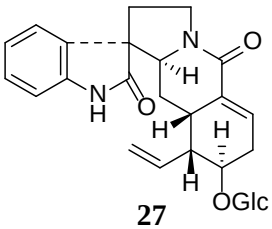

27

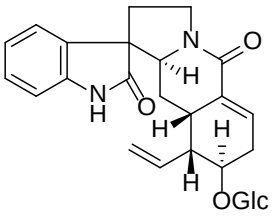

28

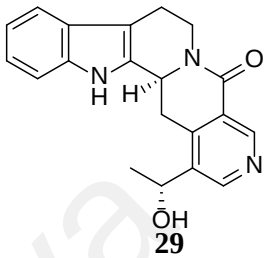

29

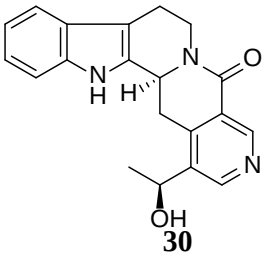

30

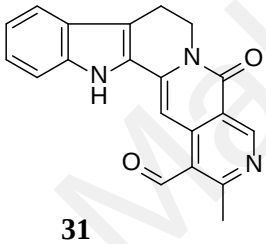

31

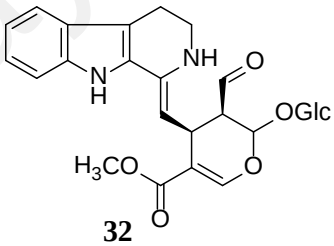

32

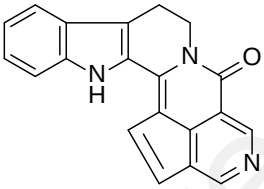

33

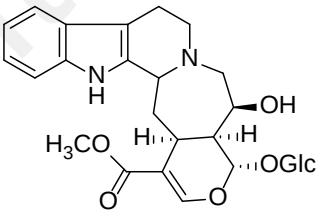

34

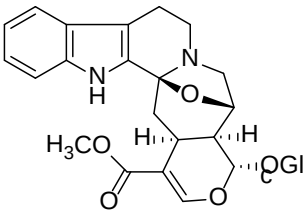

35

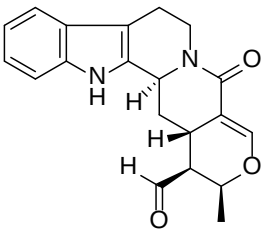

36

Figure 2.1, continued.

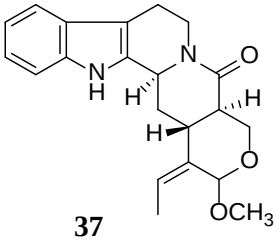

37

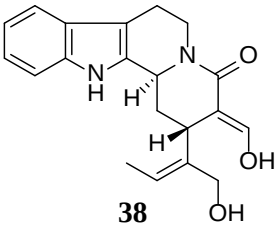

38

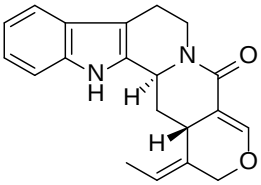

39

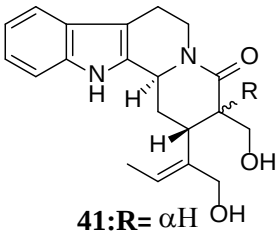

41:R= αH
40:R=βH

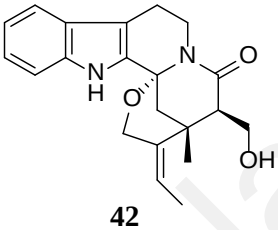

42

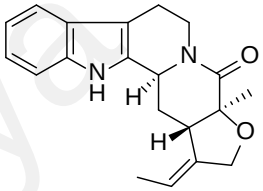

43

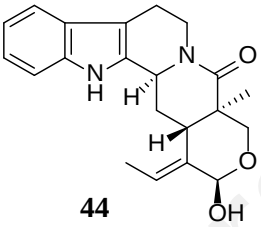

44

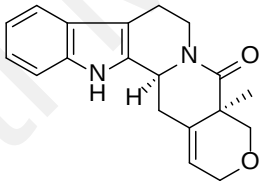

45

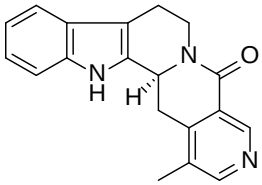

46

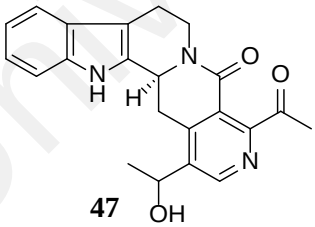

47

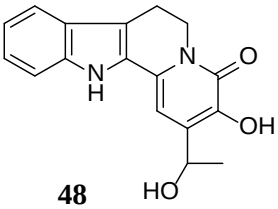

48

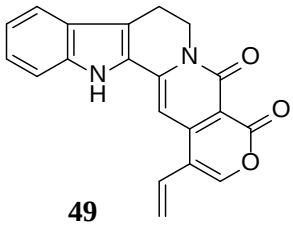

49

Figure 2.1, continued.

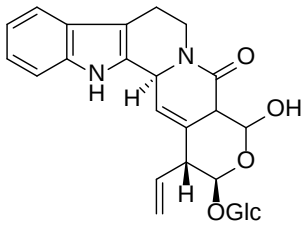

50

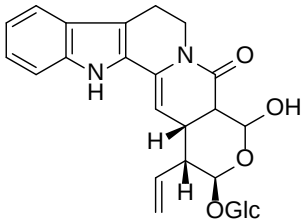

51

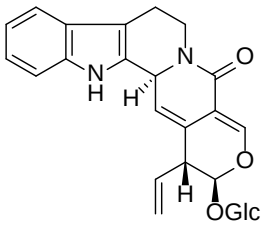

52

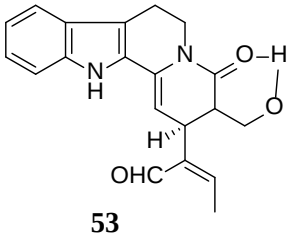

53

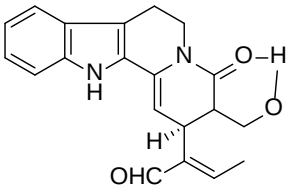

54

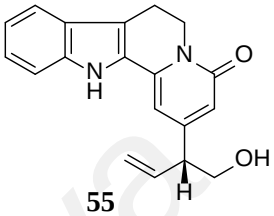

55

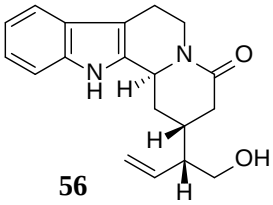

56

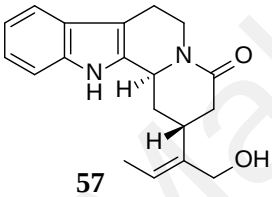

57

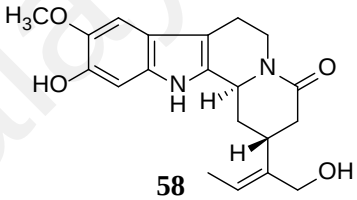

58

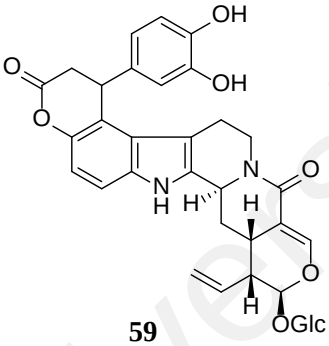

59

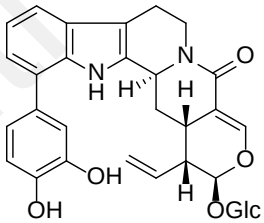

60

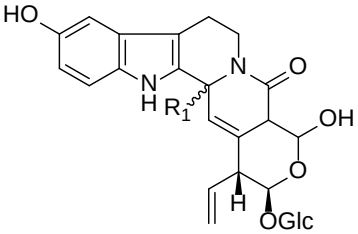

61 R=αH
62 R=βH

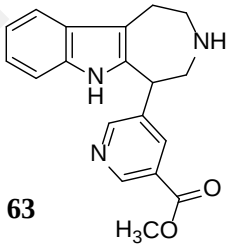

63

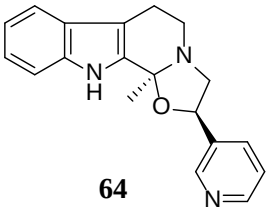

64

Figure 2.1, continued.

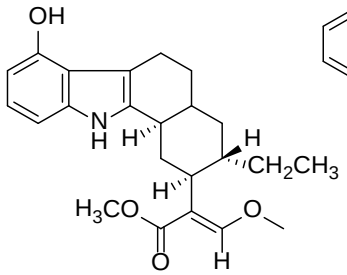

65

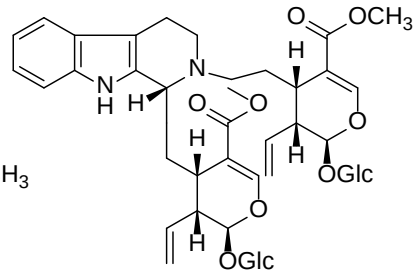

66

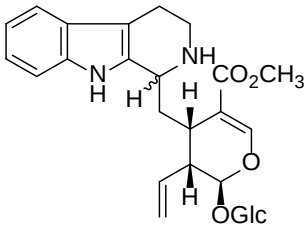

68:3*S*;
67:3*R*

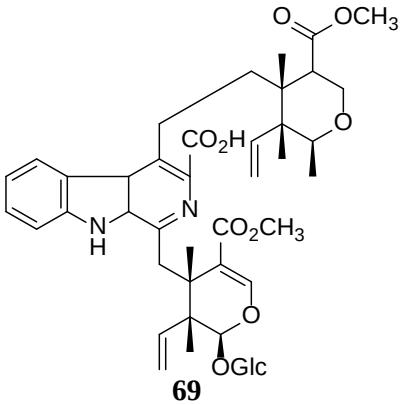

69

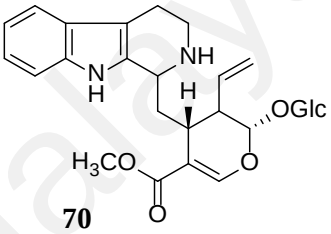

70

Figure 2.1, continued.

2.1 Phytochemical types

The following paragraph will discuss briefly in indole alkaloid and coumarin. These are main type of compound found in *O. maingayi*.

2.1.1 Indole alkaloid

An indole **(71)** (Figure 2.2) alkaloid is a nitrogen-containing bicyclic compound composed of a six-atom benzene ring fused to a five-atom pyrrole ring. Nitrogen at the centre of a pyrrole ring is responsible for the unique pharmacological properties of indole alkaloids (El-Sayed & Verpoorte, 2007).

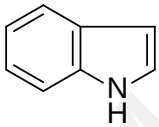

71

Figure 2.2: Structure of indole (71).

Indole alkaloids have been discovered in a variety of well-known plant families, including the Apocynaceae, Rubiaceae, Nyssaceae, and Loganiaceae (Omar et al., 2021). Among famous indole alkaloids (Figure 2.3) was isolated from plants include the antitumor drugs, vincristine **(72)** and vinblastine **(73)** and from *Catharanthus roseus* (Alam et al., 2017), antihypertensive drug, reserpine **(74)** from *Rauwolfia serpentina* (Peri & Mangipudy, 2014) and anticholinesterase drug, physostigmine **(75)** from *Physostigma venenosum* (Zhao et al., 2004) .

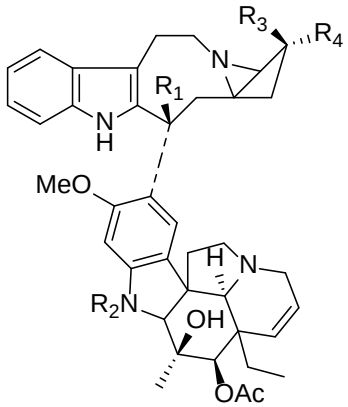

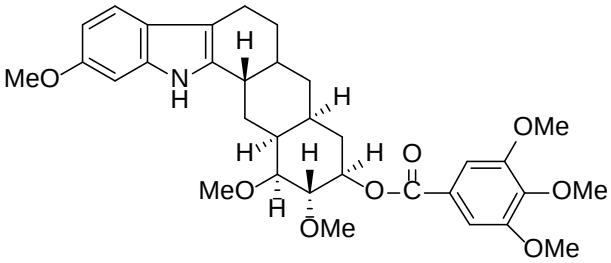

74

72: R_1=$COOCH_3$, R_2=CH_3, R_3=OH, R_4=Et
73, R_1=$COOCH_3$, R_2=CHO, R_3=OH, R_4=Et

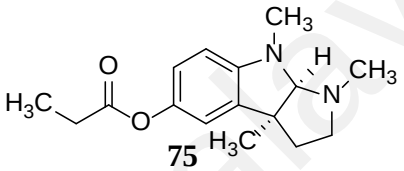

75

Figure 2.3: Structure of vincristine (72), vinblastine (73), reserpine (74) and physostigmine (75).

The primary phytoconstituents of the Rubiaceae family have been identified as indole alkaloids, which are responsible for the majority of the secondary metabolites discovered in this family. (Martins & Nunez, 2015). Several Rubiaceae genera are known to produce indole alkaloids, including *Neolamarkcia*, *Adina*, *Nauclea*, *Neonauclea*, *Anthecephalus*, *Cephalantus*, *Sarcocephalus*, *Uncaria* and *Mitragyna* (Phillipson et al., 1982). The skeleton of indole alkaloids skeleton is composed of tryptophan **(76),** tryptamine **(77)** and secologanin **(78)** (Figure 2.4).

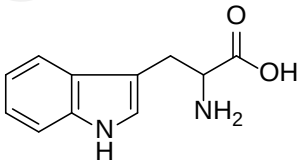

76

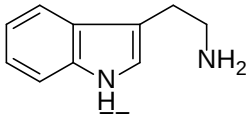

77

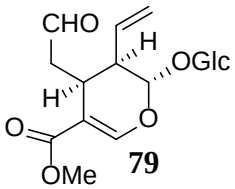

79

Figure 2.4: Structure of tryptophan (76), tryptamine (77) and secologanin (78).

Based on the structural characteristics of their skeletons, indole alkaloids can be further divided into groups. Rahman and Basha divided them to five classes as showed in Table 2.2 (Rahman & Basha, 1983).

Table 2.2: Clasification of indole alkaloids.

Class	Precursor	Example of group and compound	
		Group	**Compound**
Class I **(Corynanthe, yohimbe, strychnos type)** 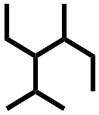	Secologanin with tryptophan/ tryptamine	Corynanthiene group	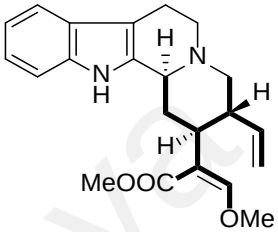 Coryanthine **(79)**
		Cadamine Group	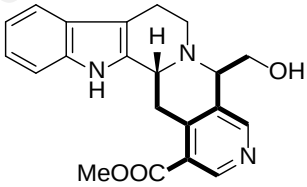 Cadamine **(4)**
		Cadambine group	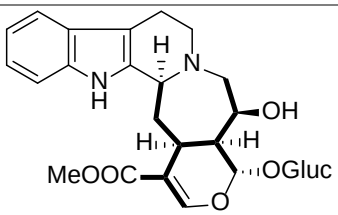 3*α*-dihydrocadambine **(34)**
		Yohimbine group	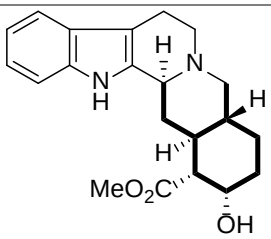 Yohimbine **(80)**

Table 2.2, continued.

Class	Precursor	Example of group and compound	
		Group	**Compound**
Class I (Corynanthe, yohimbe, strychnos type) 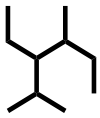	Secologanin with tryptophan/ tryptamine	Vincoside group	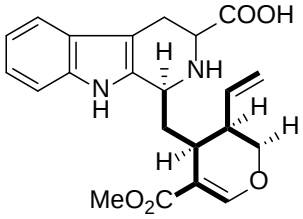 5*α*-Carboxystrictosidine **(81)**
		Ajmalicine group	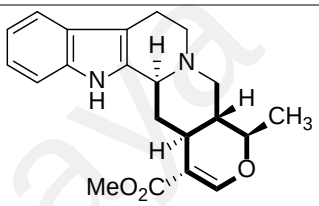 Ajamlicine **(82)**
		Cordifoline group	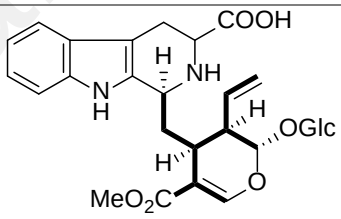 Cordifoline **(83)**
		Lyalidine group	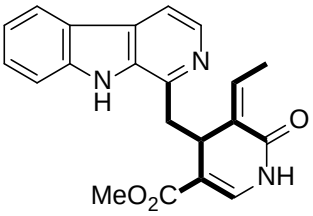 Lyalidine **(84)**
		Strictosamide group	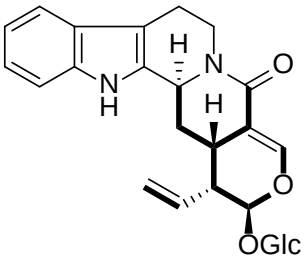 Strictosamide (**85**)
		Talboltine group	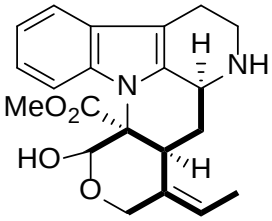 Talboltine **(86)**

Table 2.2, continued.

Class	Precursor	Example of group and compound	
		Group	**Compound**
Class I (Corynanthe, yohimbe, strychnos type) 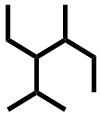	Secologanin with tryptophan/ tryptamine	Vallesiachotamine group	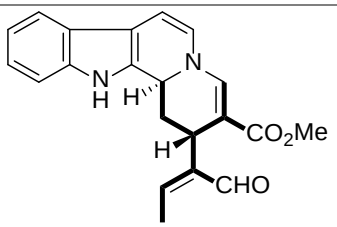 Vallesiachotamine **(87)**
		Spargine group	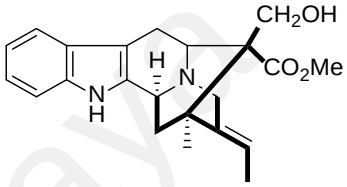 Spargine **(88)**
		Perakine group	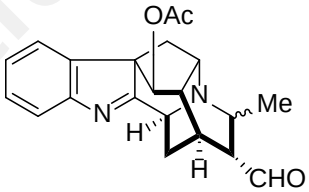 Perakine **(89)**
		Strychnine group	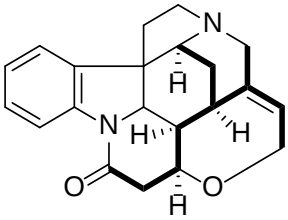 Strychnine **(90)**
		Tubofoline group	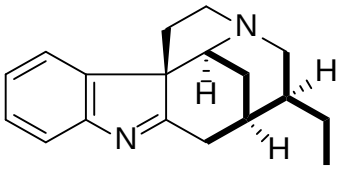 Tubofoline **91**
		Chitosenine group	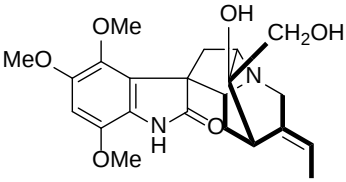 Chitosenine **(92)**

Table 2.2, continued.

Class	Precursor	Example of group and compound	
		Group	**Compound**
Class II (Aspidoserma, Hunteria type) 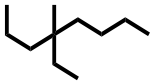	Secologanin with tryptophan/ tryptamine	Vindoline group	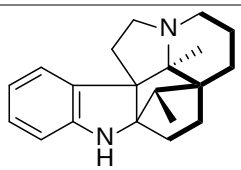 Tuboxinine **(93)**
		Quebrachamine group	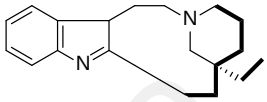 Quabrachmine **(94)**
		Aspidospermine group	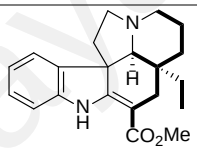 Aspidospermine **(95)**
		Buxomelline group	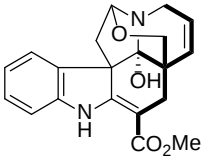 Buxomelline **(96)**
		Apodine group	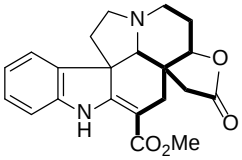 Apodine **(97)**
		Vincatine group	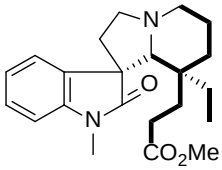 Vincatine **(98)**
		Catharanthine group	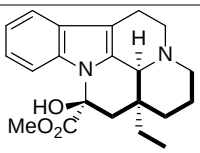 Vincamine **(99)**
		Catharanthine group	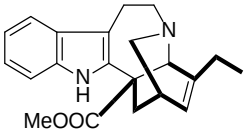 Catharanthine **(100)**

Table 2.2, continued.

Class	Precursor	Example of group and compound	
		Group	**Compound**
Class III (Iboga alkaloids and other diverse skeletons derived from tryptophan and secologanin) 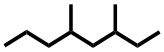	Secologanin with tryptophan/ tryptamine	Catharanthine group	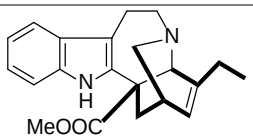 Catharanthine **(101)**
		Pandoline group	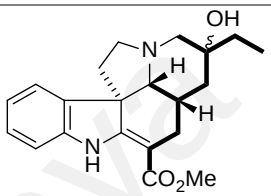 Pandoline **(102)**
		Ibophyllidine group	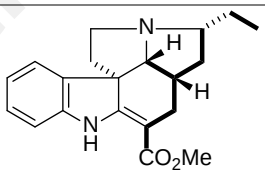 Ibophyllidine **(103)**
		Rupicoline group	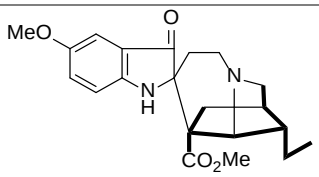 Rupicoline **(104)**
		Iboxyphylline group	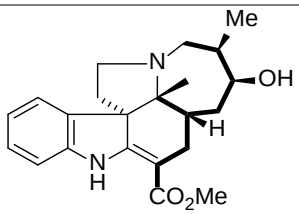 Iboxyphylline **(105)**
		Andranginine group	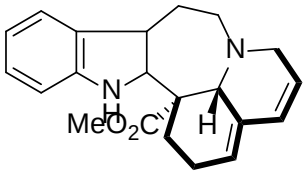 Andraginine **(106)**

Table 2.2, continued.

Class	Precursor	Example of group and compound	
		Group	**Compound**
	Subclass		
Class IV (Not derived from secologanin**)**	a) Non-trytophan	Murrayazolidine group	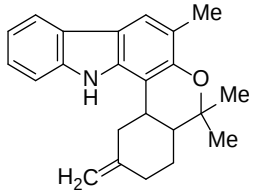 Murrayazolidine **(107)**
		Murrayanine Group	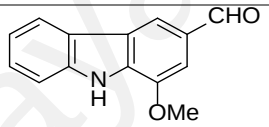 Murrayanine **(108)**
		Girnimbine group	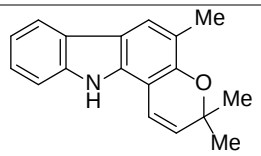 Garnimbine **(109)**
		Subincanine group	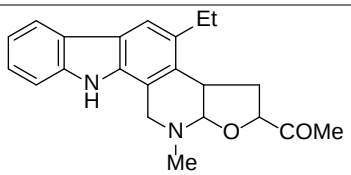 Subincanine **(110)**
		Couroupitine A group	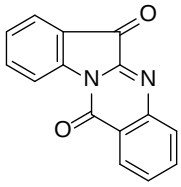 Couroupitine A **(111)**
	b) Non-isoprenoid tryptophan	Tryptophan group	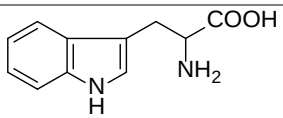 Tryptophan **(76)**

Table 2.2, continued.

Class	Precursor	Example of group and compound	
		Group	**Compound**
		Harmaline group	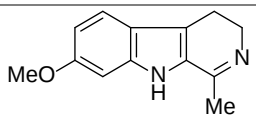 Harmaline **(112)**
		Nauclefine Group	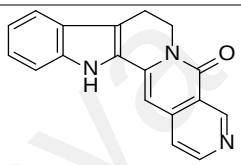 Nauclefine **(16)**
		Indolo-pyridine group	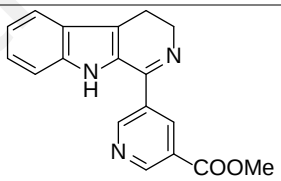 Indolo-pyridine A **(113)**
		Naufoline group	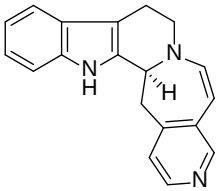 Naufoline **(114)**
		Eleacarpidine group	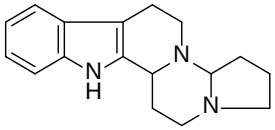 Eleacarpidine **(115)**
		Physostigmine group	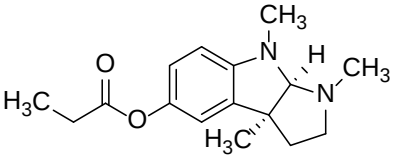 Physostigmine **(5)**

Table 2.2, continued.

Class	Precursor	Example of group and compound	
		Group	**Compound**
Class IV (Not derived from secologanin)	Subclass		
	c)Isoprenoid tryptophan	β-Cyclopiazonic acid group	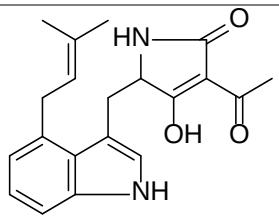 *β*-Cylopiazonic acid **(116)**
		Isopentenyl tryptophan group	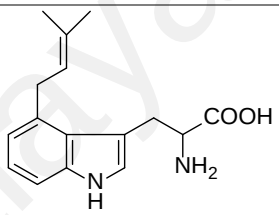 4-isopentenyl tryptophan **(117)**
		Agroclavine group	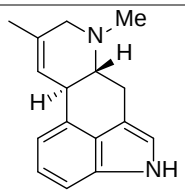 Agroclavine **(118)**
Class V Binary indole alkaloids		**Group I-I**	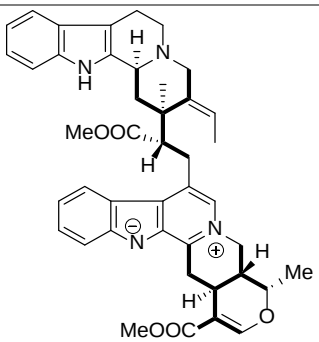 Serpentinine **(119)**
		Group II-II	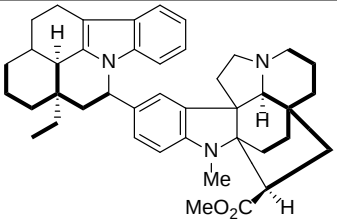 Pleiomutine **(120)**

Table 2.2, continued.

Class	Precursor	Example of group and compound	
		Group	**Compound**
		Group II-III	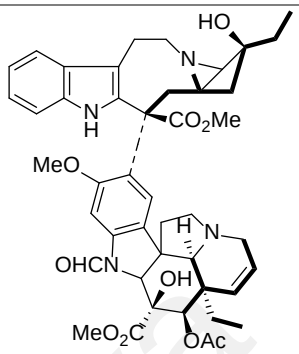 Vinblastine **(72)**
		Group IV-IV	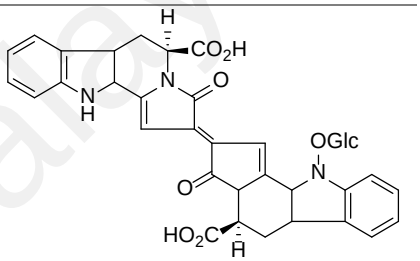 Trichotomine G **(121)**

2.1.1.1 Biosynthesis of indole alkaloid

Indole is the precursor to several vital phytochemicals found in nature. Tryptophan (**76**) with indole parents is one of the naturally occurring essential amino acids (Kaushik et al., 2013). The Mannish condensation of tryptamine **(77)** with aliphatic aldehyde possessing nine or ten carbon at the α- or β- positions of indole nucleus yields the primary form of indole alkaloids. The structures of indole **(71)**, tryptophan **(76)** and tryptamine **(77)** are depicted in Figure 2.5

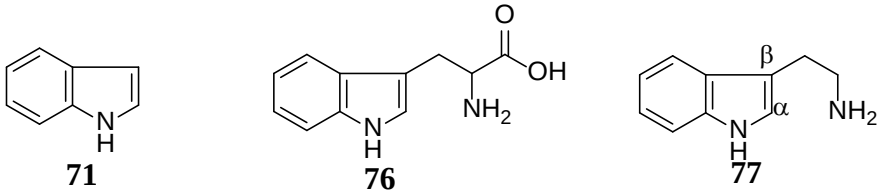

Figure 2.5: Structure of indole (71), tryptophan (76) and tryptamine (77).

Perkin and Robinson (1919) were the first to propose that the aromatic part of the indole alkaloid is derived from tryptophan **(76)**, which has been decarboxylated to tryptamine (Perkin & Robinson 1919). Experimental proof of such decarboxylation has been established by Battersby and colleagues (Battersby et al., 1969). Tryptophan **(76)** or tryptamine **(77)** could condense with an appropriate aldehyde to form a Schifff base which could then be attacked intramolecularly by the β- position of the indole nucleus to afford the corresponding indolenines **(122)** (Scheme 2.1).

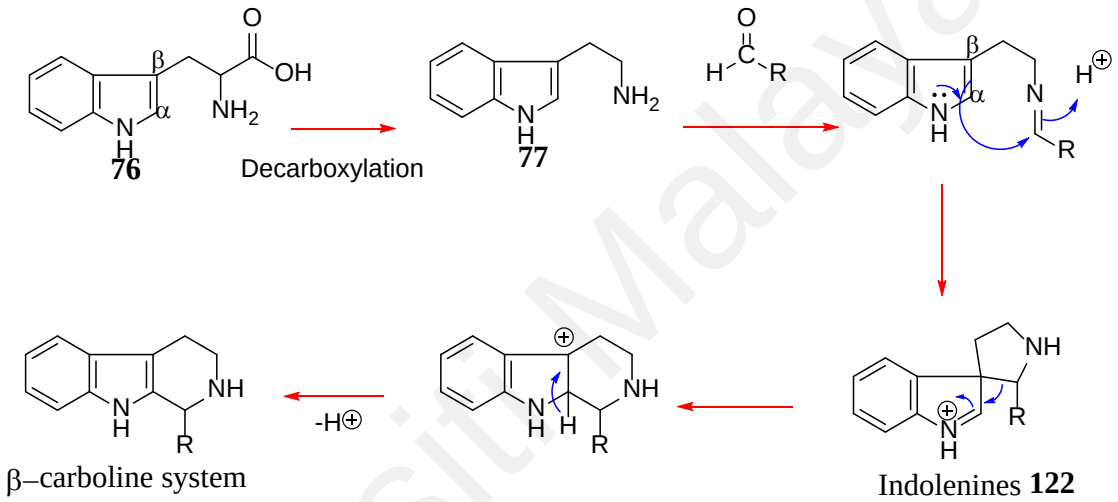

Scheme 2.1: Biosynthetic hypothesis of the *β*-carboline system from tryptamine (77).

According to Basha and Rahman (1983), cadambine **(35)** and cadamine **(4)** belong to group I (Rahman & Basha, 1983). Both cadambine **(35)** and cadamine **(4)** were considered to be biosynthesized from tryptamine **(77)** and secologanin **(78)** *via* a condensation process in the presence of enzyme strictosidine synthetase to form strictosidine **(32)** (Brown et al., 1991). The biosynthesis of cadambine **(35)** by stereospecific epoxidation of strictosidine **(32)** gives the 18,19*S*-epoxystrictosidine **(123)**. The regioselective attack by N-4 on the 18,19*S*-epoxystrictosidine **(123)** yields 3*α*-dihydrocadambine **(34)** with the formation of a seven-membered azepine ring. Oxidation of C-3 and cyclization of the alcohol leads to cadambine **(35)** (in green arrow) (Scheme 2.2).

A glycosidase enzyme hydrolyzes the glycosidic strictosidine **(35)** to generate an aglycone precursor *via* another route which indicates in blue arrow in Scheme 2.2. This aglycone hydrolyze to forms a series of reactive intermediates, which are then oxidized to form cadamine (**4)** (Heinstein et al., 1979). Neonaucline (**5)** was proposed to be biosynthesized from cadamine (**4)** (purple arrow) (Scheme 2.2). Subsequently, **4** is oxidized at C-18, followed by decarboxylation and protonation of the carbanion to afford intermediate (**5)**. Afterward, the intermediate (**5)** will be hydroxylated at C-19 followed by oxidation to yield neonaucline (**5)** (Mukhtar et al., 2012).

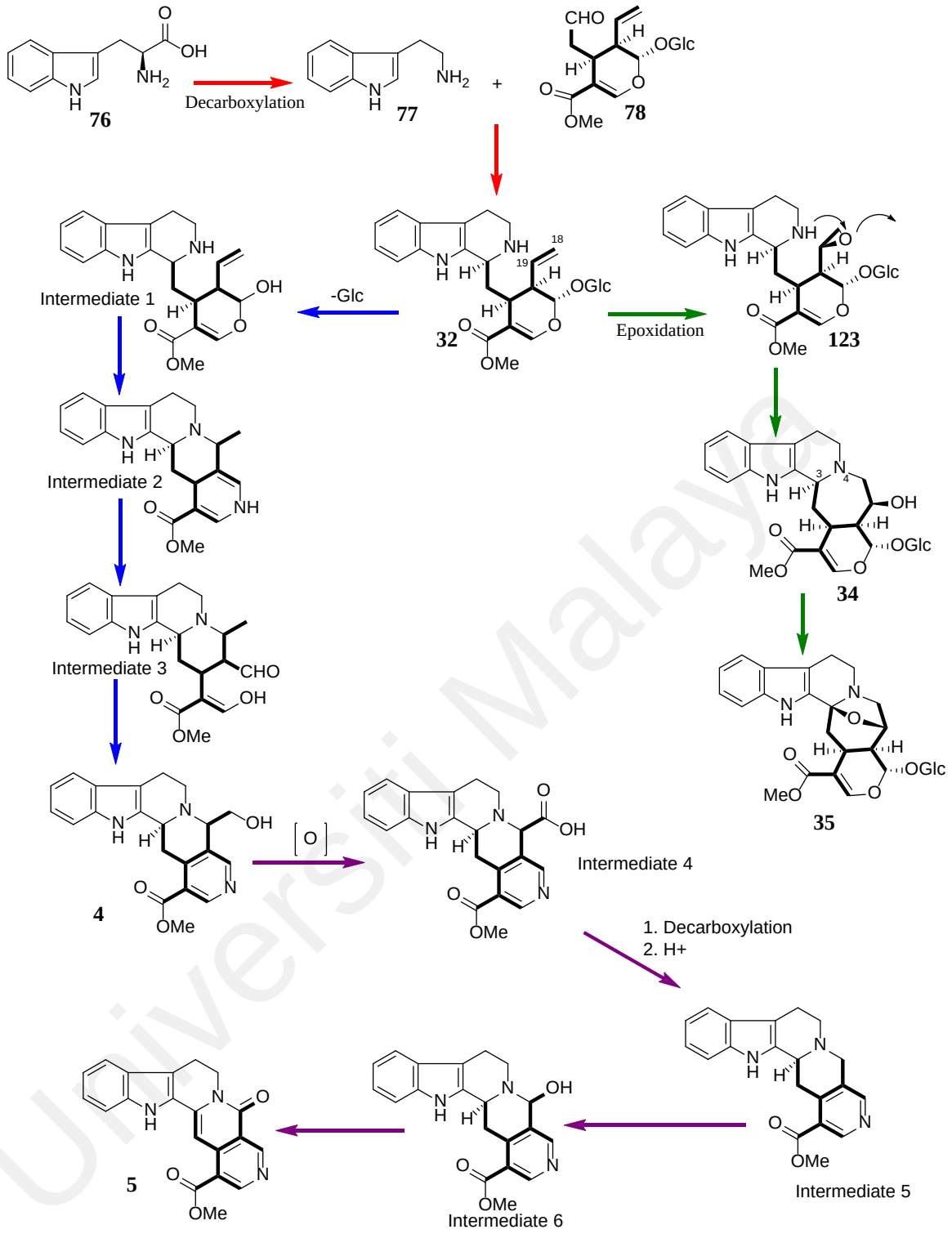

Scheme 2.2: Biosynthesis pathway of cadambine (35), cadamine (4) and neonaucline (5).

Harmane **(7),** *nor*harmane **(124)** and naucledine **(6)** belong to group IV is derived from tryptophan. Harmane **(7)** is obtained from tryptophan **(76)** *via* decarboxylation and the Pictet-Spingler reaction (Scheme 2.3). The biosynthetic route to harmane **(7)** (blue arrow) is relatively straight forward: tryptophan **(76)** decarboxylated to tryptamine **(77)**, and a

subsequent Pictet-Spingler reaction with acetaldehyde (CH_3CHO) give tetrahedron *β*-carboline intermediate. The oxidative reaction lead to formation of *β*-carboline; harmane **(7)** is an example (Stanforth, 2006). Harmane **(7)** can then be methylated to form *nor*harmane **(124)** (pink arrow). Naucledine **(6)** is an indole-pyridine group that can be biosynthesized (green arrow) through the condensation of pyridine system's two-carbon oxidized side chain with tryptamine **(77)** (Scheme 2.3). The condensation of this modified indole intermediate and the pyridine precursor, followed by decarboxylation, results in indole-pyridine alkaloids such as naucledine **(6)** (McLean & Murray, 1972).

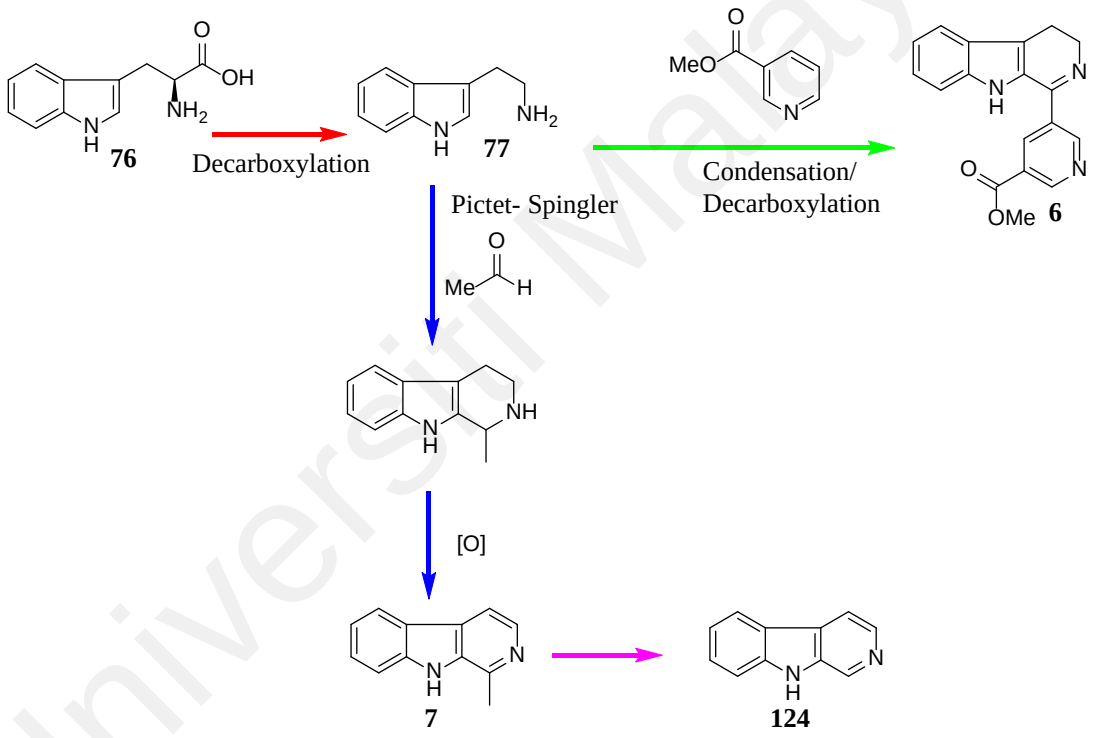

Scheme 2.3: Biosynthesis pathway of harmane (7), *nor*harmane (124) and naucledine (6).

2.1.2 Coumarin

Coumarin or 1,2-benzopyrones **(125)** (Figure 2.6) belongs to a class of polyphenolic compounds derived from plants. They are members of the benzopyrone family and possess numerous pharmaceutical applications, including anti-proliferative, anti-inflammatory, anti-coagulant, anti- cytoprotective, carcinogenic, hepatoprotective and modulatory functions, which can be interpreted as therapeutic potential for a variety of

diseases (Karayil et al., 2014). They contribute to the persistence of plants through processes such as defence against phytopathogens, regulation of oxidative stress, response to abiotic stresses, and most likely hormonal regulation (Bourgaud et al., 2006).

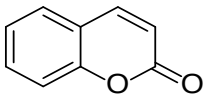

125

Figure 2.6 : Basic structure of coumarin (125).

2.1.2.1 Biosynthesis of simple coumarin

Coumarin **(125)** are ubiquitously found in higher plants originating from the phenylpropanoid pathway. Despite their importance, essential details of their biosynthesis are still remain mostly unknown (Bourgaud et al., 2006). According to Maria Joao et al., simple coumarin is biogenetically derived from shikimic acid **(126)** via cinnamic acid **(127)**. The specificity of the process in the C-2 hydroxylation produces a break (6-oxidation) of the side chain, or chain isomerization and subsequent lactonization, resulting the umbelliferon **(128)** (Maria João et al., 2015). Scheme 2.4 shows the biosynthesis of coumarin.

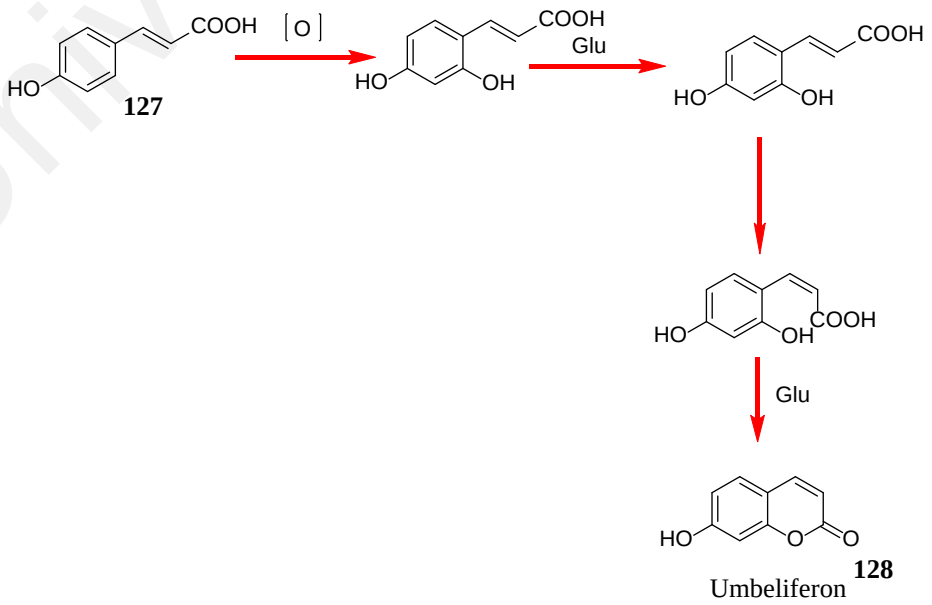

Scheme 2.4: Biosynthesis of simple coumarin.

2.2 Global Natural Products Social Molecular Networking (GNPS)

LCMS/MS based analysis has lately emerged as the benchmark for studying natural products. Notably, the usage of high-resolution mass spectrometers is growing since these devices can generate precise mass calculations for determining chemical formulas as well as MS/MS spectra for structural elucidation (Bouslimani et al., 2014). However, due to the complexity of numerous constituents in natural products, MS experiments would produce numerous spectra, making these data too broad to be manually examined (Wang et al., 2016). For this reason, the use of Molecular Networking (MN) by GNPS as an approach for mapping the spectral structural space by comparing MS/MS structural similarity is extremely beneficial (Watrous et al., 2012; J. S. Yu et al., 2022; Yu et al., 2019).

GNPS's MN allows it to visualise clusters of chemicals with similar structural properties, even if their names are unknown (Vincenti et al., 2020). As related molecules exhibit similar MS/MS profiles, clusters are produced via spectral alignment of the structurally connected compounds based on the fragmentation modes. Connections between spectra are shown as edges connecting nodes, and each chemical entity is represented as a node. Depending on library matches, the nodes may be displayed in a variety of colours, sizes, or shapes, or they might have information such as source, abundance, and mean polarity appended to them (Yang et al., 2013). Cosine scores (edges) indicate the degree of structural similarity between the molecules that are connected, with a score of one denoting structurally identical compounds (Figure 2.7) (Wang et al., 2016). When viewing exported data in Cytoscape, the map of the linked molecules appears as molecular networks (Otasek et al., 2019).

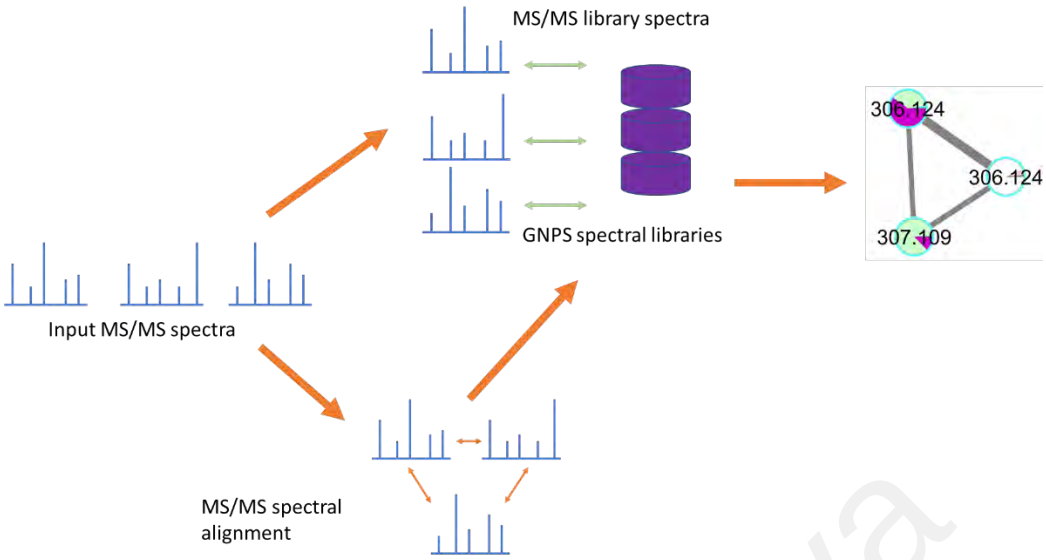

Figure 2.7: Molecular networking and library generation by GNPS.

GNPS-based molecular networking has been widely used in natural product dereplication, prioritisation and quantification, discovery, biosynthesis, and chemical ecology since its inception in 2012 (Crüsemann et al., 2017; Nothias et al., 2018; Wang et al., 2016). For instance, T. Kouamé et al. used the MN method search for a corynantheine-type indole alkaloid in the stem bark of *Corynanthe pachyceras*. Three compounds were successfully isolated, two of which previously unknown (Kouamé et al., 2020). In another case, Santos et al. apply the MN strategy to identify strictosidine-type monoterpene indole alkaloids in leaf aqueous extract *Strychnos peckii*, as strictosidine **(34)** is the precursor to most monoterpene IA. From this MN, seven strictosidine-type alkaloids were detected (Santos et al., 2020).

Targeted research on new/novel indole alkaloid analogues is proven successfully conducted using GNPS molecular networking. For example, in order to identify novel indole analogues, a GNPS molecular networking was produced for an alkaloid extract of *Palicourea sessilis* from the Rubiaceae family, which has previously reported as a producer of monoterpene indole alkaloid (MIA). The existence of many novel MIA analogues and known analogues in the extract was indicated by the molecular network, and subsequent chemical investigations enabled the separation of four new MIA (Klein-

Júnior et al., 2017). The investigation of a new vobasine–tryptamine-based monoterpene indole alkaloid pseudo-dimer from the stem bark of *Voacanga africana* is another instance of targeted molecular networking. The new analogue is a minor constituent of a thoroughly studied plant; this molecule was targeted using a molecular networking strategy, and an MS/MS-guided phytochemical study led to its isolation (Fouotsa et al., 2022). Molecular networking has aided in the comprehension of the structures of numerous compounds by providing unparalleled system-level perspectives of the chemical space in a variety of circumstances (Aron et al., 2020). In addition to providing unprecedented system-level views of the chemical space in various environments, molecular networking has helped reveal the structures of numerous compounds.

2.3 Anticholinesterase Activity

Alzheimer's disease (AD) is a progressive neurodegenerative disease characterized by the presence of amyloid-β deposits, low level of acetylcholine, τ-protein aggregation, and oxidative stress (Korabecny et al., 2014; Zhan et al., 2010). Despite the fact that the pathophysiology of AD is not entirely understood, the "cholinergic hypothesis" is the primary mechanistic theory that escalated out (Cavdar et al., 2019). According to the mechanistic cholinergic hypothesis, dysfunction of acetylcholine-containing neurons in the brain significantly contributes to the cognitive decline observed in elderly and Alzheimer's disease patients (Terry & Buccafusco, 2003).

Cholinesterase inhibitors are frequently used to treat Alzheimer's disease and other dementias symptoms (Pohanka, 2014). Cholinesterase (ChE) is a critical enzyme that has been classified into two subgroups based on their catalytic characteristics. They are acetylcholinesterase (AChE) and butyrylcholinesterse (BChE). AChE is an enzyme that promotes the decomposition (hydrolysis) of tiny substrate such as acetylcholine (Ach). Meanwhile, BChE may adapt to the bulkier substrates like benzoyl or butyryl-choline and catalyse their decomposition (Rashid & Ansari, 2014). Figure 2.8 show the structure

of (a) acetylcholinesterase (AChE), (b) butyrylcholinesterse (BChE) and (c) benzoyl (ligand).

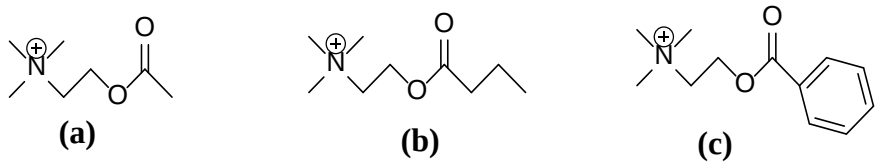

Figure 2.8: Structure enzymes (a) acetylcholinesterase (AChE), (b) butyrylcholinesterse (BChE) and (c) benzoyl (ligand).

Butyrylcholinesterase (BChE) and acetylcholinesterase (AChE) are enzymes that break down acetylcholine, where acetylcholine is a neurotransmitter essential for cognitive function and neuromuscular transmission. However, some differences between the two enzymes may favoure BChE in certain situations (Kumar, 2015). BChE, also recognized as pseudocholinesterase or nonspecific cholinesterase, is found in more tissue throughout the body than AChE, such as in the blood, liver, and other tissues, while AChE which is only located in the neuro-muscular junction and in the central nervous system. This broader distribution may make BChE more accessible as a therapeutic target (Colović et al., 2013; Mushtaq et al., 2014). Additionally, BChE has a broader substrate specificity than AChE, where it can cleave a more comprehensive range of compounds (Pope & Brimijoin, 2018). Although AChE is the primary enzyme responsible for the breakdown of acetylcholine, BChE plays a more supporting role. Because the important enzyme remains active to maintain normal physiological function, blocking BChE may have less negative effects than inhibiting AChE (Darvesh et al., 2003). Due to the limited choice of the clinically available cholinesterase inhibitors, researchers are still looking for new effective inhibitors, with plants being the best source. Several AChE and BChE inhibitors have been identified from various natural sources (Konrath et al., 2013). Due to their complicated nitrogen-containing structures, alkaloids are regarded to be the most promising natural compounds for treating AD. (Portelius et al., 2006). Physostigmine **75**, an indole alkaloid discovered for the first time in 1864 from *Physostigmina venenosum*

Balf., was employed in therapy prior to the discovery of ACh as neurotransmitter (Erdogan Orhan et al., 2011). Physostigmine **(75)**, on the other hand, is quite polar, being distributed throughout the body with only a small amount reaching the central nervous system. Both AChE and BChE are inhibited by **75** in a similar sub micromolar range (concentration required to inhibit 50% of the enzyme (IC_{50}) of 0.015 and 0.016 mm, respectively) (Iijima et al., 1992; Thomsen et al., 1991). The carbamate position is essential for physostigmine **(75)** activity since the inhibitory activity is lost when the ester bond of physostigmine (**75)** is hydrolysed, forming eseroline. Tabulation data in the Table 2.3 and Figure 2.9 revealed that indole alkaloids from plants were active AChE inhibitor candidate.

Table 2.3: Indole alkaloid isolated from plant active towards anticholinesterase activity.

Indole alkaloid	AChE IC_{50} (µM)	BChE IC_{50} (µM)	Plant	Reference
Harmane **(7)**	330 ± 5.0	90 ± 0.20	*Simira glaziovii*	(Torres et al., 2012)
Turbinatine **(129)**	1.86	NT	*Chimarrhis turbinata*	(Cardoso et al., 2004)
Naucletine **(15)** Angustidine **(17)** Nauclefine **(14)** Angustine **(13)** Naucline **(16)** Angustoline **(18)** Harmane **(7)** 3,14-Dihydroangustoline **(19)** Naucledio**l (130)**	ND 21.72 ND ND 261.89 15.429	63.14 ND 7.70 4.98 38.25 25.10 13.18 49.77 8.756	*Nauclea officinalis*	(Liew et al., 2015) (Liew et al., 2023)
7-Hydroxyisopaynantheine **(131)** 3-Dehydropaynantheine **(132)** Mitraciliatine **(133)** Speciociliatine N(4)-oxide **(134)**	10.3 ± 1.3 4.1±1.0 5.2±1.2 10.2±0.5	NT NT NT NT	*Mitragyna diversifolia*	(Cao et al., 2013)
Geissoschizoline **(135)** Geissoschizone **(136)** 3′,4′,5′,6′-Tetradehydrogeissospermine **(137)**	5.86±0.31 8.50± 0.43 0.45± 0.01	7.89 ± 0.33 11.46± 0.44 0.32 ± 0.02	*Geissospermum vellosii*	(Lima et al., 2020)
Oleraindole A **(138)** Oleraindole B **(139)**	55.12±0.20 46.76±0.08		*Portulaca oleracea*	(Zhao et al., 2019)
Coronaridine **(140)** Voacangine **(141)**	8.6 4.4		*Ervatamia hainanensis*	(Zhan et al., 2010)
Alstolarines B **(142)**	19.3		*Alstonia scholaris*	(Zhang et al., 2020)
Macusine B **(143)** Vinorine **(144)** Isoreserpiline **(145)** Rescinnamine **(146)**	48.39 35.06 24.89 11.01		*Rauvolfia reflexa*	(Fadaeinasab et al., 2015)
(−)-2-Ethyl-3[2-(3-ethylpiperidinyl)-ethyl]-1H-indole **(147)**		0.65 ± 0.16	*Vinca minor L.*	(Vrabec et al., 2022)
Geissoschizine methyl ether **(148)**	3.7 ± 0.3		*Uncaria rhynchophylla*	(Yang et al., 2012)

*ND= Not Determine, NT=Not Tested

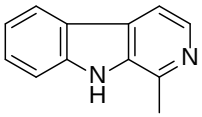

7

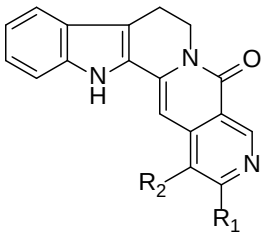

13; R_1=H, R_2=CH_2CH_2
14; R_1=H, R_2=H
15; R_1=H, R_2=$COCH_3$
17; R_1=CH_3, R_2=H
18; R_1=H, R_2=$COHCH_3$

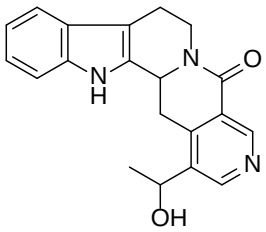

19

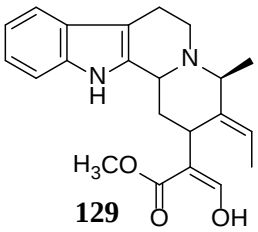

129

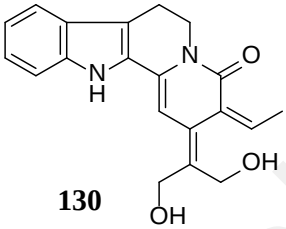

130

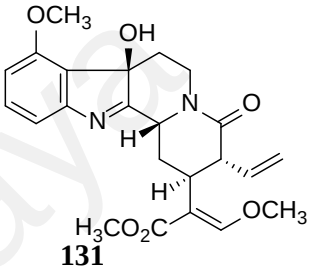

131

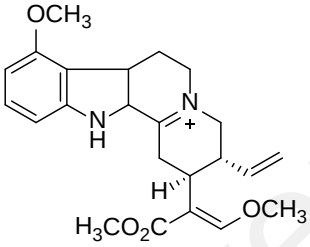

132

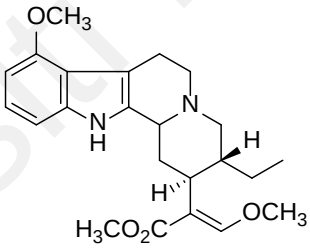

133

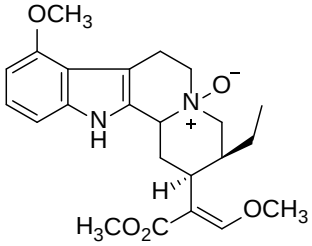

134

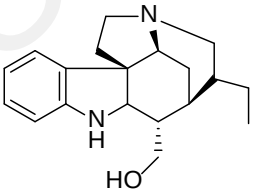

135

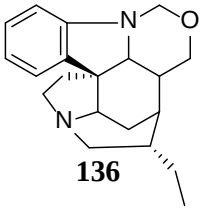

136

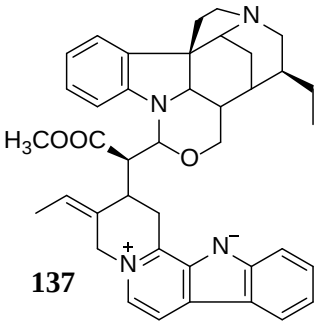

137

Figure 2.9: Structure of indole alkaloids isolated from plant active towards anticholinesterase activity.

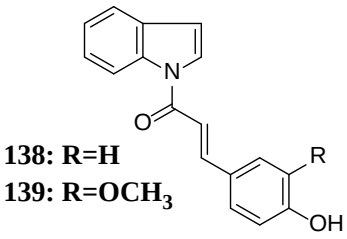

138: R=H
139: R=OCH$_3$

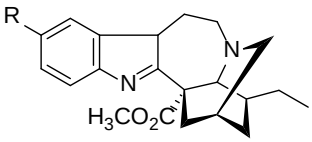

131; R=H
141; R=OCH3

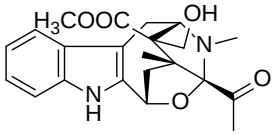

142

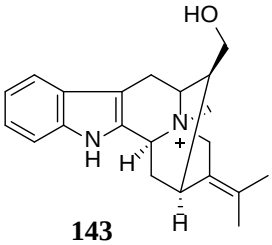

143

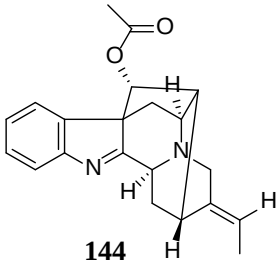

144

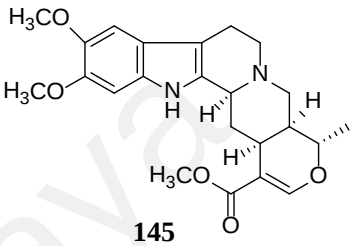

145

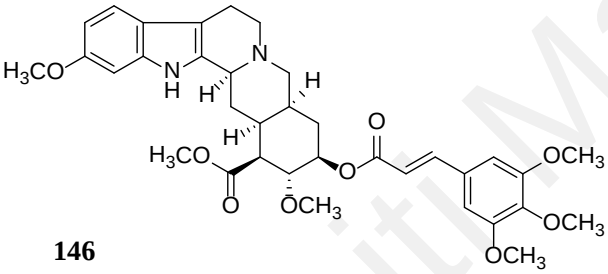

146

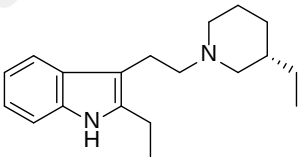

147

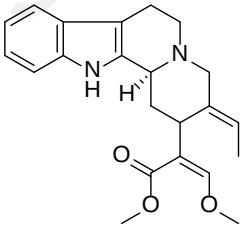

148

Figure 2.9, continued.

CHAPTER 3: RESEARCH METHODOLOGY

The following subsections will discuss briefly on experimental activities and there are three subsections; 3.1 Phytochemical analysis, 3.2 Featured Based Molecular Networking and 3.3 Anticholinesterase activity.

3.1 Phytochemical Analysis

3.1.1 Plant Material

The plant *Ochreinauclea maingayi* (Figure 1.2) was collected at Ulu Sat Reserve Forest, Machang, Kelantan, by Mr. Din Mat Nor and Mr, Teo Leong. The plant identification was done by Prof. Colin E. Ridsdale from Leiden University, Leiden, Netherlands. The voucher specimen with herbarium series number KL5595, was deposited in the Department of Chemistry's herbarium at Universiti Malaya.

3.1.2 Chemical and reagents

1. *Dichloromethane (industrial grade)
2. *Hexane (industrial grade)
3. *Methanol (industrial grade)
4. 25% ammonia solution
5. Celite
6. Chloroform AR grade
7. Deuterated chloroform, $CDCl_3$ with 99.8 atom % D (with silver stabilize)
8. Deuterated pyridine, C_5D_5N with 99.8 atom % D
9. Methanol AR grade
10. Methanol spectroscopy grade
11. Silica gel 60 for column chromatography, (0.040-0.063mm)
12. Slilica Gel 60 F254, pre-coated glass plate

*note: solvent was distilled prior to use

3.1.3 Instrumentations

3.1.3.1 Nuclear Magnetic Resonance (NMR)

All the NMR spectra were recorded on a BRUKER Advance III 400 NMR and BRUKER Advance III 600 NMR. Spectrometer System using deuterated solvent such as chloroform ($CDCl_3$), methanol (CD_3OD), and pyridine (C_5D_5N).

3.1.3.2 Infrared (IR)

The IR spectra were obtained through Perkin-Elmer 1600 and Perkin-Elmer RX1 FT-IR spectrophotometer series using chloroform as solvent.

3.1.3.3 Ultraviolet (UV)

The Shimadzu UV-250 Ultraviolet-Visible Spectrophotometer was used to record the UV spectra. Spectroscopic grade methanol (CH_3OH) was used as solvent.

3.1.3.4 Liquid Chromatography Mass Spectrum (LCMS)

LCMS spectra for purified compound were obtained from quadruple time of flight (Agilent 1260-6530 Infinity) attached with 1260 DAD detector for profiling. Column used was ZORBAX Eclipse XDB (2.1 mm i.d x 100 mm, 1.8 µm) by Agilent.

Another LCMS used is an Agilent 1260 Infnity HPLC coupled to an Agilent 6530 ESI-Q-TOF-MS (ElectroSpray Ionization Quadrupole Time of Flight Mass Spectrometry) operating in positive mode. A Sunfire® analytical C18 column (150×2.1mm; i.d. 3.5 µm, Waters).

All sample were filtered through Whatman 13 mm, 0.2 µm nylon membrane syringe before use 1 µL of sample was injected into the instrument.

3.1.3.5 Optical rotation

Optical rotations $[\alpha]_D^{20}$ values were measured on Jasco P-1020 digital polarimeter using methanol as a solvent.

3.1.4 Separation techniques

3.1.4.1 Column Chromatography (CC)

All the solvents used in this experiment are industrial grade (distilled) or AR grade. (distilled). Column chromatography was performed using Silica Gel 60 (70 – 230 mesh). A slurry of silica gel (approximate ratio 30:1 silica gel to sample) was poured into a glass column of appropriate size with gentle tapping to remove trapped bubbles. The crude extract was first dissolved in the fewest solvents possible before being loaded onto the packed column. The extract was diluted with a suitable solvent system at a specific flow rate and collected using fractions, which were collected and evaporated in test tubes, following that, TLC monitoring was used to combine fractions with the same R_f.

$$R_f = \frac{Distance\ moved\ by\ solute}{Distance\ moved\ by\ solvent} \tag{3.1}$$

3.1.4.2 Thin Layer Chromatography (TLC)

The isolated compounds' spots were visualised using aluminum-supported silica gel plates. After spraying or dipping with required reagents, UV light (254 and 365 nm) was used to examine spots or bands on the TLC.

3.1.4.3 Preparative Thin Layer Chromatography (PTLC)

PTLC was used to separate fractions and compounds that could not be separated using CC. Silica gel plate was loaded with 20 mg of sample. The plate was developed in a covered glass chamber using a suitable solvents system. The separated compounds were visualized and marked under UV lights (254 and 365 nm). The designated section was then scraped off and placed in a conical flask to be extracted with the appropriate solvents several times.

3.1.5 Detector Reagents

3.1.5.1 Mayer Reagents

In 60 mL of distilled water, 1.4 g of mercuric iodide was mixed with 5.0 g of potassium iodide in 10 mL of water. After that, the mixture was concentrated to make a 100 ml solution. The formation of a white precipitate indicated a positive test result when the aqueous layer (acidified) was treated with 2-3 drops of Mayer's reagent.

3.1.5.2 Dragendorff's Reagent

A stock solution of Dragendorff's reagent is a mixture of equal parts solution A and solution B. The solution A contains 0.85 g bismuth (III) nitrate in 10 mL of glacial acetic acid and 40 mL of distilled water. Whilst solution B consists of 8.0 g potassium iodide in 200 mL of distilled water (200 ml). For the spraying reagent, 20 mL of stock solution was diluted with pure water to 60 mL. The dried TLC plate was equally sprayed with Dragendorff's Reagent in a working hood. The alkaloid compounds were detected by having orange-brown spots to indicate a favourable reaction, and the results were recorded immediately after colour testing as the orange-brown spots faded over time.

3.1.5.3 Vanillin-sulphuric acid vapour

The 0.5 g vanillin in 2 ml concentrated H_2SO_4 was added with cooling to 8 ml ethanol before spraying onto the TLC plate. On dried chromatography TLC plates, vanillin reagent was sprayed. The plates were then heated at 100-105 ^{o}C until the colours were fully developed. Positive reactions will produce a rainbow of coloured spots that detect triterpenes, steroids, higher alcohols, phenols, and essential oils.

3.1.6 Extraction, fractionation, and isolation of *O. maingayi*

3.1.6.1 Extraction of *O.maingayi*

The extraction process was carried out using simple maceration method. The dried and grounded stem bark of *O. maingayi* (2.0 kg) was first defatted with hexane (10 L) for three days period at room temperature. The resulting slurry was processed through a filter, and the plant material that was left behind was soaked in an ammonia solution with a concentration of twenty-five percent (1 L), after which it was left for two hours to allow the nitrogen-containing compounds in the plant to aggregate. The basified residual plant material was then successively re-extracted with dichloromethane (15 L, three days) and the process was repeated twice. The liquid extracts were dried under using rotary evaporator under reduced pressure, yielding 10 g of DCE. The yield of crudes from the bark extract from *O. maingayi* is given in Table 3.1.

Table 3.1: Yield of the crude extracts from the barks of *O. maingayi.*

Plant part	Amount (Kg)	Crude	Yield of crude (g)	Percentage of yield (%)	Mayer test
Bark	2.0	n-hexane	3.2	0.32	
		CH_2Cl_2	13.0	1.30	+3

3.1.6.2 Fractionation of *O. maingayi*

The DCE crude (10 g) was subjected to column chromatography (CC) separation over silica gel (Merck silica gel, 720-230 mesh) as the stationary phase. The gradient elution method was used for all separations. Dichloromethane and methanol (Table 3.2) were used as the solvent system, which acted as mobile phases.

Table 3.2: Solvent system DCM: MeOH.

DCM	MeOH
100	0
99	1
98	2
97	3
96	4
95	5
94	6
93	7
90	10
80	20
70	30
30	60
0	100

The solvent eluents were collected using a test tube (10 ml), and the alternated test tube was then tested for purity using detector reagents on thin layer chromatography (TLC). Test tubes that produced spots on the TLCs with the same R_f values were combined and treated as a fraction. Each fraction was either subjected to repeated CC or other chromatography techniques such as PTLC and MC. Fractionation of DCE eluted with CH_2Cl_2/CH_3OH (100: 1 to 1: 100, *v/v*), yielding ten fractions (F1-F10) as tabulated in Table 3.3.

Table 3.3: List of eluents of fractions and respective yield and percentage of yield from CC.

Fraction	Eluent CH_2Cl_2: MeOH	Weight (g)	% of yield
1	100:0	0.401	4.0
2	100:0	0.240	2.4
3	100:0	0.281	2.8
4	100:0	0.681	6.8
5	99:1	0.217	2.2
6	99:1	0.850	8.5
7	99:1	1.200	12.0
8	98:2	0.27	2.7
9	97:3	0.376	3.8
10	96:4	0.597	6.0
Flush	0:100	3.011	30.0

3.1.6.3 Isolation and purification fractions of *O. maingayi*

Preparative PTLC purification of **F10** afforded **A** (6.0 mg, CH_2Cl_2: CH_3OH; 94:6, saturated with NH_4OH; R_f=0.56) and **B** (110.0 mg, CH_2Cl_2: CH_3OH; 94:6, saturated with NH_4OH; R_f=0.11), respectively. After purification by PTLC of **F9, C** and **A** (3.6 mg and 2.0 mg, CH_2Cl_2: CH_3OH; 95:5, saturated with NH_4OH; R_f=0.83 and 0.54) were obtained. PTLC was used to isolate compound **D** (2.3 mg, CH_2Cl_2: CH_3OH; 99:1, saturated with NH_4OH; R_f=0.75) from **F8**. **F7** was subjected to MC eluted with CH_2Cl_2: CH_3OH (100: 1 to 1: 100, *v/v*) to five sub-fraction and then sub-fraction 5(1) was purified with PTLC to obtain **E** (1.6 mg, CH_2Cl_2: CH_3OH; 99:1, saturated with NH_4OH) and **F** (3.5 mg, CH_2Cl_2: CH_3OH; 99:1, saturated with NH_4OH; R_f=0.43). Meanwhile, **F6** purification yielded **G** (2.8 mg, CH_2Cl_2: CH_3OH; 99:1, saturated with NH_4OH; R_f= 0.51) using PTLC. After purification with PTLC, three compounds were obtained from **F5**: **H** (3.2 mg,

CH_2Cl_2: CH_3OH; 99:1, saturated with NH_4OH; R_f=0.73), **I** (2.2 mg, CH_2Cl_2: CH_3OH; 99:1, saturated with NH_4OH; R_f= 0.38) and **J** (1.8 mg, CH_2Cl_2: CH_3OH; 99:1, saturated with NH_4OH; R_f= 0.59). **F4** was also purified using PTLC, yielding **K** (80 mg, CH_2Cl_2: CH_3OH; 100:0). **F3** was separated by MC to give four subfractions (C1-C4), C4 was purified with PTLC to afford compound **L** (6.4, CH_2Cl_2: CH_3OH; 99:1; R_f=0.78) while C3, also purified by PTLC, yielded **M** (2.7mg, CH_2Cl_2: CH_3OH; 99:1; R_f= 0.65). Preparative thin layer chromatography (PTLC) was used to separate **F2** into **N, O** and **P** (40.0, 5.2, and 3.0 mg, CH_2Cl_2:100; R_f= 0.79,0.28,0.14), respectively. Purification **F1** eluted by microcolumn (MC) with hexane/ethyl acetate (100: 1 to 1: 100, *v/v)* gave ten sub-fractions (A1-A10) monitored with TLC, sub-fraction A7 yielded **Q** (25.0mg, hexane/ethyl acetate (94:6, v/v)). Scheme 3.1 simplifies the schematic flow of the isolating of all compounds from the barks of *O. maingayi*.

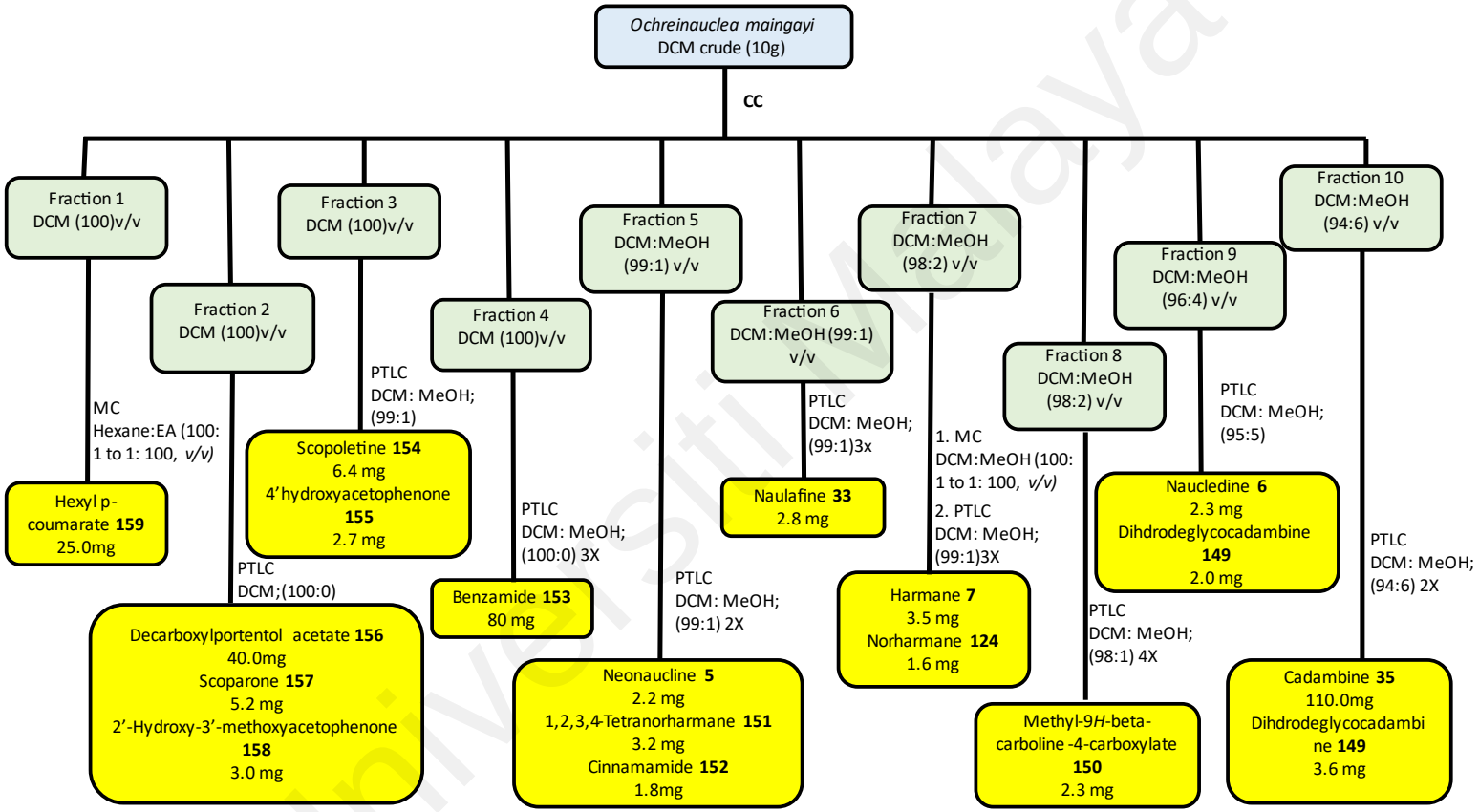

Scheme 3.1: The schematic flow of the isolation of all compounds from the barks of *O.mangayi*.

3.2 Feature Based Molecular Networking

Feature based molecular networking (FBMN) is an analysis method created by the GNPS to supplement existing chromatographic feature identification and alignment methods (Nothias et al., 2020). Isomer separation and quantitative analysis techniques like ion mobility spectrometry are made possible. Figure 3.1 shows the overall workflow of FBMN. After collecting crude and fractions LCMS/MS data, we used the MSConvert programm in the Proteowizard suite to transform the .RAW LCMS/MS data into the .mzXML format. Each .mzXML file was run through MZmine 2 v53 to produce the.mgf data. Massive molecular networking was generated by exporting and uploading the.mgf pre-clustered spectral data file and its corresponding.csv metadata file (for RT and integration) to GNPS (Global Natural Product Social Molecular Networking) (MN). In order to visualise and assess the constructed molecular network, Cytoscape software (ver3.8.2) is used.

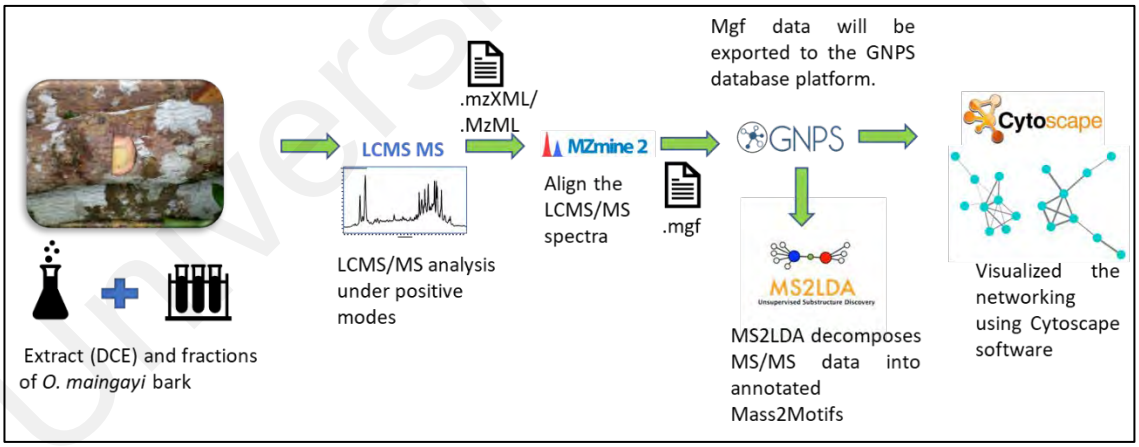

Figure 3.1: Feature based molecular networking workflow.

3.2.1 LCMS/MS Orbitrap analysis

For LCMS/MS analysis, the crude extracts were dissolved in LCMS grade MeOH at a 1.0 mg/mL. The experiments were carried out on a Thermo Scientific Orbitrap Fusion Tribrid. The samples were injected and chromatographically separated on an Accucore TM Vanquish C18+ Dim. (2.1 x100 mm) at 40 °C using a 1.0 µL injection volume. The separation was achieved with a binary LC solvent system controlled by Mobile phase A consisting of 99.9 percent water/0.1 percent formic acid (LCMS grade) and mobile phase B containing 100 percent MeOH (LCMS grade), which were pumped at a rate 0.250 mL/min, According to the following gradient sequence of percentage Solvent B increment: maintained at 5 percent from 0 to 2 min, increased from 5 to 100 percent from 2 to 30 min, maintained at 100 percent until 40 min. Positive mode MS/MS analysis was carried out, with the following optimised operating conditions: column temperature 40 °C; capillary temperature 325°C; spray voltage, 3.5 (+) and 2.5 (-) kV; sheath gas flow rate (Arb): 50, auxiliary gas flow rate (Arb): 10; Sweep gas (Arb): 1; RF lens (percent): 60; Scan range (m/z): 100-1000; Collision-induced dissociation (CID) energy was adjusted to 30 percent . The Thermo Xcalibur software, version 4.3, was used for the recording and processing of all the data.

3.2.2 MZmine 2 v53 parameters

The MS/MS data files were first converted from the .raw (Orbitrap) standard data format to .mzXML format using MSConvert Software from ProteoWizard package (Chambers et al., 2012). After that, all .mzXML files were then processed using MZmine 2 v53 (Pluskal et al., 2010). The mass detection was realised by keeping the noise level at 5.0E5 at MS1 and 5.0E4 at MS2. The ADAP chromatogram builder was used with a minimum group size of the scan of 5, a group intensity threshold of 3.0E5, a minimum highest intensity of 3.0E5, and a m/z tolerance of 0.001 Da (or 5ppm). The ADAP wavelet deconvolution algorithm was used with the following standard setting: a chromatographic

threshold =1%, a search minimum in RT range min = 0.30, a minimum relative height = 1%, a minimum absolute height = 5.0E5, a minimum ratio peak top/edge = 2, and a peak duration range (min) = 0 to 2 min. Isotopologues were categorised by using an algorithm called the isotopic peak grouper with a m/z tolerance of 0.006 Da (20 ppm) and an RT tolerance of 0.5 min. These parameters were used to determine how closely isotopologues were related to one another. The join aligner module was used to accomplish peak alignment, with the following parameters: a m/z tolerance of 0.001 Da (or 5 ppm), a weight for RT value of 2.0, and an absolute RT tolerance of 0.3 minutes. The feature list row filler peak m/z was 100 to 1000, which kept the MS2 scan and reset the ID. The gap in the peak list was filled using a gap filler module with the same RT and m/z range (the m/z tolerance was set to either 0.001 or 5ppm). Eventually, the .mgf preclustered spectral data file and its corresponding.csv metadata file (for RT and integration) were exported using the dedicated "Export/Submit for GNPS/FBMN" option. Figure 3.2 shows the overall workflows of MZmine 2 V53.

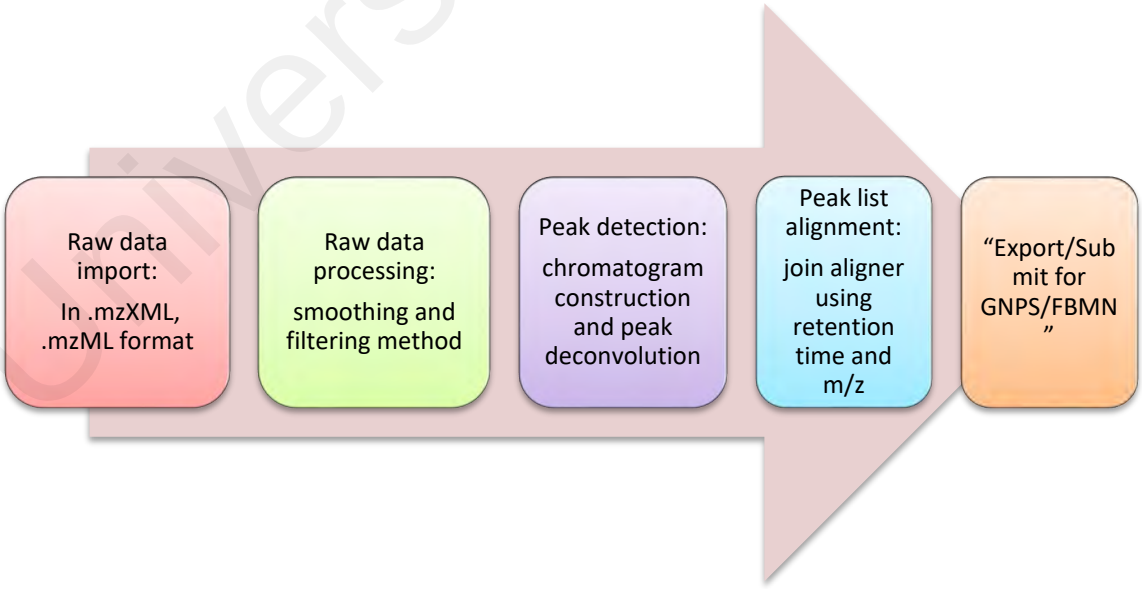

Figure 3.2: Overall workflows of MZmine 2 v53.

3.2.3 Molecular Networking parameters

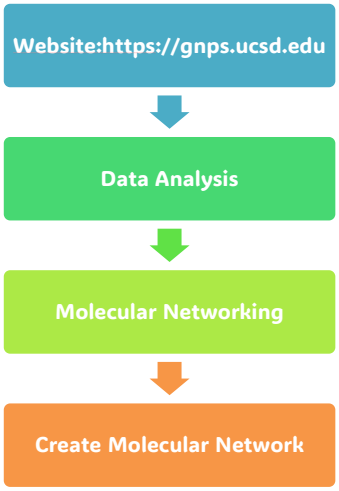

Figure 3.3: Molecular Networking online workflow.

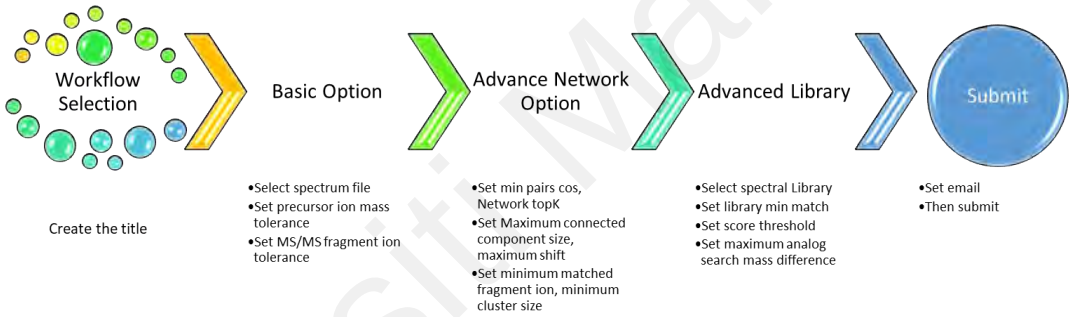

Figure 3.4: Parameter of workflow selection.

A molecular network (Figure 3.3) was created using the online workflow on the GNPS (Wang et al., 2016).The workflow parameter (Figure 3.4) started with creating the title of MN. When processing the data, a filter was applied to remove of any MS/MS fragment ions within +/- 17 Da of the precursor m/z. MS/MS spectra were window-filtered by selecting only the top six fragment ions in the +/- 50 Da window across the entire spectrum. After that, a tolerance of 0.02 Da was applied to the precursor ion mass, and a tolerance of 0.03 Da was applied to the MS/MS fragment ion. Then, a network was constructed with filtered edges, each of which needed to have a cosine score that was greater than 0.6 and more than six peaks that matched. Furthermore, the connections between two nodes were allowed to remain in the network if and only if each of the nodes

appeared in the top 10 most similar nodes of the other node's respective set. In the end, the maximum size of a molecular family was increased to 100, and the edges with the lowest score were removed from the molecular families until the size of the molecular family dropped below the threshold. For a match to be considered valid between the network and library spectra, it needed to have a score greater than 0.7 and at least 6 peaks that were identical. For MN analysis, a matching score threshold of 0.7 was utilised to confidently identify the compound. The spectral libraries (**a** Workflow-view all library) (Figure 3.5) of the GNPS were then searched using the network's spectra as the search criteria. Cytoscape software (ver 3.8.2) (**b** download direct cytoscape preview) (Figure 3.5) was used to perform statistical analysis and data visualisation on the molecular networking information.

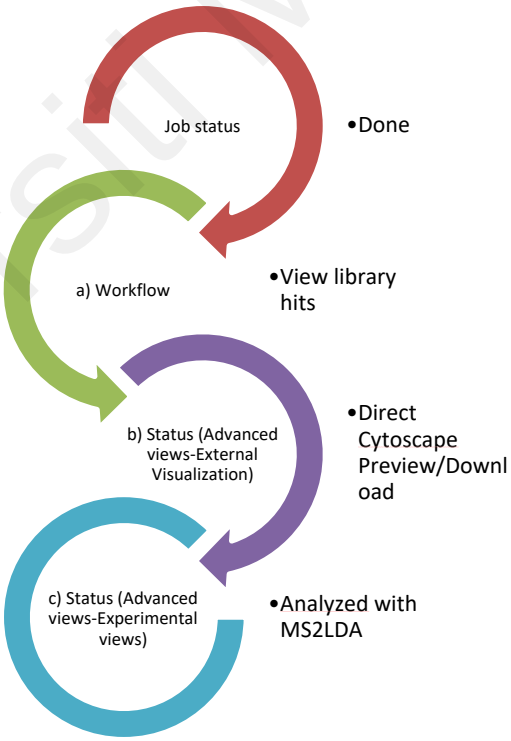

Figure 3.5: MN workflow status.

3.2.4 MS2LDA unsupervised substructure annotation

The fragmentation spectra were mined for co-occurring fragments and neutral losses using the latent Diriclet allocation algorithm on the MS2LDA web app. The MS/MS of MN analysis were re-analysed with MSLDA (**c** Status -Advanced views-Experimental views-analyzed with MS2LDA) (Figure 3.5), the dataset of MSLDA from GNPS were upload to MS2LDA (Figure 3.6). The following parameters were used for this task: isolation_window (0.5), min_ms2_int (500), n_its (1000), K (60), ms2_bin (0.005 Da), Zero MotiftDB. The result of the MS2LDA annotation is publicly available at the following link: https://ms2lda.org/basicviz/toggle_public/2353/. The inspection and the annotation of the Mass2Motifs were realized on the MS2LDA.org Web app.

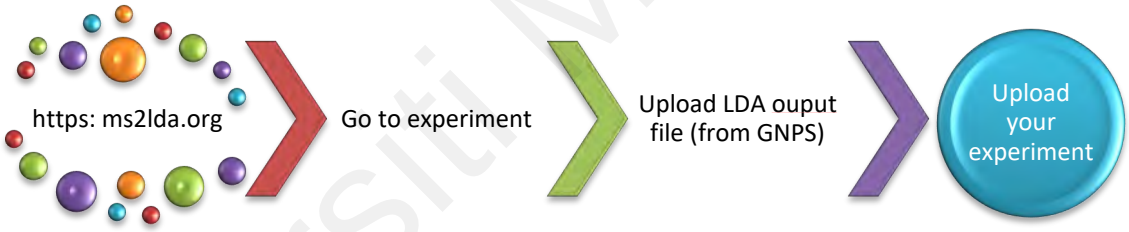

Figure 3.6: MS2LDA experimental workload.

3.2.5 Library search parameter

The converted raw (.mzXML) data of DCE and fractions F1-F10 were run under Library search, the precursor ion mass tolerance was set to 0.02 Da with a MS/MS fragment ion tolerance of 0.03 Da. The minimum match peak was set to 6 or 4 spectra, with threshold score were set on default value 0.7 (Figure 3.7).

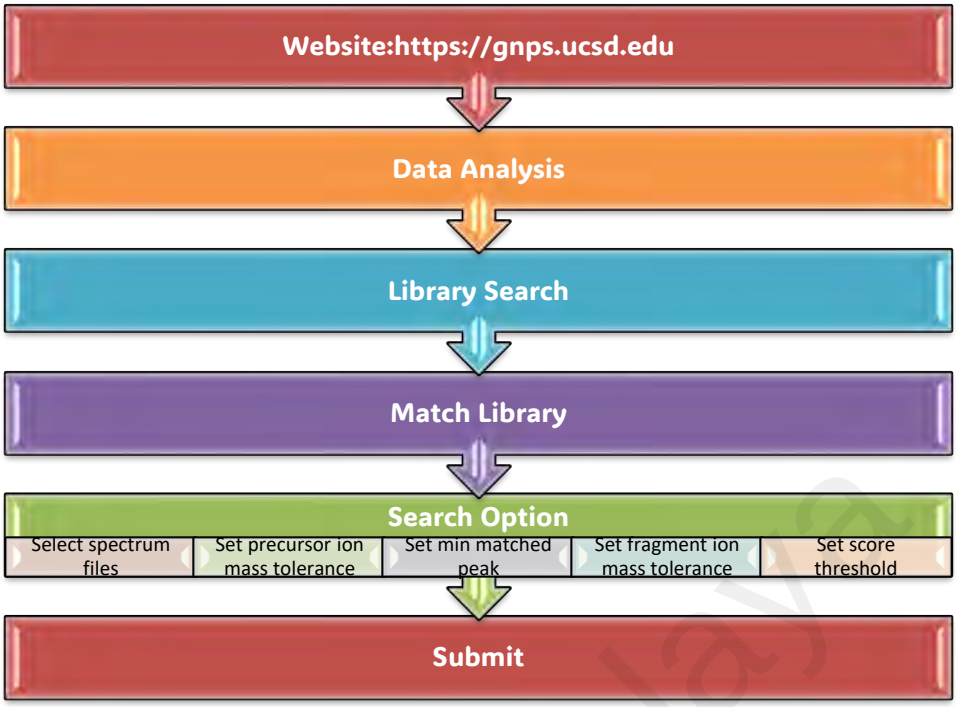

Figure 3.7: Library Search workflow.

3.3 Anticholinesterase activity

3.3.1 Chemicals and enzyme

Acetylcholinesterase (AChE) from Electrophorus electricus, butyrylcholinesterase (BChE) from equine serum, 5,5'-dithiobis (2-nitrobenzoic acid) (DTNB), acetylthiocholine iodide, donepezil and S-butyrylthiocholine chloride were purchased from Sigma-Aldrich Co. LLC. (St. Louis, MO, USA). Disodium hydrogen phosphate anhydrous was purchased from Merck (Darmstadt, Germany), while Sodium dihydrogen phosphate anhydrous was purchased from R&M Chemicals (Essex, UK). All other solvents and reagents employed were of analytical quality.

3.3.2 *In vitro* cholinesterase inhibitory activity

The sample (fractions and compounds) were dissolved in methanol at 1 mg/ml at the start. Before executing the experiment, the samples were filtered through a 0.22 µM sterile

filter (JETBIOFIL) and stored at 4 ºC. Ellman's microplate assay was used to assess the isolated compounds' cholinesterase inhibitory efficacy (Ellman et al., 1961). A 96 well microplate was filled with 140 µL of 0.1 M sodium phosphate buffer with pH 8, followed by 20 µL of the sample and 20 µL of 1U of AChE or BChE enzyme. Subsequently, 10 µL of 10 mM DTNB was then added, followed by 10 µL of 14 mM of acetylthiocholine iodide or S-butyrylthiocholine chloride. The absorbance of the coloured end-product was measured at 412 nm at designated intervals for 30 minutes after the initiation of enzymatic reaction using a Tecan Infinite 200 ProMicroplate Spectrometer (Switzerland). Donepezil was used as the standard. Each test sample was conducted in three times. The absorbance of the test sample was corrected by subtracting the absorbance of its respective blank. Five concentrations were used to estimate the 50% inhibitory concentration (IC_{50}) for the active compounds.

3.3.3 Kinetic study

Studies of enzyme kinetics were performed in the same way that enzyme inhibition assays are. The enzyme inhibition kinetics were studied in the absence and the presence of three concentrations of inhibitors (0, 10, 20, 30 µM) at varied concentrations of the substrates, S-butyrylthiocholine chloride (1.75 - 14 mM) using a Lineweaver-Burk plot and reciprocal plots of 1/V versus 1/[S]. The inhibition constant (*Ki*) was estimated from the secondary plot of the Lineweaver–Burk plot.

3.3.4 Molecular Docking

Autodock 3.0.5 and AutoDockTools (ADT) were used to undertake molecular docking studies on the indole alkaloids (Morris et al., 1998). To summarise, the two-dimensional structures of the indole alkaloids were constructed using Hyperchem 8 and energy minimization was carried out with a convergence criterion of 0.05 kcal/(molA). The three-dimensional crystal structures of BChE from *Homo sapiens* (PDB ID: 2WIJ)

(Carletti et al., 2009) that retrieved from the Protein Data Bank (PDB). ADT was used to eliminate all water molecules from the protein before adding hydrogen atoms non-polar hydrogens and lone pairs were then merged and each atom was assigned with Gasteiger partial charges. A g rid box with 60×60×60 points and 0.375 spacing was positioned at the centre (X= -16.187, Y= -36.783, Z= -22.704) of the active site gorge. One hundred separate dockings were performed for each experiment, with a population size of 150 and 2,500,000 energy assessments. The conformations from the docking experiments were analyzed and visualized using Acceryls Discovery Studio 3.5 (Accelrys Inc., San Diego, CA, USA) and PyMOL 2.5 (Schrödinger, Inc., New York, USA).

CHAPTER 4: RESULTS AND DISCUSSION

The bark from *O. maingayi* has been studied. The extraction was accomplished using the simple maceration method. The dried and crushed bark was first defatted with hexane. After that, the bark was soaked in dichloromethane to obtain dichloromethane crude extract (DCE). Then, the DCE was subjected to column chromatography (CC), and ten fractions were successfully extracted from the CC (F1-F10). The DCE and all fractions were subjected to molecular networking to detect the presence of several types of compound scaffolds.

The chromatographic isolation method yielded seventeen compounds; nine indoles alkaloid in which one is new; dihydrodeglycocadambine **(149)**. The known compounds are neonaucline **(5)**, naucledine **(6)**, harmane **(7),** naulafine **(33)**, cadambine **(35)**, *nor*harmane **(124)**, methyl 9*H*-*β*-carboline-4-carboxylate **(150)**, and 1,2,3,4-tetrahydronorharmane-1-one **(151)**. Besides, eight non-alkaloidal compounds were also isolated; cinnamamide **(152),** benzamide **(153),** scopoletine **(154)**, 4'hydroxyphenone **(155),** decarboxylportentol acetate **(156)**, scoparone **(157)**, 2'-Hydroxy-3'-methoxyacetophenone **(158)** and hexyl-*p*-coumarate **(159)**.

The DCE was screened toward anticholinesterase activity. The results showed that the DCE inhibited BChE moderately, with more than 54% of inhibition at 100 µg/mL Therefore, all fractions were subjected to screening towards BChE inhibitor activity. F7 and F9 inhibited BChE by more than 80% at 100 µg/mL. These active fractions yielded three active compounds: harmane **(7)**, naucledine **(6)** and dihydrodeglycocdambine (**149)**. All these compounds were then subjected to BChE inhibitory activity.

The following subsections will discuss briefly on all the findings which divided into three subsections: 4.1 Molecular Networking analysis, 4.2 Isolation and structural elucidation of compounds and 4.3 Anticholinesterase activity.

4.1 Molecular Networking (MN) Analysis

MN strategy begins by analyzing the LCMS/MS profile (Figure 4.1) of the DCE extracted from the bark of *O. maingayi* in positive ion mode. More than 1000 MS/MS spectra between 70 and 1000 m/z were generated.

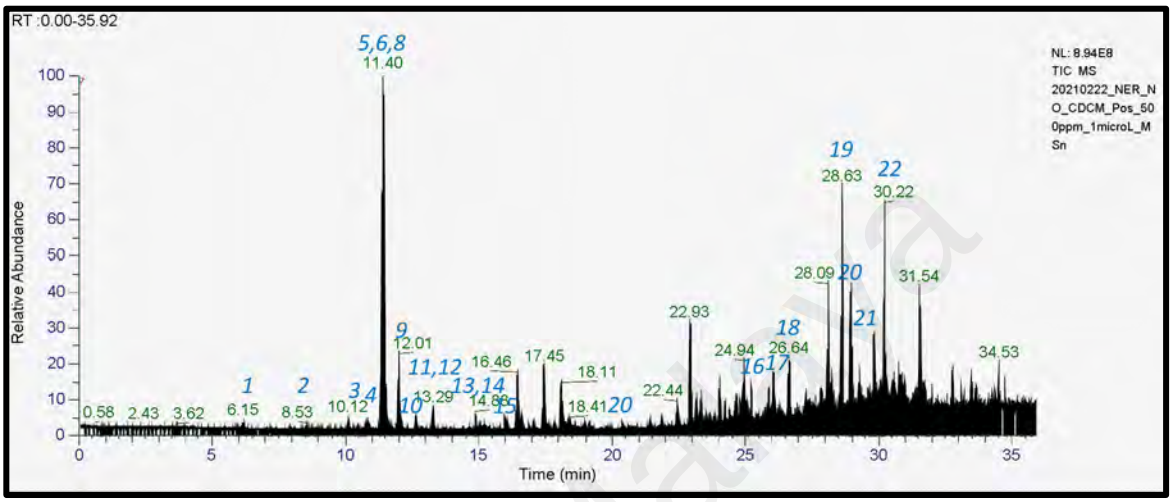

Figure 4.1: Chromatogram of DCE bark of *Ochreinauclea maingayi* in positive mode

The raw data of LCMS/MS for the DCE and ten fractions (F1-F10) (fractionation of crude using column chromatography) were converted to .mgf data file using FBMN. The complete FBMN MS/MS spectral data of DCE and fractions is employed to generate the molecule networks map for analysis. Prior to network formation, connections between nodes are computationally established within the GNPS platforms (https://gnps.ucsd.edu/ProteoSAFe/accessed on 16 August 2021) by transforming the MS/MS spectra into vectors and evaluating their similarities, which leads to the creation of massive network MN indicated as **(a)** (Figure 4.2). The colourful circles are called nodes, and the number on the nodes is the precursor ion mass. These nodes represent the molecular weight and key fragment data of each compound. The grey lines are called edges, when two or more nodes are connected by an edge, it indicates that their MS/MS fragmentation patterns are similar and can be mapped to the same cluster. Each cluster has several nodes (nodes ≥ 2) which depicted the fractions contained within those nodes. Different colour in the nodes represent different fractions.

Analysis of MN detected twenty-two compounds that matching with GNPS library database that have been list in Table 4.1 and 4.2, and identified the compound from previously study by analysed their fragmentation patterns. The massive network MN (Figure 4.2) visualized two main clusters (A and B), and forty-one non-prioritized clusters and self-loop nodes. Self-loop nodes occur due to the cosine score below than 0.65, which is it can't form the cluster. Cluster A contain indole alkaloids, mainly of the cadambine-type. Cluster B contain triterpenoids and fatty acids. From the non-prioritized nodes and the self-loops nodes; indole alkaloids, triterpenoids, coumarins and benzene derivatives were detected. All identified compounds, along with their respective retention times (RT), precursor ion m/z, parent name, molecular formula, ion type, prediction fractions and key fragments, are listed at Table 4.3.

Table 4.1: Dereplicated compounds from GNPS library

Compounds	Shared name	Library	Matching score	RT (second)
Geissoschizine methyl ether	264	GNPS lib	0.92	937.29
Cyclo(*L*-Phe-*D*-Pro)	1484	GNPS lib	0.85	714.65
Trans-Ferulic acid	897	NIST14	0.84	1776.18
1,2,3,4-Tetranorharmane-1-one	779	Massbank	0.82	912.81
Scopoletine	89	Massbank	0.79	645.03
***Nor*harmane**	896	Massbank	0.77	532.97
Oleanolic acid	1589	GNPS lib	0.76	1828.45
9(10)-EpOME	46	NIST14	0.76	1595.33
Di-*O*-methylfraxetin	247	GNPS lib	0.72	838.88
Glycyrrhetic acid	1326	GNPS lib	0.72	1594.59
Betulinic acid	17	GNPS lib	0.71	1723.70
Phytosphingosine	769	NIST14	0.71	1507.24

Table 4.2: Dereplicated compound from LS of GNPS

Compounds	Library class	RT (second)	Library	Matching score	Crude/ Fraction
Cadambine	Bronze	686.39	MIADB	0.84	Crude
Harmane	Bronze	610.76	GNPS lib	0.95	F10
Geissoschizine methyl ether	Gold	939.25	NIST14	0.91	F9, F10
1,2,3,4-Tetranorharmane-1-one	Bronze	914.55	Massbank	0.82	Crude, F6, F10,
Scopoletine	Bronze	646.77	Massbank	0.93	Crude, F3, F4
***Nor*harmane**	Bronze	534.29	Massbank	0.89	Crude F9, F10
Benzamide	Gold	370.95	GNPS lib	0.95	F6, F10
Scoparone	Bronze	764.63	Massbank	0.96	F2
9(10)-EpOME	Bronze	1605.13	GNPS lib	0.93	F4
Betulinic acid	Bronze	1723.70	GNPS lib	0.89	F4
Oleanolic acid	Bronze	1824.12	GNPS lib	0.87	F2,F4, F5
Di-*O*-methylfraxetin	Gold	840.04	GNPS lib	0.74	F3
Cyclo(*L*-Phe-*D*-Pro)	Bronze	716.29	GNPS lib	0.74	F6
Ursolic acid	Bronze	1745.19	GNPS lib	0.89	F3, F6
Phytosphingosine	Bronze	1509.85	NIST14	0.72	F10
Cinnamamide	Bronze	676.80	NIST14	0.71	F5

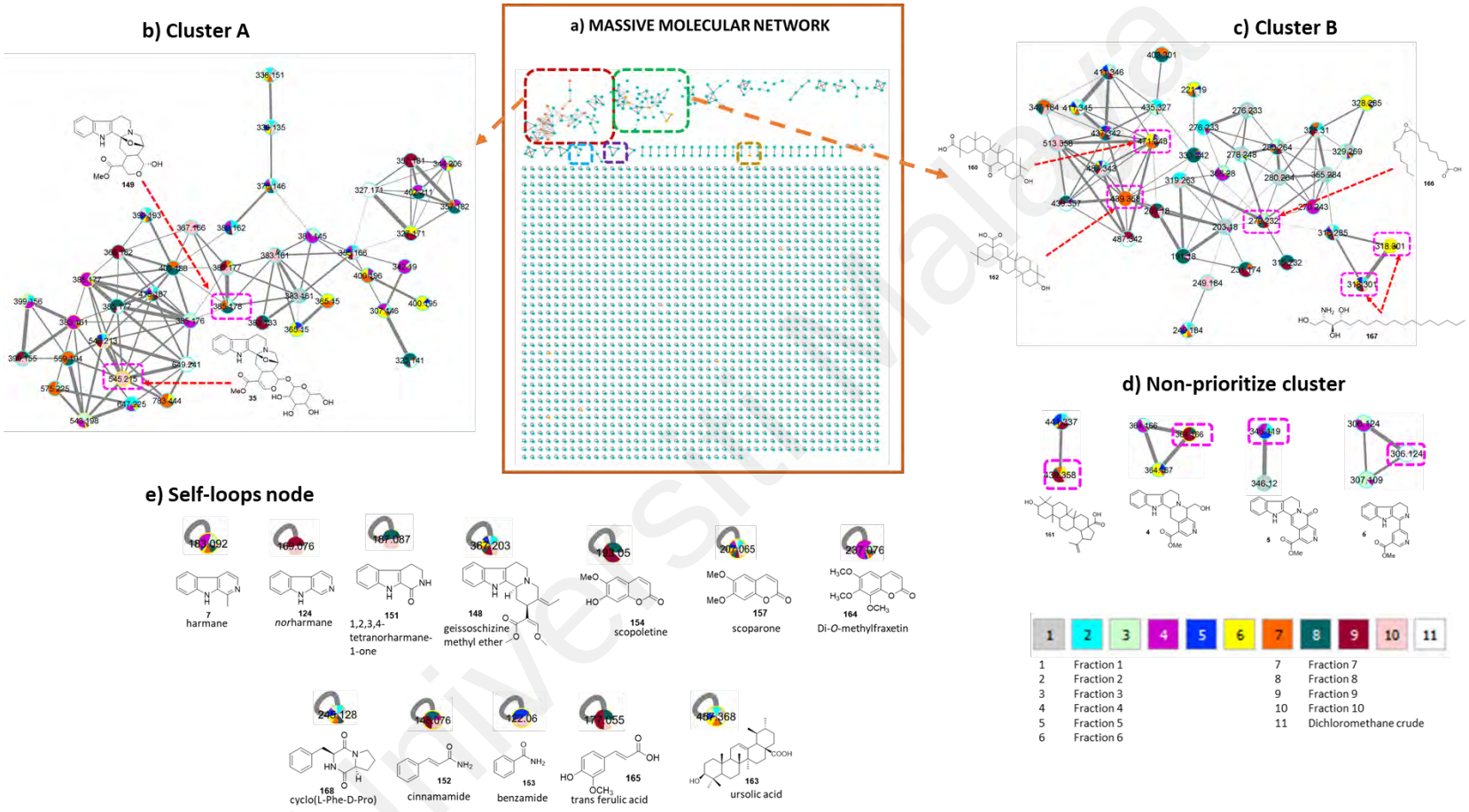

Figure 4.2: (a) Massive MN of the bark of *O. maingayi* (b) Cluster A (c) Cluster B (d) Non-prioritized clusters (e) Self-loop nodes.

Table 4.3: Chemical constituents identified in the dichloromethane crude extract (DCE) of the bark of *O. maingayi.*

Peak No	Compound	Precursor ion mass (m/z)	Node Parent	Molecular Formula	RT means (min)	Ion type	Predicted fractions	Key fragment (m/z)
	IA (Cluster A, non-prioritized cluster and selfloops)							
2	*Nor*harmane[a] **(124)**	169.076	896	$C_{11}H_9N_2$	8.88	$[M+H]^+$	F10,F9,F8,F5	142,115
3	Harmane[ab]**7**	183.091	804	$C_{12}H_{11}N_2$	10.41	$[M+H]^+$	F6,**F7**,F8,F9,F10,F1, F2,F3,F4	142,115
6	Dihydrodeglycocadambine[c]**1 49**	385.177	803	$C_{21}H_{25}N_2O_5$	11.23	$[M+H]^+$	F8,F9,**F10**	367,227,183,170,144
7	Cadambine[a] **35**	545.215	492	$C_{27}H_{23}N_2O_{10}$	11.43	$[M+H]^+$	F9,**F10**	383,365,227,170,144,139
8	Naucledine[b] **6**	306.124	956	$C_{18}H_{16}N_3O_2$	11.75	$[M+H]^+$	F10,**F9**,F8,F6	159,144
11	Cadamine[b] **4**	364.167	900	$C_{21}H_{22}N_3O$	13.2	$[M+H]^+$	F6,F7,F5,F9	346,317,144
13	Neonaucline[b] **5**	346.119	533	$C_{20}H_{16}N_3O_2$	14.39	$[M+H]^+$	F4,**F5**,F2,F7,F6	286,144
14	1,2,3,4-Tetranorharmane-1-one [a] **151**	187.087	779	$C_{11}H_{11}N_2O$	15.21	$[M+H]^+$	F2,F8,F9,F10,F6,F4, F3	158,142,130,115
15	Geissoschizine methyl ether[a] **148**	367.203	264	$C_{22}H2_6N_2O_3$	15.62	$[M+H]^+$	F8,F9,F10	170,144,130,108,75
	Triterpene (Cluster B, non-prioritized cluster and Selfloops)							
17	Glycyrrhetic acid[a] **160**	471.348	1326	$C_{30}H_{47}O_4$	26.57	$[M+H]^+$	F6,F7,F5,F4,F1	189,175,133,119,107,95
19	Betulinic acid[a] **161**	439.358	1589	$C_{30}H_{46}O_2$	28.72	$[M+H]^+$-H_2O	F9,F10, F7,F8,F6	393,259,243,213,179,137,95

Peak numbers correspond to the numbering of peaks that appear in the total ion chromatogram (TICs). a) Structural hit obtained from GNPS spectral library matching. b) Compounds previously reported in the leaves of *O. maingayi* [10].c) Predicted compoound

Table 4.1, continued.

Peak No	Compound Identifications	Precursor ion mass (m/z)	Node	Molecular Formula	RT means (min)	Ion type	Predicted Fractions	Key fragment (m/z)
	Triterpene (Cluster B, non-prioritized cluster and Selfloops)							
22	Oleanolic acid[a] **162**	439.358	17	$C_{30}H_{46}O_2$	30.47	$[M+H]^+$-H_2O	F7,F8,F9,F10	215,203,189,147,133,119,107,95,81,69
20	Ursolic acid[a] **163**	457.368	235	$C_{30}H_{48}O_3$	29.19	$[M+H]^+$	F3,F2, F6,F5	411, 203,191,163
	Coumarine (Selfloops)							
4	Scopoletine[a] **154**	193.050	89	$C_{10}H_9O_4$	10.75	$[M+H]^+$	F4,**F3**	150,133,122,94,77,66
10	Scoparone[a]**157**	207.065	39	$C_{11}H_{11}O_4$	12.73	$[M+H]^+$	F1,**F2**,F3,F4,F5,F6,F7,F8,F9	163,151,146,135,118,107,91
12	Di-*O*-methylfraxetin[a] **164**	237.076	247	$C_{10}H_9O_5$	13.98	$[M+H]^+$	F4,F3,F5,F7,F8	207,179,147,133,123,91
	Cinnamic acid (Cluster B)							
21	Trans ferulic acid[a] **165**	177.055	897	$C_{10}H_{11}O_4$	29.60	$[M+H]^+$	F8,F9,F10	117,89,78
	Fatty acid (Cluster B)							
28	9(10)-EpOME[a] **166**	279.232	46	$C_{18}H_{33}O_3$	26.59	$[M+H]^+$-H_2O	F8,F9,F10,F7,F1,F4,F5,F6	135,123,109,95,81,67

Peak numbers correspond to the numbering of peaks that appear in the total ion chromatogram (TICs). a) Structural hit obtained from GNPS spectral library matching. b) Compounds previously reported in the leaves of *O. maingayi* [10].c) Predicted compound

Table 4.1, continued.

Peak No	Compound Identifications	Precursor ion mass (m/z)	Node	Molecular Formula	RT means (min)	Ion type	Predicted Fractions	Key fragment (m/z)
	Fatty acid (Cluster B)							
16	Phytosphingosine[a] **167**	318.301	769	$C_{18}H_{40}NO_3$	25.11	$[M+H]^+$	F6,F7,F2,F4,F5	300,282,270,252,95,83
	Amide (Selfloops)							
9	cyclo(L-Phe-D-Pro) [a] **168**	245.128	1484	$C_{14}H_{17}N_2O_2$	11.90	$[M+H]^+$	F3, F2,F1,F6,F5,F7,F8,F9,F4	154,120,98,70
1	Benzamide[ab]**153**	122.060	663	C_7H_8NO	6.15	$[M+H]^+$	F5,F1,F8,F10	105,95,77
5	Cinnamamide[a,b]**152**	148.076	1721	$C_9H_{10}NO$	11.28	$[M+H]^+$	F4,F8,F10,F10	131,103

Peak numbers correspond to the numbering of peaks that appear in the total ion chromatogram (TICs). a) Structural hit obtained from GNPS spectral library matching. b) Compounds previously reported in the leaves of *O. maingayi* [10].c) Predicted compound

4.1.1 Cluster A

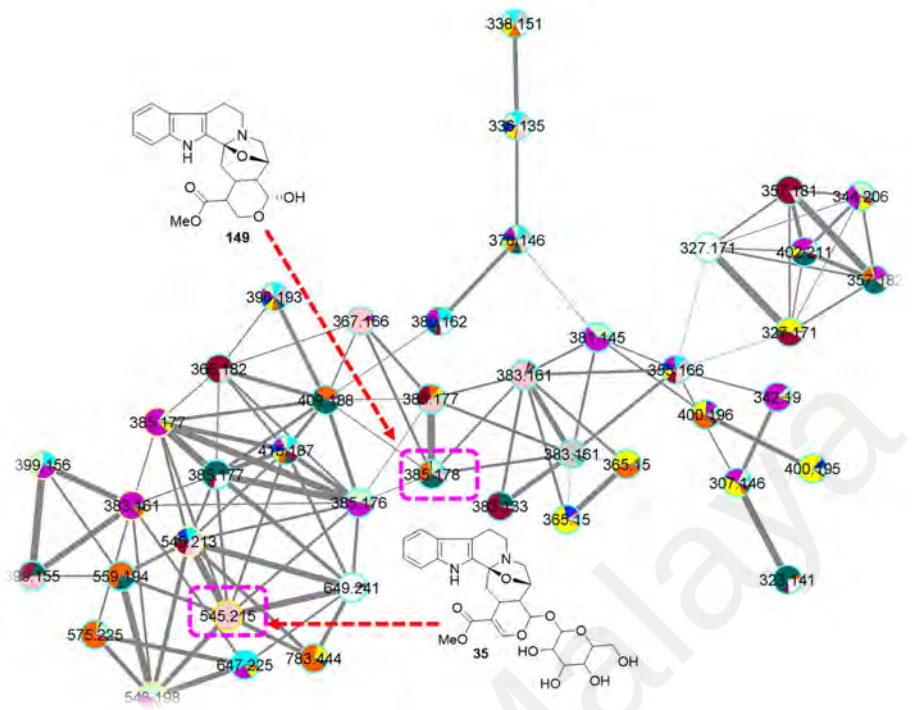

Figure 4.3: Cluster A.

Cluster A (Figure 4.3) is a main cluster in this MN analysis, with forty-three nodes. cadambine **(35)** appeared to this cluster, this suggest that cadambine-type alkaloids are the most abundant in this plant since they have their own cluster which is Cluster A. To further this analysis, we utilized the web based MS2LDA (van der Hooft et al., 2016; Wandy et al., 2017) to process our MS/MS data and explore the results through interactive visualizations. The fragmentation spectrum is decomposed by MS2LDA into blocks of co-occurring fragments and losses. These blocks are referred to as "Mass2Motifs." This process indicated that Cluster A exhibited a Mass2motif (motif_370) (Appendix 1) with significant peak at m/z 333.124 ,227.120 and 170.075 shared by 16 parent masses that possess indole alkaloids (IA) scaffold. Out of these, two parent masses, Parent: 492 and Parent: 803, show characteristic fragmentation patterns belonging to IA scaffold of cadambine-type (Gai et al., 2013). The details of Parent: 492 and Parent: 803 MS/MS spectra, the protonated molecular ions, and the fragmentation pathway are shown in Scheme 4.1and Scheme 4.2, respectively. The analysis of Parent: 492 fragmentation

patterns led to the identification of cadambine **(35)** (Scheme 4.1), the analysis of Parent: 803 led to the discovery of the new compound dihydrodeglycocadambine **(149)**. Compound **(149)** is formed from the loss of hexose sugar moiety and addition of two hydrogen at C-16 and C-17, therefore the double bond that is present in cadambine **(35)** is noted absent in dihydrodeglycocadambine **(149)** (Scheme 4.2). This MN strategy, help to accelerate workflow to isolate and elucidate all the compounds including the finding of new indole alkaloid, dihydrodeglycocadambine (**149)** (Osman et al., 2023). Further discussion on the new compound is in subchapter 4.2.1 (Page 81-88).

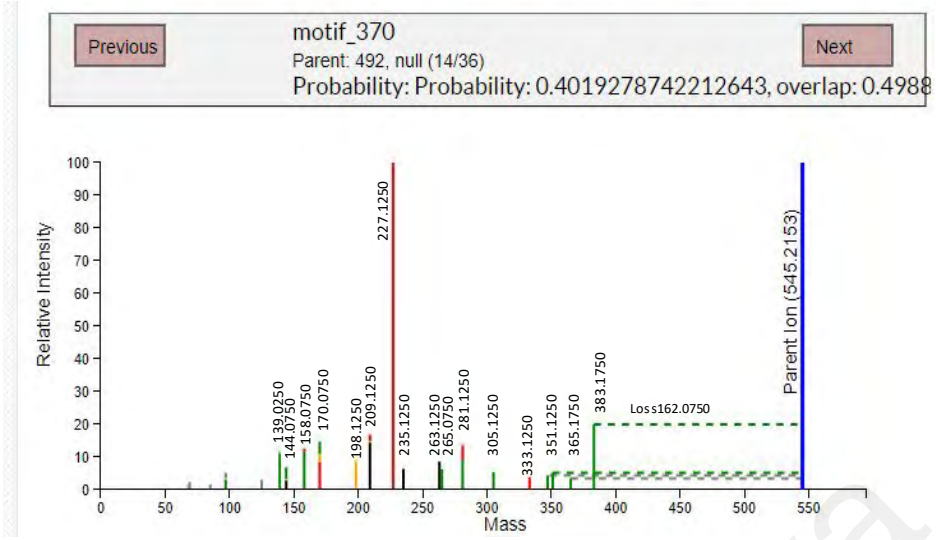

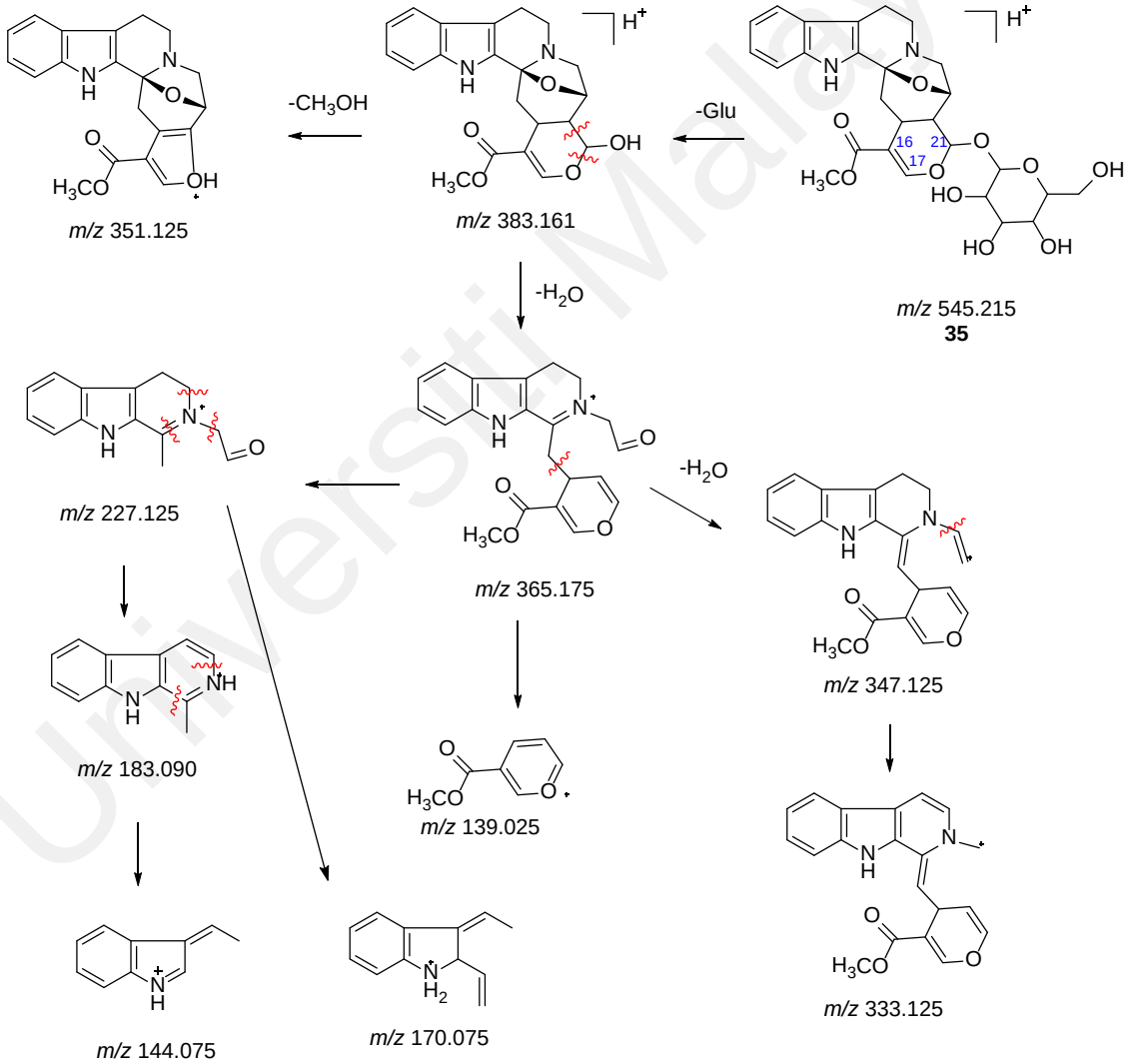

Scheme 4.1: Mass spectra and fragmentation pathway of mass motif for cadambine (35) (Parent :492) (Gai et al., 2013).

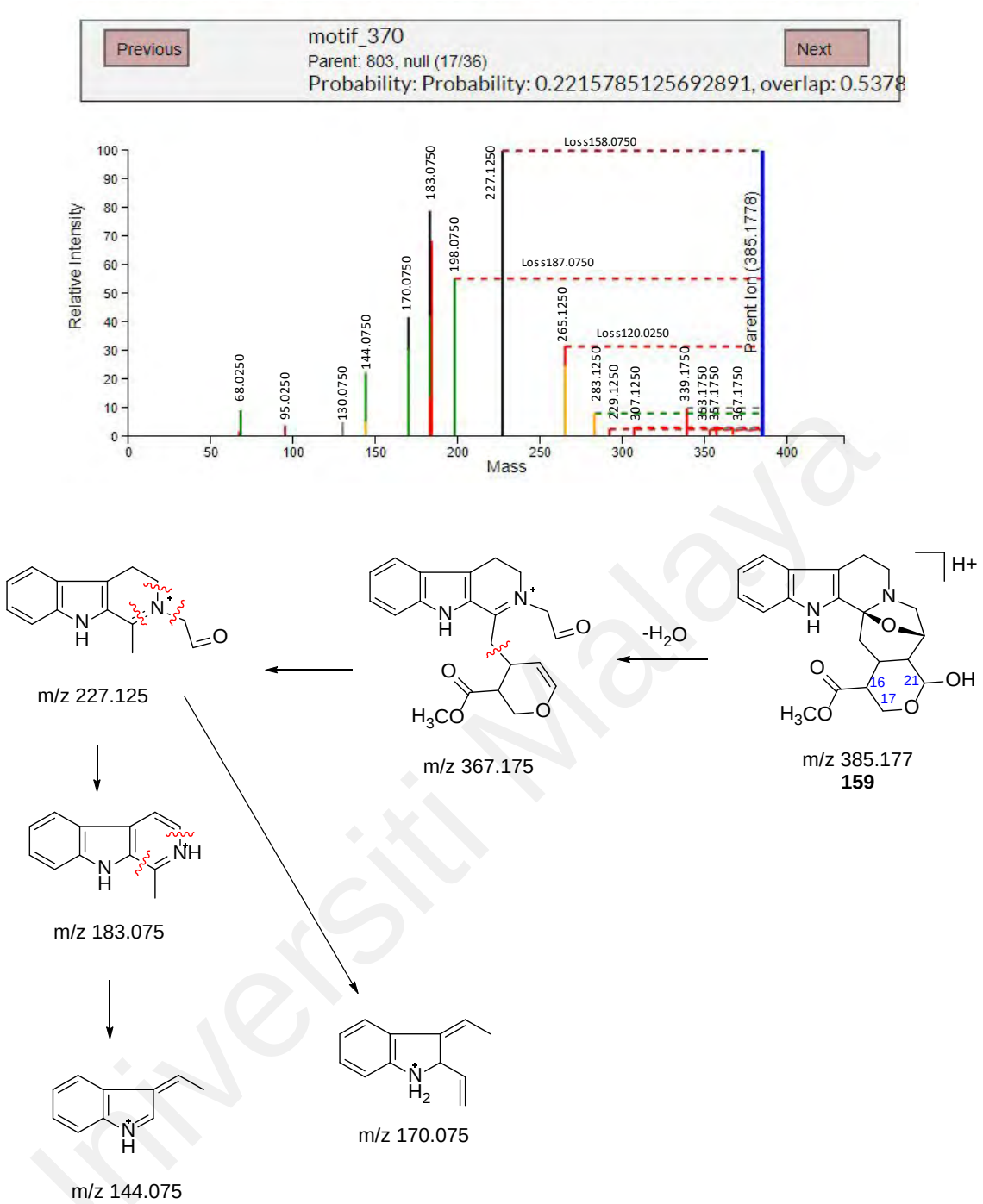

Scheme 4.2: Mass spectra and fragmentation pathway of mass motif for dihydrodeglycocadambine (149) (Parent: 803).

4.1.2 Cluster B

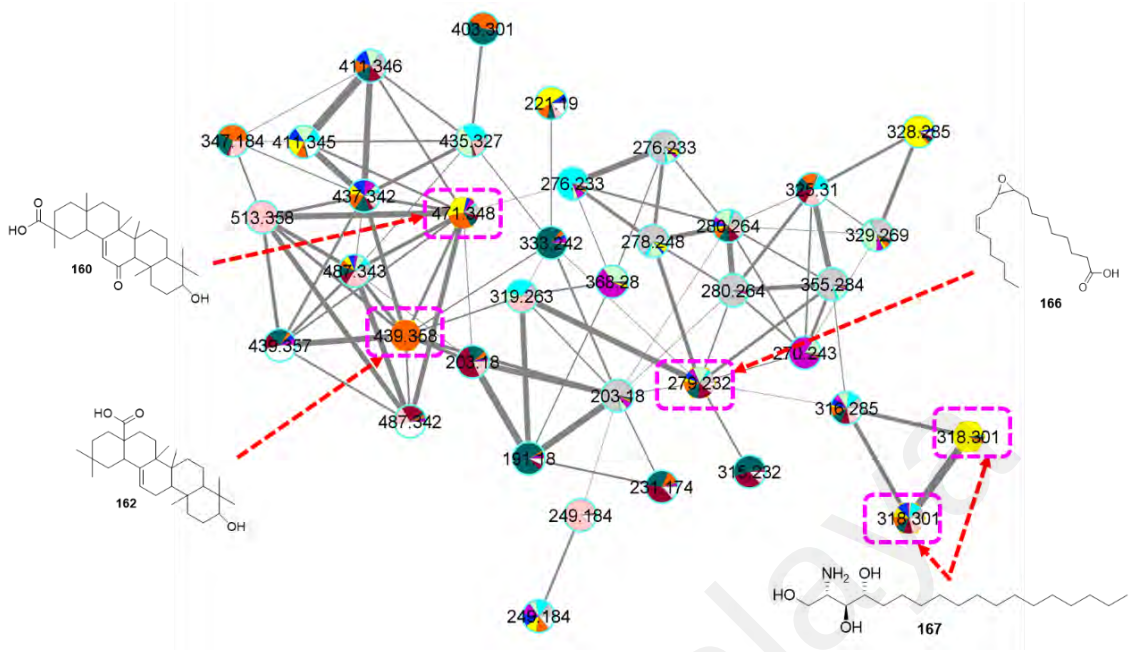

Figure 4.4: Cluster B.

Cluster **B** (Figure 4.1.3) is the second main cluster with thirty-seven nodes. Four nodes were hit by GNPS library matching (Table 4.1 and Table 4.2). Two nodes are from triterpenoid subclass, glycrrhetic acid **(160)** with precursor ion *m/z* 471.348 $[M+H]^+$ and oleanolic acid **(162)** with precursor ion *m/z* 457.358 $[M+H]^+$-H_2O. Both compounds are oleanane-type triterpenoid, where they possess similar fragmentation pattern at m/z 189, 133,119,107 and 95 (Lourenço et al., 2021). Another two nodes that matched by GNPS library matched were fatty acid subclass, phytosphingosine **(167)** and 9(10)-EpOMe (leukotoxin A) **(166)** with precursor in mass at *m/z* 318.301 $[M+H]^+$ and *m/z* 279.232 $[M+H]^+$-H_2O, respectively.

4.1.3 Non-prioritize cluster

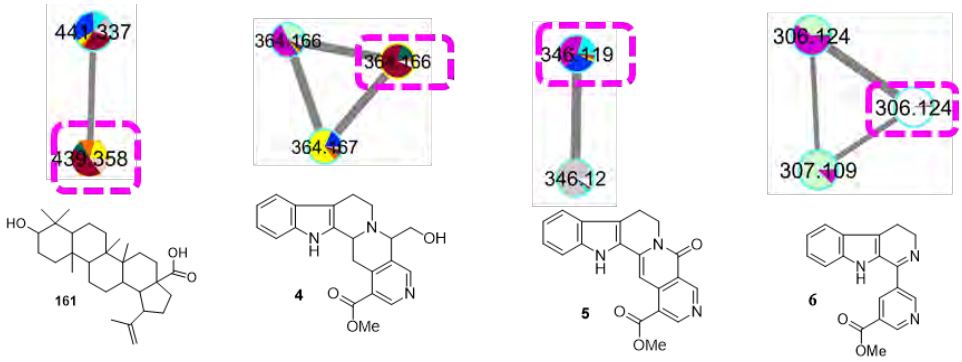

Figure 4.5: Non-prioritize cluster.

Another triterpenoid compound, betulinic acid **(161)**, with precursor ion mass *m/z* 439.358 $[M+H]^+$-H_20, was annotated by GNPS library matching (Table 4.1) as non-prioritize cluster (Figure 4.5). Betulinic acid **(161)** is a well-known lupane-type triterpenoid.

Apart from those compounds identified by matching with GNPS library and Library Search data, other compounds can be predicted in massive network MN by analyzing their fragmentation patterns. From the non-prioritize cluster (Figure 4.5), three compounds were predicted; cadamine **(4)** (*m/z* 364.167 $[M+H]^+$), neonaucline **(5)** (*m/z* 346.119 $[M+H]^+$), and naucledine **(6)** (*m/z* 306.124 $[M+H]^+$) (Mukhtar et al., 2012). These three compounds could not be identified either due to the absence of the data in the GNPS library database (Naphen, 2019). However, the proposed fragmentation pathway represents node 900 (Scheme 4.3), 533 (Scheme 4.4) and 956 (Scheme 4.5) strengthening the existence of cadamine **(4)**, neonaucline **(5)** and naucledine **(6)** in the examined *O. maingayi* DCE extract.

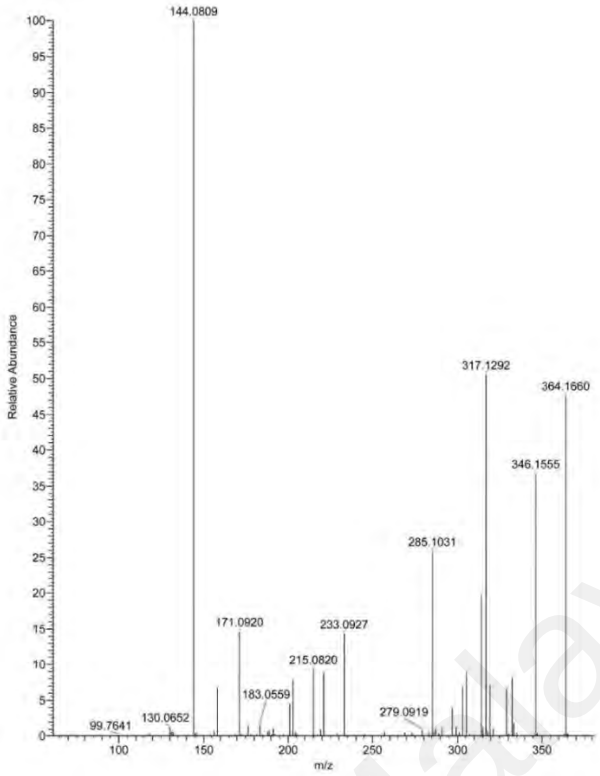

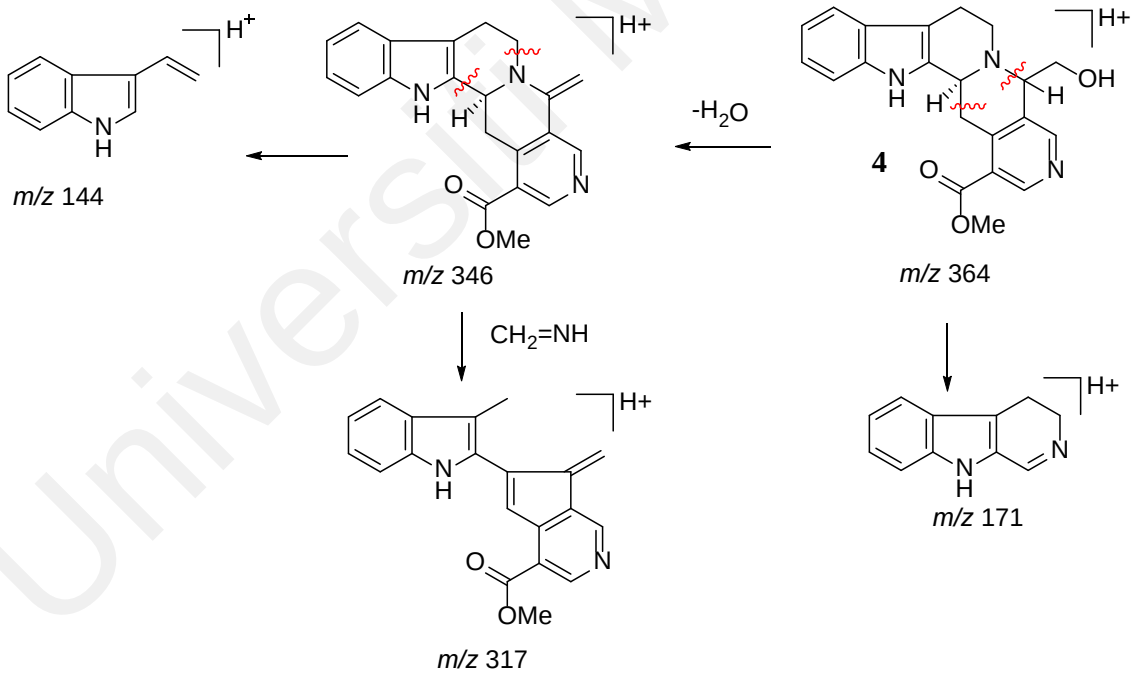

Scheme 4.3: Mass spectra and fragmentation pathway of cadamine (4) (Parent: 900).

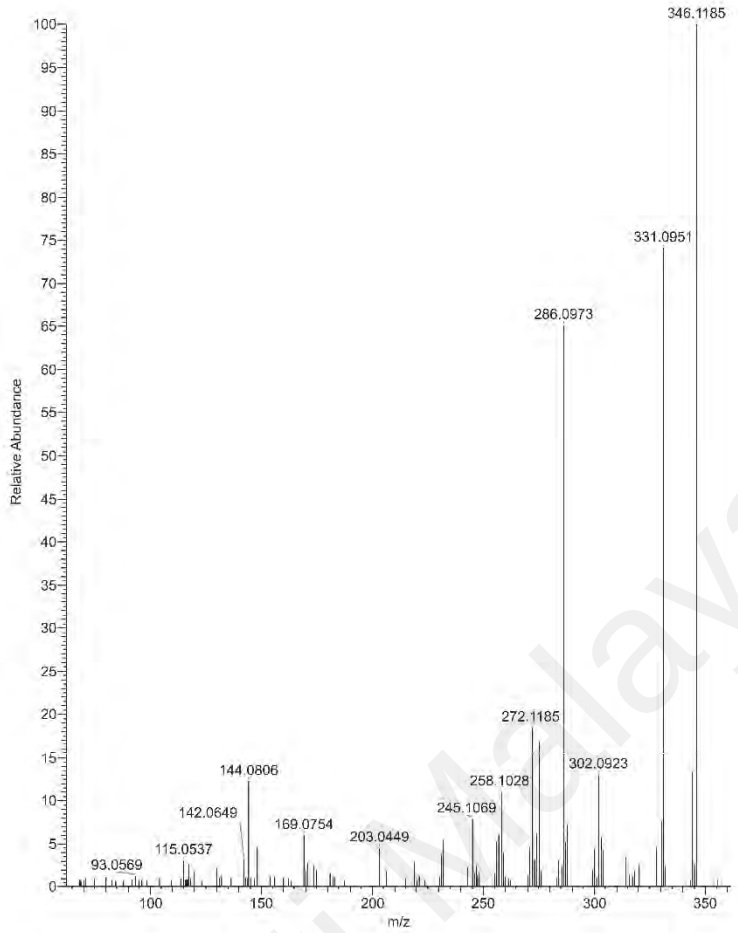

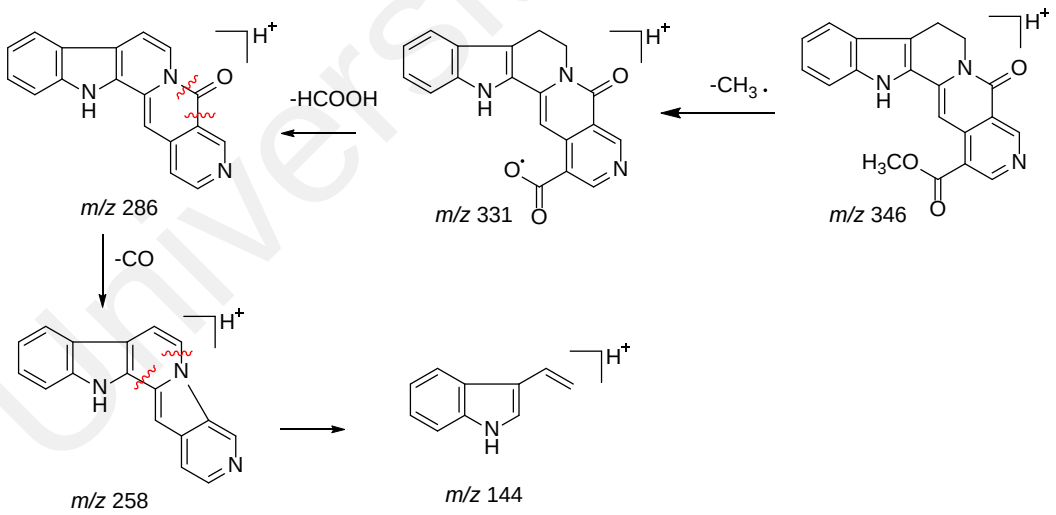

Scheme 4.4: Mass spectra and fragmentation pathway of neonaucline (5) (Parent: 533).

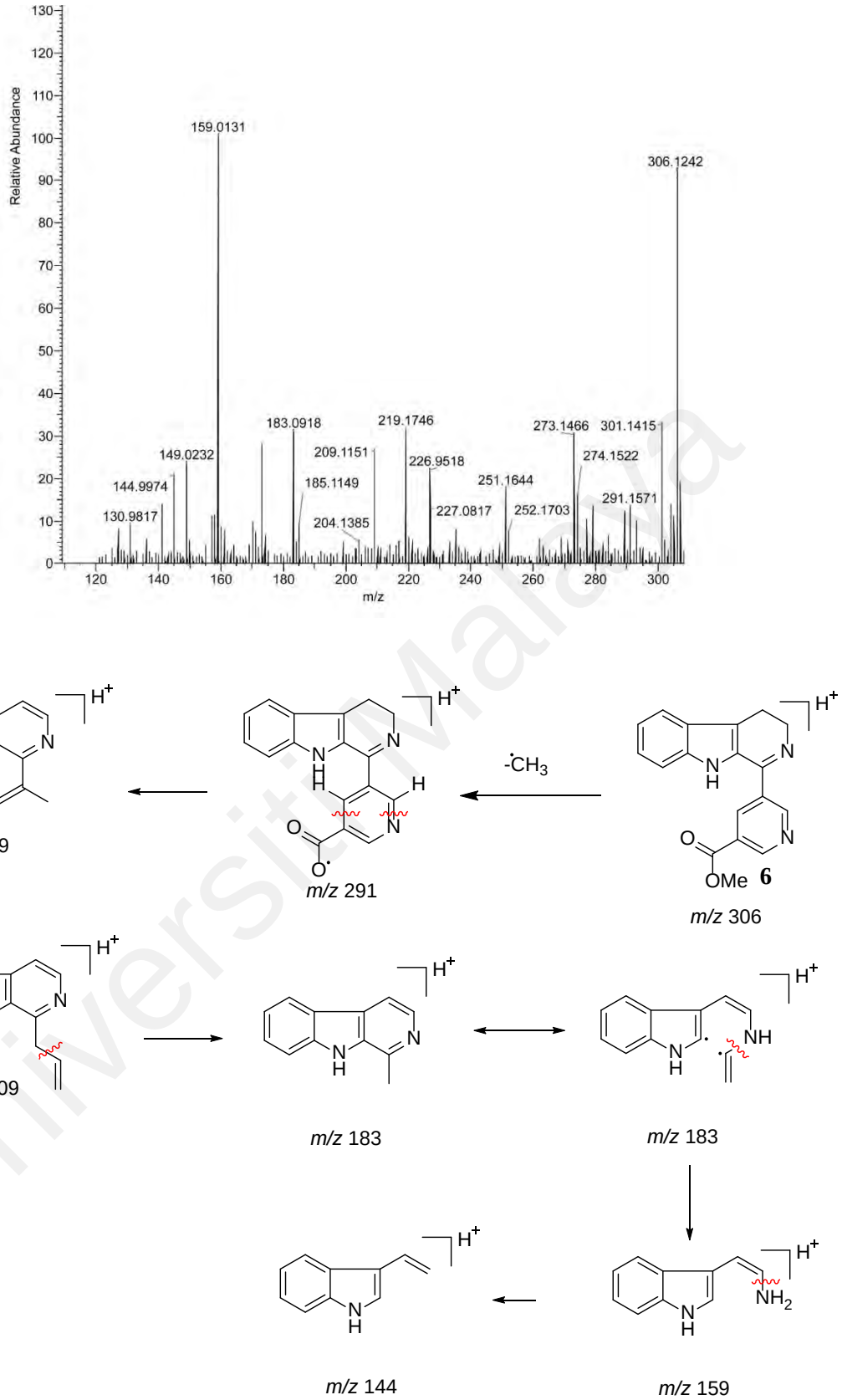

Scheme 4.5: Mass spectra and fragmentation pathway of naucledine (6) (Parent: 956).

4.1.4 Self-loop nodes

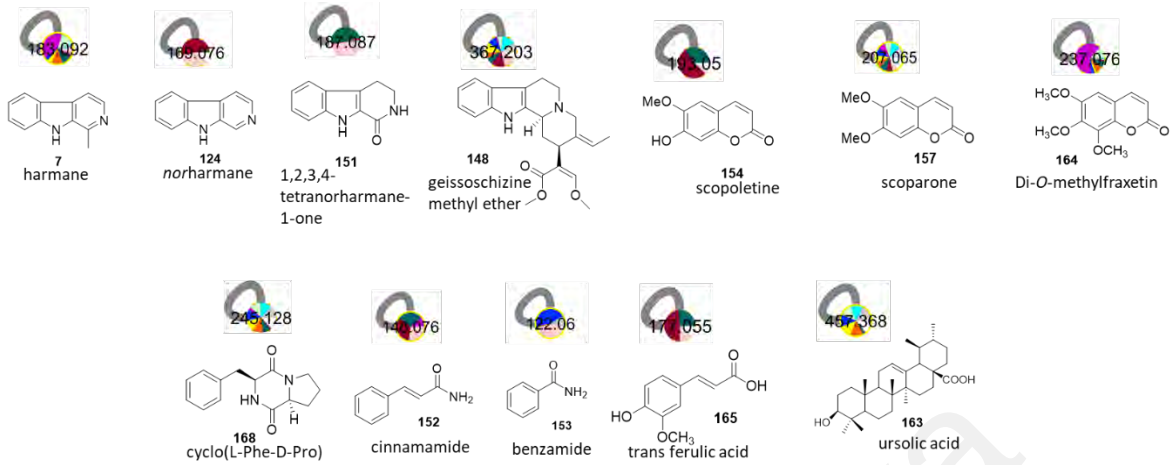

Figure 4.6: Self-loop nodes.

Twelve of self-loop nodes (Figure 4.6) revealed matching with GNPS library and Library search; four indole alkaloids; harmane **(7)** (*m/z* 183.091 $[M+H]^+$) , *nor*harmane **(124)** (*m/z* 169.076 $[M+H]^+$), 1,2,3,4-tetranorharmane-1-one (m/z 187.087 $[M+H]^+$) **(151)** and geissoschizine methyl ether **(148)** (*m/z* 367.203 $[M+H]^+$), three coumarins scaffold; scoparone **(157)** (*m/z* 183.091 $[M+H]^+$), scopoletine **(154)** (*m/z* 193.050 $[M+H]^+$) and Di-*O*-methylfraxetin **(164)** (*m/z* 237.076 $[M+H]^+$), one triterpenoid; ursolic acid **(163)** (m/z 457.368 $[M+H]^+$) and benzene derivative; trans ferulic acid **(165)** (*m/z* 177.055 $[M+H]^+$**)**, benzamide **(153)** (*m/z* 122.060 $[M+H]^+$), cinnamamide **(152)** (*m/z* 148.076 $[M+H]^+$) and cyclo(L-Phe-D-Pro) **(168)** (*m/z* 245.128 $[M+H]^+$).

4.2 Isolation and structural elucidation of compounds

The DCE of *O. maingayi* was fractionated to ten fractions (F1-F10). Seventeen compounds (Table 4.4) were successfully isolated, nine from them is indole alkaloids appear as major chemical constituents, followed by two coumarins, two amides, one polyketide and three phenolics. The structural elucidation as determined by various spectroscopic methods; 1D and 2D (^{1}H NMR, ^{13}C NMR, DEPT, COSY, HMBC HMQC), IR, MS, UV and by comparison with the literature data. Table 4.4 is summarises all the isolated compounds, their classification and page number.

Table 4.4: Chemical constituents of the bark extract of *O.maingayi.*

Fraction	Compound	Compounds name	Type	Page
F10	Compound A	Dihydrodeglycocadambine **(149)**	Indole alkaloid	81
F10	Compound B	Cadambine **(35)**	Indole alkaloid	89
F9	Compound C	Naucledine **(6)**	Indole alkaloid	94
F8	Compound D	Methyl 9*H*-*β*-carboline- 4-carboxylate **(150)**	Indole alkaloid	97
F7	Compound E	*Nor*harmane **(124)**	Indole alkaloid	101
F7	Compound F	Harmane **(7)**	Indole alkaloid	104
F6	Compound G	Naulafine **(33)**	Indole alkaloid	107
F5	Compound H	Neonaucline **(5)**	Indole alkaloid	111
F5	Compound I	1,2,3,4-Tetrahydronorharmane-1-one **(151)**	Indole alkaloid	115
F5	Compound J	Cinnamamide **(152)**	Amide	118
F4	Compound K	Benzamide **(153)**	Amide	121
F3	Compound L	Scopoletine **(154)**	Coumarin	124
F3	Compound M	4'-Hydroxyacetophenone **(155)**	Phenolic	127
F2	Compound N	Decarboxyportentol acetate **(156)**	Polyketide	130
F2	Compound O	Scoparone **(157)**	Coumarin	133
F2	Compound P	2'-Hydroxy-3'-methoxyacetophenone **(158)**	Phenolic	136
F1	Compound Q	Hexyl *p*-coumarate **(159)**	Phenolic	139

4.2.1 Compound A: Dihydrodeglycocadambine (149)

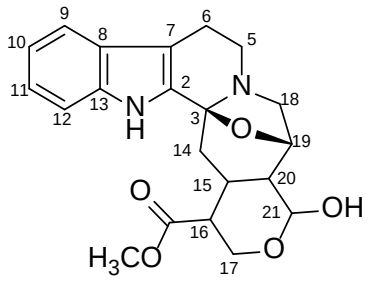

Compound **A** was obtained as an optically active, light yellow, and amorphous solid $[\alpha]_D^{25}$= +57.3 (*c* 0.0004, MeOH). It has the molecular formula $C_{21}H_{23}N_2O_5$ as deduced from the LC-ESI analysis (Figure 4.9) $[M+H]^+$, and *m/z* 385.1754 (calc. for $C_{21}H_{25}N_2O_5$, 385.1764). The UV spectrum (Appendix 2) reveals a maximum absorption at 222 and 274 nm, which reveals an indole chromophore (Albinsson & Norden, 1992), while the IR (Appendix 19) gives a broad band at 3339 cm^{-1} due to O-H stretching and a sharp strong band at 1731 cm^{-1} due to a C=O group (Pavia et al., 2009).

An analysis of the ^{1}H NMR (Figure 4.10) and HSQC (Figure 4.12) indicated four aromatics signal characteristic of unsubstituted indole moiety appearing at δ_H 7.74, (*d*, *J* = 7.6), H-9; δ_H 7.28, (*t*, *J* = 7.6), H-10; δ_H 7.34, (*t*, *J* = 7.6), H-11; and δ_H 7.67, (*d*, *J* = 7.6), H-12. The ^{13}C NMR (Figure 4.11) indicate a total of twenty one carbons in the structure which belong to five quaternary carbons (δ_c 135.1,C-2; 92.3,C-3; 111.1 C-7; 127.2, C-8; and 138.4, C-13), nine methines (δ_c 119.9,C9; 119.7,C10; 122.7,C11; 111.4,C12; 29.8,C15; 48.9,C16; 74.8,C19; and 50.3,C20), five methylenes (δ_c 53.2,C-5; 22.8,C-6; 47.9,C-14; 67.8,C-17; and 57.3,C-18), one hemiacetal carbon (δ_c 97.1,C21), one methoxy group (δ_c 52.0,C-23), and one carbonyl groups (δ_c 173.0,C-22).

Further analysis of the ^{1}H and^{13}C NMR spectroscopic data (Figure 4.10, Figure 4.11) indicated that **A** was structurally related to compound **B**, except for the following two differences: firstly, the absence of glucosyl moiety at C-21, which suggested that **A** was the aglycone to compound **B**, and secondly the double bond at C16-C17. The location of the substituents and the ring arrangement were further confirmed by cross

peaks in the HMBC spectra (Figure 4.7, Figure 4.14). The correlation of H-16/C-22 (δ_c 173.0), OMe-/C-22 (δ_c 173.0), and H-16/C-20 (δ_c 50.3) proves that the ester group is situated at δ_c 48.9, C-16. The cross peaks between H-17/C-21 (δ_c 97.1) and H-20/C-21 indicate the location of a hydroxyl group at C-21. Finally, the linkages between the rings C, D, E were assigned with the aid of the HMBC spectrum. The cross peak between H- 18/C-5 and H-14/C-3 further confirms that the indole rings (A-C) and D are fused via a H-18/C-20 and H-16/C-20 suggests that ring D is connected through a tetrahydropyran ring E through C-20.

The relative stereochemistry of **A** was confirmed from the NOESY spectrum (Figure 4.15) and by comparison of its correlations with those of a similar skeleton (Yuan et al., 2020). The stereochemistry at C-20 could be ascertained by the NOESY relationship between H19 and H-20. The presence of a chiral carbon at C-19 as indicated by the O-bridged complex between C-3 and C-19 exists as a β-configuration. This β-configuration leads to the assignment of the proton at C-19 as an α-configuration. The NOESY spectrum of H-19 correlates with H-20 as an α-configuration. In addition, H-20 correlates with H-21 in the COSY spectrum (Figure 4.13); however, there is no correlation between H-20 and H-21 in the NOESY spectrum. Thus, it can be deduced that H-21 has a different configuration than H-20 and is assigned as a *β*-configuration. There are two geminal protons for C-17 (H17α and H17β). H-17β shows correlation with H-21β. It also proves that H16 exists as an α -configuration due to the direct correlation of H17α and H16α. There is a direct correlation between H-15 and H-16 and between H-15 and H-20; therefore, we can presume that H-15 also exists as α-oriented.

The ^{1}H NMR and ^{13}C NMR spectral assignments performed by extensive 2D-NMR experiments (COSY, HSQC and HMBC) are summarized in Figure 4.7 and Table 4.3. From thorough analysis of 1D and 2D NMR proved that **A** is a new indole alkaloid namely dihydrodeglycocadambine **(149)** a derivative of **B** (Osman et al., 2023).

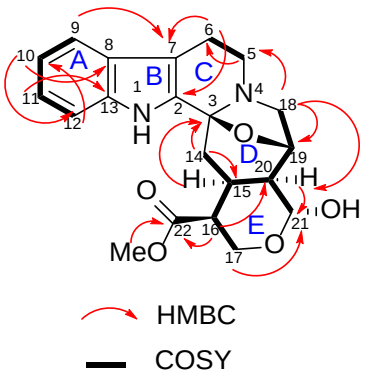

Figure 4.7: Selected key correlation of dihydrodeglycocadambine (149).

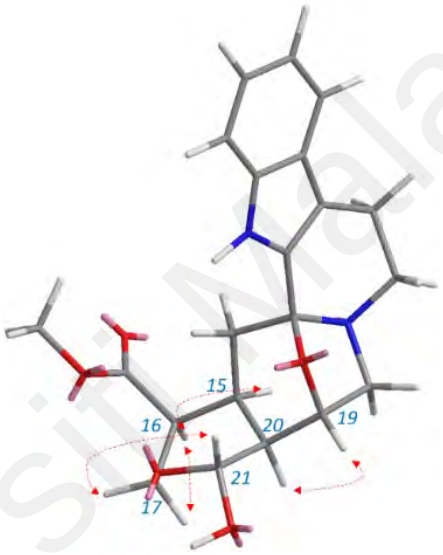

Figure 4.8: Selected NOESY correlation of dihydrodeglycocadambine (149).

Table 4.5: ^{1}H NMR (600 MHz) and ^{13}C NMR (150 MHz) spectral data of dihydrodeglycocadambine (149) in C_5D_5N.

Dihydrodeglycocadambine (149)					
Position	δ_H (*m*, *J* in Hz)	δ_C	COSY	HMBC	NOESY
NH	12.48 (*br s*)				
2		135.1			
3		92.3			
5	3.18, (*d*, *J*= 8.1) 2.81-2.86, (*m*)	53.2	6		
6	2.81-2.86, (*m*)	22.8	5	2,7	
7		111.1			
8		127.2			
9	7.74, (*d*, *J*=7.6)	119.9	10	7	
10	7.28, (*t*, *J*=7.6)	119.7	9,11	8	
11	7.34, (*t*, *J*=7.6)	122.7	10,12	13	
12	7.67, (*d*, *J*=7.6)	111.4	11	10	
13		138.4			
14a **14b**	2.28, (*dd*, *J*=12.0,12.0) 2.09, (*dd*, *J*=12.0, 4.7)	47.9	15	3	
15	2.81-2.86, (*m*)	29.8	14,20	3	
16	2.65, (*m*)	48.9	15,17	22,20	
17a **17b**	4.33, (*dd*, *J*=11.5,4.3) 3.97, (*m*)	67.8		21,	16 21
18a **18b**	2.62, (*d*, *J*=10.1) 2.81-2.86, (*m*)	57.3	19	5,19,20	
19	5.22, (*dd*, *J*=2.0,1.9.6.3,6.2)	74.8	20		20
20	2.20, (*m*)	50.3	21	21	19
21	5.04, (*br d*, *J*=8.6)	97.1			
22		173.0			
OMe	3.49, (*br s*)	52.0		22	

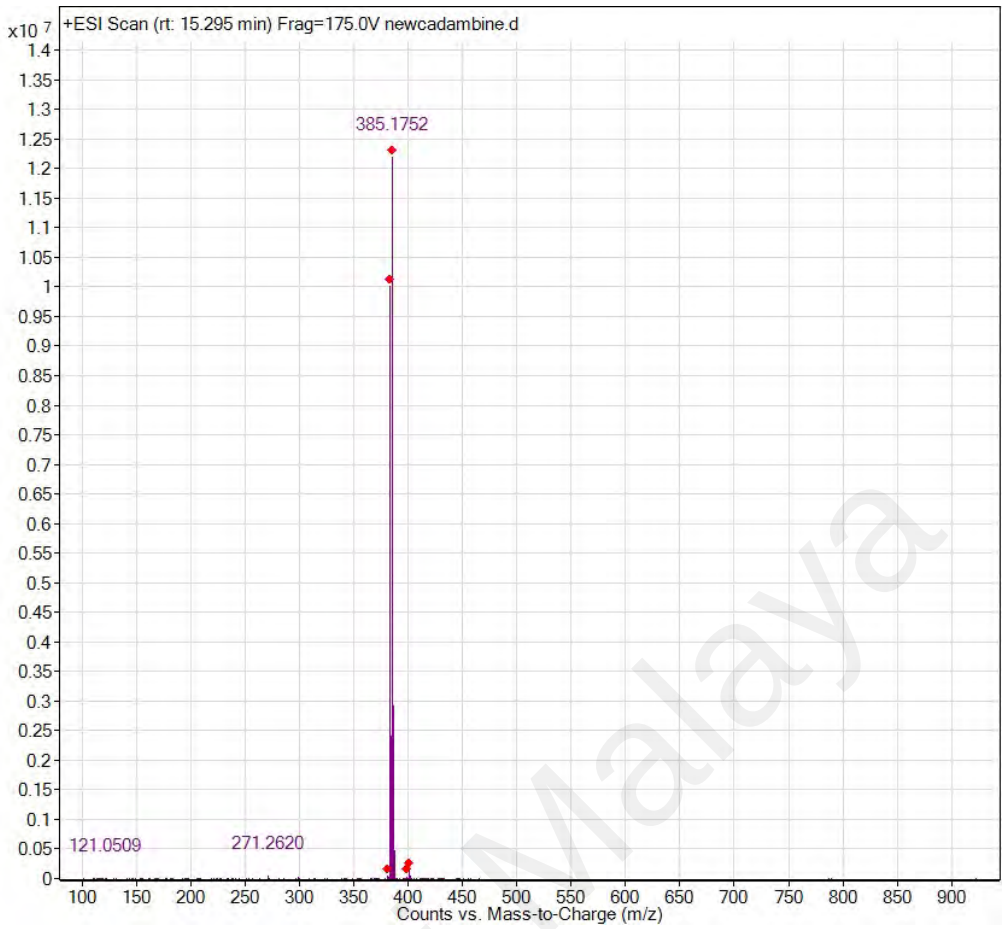

Figure 4.9: LC-ESI spectrum of dihydrodeglycocadambine (149).

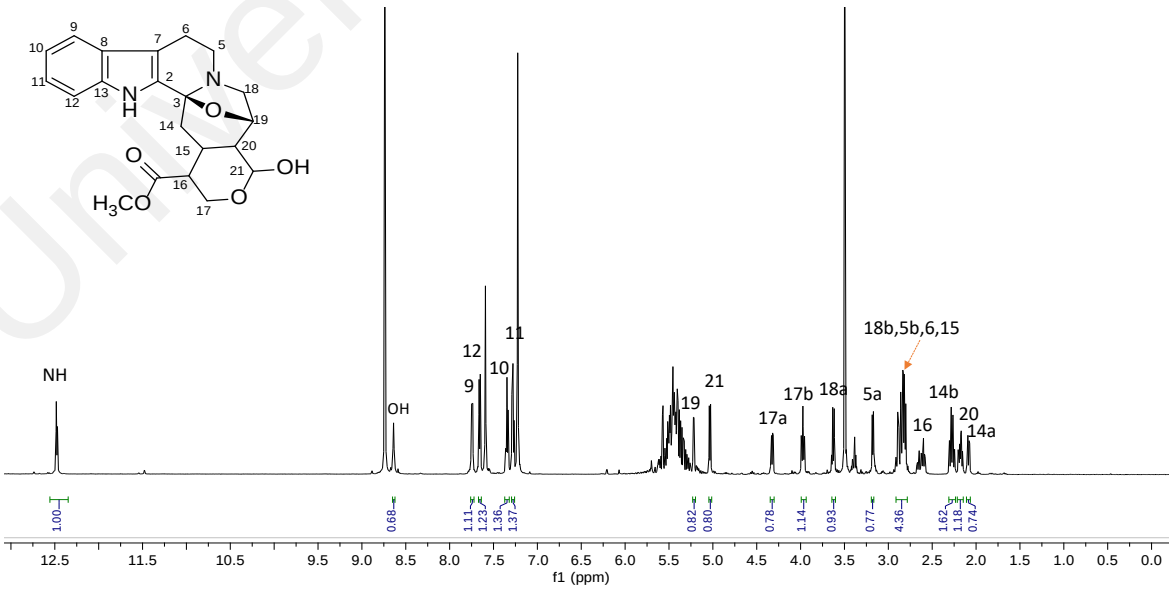

Figure 4.10: ^{1}H NMR spectrum of dihydrodeglycocadambine (149).

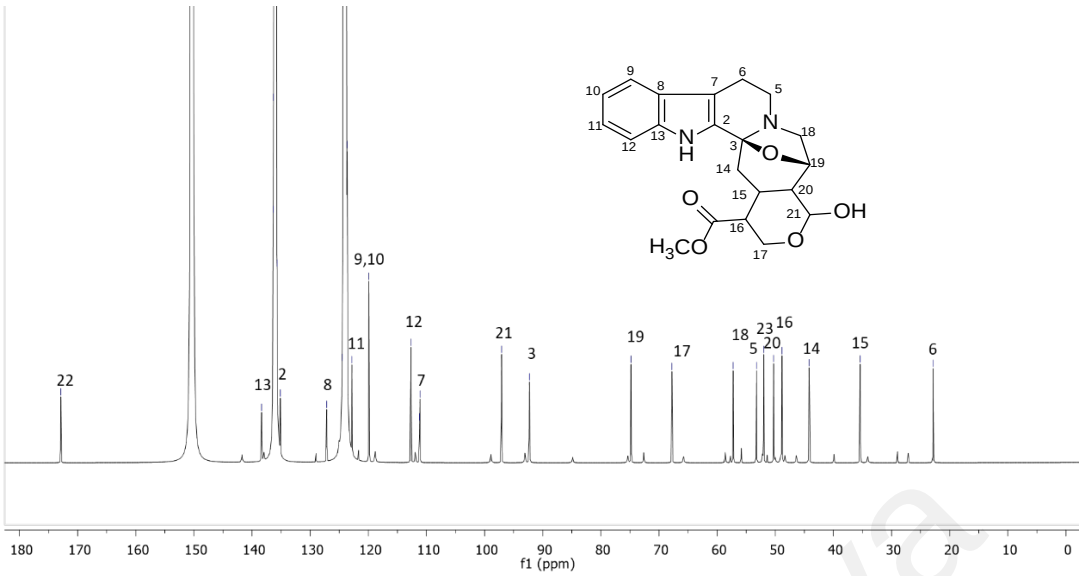

Figure 4.11: ^{13}C NMR spectrum of dihydrodeglycocadambine (149).

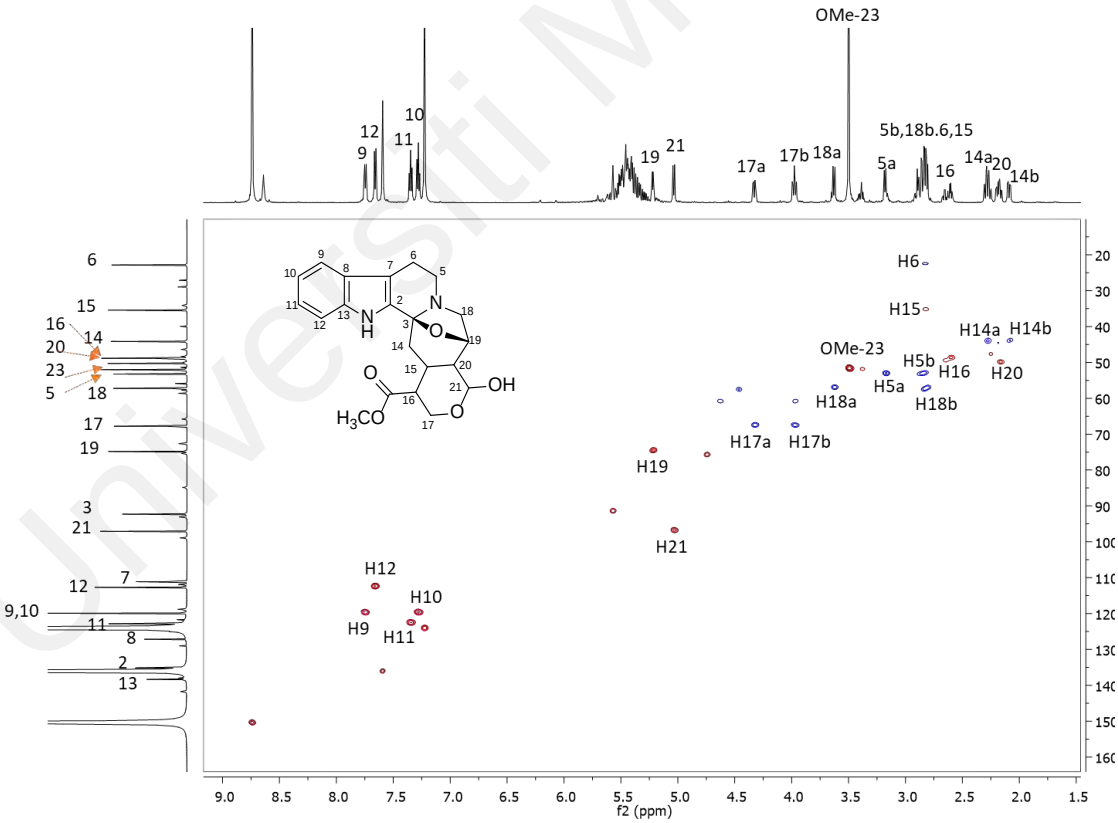

Figure 4.12 : HSQC spectrum of dihydrodeglycocadambine (149).

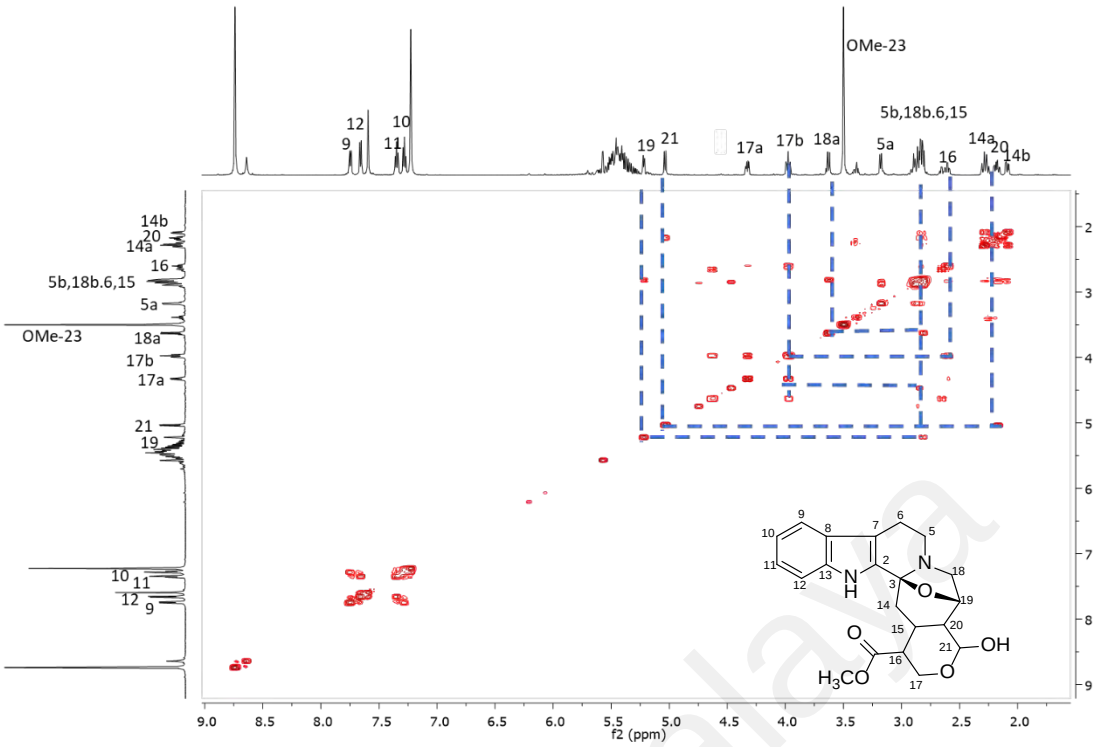

Figure 4.13: COSY spectrum of dihydrodeglycocadambine (149).

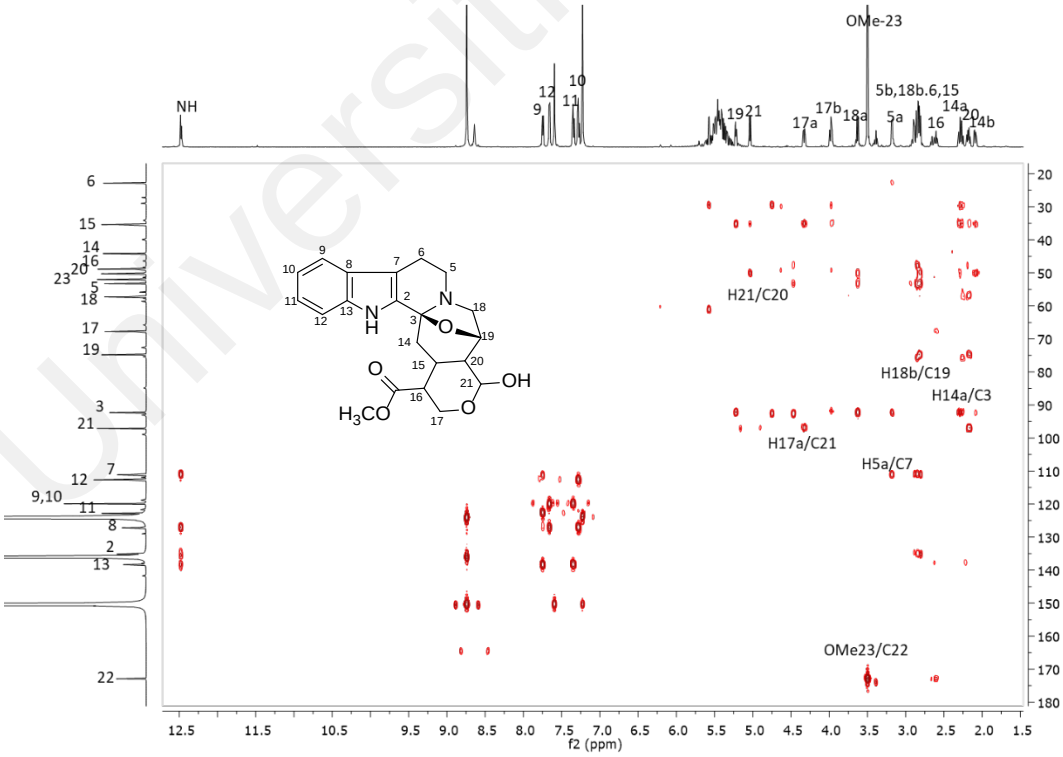

Figure 4.14: HMBC spectrum of dihydrodeglycocadambine (149).

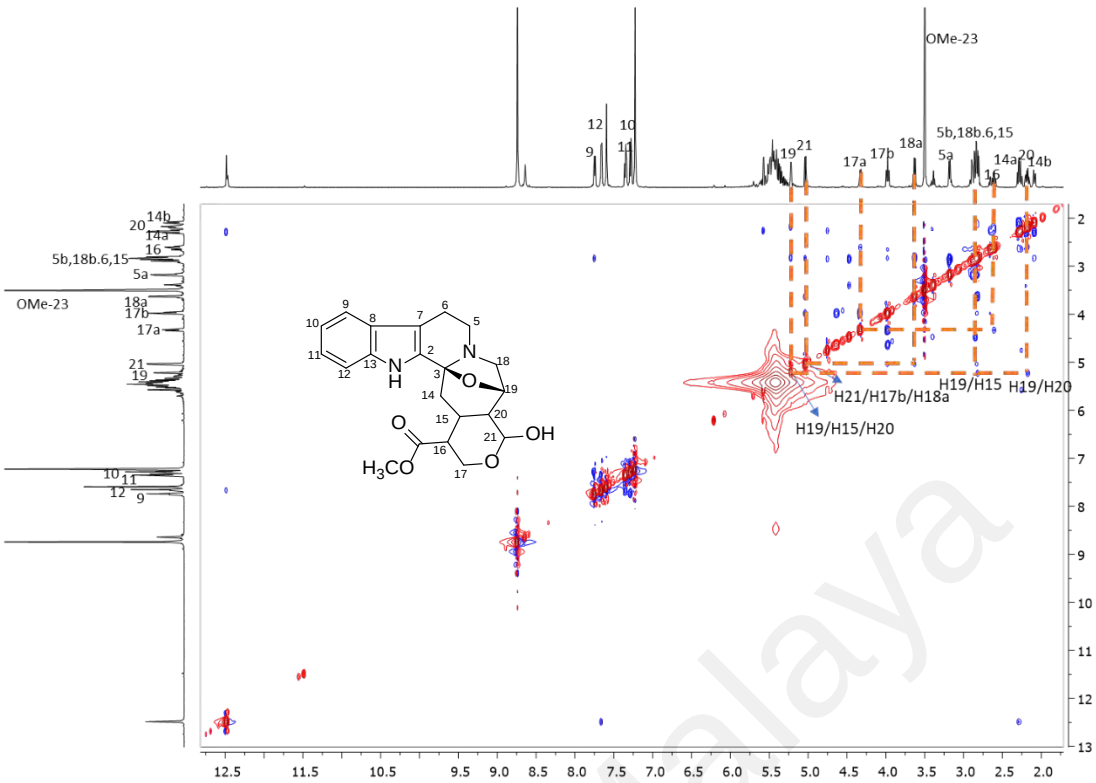

Figure 4.15: NOESY spectrum of dihydrodeglycocadambine (149).

4.2.2 Compound B: Cadambine (35)

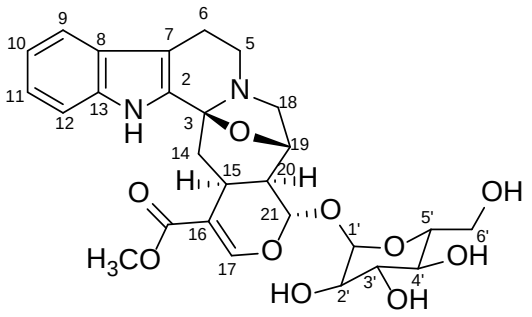

Compound **B** was isolated as a white amorphous solid with $[\alpha]_D^{25}$ = -122.77 (c=0.001, MeOH). Its molecular formula was established as $C_{27}H_{33}N_2O_{10}$ based on LC-ESI spectrum (Figure 4.16), which showed a pseudomolecular ion peak at *m/z* 545.2135 $[M+H]^+$; (calc. 545.2135). The IR spectrum (Appendix 20) revealed absorption bands at 3295, 1683 and 1072 cm^{-1} indicated of OH, C=O and C-O group, respectively (Pavia et al., 2009). The UV spectrum (Appendix 3) showed the existence of indole moiety by the observed maximum absorptions at 232 and 274 nm (Albinsson & Norden, 1992).

The ^{1}H NMR spectrum of **B** (Figure 4.17, Figure 4.18) displayed signals for an unsubstituted indole nucleus at δ_H 7.69 (*d*, *J*=7.7), 7.23 (*t*, *J*=7.7), 7.27 (*t*, *J*=7.7) and 7.51 (*d*, *J*=7.7) attributed to H-9, H-10, H-11 and H-12, respectively. Two methylene H-5 and H-6 appear at δ_H 2.74 -3.01 (m) and δ_H 2.80 (m), δ_H 4.63 (*dd*, *J*=3.0, 12). The former protons are more deshielded than the latter because C-5 is adjacent to N-4. These are signals of the tetrahydro *β*-carboline part of compound **B.**

The tetrahydro *β*-carboline moiety is fused to another ring that contains an oxygen bridge between C-3 and C-19. From biosynthesis of cadambine **(35)**, the oxygen or ether bridge is formed where C-18 of strictosidine **(32)** (precursor) has cyclized to N-4 (Brown & Fraser, 1974) to form azepine ring. The olefinic proton H-17 signal appeared downfield at δ_H7.65 as a singlet due to the adjacent O-atom. The methoxy proton of the ester functionality resonated as a singlet peak at δ_H 3.60. Proton H-21, attached to carbon C-21, substituted by two oxygen atoms, is the most downfield doublet at δ_H 5.82 (*J*=9.2).

The ^{13}C NMR spectrum (Figure 4.19) is in agreement with the molecular formula indicated by the mass spectrum, showing twenty-seven carbons: six quaternary, eight methines, five methylene, one methyl, one carbonyl, and six glucose carbon, respectively. The carbonyl signal present at the very downfield region at δc 167.6 in the spectrum. The typical glucose signals (Agrawal, 1992) can be seen at the upfield region between δc 63.6 to 76.4 (C-6' to C-2'). The anomeric C-1' signal resonates in the downfield region at δc 103.0 because two oxygen atoms flank it.

Through analysis of all NMR spectra (^{1}H, ^{13}C, COSY, HSQC, HMBC and NOESY) and upon comparison with the literature review with literature (Yuan et al., 2020) (Table 4.6) confirm that **B** is the known cadambine **(35)** that was first isolated from the leaves of *Neolamarckia cadamba*. It is the major indole alkaloid found in the bark of *O. maingayi*. Cadambine **(35)** reported as potent toward DNA topoisomerase IB inhibitory activity and moderately active on anticholinesterase activity (Kumar et al., 2015; P. Yu et al., 2022).

Table 4.6: ^{1}H NMR (600 MHz) and ^{13}C NMR (150 MHz) spectral data of cadambine (35) in C_5D_5N.

	Cadambine (35)		**Cadambine (Yuan et al., 2020)**	
Position	δ_H (*m*, *J* in Hz)	δ_C	δ_H (*m*, *J* in Hz) in CD_3OD	δ_C in CD_3OD
1				
2		134.6		133.2
3		92.1		93.0
5	3.01 (*m)* 2.74 (*m*)	53.0	3.16 (*m*) 2.79 (*m*)	53.9
6	2.80 (*m*) 4.63 (*dd*, *J*=3.0, 12.2)	22.8	2.80 (*brs*)	22.8
7		110.8		111.6
8		127.0		127.0
9	7.69 (*d*, *J*=7.7)	119.9	7.47 (*d*, *J*=7.8)	120.2
10	7.23 (*t*, *J*=7.7)	119.9	7.00 (*t*, *J*=7.8)	120.1
11	7.27(*t*, *J*=7.7)	122.8	7.11 (*t*, *J*=7.8)	123.4
12	7.51 (*d*, *J*=7.7)	112.6	7.33 (*d*, *J*=7.8)	112.6
13		138.4		136.3
14	2.33 (*t*, *J*=12.5) 2.38 (*dd*, *J*=5.9, 13.1)	44.1	2.06 (*m*)	43.1
15	3.48 (*m*)	26.41	3.26 (*m*)	26.9
16		110.8		111.3
17	7.65 (*s*)	153.4	7.57 (*s*)	154.4
18	3.14 (*d*, *J*=10.2) 2.86 (*m*)	59.4	3.51 (*brd*, *J*=10.8) 3.02 (*dd*, *J*=10.8,7.3)	59.4
19	5.10 (*d*, *J*=7.1)	73.8	4.94 (*brd*, *J*=7.3)	74.6
20	1.78 (*m*)	40.9	1.76 (*m*)	41.1
21	5.82 (*d*, *J*=9.2)	98.2	5.84 (*d*, *J*=9.3)	97.6
22-C=O		167.6		168.9
23-OCH3	3.60 (*bs*)	51.5	3.65 (*s*)	51.9
1'	5.19 (*d*, *J*=7.8)	103.0	4.80 (*d*, *J*=7.9)	101.7
2'	4.16 (*m*)	75.4	3.30 (*m*)	74.9
3'	4.30 (*t*, *J*=8.9)	78.0	3.42 (*t*, *J*=9.0)	78.1
4'	4.20 (*m*)	72.4	3.28 (*m*)	71.7
5'	3.97 (*ddd*, J=7.0, 2.4)	79.0	3.34 (*m*)	78.5
6'	4.48 (*dd*, *J*=11.8, 2.4) 4.17 (*m*) overlapp	63.6	3.87 (*dd*, *J*=12.1, 2.3) 3.61 (*dd*, *J*=12.1, 6.4)	62.9

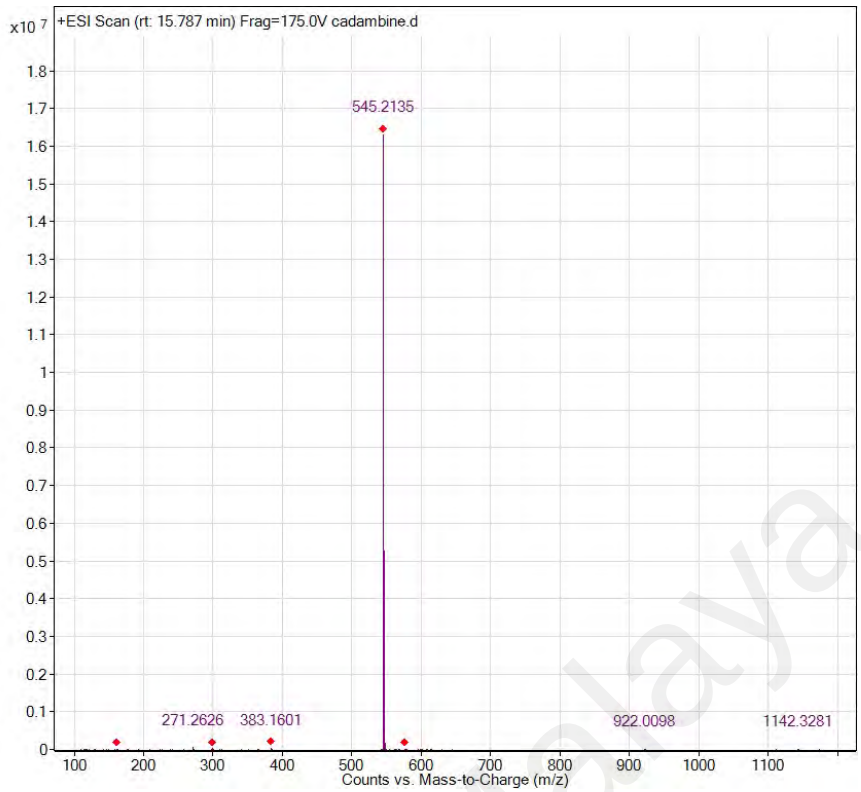

Figure 4.16: LC-ESI spectrum of cadambine (35).

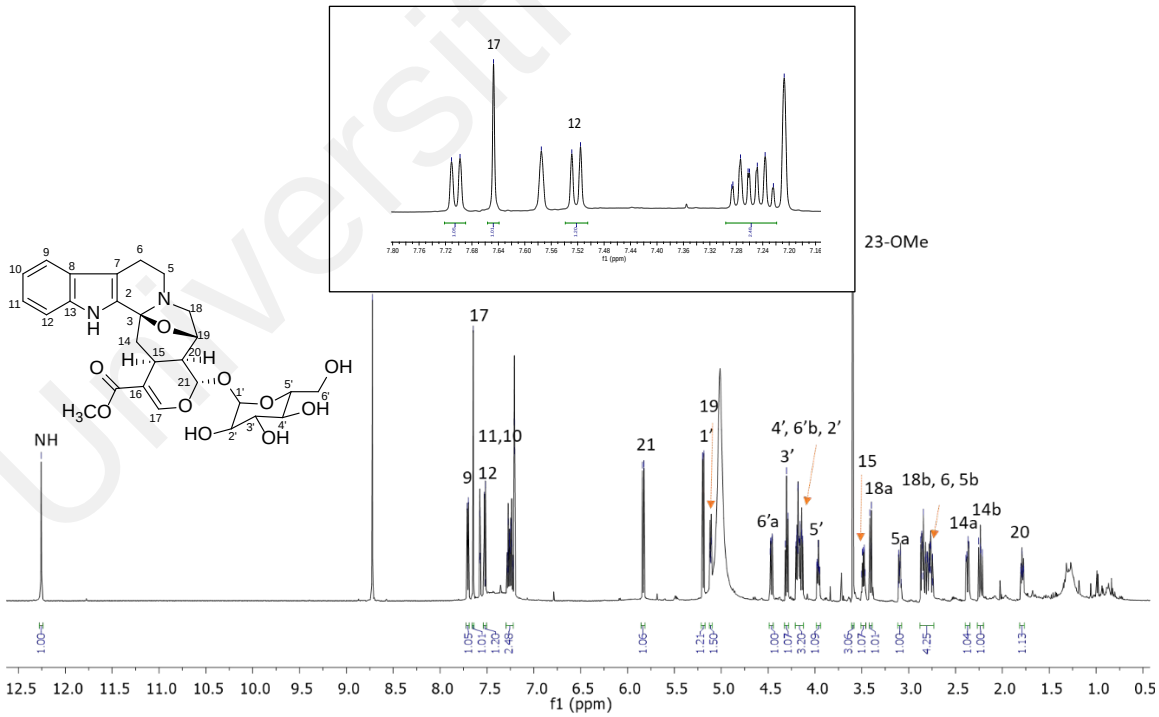

Figure 4.17: ^{1}H NMR spectrum of cadambine (35).

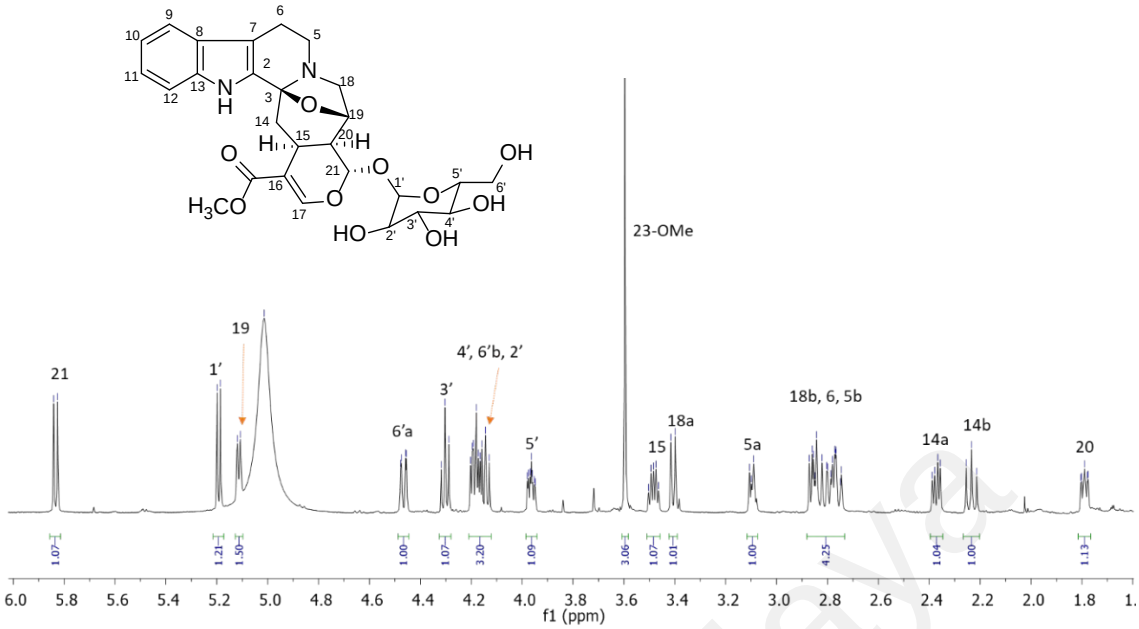

Figure 4.18: ^{1}H NMR spectrum (expand) of cadambine (35).

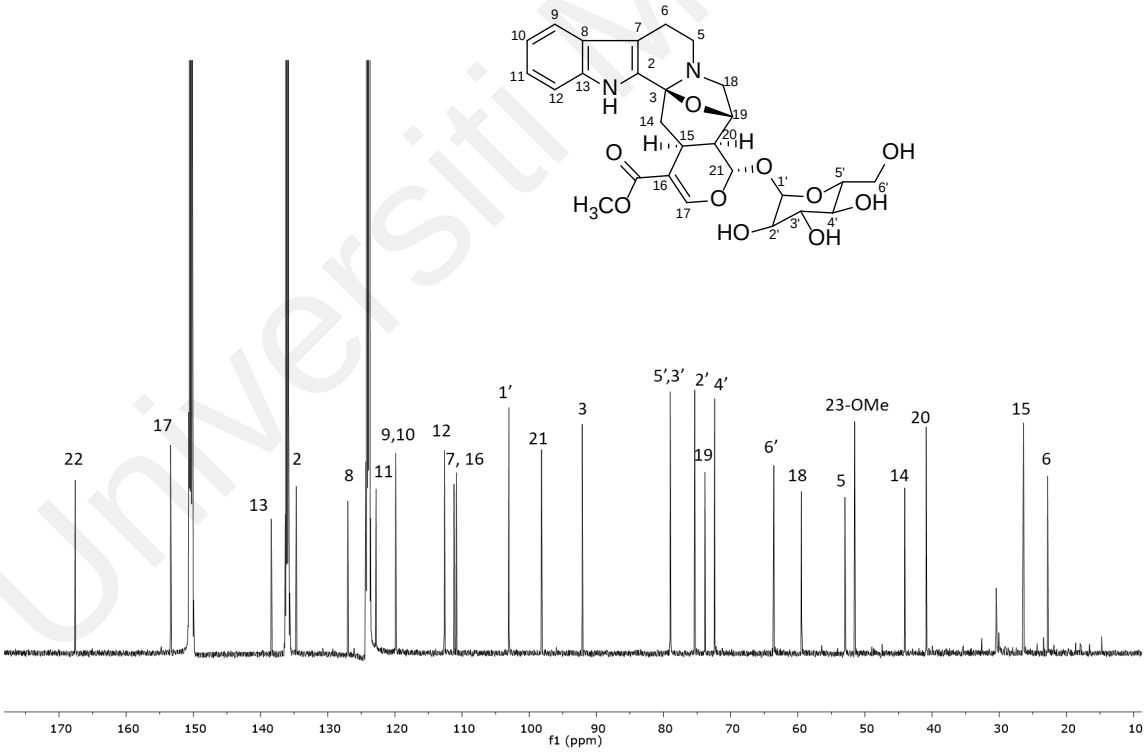

Figure 4.19: ^{13}C NMR spectrum of cadambine (35).

4.2.3 Compound C: Naucledine (6)

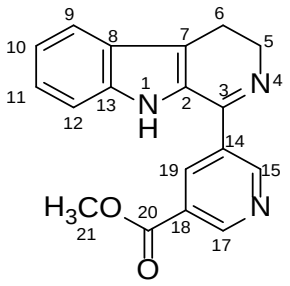

Compound **C** was yielded as a yellow amorphous solid. The UV spectrum (Appendix 4) showed absorption maxima at 329, 280 and 220 nm, were consistence with the presence of indole chromophore (Kam & Choo, 2004; Mukhtar et al., 1997; Zhou et al., 2008). The IR spectrum (Appendix 21) showed an absorption band at 3402 cm^{-1}, which indicates the presence of the N-H group and the carbonyl group appeared at 1731 cm^{-1} (Pavia et al., 2009). A molecular formula was determined to be $C_{18}H_{16}N_3O_2$ by LC-ESI spectrum (Figure 4.20) at *m/z* 306.1236, $[M+H]^+$ (calc. 306.1244).

The ^{1}H NMR spectrum (Figure 4.21) of compound **C** possess the same indole aromatic substitution pattern a compound **B**. Analysis of the spectroscopic data (Table 4.7) corroborated that **C** was indolopyridine-type alkaloid significantly different from that **B**, which is cadambine-type. Three pyridine proton signals were observed in association with 3, 5-disubstituted pyridine Three pyridine proton signals corresponding to 3, 5-disubstituted pyridine were detected at δ_H 9.18 (*d*, *J*=2.0 Hz, H-17), 9.30 (*d*, *J*=2.0 Hz, H-15) and 8.68 *(t*, *J*=2.0 Hz, H-19). Additionally, the signal of the methoxy group was identified as a singlet at δ_H 3.98, which correlates with C-20 and indicates the presence of an ester group attached to C-18.

The ^{13}C NMR (Figure 4.22) spectra were in agreement with the molecular formula deduced from the mass spectrum, accounting for all 18 carbons: seven quaternary, seven methines, two methylene, one methyl and one carbonyl carbons.

The analysis of accumulated data (HSQC, COSY and HMBC) and comparison to values in the literature (Table 4.7) (Mukhtar et al., 2012; Murray, 1969), that confirmed

C is naucledine **(6)** were previously isolated from *Nauclea diderichii*. It also showed good vasorelaxant activity on isolated rat aorta (Mukhtar et al., 2012).

Table 4.7: ^{1}H NMR (600 MHz) and ^{13}C NMR (150 MHz) spectral data of naucledine (6) in $CDCl_3$.

	Naucledine (6)		**Naucledine (Mukhtar et al., 2012)**	
Position	δ_H (*m*, *J* in Hz)	δ_C	δ_H (*m*, *J* in Hz) in $CDCl_3$	δ_C in $CDCl_3$
1			8.35 (*s*)	
2		127.0		126.3
3		156.2		156.3
4				
5	4.10 (*t*, *J*=6.9)	49.1	4.13 (*t*, *J*=6.8)	49.3
6	3.81 (*t*, *J*=6.9)	19.2	3.03 (*t*, *J*=6.8)	19.3
7		118.9		119.0
8		125.4		125.4
9	7.67 (*d*, *J*=7.5)	120.2	7.68 (*d*, *J*=8.3)	120.3
10	7.20 (*t*, *J*=7.5)	120.2	7.23 (*dd*, *J*=8.3)	120.9
11	7.32 (*t*, *J*=7.5)	125.3	7.33 (*dd*, *J*=8.3)	125.5
12	7.41 (*d*, *J*=7.5)	112.3	7.42 (*d*, *J*=8.3)	112.4
13		137.0		136.9
14		126.17		125.4
15	9.26 (*t*, *J*=2.0)	136.5	9.30 (*t*, *j*=1.9)	136.5
17	9.18 (*d*, *J*=2.0)	152.8	9.18 (*d*, *J*=1.9)	152.6
18		133.3		133.3
19	8.68 (*d*, *J*=2.0)	151.6	8.68 (*d*, *J*=1.9)	151.8
20		165.3		165.5
21	4.00 (*s*)	52.8	3.98 (*s*)	52.8

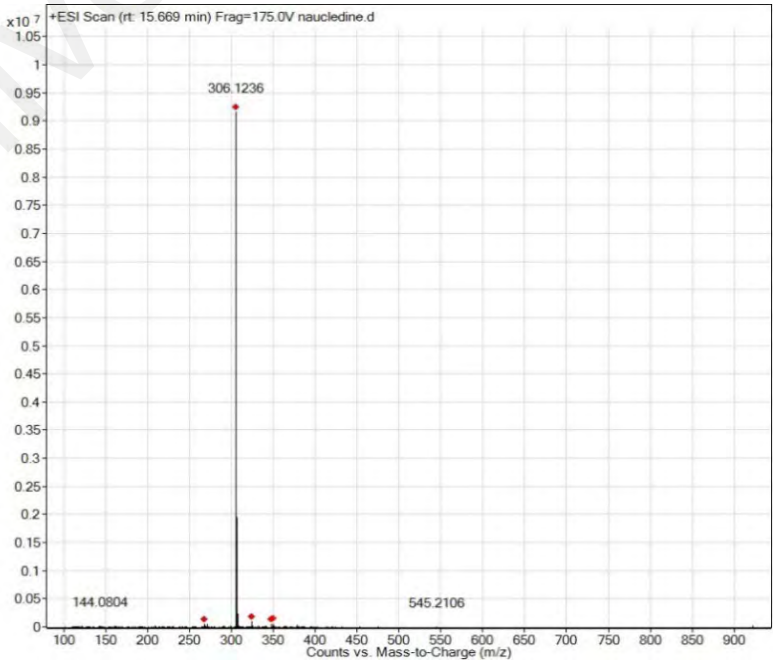

Figure 4.20: LC-ESI spectrum of naucledine (6).

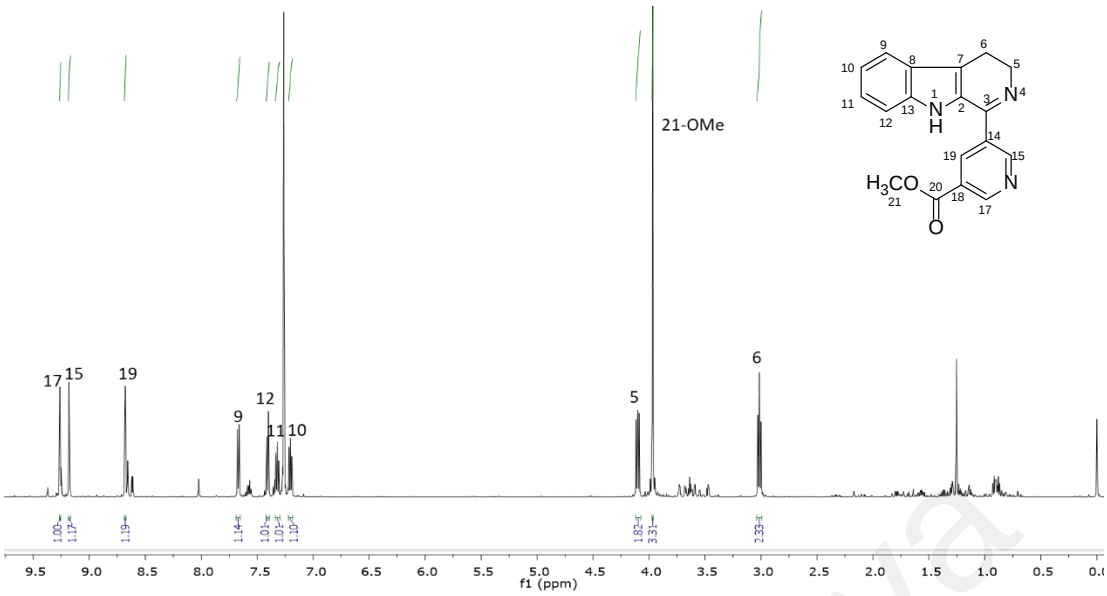

Figure 4.21: ^{1}H NMR spectrum of naucledine (6).

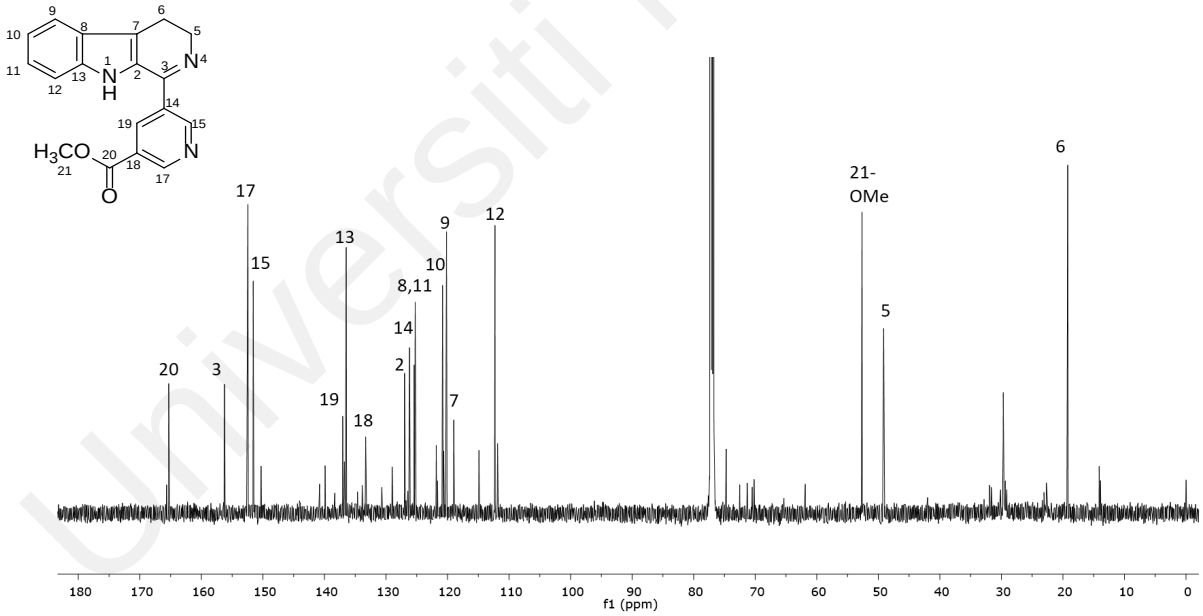

Figure 4.22: ^{13}C NMR spectrum of naucledine (6).

4.2.4 Compound D: Methyl *9H-β*-carboline-4-carboxylate (150)

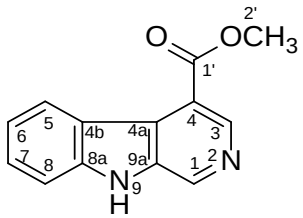

Compound **D** was obtained as a dark yellow amorphous solid. The LC-ESI spectrum (Figure 4.23) gave a pseudomolecular ion peak at m/z 227.1155 (calc. 227.0821) $[M+H]^+$, which agrees with the molecular formula $C_{13}H_{11}N_2O_2$. In UV spectrum (Appendix 5), absorption maxima were observed at 206, 298, 312, 366 and 381 nm characteristic of *β*-carboline (Parameswaran et al., 1997). The IR spectrum (Appendix 22) showed absorption bands at 2919 and 2919 and 1723cm^{-1} indicated the present of conjugated carbonyl carbon.

Analysis of ^{1}H NMR spectrum (Figure 4.24), showed that compound **D** was resembled of **H** and **F** but substituted at C-4. In HMBC spectrum (Figure 4.26), the methoxy group showed J_3 correlated to carbonyl carbon at 1' and H-3/C-1' prove the attachment of ester functionality.

^{13}C NMR data (Figure 4.25) indicate the presence of six methines, six quaternary carbons and one methyl groups.

Complete analysis assignments of **D** were establish by ^{1}H, ^{13}C NMR, COSY, HMQC and HMBC spectra and literature review (Table 4.8) (Bartoli et al., 2008) prove the structure of **D** is methyl *9H-β*-carboline-4-carboxylate **(150)**. There are no biological activities reported on this compound yet.

Table 4.8: ^{1}H NMR (600 MHz) and ^{13}C NMR (150 MHz) spectral data of methyl *9H-β*-carboline-4-carboxylate (150) in $CDCl_3$.

	Methyl *9H-β*-carboline-4-carboxylate (150)		**Methyl *9H-β*-carboline-4-carboxylate (Bartoli et al., 2008)**
position	δ_H (*m*, *J* in Hz)	δ_C	δ_H (*m*, *J* in Hz) in DMSO-d_6
1	9.02 (*s*)	151.2	9.12 (*s*)
2			
3	8.58 (*s*)	151.2	8.75-8.28 (*m*)
4		125.7	
4a		108.9	
4b		126.7	
5	7.52(*d*, *J*=7.8)	118.2	8.75-8.28 (*m*)
6	7.13(*t*, *J*=7.8)	119.5	7.23-7.36 (*m*)
7	7.22(*t*, *J*=7.8)	121.9	7.60-7.71 (*m*)
8	7.45(*d*, *J*=7.8)	111.1	7.60-7.71 (*m*)
8a		136.4	
9-NH			
9a		138.5	
1'		167.6	
2'	4.08 (*s*)	52.9	4.10 (*s*)

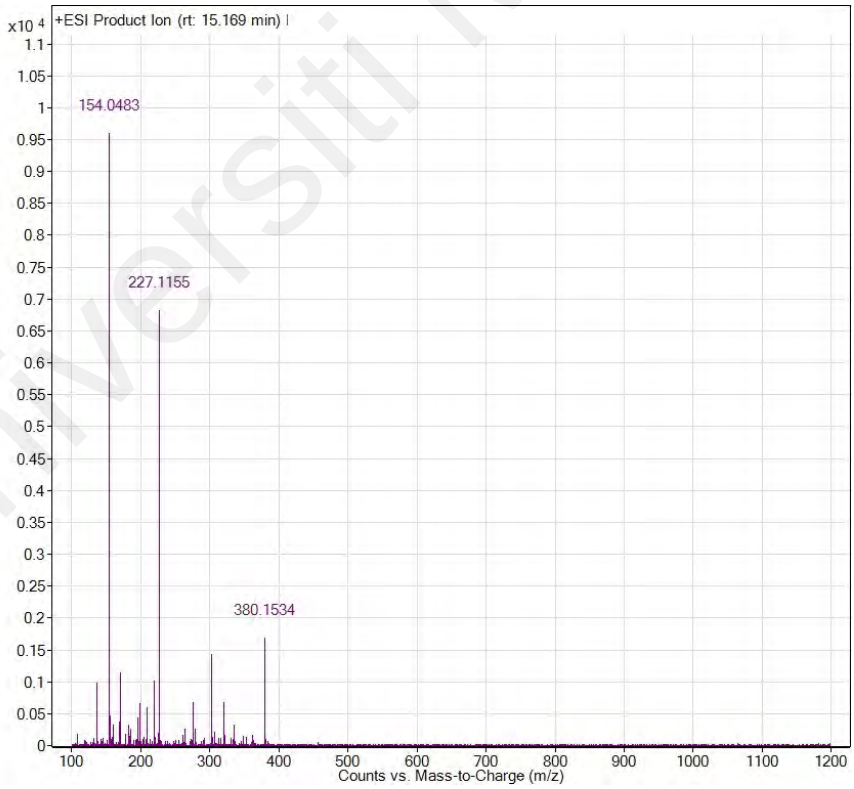

Figure 4.23: LC-ESI spectrum of methyl *9H-β*-carboline-4-carboxylate (150).

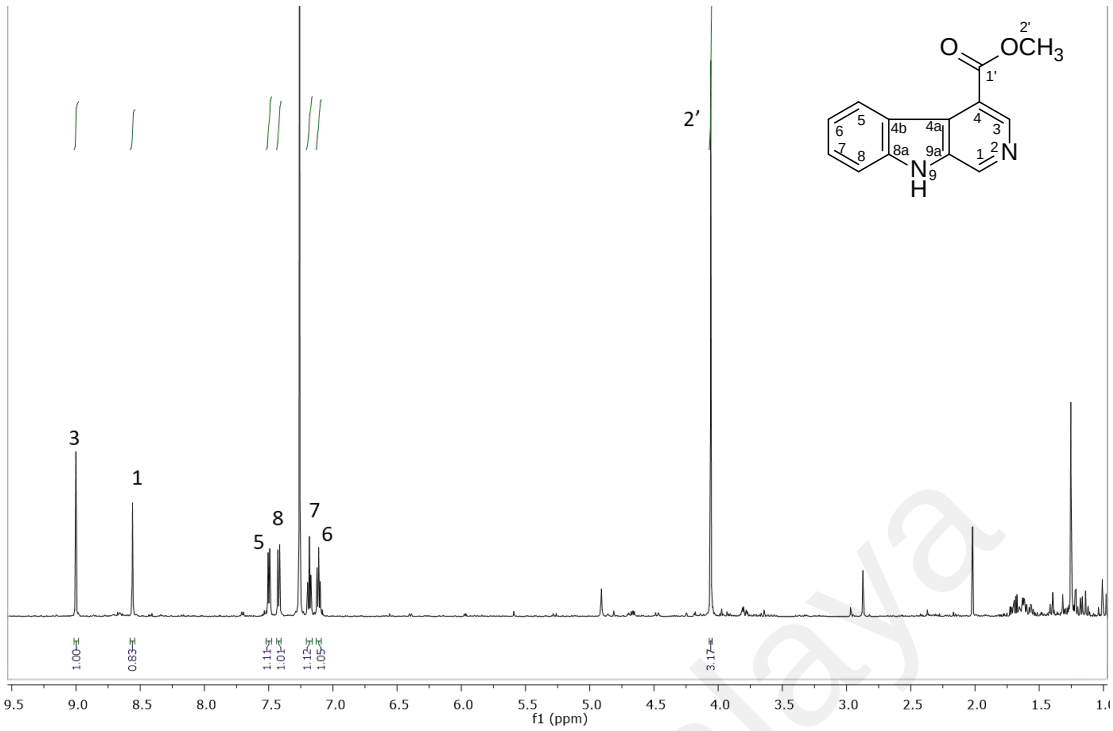

Figure 4.24: ^{1}H NMR spectrum of methyl *9H-β*-carboline-4-carboxylate (150).

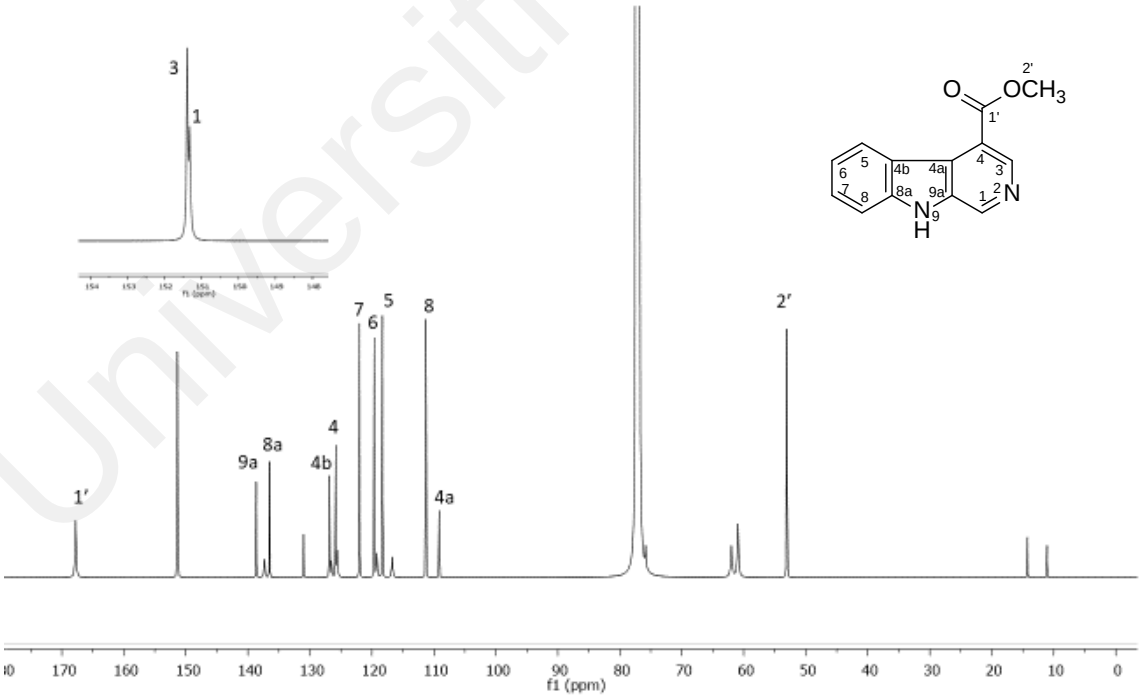

Figure 4.25: ^{13}C NMR spectrum of methyl *9H-β*-carboline-4-carboxylate (150).

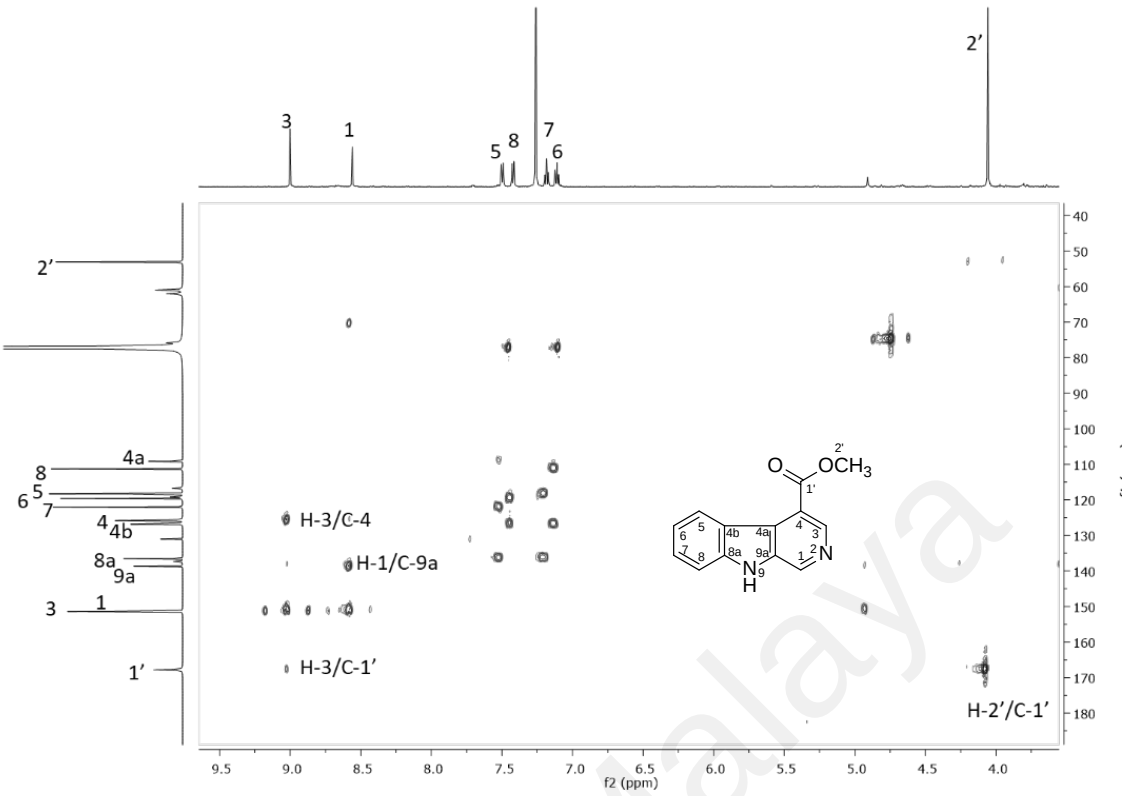

Figure 4.26: HMBC spectrum of methyl *9H-β*-carboline-4-carboxylate (150).

4.2.5 Compound E: *Nor*harmane (124)

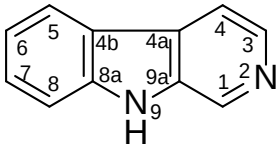

Compound **E** was separated as a brownish amorphous solid. The IR spectrum (Appendix 23) of this alkaloid showed absorption for the NH function at 3166 cm-1 and the aromatic system at 2924 cm^{-1}. The UV spectrum (Appendix 6) showed *β*-carboline characteristic with absorption maxima at 211, 234, 288,304, and 350 nm (Parameswaran et al., 1997). The molecular formula was determined by LC-ESI (Figure 4.27) with *m/z* 169.0760 $[M+H]^+$ (calc 169.0767) as $C_{11}H_9N_2$.

In the ^{1}H NMR spectrum (Figure 4.28) of compound **E,** proton signals in the aromatic regions of δ_H 7.61 (*d*, *J* = 8.0 Hz, H-5), δ_H 8.01 (*d*, J=8.0 Hz, H-8), δ_H 7.25 (*t*, *J* = 8.0 Hz , H-6), δ_H 7.61 (*t*, *J* = 8.0 Hz, H-7) and two downfield methine signals at δ_H 8.32 (*d*, *J* = 5.6, H-3) and δ_H 8.11 (*d*, *J* = 5.6, H-4), indicating the presence of *β*-carboline. Meanwhile, a broad singlet signal appeared at δ_H 9.29 belonging to NH in the upfield region.

The ^{13}C-NMR spectrum (Figure 4.29) showed eleven signals representing eleven carbons. Four quaternary carbons appeared at 120.5(C-4b), 132.8 (C-4a), 142.4(C-8a) and 135.7 (C-9a), while another seven peaks at 112.7(C-5), 115.6 (C-4), 120.5(C-6), 122.3(C-8), 129.9 (C-1),130.6 (C-7) and 131.8 (C-3) were assigned to CH aromatic.

The structure of **E** or *nor*harmane **(124)** was determine from the analysis of spectral data (^{1}H, ^{13}C NMR, COSY,HSQC and HMBC) and a comparison with the literature (Table 4.9) (Parameswaran et al., 1997). **124** was reported to has potential as anti-cancer (Sahoo et al., 2019).

Table 4.9: ^{1}H NMR (600 MHz) and ^{13}C NMR (150 MHz) spectral data of *nor*harmane (124) in $CDCl_3$.

	***nor*harmane (124)**		***nor*harmane (Parameswaran et al., 1997)**	
Position	δ_H (*m*, *J* in Hz)	δ_C	δ_H (*m*, *J* in Hz) $CDCl_3$	δ_C in $CDCl_3$
1	9.29 (*s*)	129.9	8.97 s	129.29
2				
3	8.32 (*d*, *J*=5.6)	131.8	8.45 (*d*, *J*=5.0)	133.34
4	8.11 (*d*. *J*=5.6)	115.6	7.97 (*d*, *J*=5.0)	114.92
4a		132.8		136.07
4b		120.5		120.20
5	7.59 (*d*, *J*=8.0)	112.7	7.55 (*m*)	111.81
6	7.25 (*t*, *J*=8.0)	120.5	7.30 (*m*)	121.40
7	7.61 (*t*, *J*=8.0)	130.6	7.55 (*m*	128.75
8	8.01 (*d*, *J*=8.0	122.3	8.13 (*d*, *J*=7.8	121.86
8a		142.4		140.83
9	10.5 (*s*)		9.43 (*s*)	
9a		135.7		138.40

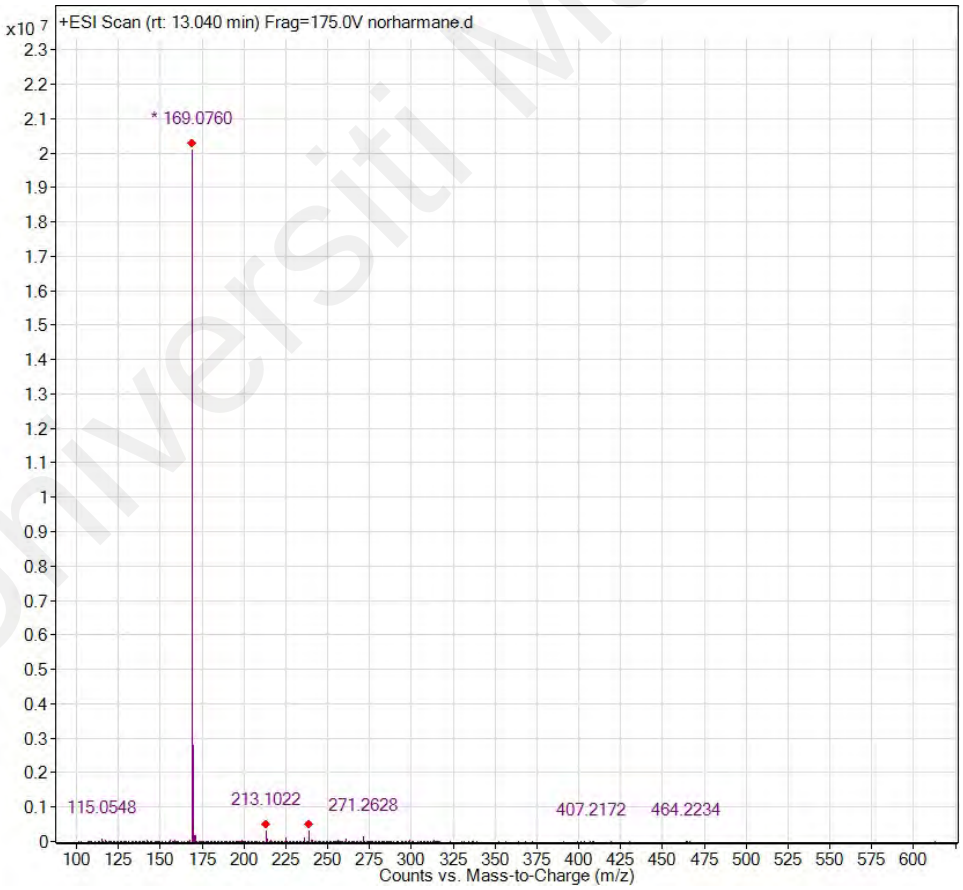

Figure 4.27: LC-ESI spectrum of *nor*harmane (124).

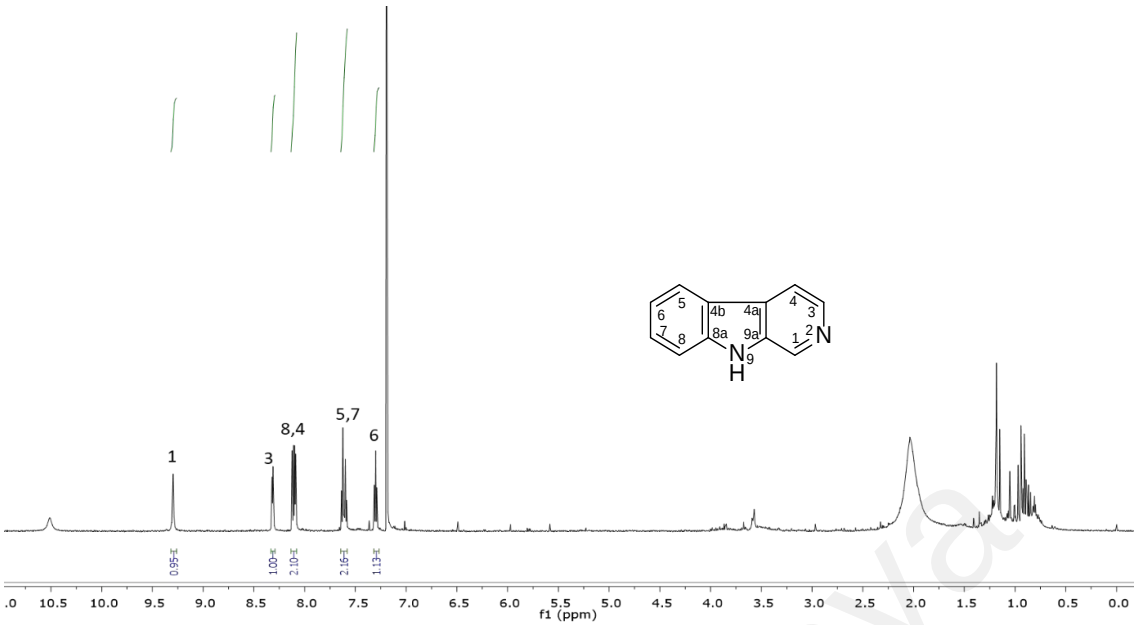

Figure 4.28: ^{1}H NMR spectrum of *nor*harmane (124).

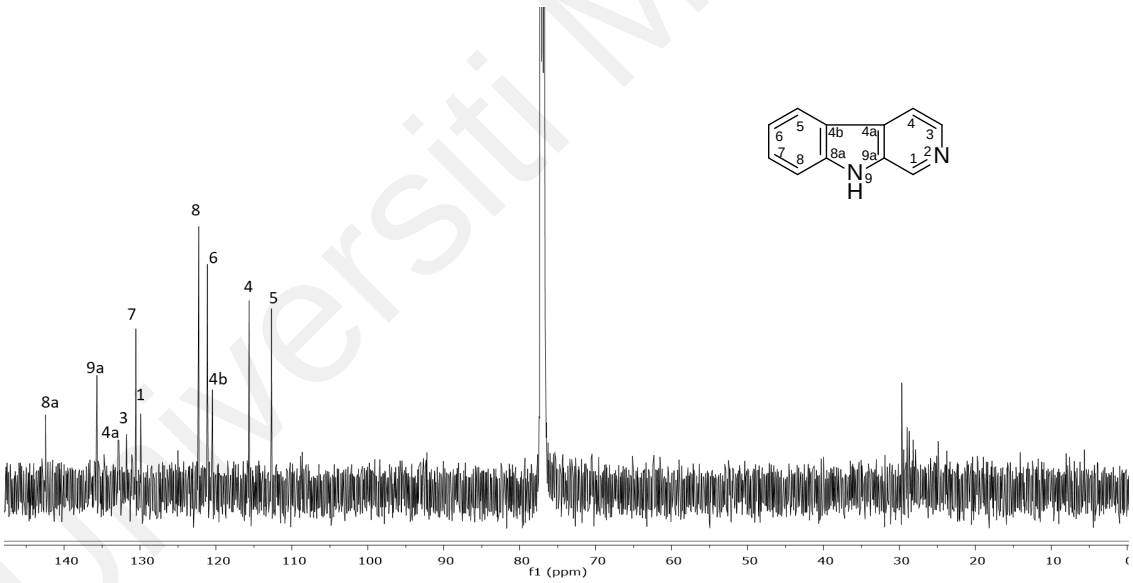

Figure 4.29: ^{13}C NMR spectrum of *nor*harmane (124).

4.2.6 Compound F: Harmane (7)

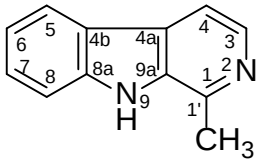

Compound **F** is afforded as a brownish amorphous solid. It has the molecular formula of $C_{12}H_{10}N_2$, as deduced from the LC-ESI spectrum, which appeared as a pseudo molecular ion peak at *m/z* $[M+H]^+$ 183.0994 (Figure 4.30) (calc.183.0923). The IR spectrum (Appendix 24) of **F** showed a broad absorption band at 3145 cm^{-1}, indicating the presence of the N-H group. The UV spectrum (Appendix 7) showed absorption maxima at 348, 335, 287, and 243 nm which are characteristic of the *β*-carboline moiety (Parameswaran et al., 1997).

Compound **F** resembles compound **E** *nor*harmane **(124)**), but a singlet proton signal in the upfield region assigned to H-1 has disappeared in **E** (Figure 4.31). A methyl signal from H-1' appeared at δ_H 2.83, with this methyl attached to C-1, representing a methyl group attached to *β*-carboline skeleton. The ^{13}C NMR (Figure 4.32) of compound **F** showed twelve carbon signals: five quaternary, six methines, and one methyl groups.

From the analysis of the spectroscopic data obtained (^1H, ^{13}C NMR, HSQC, COSY and HMBC) and comparison with literature values (Table 4.10) (Aassila et al., 2003), the structure of compound **F** as harmane **(7)** was confirmed. The beta-carboline, **7** was first found in *Perganum harmala* of the family Nitrariaceae (McKenzie et al., 1975)**.** Harmane **(7)** was reported has anti-anxiety and antidepressant effect, acetylcholinesterase inhibitory, antiplatelet effect, antidiabetic, antihypertensives, and antiparasitic (Aricioglu & Altunbas, 2003; Khan et al., 2017).

Table 4.10: ^{1}H NMR (600 MHz) and ^{13}C NMR (150 MHz) spectral data of harmane (7) in $CDCl_3$.

	Harmane (7)		Harmane (Aassila et al., 2003)	
Position	δ_H (*m*, *J* in Hz)	δ_C	δ_H (*m*, *J* in Hz) in$CDCl_3$	δ_C in $CDCl_3$
1		141.6		142.9
2 N				
3	8.30 (*d*, *J*=5.4)	137.8	8.31(*d*, *J*=5.3)	139.0
4	7.84 (*d*, *J*=5.4)	112.9	7.84 (*d*, *J*=5.3)	113.0
4a		128.5		128.3
4b		121.8		122.8
5	8.12 (*d*, *J*=7.8)	121.8	8.12 (*d*, *J*=7.9)	122.0
6	7.29 (*m*)	121.1	7.28 (*m*)	120.4
7	7.55 (*m*)	128.5	7.55 (*m*)	128.5
8	7.55 (*m*)	111.6	7.56 (*m*)	119.9
8a		140.4		140.7
9-NH				
9a		131.7		135.7
1'	2.83 (*s*)	19.8	2.8 (*s*)	20.0

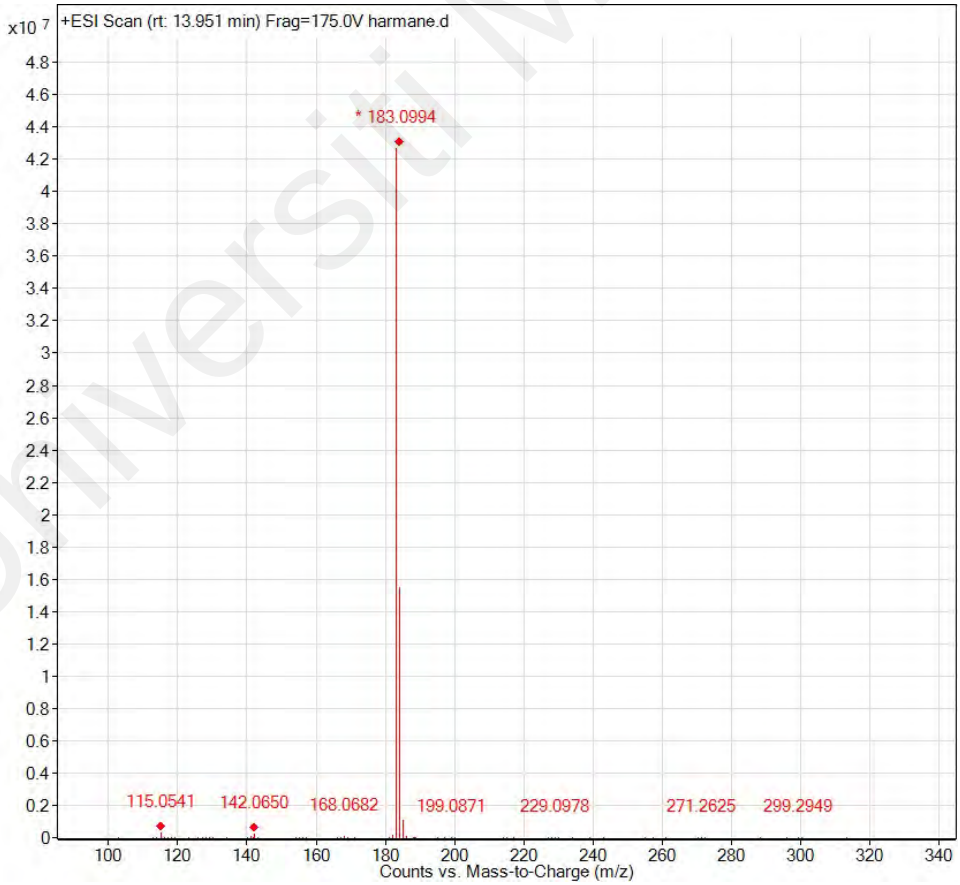

Figure 4.30: LC-ESI spectrum of harmane (7).

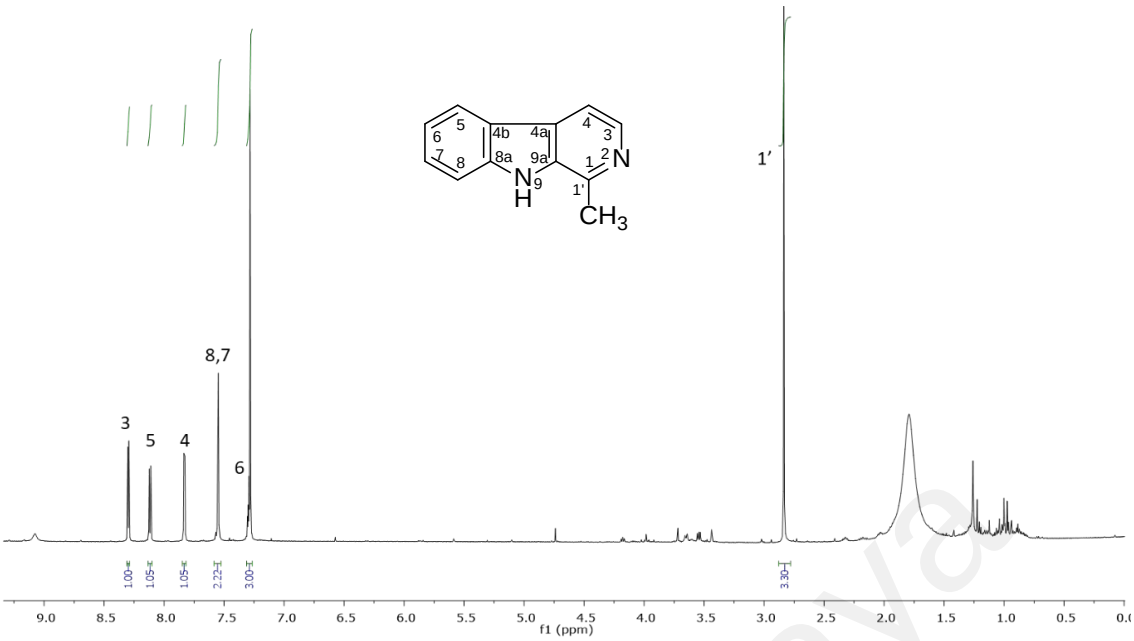

Figure 4.31: ^{1}H NMR spectrum of harmane (7).

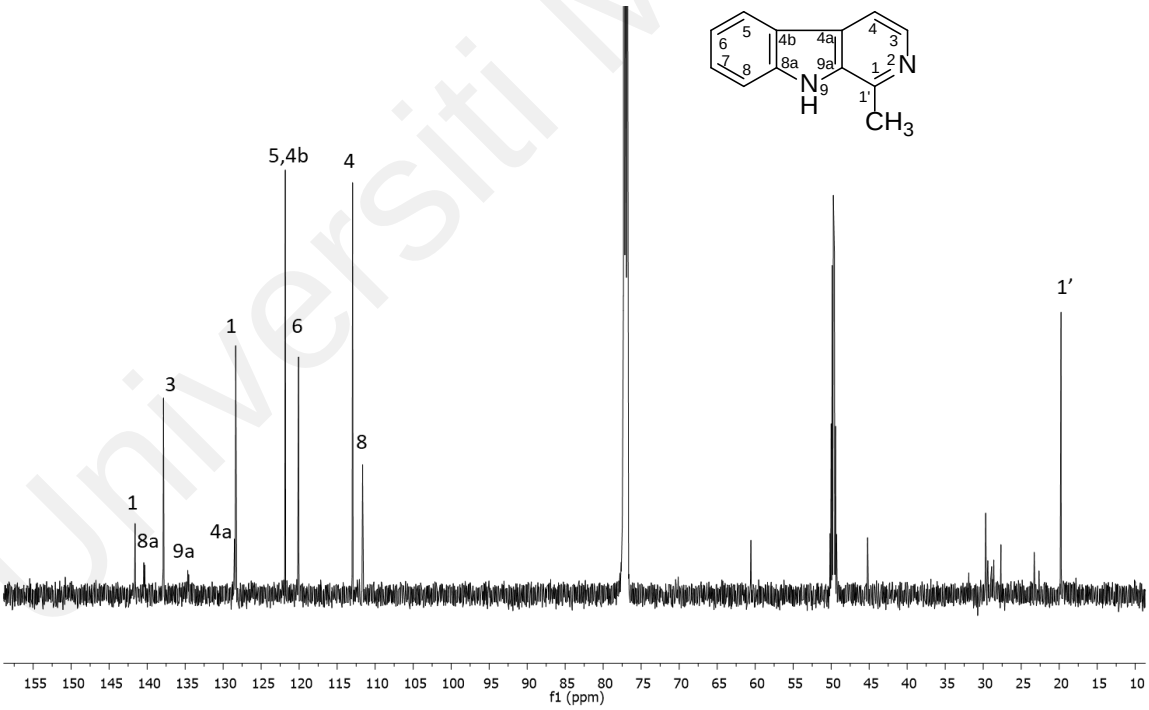

Figure 4.32: ^{13}C NMR spectrum of harmane (7).

4.2.7 Compound G: Naulafine (33)

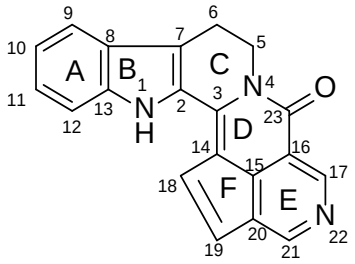

Compound **G** was afforded as a reddish-brown amorphous solid. The LC-ESI was the presence of pseudomolecular ion peak *m/z* 312.1155 (Figure 4.33) (calc. 312.1138) $[M+H]^+$ which were consistent with the molecular formula $C_{20}H_{14}N_3O$. This compound **G** gave UV (Appendix 8) absorption maxima at 205, 302, 314, 366 and 385 nm characteristic of indole chromophore (Hotellier et al., 1979). IR spectrum (Appendix 25) indicated absorption at 3351 and 1667 cm^{-1} corresponded to NH and CO groups (Pavia et al., 2009).

The ^{1}H NMR spectrum showed (Figure 4.34) that hexacyclic compound **G** exhibited eight aromatic methine protons, resonating between δ_H 7.09 to 9.28. Four protons were assignable to H-9, δH 7.68 (*d*, *J*=7.8); H-10, 7.24 (*t*, *J*=7.8); H-11, δ_H 7.39 (*t*, *J*=7.8) and H-12, δH 7.52 (*d*, *J*= 7.8). These protons were part of the indole moiety. At ring E, two deshielded aromatic protons, H-21 and H-17, appeared as a singlet at δ_H 9.28 and 8.85 due to the inductive effect by N-22 atom. The remaining two methine proton at δ_H 7.09 (*d*, *J*=5.0) and 7.31 (*d*, *J*=5.0) attached to C-18 and C-19 appeared as pair of doublets peaks, depicted the presence of the pentacyclic ring (ring-F) fused to the ring-D and E.

The ^{13}C NMR spectrum (Figure 4.35) revealed twenty carbons; eight aromatic methines, two methylene group, and ten quaternary carbons, including one lactam carbon which were agreement with the molecular formula of **G**.

Detailed analysis of the spectral data (COSY, HSQC, HMBC) and comparison with the literature review (Hotellier et al., 1979; Repke et al., 1988) (Table 4.11) confirmed

that structure **G** is naulafine **(33)**. However, no biological active reported on naulafine **(33)**.

Table 4.11: ^{1}H NMR (600 MHz) and ^{13}C NMR (150 MHz) spectral data of naulafine (33) in $CDCl_3$.

	Naulafine (33)		**Naulafine (Repke et al., 1988)**	
Position	δ_H (*m*, *J* in Hz)	δ_C	δ_H (*m*, *J* in Hz) in $DMSOd_6$,	δ_C in $DMSOd_6$,
1-NH				
2		140.7		140.3
3		140.1		139.8
4				
5	4.57 (*t*, *J*=6.7)	41.1	4.45 (*t*, *J*=6.6)	40.7
6	3.22 (*t*, *J*=6.7)	20.3	3.19 (*t*, *J*=6.6)	19.5
7		111.2		110.2
8		127.7		126.8
9	7.68 (*d*, *J*=7.8)	121.0	7.71(*d*, *J*=7.9)	120.2
10	7.24 (*t*, *J*=7.8)	121.4	7.15(*dd*, *J*=7.9, 8.0)	120.4
11	7.39 (*t*, *J*=7.8)	126.7	7.35(*dd*, *J*=8.0,8.0)	125.8
12	7.52 (*d*, *J*= 7.8)	112.1	7.60(*d*, *J*=8.0)	112.8
13		139.8		137.4
14		120.9		120.4
15		132.0		131.9
16		116.8		116.1
17	8.85 (*s*)	143.9	8.89 (*s*)	143.5
18	7.09 (*d*, *J*=5.0)	125.8	7.16 (*d*, *J*=5.0)	134.1
19	7.31 (*d*, J=5.0)	125.1	7.82 (*d*, *J*=5.0)	127.3
20		125.4		124.6
21	9.28 (*s*)	146.1	9.07 (*s*)	144.3
23		162.2		161.2

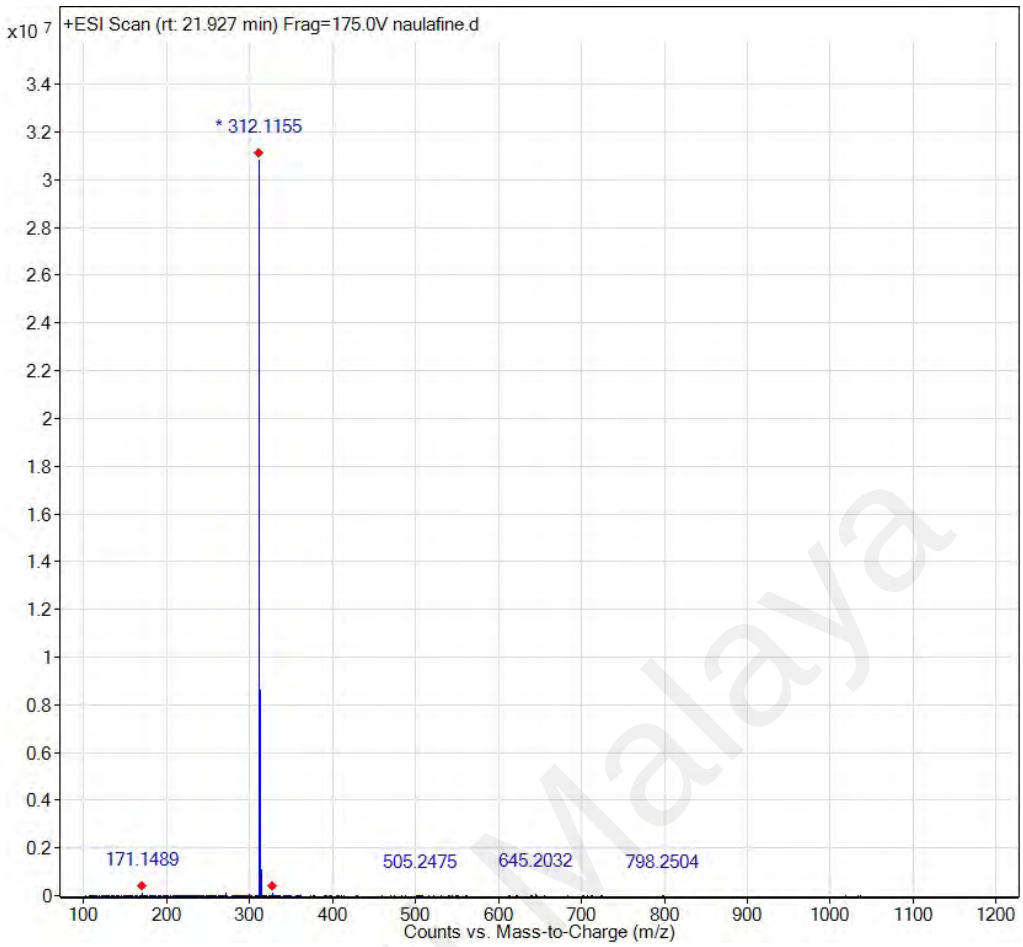

Figure 4.33: LC-ESI spectrum of naulafine (33).

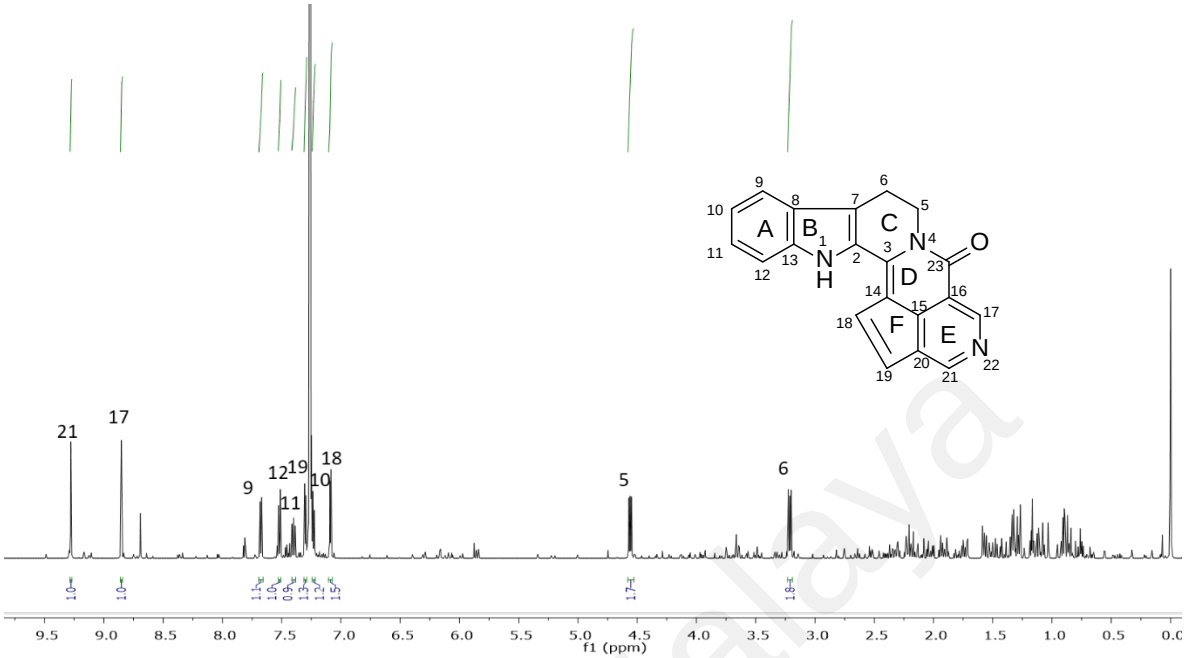

Figure 4.34: ^{1}H NMR spectrum of naulafine (33).

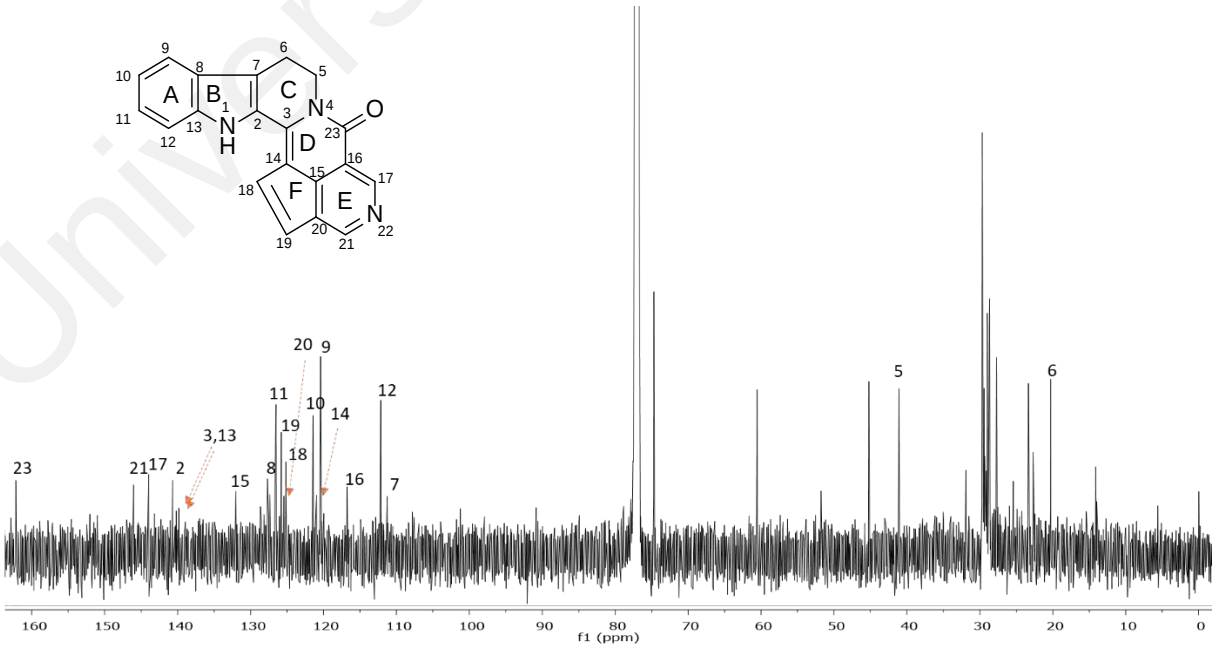

Figure 4.35: ^{13}C NMR spectrum of naulafine (33).

4.2.8 Compound H: Neonaucline (5)

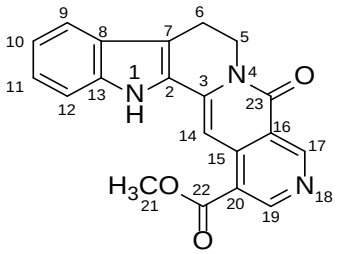

Compound **H** was yielded as a yellowish amorphous solid. In the UV spectrum (Appendix 9), absorption maximum was observed at 382, 298 and 205 nm which characteristic of an indole chromophore (Kam & Choo, 2004; Mukhtar et al., 1997; Zhou et al., 2008). The IR spectrum (Appendix 26) revealed absorption bands at 3364 and 1731 cm^{-1} for the stretching vibrations of NH and CO groups, respectively (Pavia et al., 2009). The LC-ESI spectrum (Figure 4.36) of **H** showed a pseudomolecular ion peak, at *m/z* 346.0926, $[M+H]^+$ (calc. 346.1193) that corresponded to the molecular formula of $C_{20}H_{16}N_3O_3$.

The ^{1}H NMR (Figure 4.37) and ^{13}CNMR (Figure 4.38) spectroscopic data of compound **H** show similarity to **G** (naulafine **(33)**). However, a significant difference can be seen in **H**, where it lacks the ring-F of **G**. The first detectable difference is that the proton signal at δ_H 7.87 exists as a singlet peak belonging to H-14. Second, the presence of ester functionality is inferred from the methoxy singlet at δ_H 4.01, which correlates with the carbonyl carbon δ_c 166.4 that attached to C-20 on ring E.

All these signals are reminiscent of the known alkaloid neonaucline **(5)**. Through analysis of COSY, HSQC and HMBC and comparison with literature review (Table 4.12) confirm the identify of **H** is neonaucline **(5)**. Hence, Neonaucline **(5)** were originated found on *O. mangayi* and reported with significant activity on vasorelaxant assay (Mukhtar et al., 2012), recently it was reported found in *Nauclea orientalis* from genus *Nauclea* (Liu et al., 2018).

Table 4.12: ^{1}H NMR (600 MHz) and ^{13}C NMR (150 MHz) spectral data of neonaucline (5) in $CDCl_3$.

	Neonaucline (5)		**Neonaucline (Mukhtar et al., 2012)**	
position	δ_H (*m*, *J* in Hz)	δ_C	δ_H (*m*, *J* in Hz) in $CDCl_3$	δ_C in $CDCl_3$
1			8.72 (*s*)	
2		127.3		127.4
3		138.2		138.2
4				
5	4.53 (*t*, *J*=6.7)	40.6	4.54 (*t*, *J*=6.8)	40.7
6	3.19 (*t*, *J*=6.7)	19.8	3.19 (*t*, *J*=6.8)	19.4
7		116.9		116.9
8		125.9		125.7
9	7.62 (*d*, *J*=7.9)	119.9	7.64 (*d*, *J*=7.8)	119.9
10	7.20 (*t*, *J*=7.9)	120.9	7.18 (*dd*, *J*=7.8,7.8)	120.9
11	7.35 (*t*, *J*=7.9)	125.6	7.35 (*dd*, *J*=7.8,7.8)	125.6
12	7.45 (*d*, *J*=7.9)	111.8	7.46 (*d*, *J*=7.8)	119.9
13		138.6		138.6
14	7.87 (*s*)	94.9	7.88 (*s*)	95.1
15		141.8		141.9
16		117.8		117.8
17	9.32 (*s*)	155.5	9.32 (*s*)	154.2
18				
19	9.68 (*s*)	154.4	9.69 (*s*)	155.4
20		120.4		120.4
21		166.4		166.4
22-OMe	4.01 (*s*)	52.4	4.00 (*s*)	52.5
23		161.4		166.4

Figure 4.36: LC-ESI spectrum of neonaucline (5).

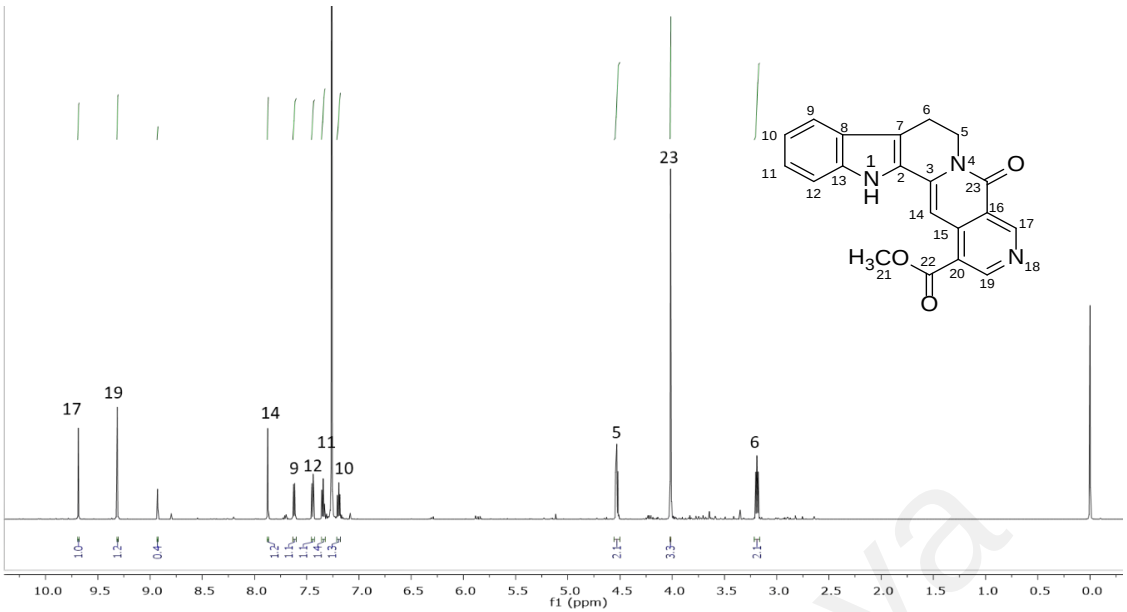

Figure 4.37: ^{1}H NMR spectrum of neonaucline (5).

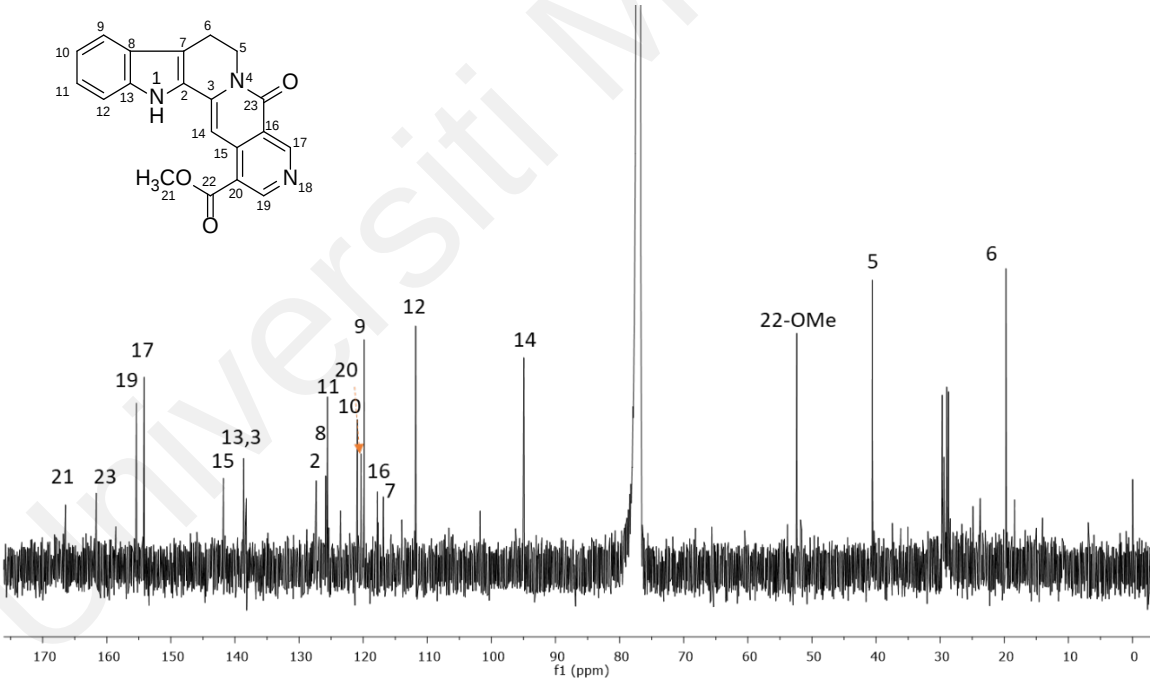

Figure 4.38: ^{13}C NMR spectrum of neonaucline (5).

4.2.9 Compound I: 1,2,3,4-Tetrahydronorharmane-1-one (151)

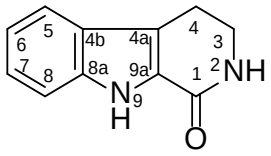

Compound **I** was isolated as a brownish amorphous solid. The LC-ESI spectrum showed a pseudomolecular ion peak at m/z 187.0896 $[M+H]^+$ (Figure 4.39), corresponding to the molecular formula $C_{11}H_{11}N_2O$ (calc 187.0872) $[M+H]^+$. In the UV spectrum (Appendix 10), absorption maxima of this compound were observed at 299 and 201 nm. In the IR spectrum (Appendix 26), absorption peaks were observed at 3233 and 1655 cm^{-1} observed due to NH and CO stretching respectively.

Analysis of the ^1H NMR spectrum (Figure 4.40), showed that **I** has similarity to **F**. However, the presence of two methylene protons at δ_H 3.73 (*dt*, J= 2.6, 7.0 Hz, H-7) and δ_H 7.32 (d, *J*= 7.0 Hz, H-4) shows that **I** do not have a double bond at C-3 and C-4. A broad singlet can be observed at δ_H 9.1 which was assigned to NH-9.

The ^{13}C NMR spectrum (Figure 4.41) of **I** showed a total of eleven carbon signals: two methylenes (42.3;C-3, 20.8;C-4), four methines (111.9;C-5, 120.4; C-6, 125.3; C-7, 112.4; C-8), four quaternary carbons (120.0; C-4a, 125.0;C-4b, 137.2; C-8a, 126.3; C-9a) and one carbonyl carbon (162.0; C-1). C-1 appeared at downfield region, the HMBC correlation of H-3 with this carbonyl signal indicating the presence of an oxo-*β*-carboline skeleton.

Based on the analysis of spectral data obtained (^1H, ^{13}C NMR, HSQC, COSY and HMBC) and comparison with literature values (Table 4.13) (Rao et al., 2003), the structure of compound **I** is 1,2,3,4-tetranorharmane-1-one **(151)** was confirmed. There are no biological active reported in **151**.

Table 4.13 : ^{1}H NMR (600 MHz) and ^{13}C NMR (150 MHz) spectral data of 1,2,3,4-tetranorharmane-1-one (151) in $CDCl_3$.

	1,2,3,4-tetranorharmane-1-one (151)		**1,2,3,4-tetranorharmane-1-one (Rao et al., 2003)**	
position	δ_H (*m*, *J* in Hz)	δ_C	δ_H (*m*, *J* in Hz) in $CDCl_3$	δ_C in $CDCl_3$
1		162.9		164.5
2-NH	5.7 (*s*)			
3	3.73 (*t*, *J*=7.0)	42.3	3.64 (*t*, *J*=14.2)	41.8
4	3.02 (*t*, *J*=7.0)	20.8	3.02 (*t*, *J*=14.1)	20.6
4a		120.0		120.0
4b		125.0		125.0
5	7.62 (*d J*=8.0)	111.9	7.59 (*d*, *J*=8.3)	111.9
6	7.16 (*t J*=8.0)	120.4	7.23 (*d*, *J*=8.5)	120.2
7	7.32 (*t J*=8.0)	125.3	7.26 (*t*, *J*=8.5)	124.9
8	7.46 (*d J*=8.0)	112.4	7.43 (*d*, *J*=8.3)	112.4
8a		137.2		
9-NH	9.1 (*s*)			
9a		126.3		125.8

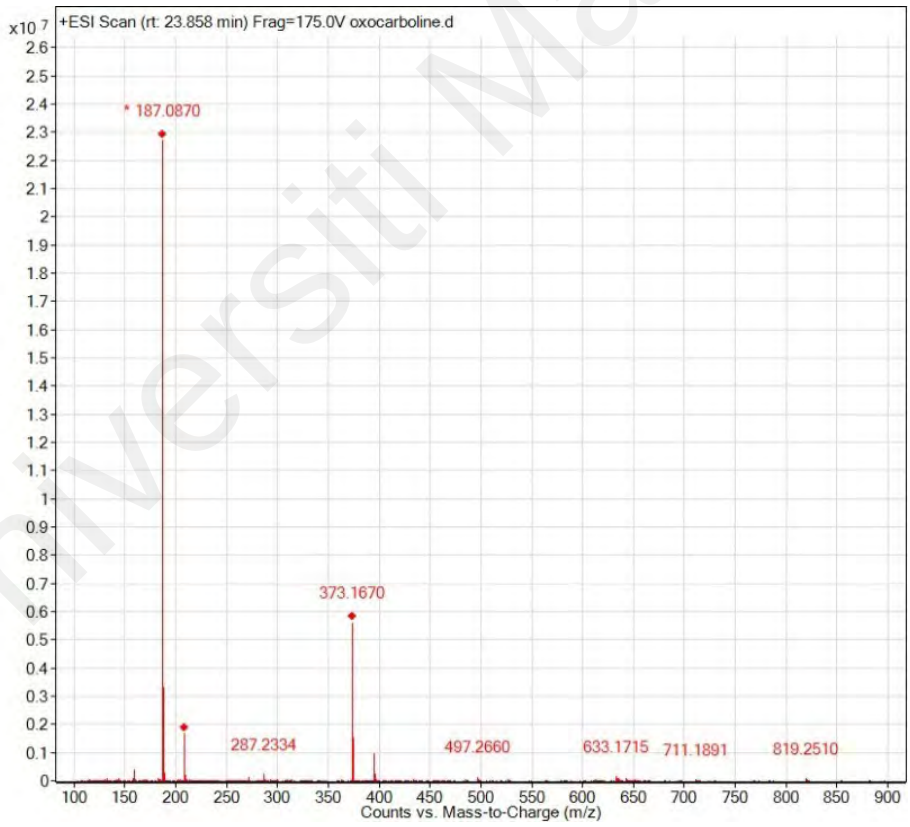

Figure 4.39: LC-ESI spectrum of 1,2,3,4-tetrahydronorharmane-1-one (151).

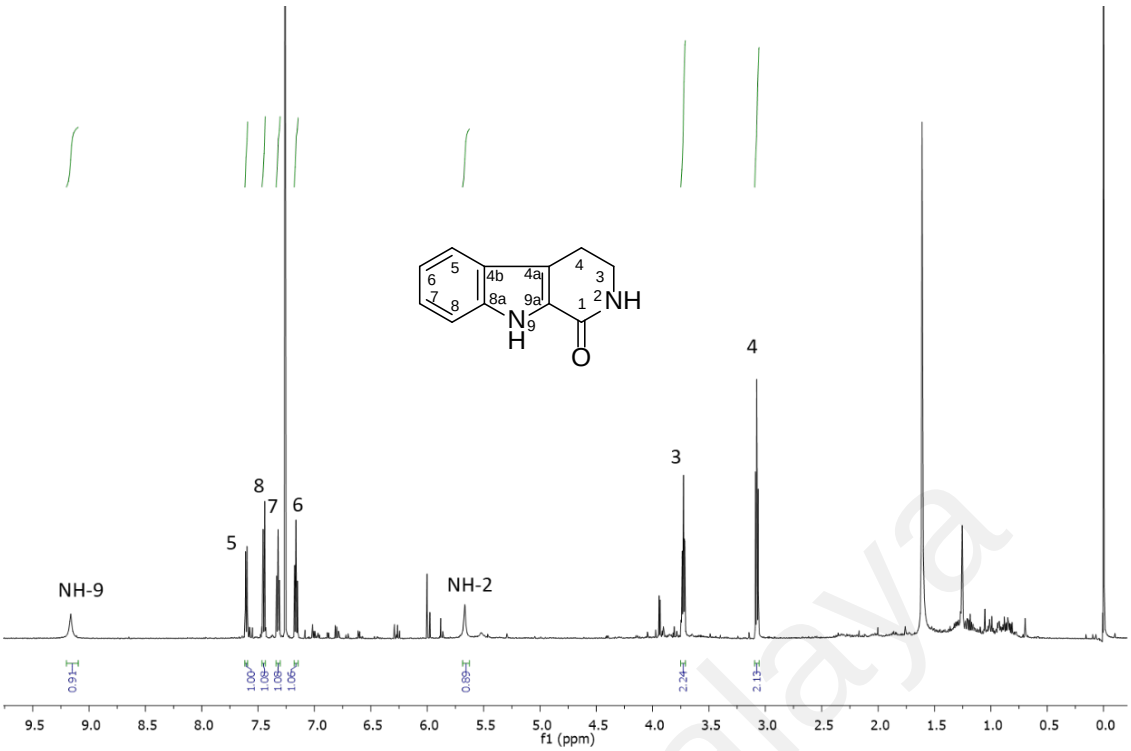

Figure 4.40: ^{1}H NMR spectrum of 1,2,3,4-tetrahydronorharmane-1-one (151).

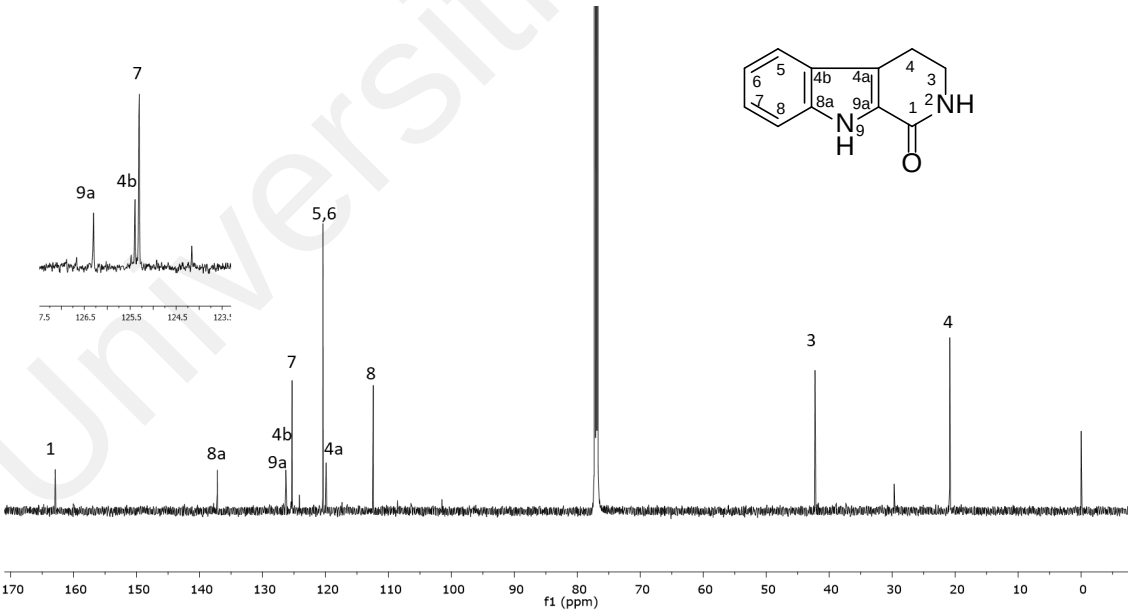

Figure 4.41: ^{13}C NMR spectrum 1,2,3,4-tetrahydronorharmane-1-one (151).

4.2.10 Compound J: Cinnamamide (152)

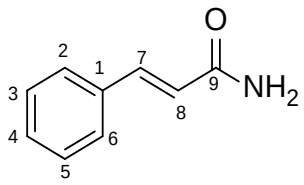

Compound **J** was obtained as a white amorphous solid. The LC-ESI spectrum (Figure 4.42) for compound **J** showed a pseudomolecular ion peak at *m/z* 148.0753 $[M+H]^+$ (calc 148.0763) corresponding to the molecular formula $C_9H_{10}NO$. The UV spectrum (Appendix 11) showed the absorption maxima at 266 nm. The IR spectrum (Appendix 27) of this compound showed significant peaks at 3368 and 1655 cm^{-1} conforming the presence of amide group and carbonyl group.

The proton signals at δ_H 6.46 (*br d, J*= 15.7 Hz, H-8) and δ_H 7.65 (*br d, J*= 15.7 Hz, H-7) in the ^1H NMR spectrum (Figure 4.43) represent a trans-substituted double bond. The presence of a monosubstituted aromatic ring could be deduced from the proton signals observed at δ_H 7.39-7.37 (*m*, H-2 & H-6) and 7.51 (*m*, H-3, H4, H-5) respectively. The presence of the NH_2 group was indicated by the broad signals at δ_H 5.59.

In the ^{13}C NMR spectrum (Figure 4.44), nine carbons appeared in agreement with the molecular formula of **J**. Two overlapping carbon peaks at δ_c 128.0 (C-2 with C-6) and 128.9 (C-3 with C-5) showed at the same chemical shift, which is due to the equivalence of the environment in the aromatic ring.

The detailed analysis of the NMR data is shown in Table 4.14. The comparison of the data with values from the literature confirms the structure of **J** is cinnamamide **(152)** (Ernawati et al., 2020; Saidi, 2010). Cinnamamide **(152)** or cinnamic acid amide, is a well-known natural product compound. **152** and its derivatives have a wide range of biological activity, including anticancer, anti-inflammatory, anti-trypanosomal, antitubercular, anti-microbial, antiviral, anti-diabetic and anti-malarial (Gaikwad et al., 2019).

Table 4.14 :^{1}H NMR (600 MHz) and ^{13}C NMR (150 MHz) spectral data of cinnamamide (152) in $CDCl_3$.

	Cinnamamide (152)		Cinnamamide (Ernawati et al., 2020)	
Position	δ_H (*m*, *J* in Hz)	δ_C	δ_H (*m*, *J* in Hz) in $CDCl_3$	δ_C in $CDCl_3$
1		134.6		134.5
2	7.51 (*m*)	128.0	7.47 (*dd*, J=9.75)	128.1
3	7.39-7.37 (*m*)	128.9	7.35 (*dt*, *J*=3.9, 9.75)	128.9
4	7.39-7.37 (*m*)	130.1	7.35 (*dt*, *J*=3.9, 9.75)	130.2
5	7.39-7.37 (*m*)	128.9	7.35 (*dt*, *J*=3.9, 9.75)	128.9
6	7.51 (*m*)	128.0	7.47 (*dd*, *J*=9.75	128.1
7	7.65 (*d*, *J*=15.7)	142.6	7.64 (*d*,*J*=16)	143.1
8	6.46 (*d*, *J*=15.7)	119.6	6.43 (*d*,*J*=16)	119.2
9		168.1		168.3
NH_2	5.59 (*bs*)			

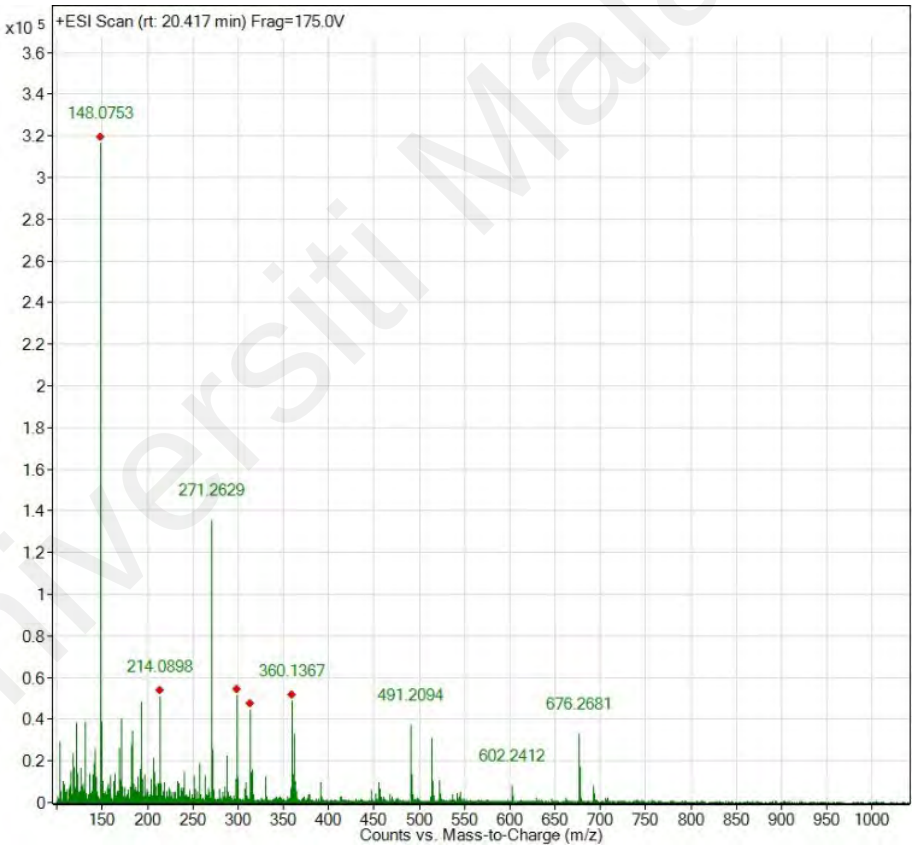

Figure 4.42: LC-ESI spectrum of cinnamamide (152).

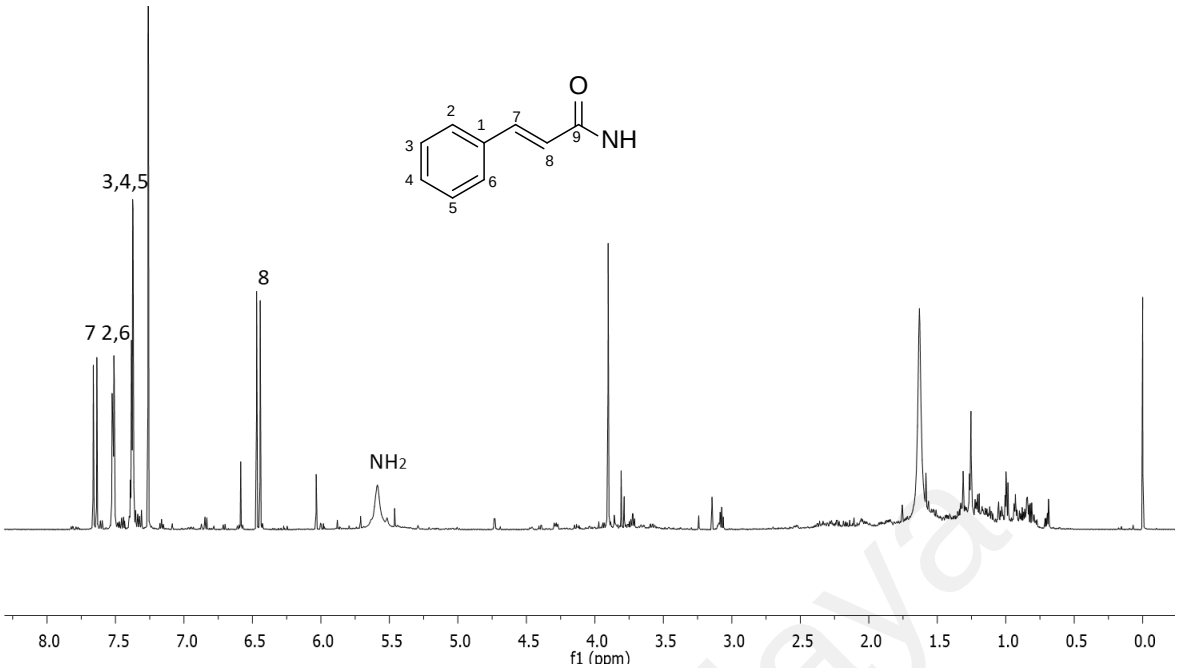

Figure 4.43: ^{1}H NMR spectrum of cinnamamide (152).

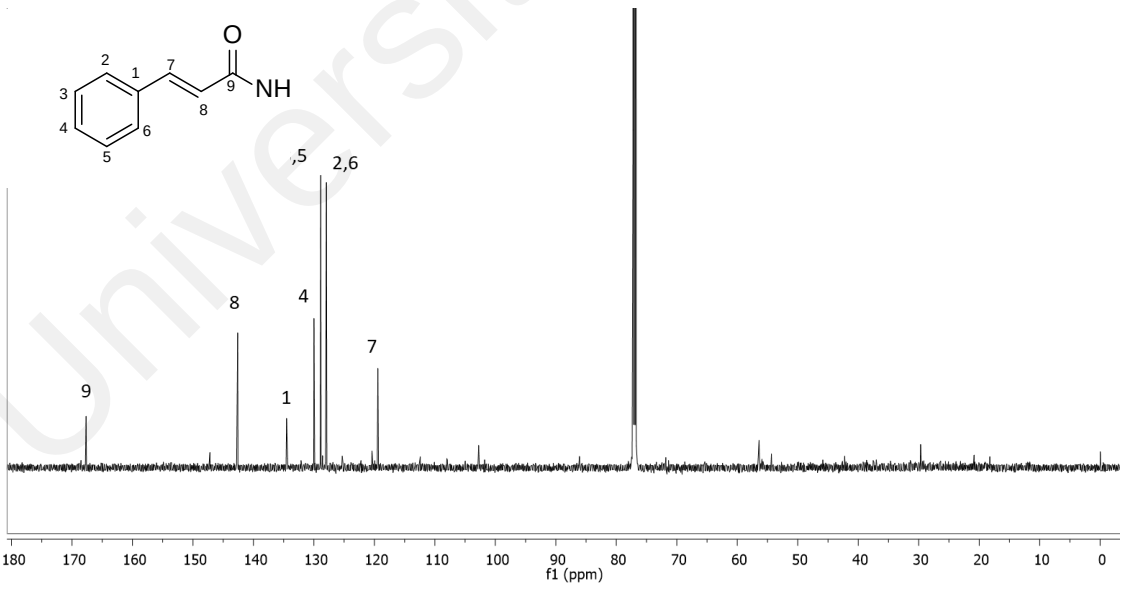

Figure 4.44: ^{13}C NMR spectrum of cinnamamide (152).

4.2.11 Compound K: Benzamide (153)

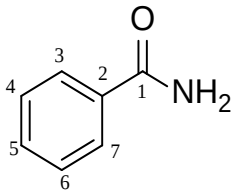

Compound **K** was isolated as a crystalline needle. LC-ESI showed a pseudomolecular ion peak at *m/z* 122.0598 (Figure 4.45) (calc 122.0606) $[M+H]^+$ with agreement of the molecular formula C_7H_8NO. The IR spectrum (Appendix 28) exhibited a strong peak at 1646 cm^{-1} attributed to a conjugated carbonyl group, while the peak at 3365 cm^{-1} indicated the binding of amide in the structure. The UV spectrum (Appendix 12) displayed the absorption maxima at 241 nm.

In the ^{1}H NMR spectrum (Figure 4.46), two triplets and one doublet signal appeared in the aromatic region, indicating that the ring was monosubstituted. The doublet peak of H-3 and H-7 appeared at δ_H 7.85 (*d*, *J*=7.4), while the proton signal H-4 and H-6 appeared as a triplet at δ_H 7.47 (*t*, *J*=7.4). In addition, signal H-5 appeared as a triplet peak at δ_H 7.55 (*t*, *J*=7.4). The broad singlet peak of NH_2 appeared at δ 6.32.

The ^{13}C NMR spectrum (Figure 4.47) confirms that seven carbon atoms are present. Two groups of methine carbon peaks, C-3 with C-7 and C-4 with C-6, overlapped at δc 127.3 and 128.6, respectively. C-5 was another methine carbon that appeared at δc 133.4. Two quaternary carbon signals, C-1 and C-2 showed peaks at δc 169.4 and 131.9, respectively.

Analysis of the spectroscopic data and comparison with data from literature (Table 4.15) (Saidi, 2010; Wu et al., 2012), confirmed that compound **K** is benzamide **(153)**. Benzamide **(153)** derivatives have many medical uses, such as killing microbes, relieving pain, reducing inflammation, fighting cancer, protecting the heart, and more. Because of this biological importance, scientists have been working on making a lot of new benzamide compounds (Asif, 2016).

Table 4.15: ^{1}H NMR (400 MHz) and ^{13}C NMR (100 MHz) spectral data of benzamide (153) in $CDCl_3$.

	Benzamide (153)		**Benzamide (Wu et al., 2012)**	
Position	δ_H (*m*, *J* in Hz)	δ_C	δ_H (*m*, *J* in Hz) in $CDCl_3$	δ_C in $CDCl_3$
NH_2	6.32 *br s*	-	6.04 (*bs*)	
1	-	169.4		169.9
2	-	133.4		133.3
3	7.85 (*d*, *J*=7.4)	127.3	7.73-7.80 (*m*)	127.4
4	7.47 (*t*, *J*=7.4)	128.6	7.34-7.51 (*m*)	128.7
5	7.55 (*t*, *J*=7.4)	131.9	7.34-7.51 (*m*)	132.1
6	7.47 (*t*, *J*=7.4)	128.6	7.34-7.51 (*m*)	128.7
7	7.85 (*d*, *J*=7.4)	127.3	7.73-7.80 (*m*)	127.4

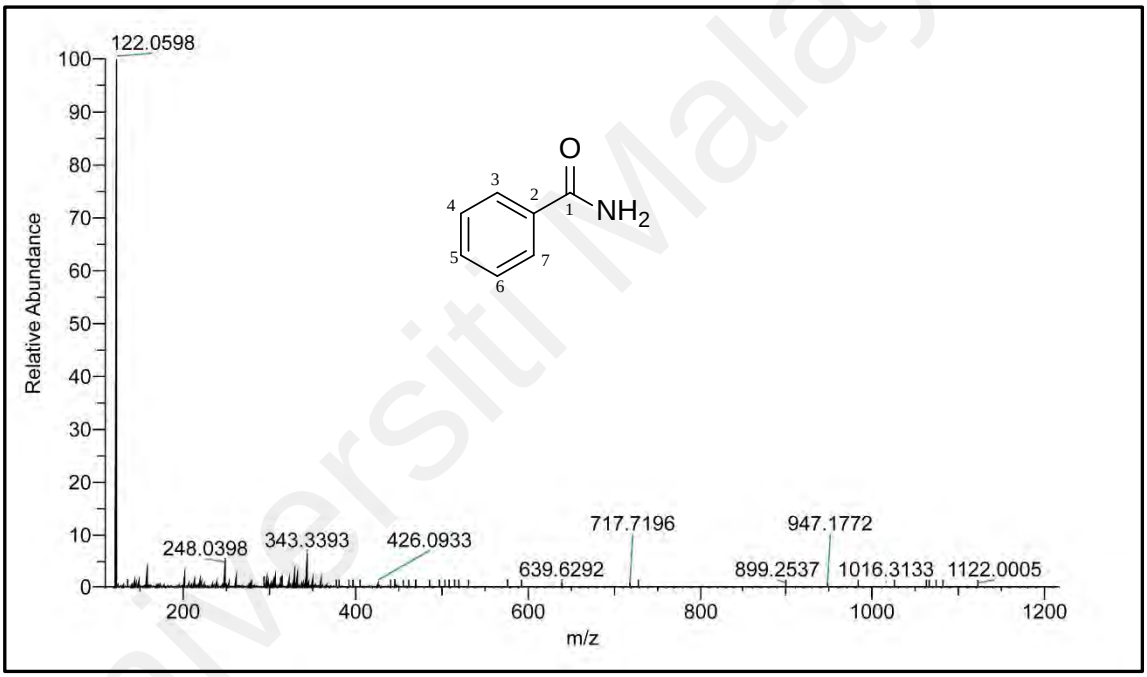

Figure 4.45: LC-ESI spectrum of benzamide (153).

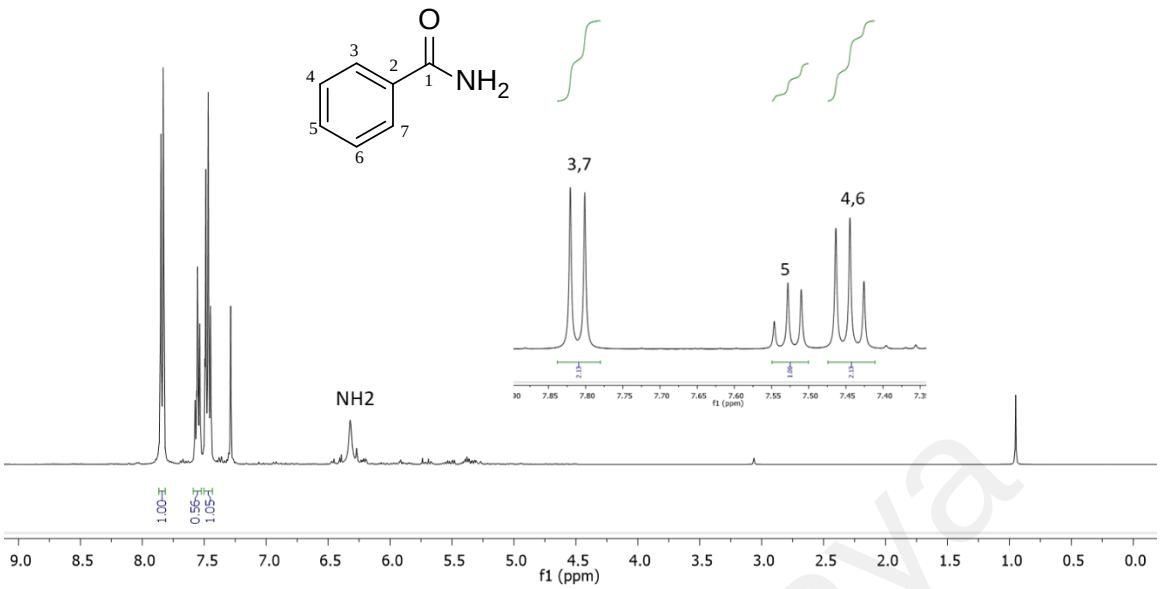

Figure 4.46: ^{1}H NMR spectrum of benzamide (153).

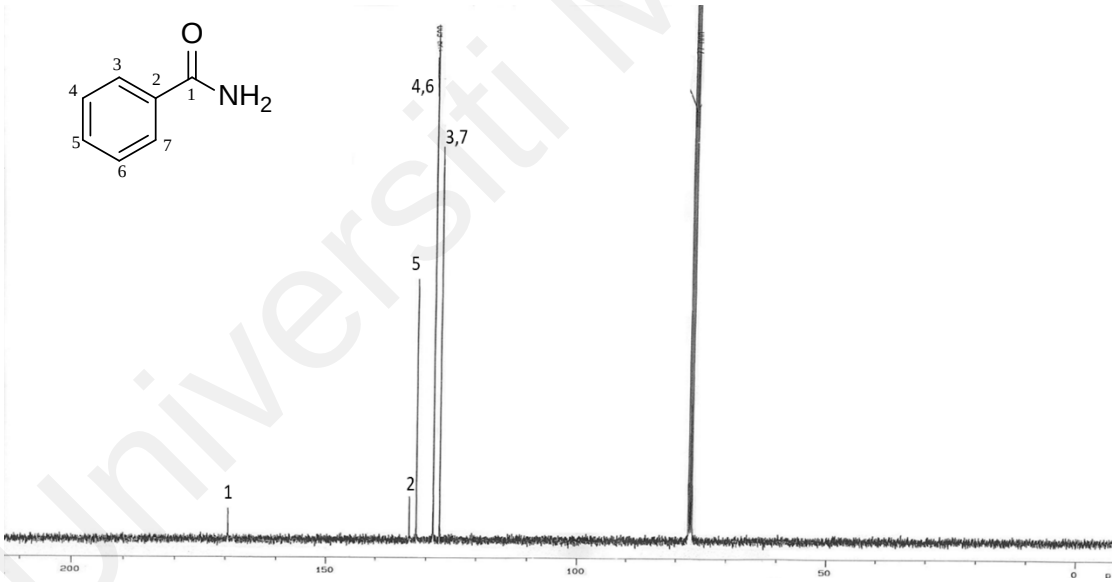

Figure 4.47: ^{13}C NMR spectrum of benzamide (153).

4.2.12 Compound L: Scopoletine (154)

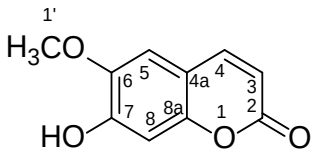

Compound **L** was isolated as pale yellow amorphous and exhibited blue fluorescence under UV light. The LC-ESI spectrum (Figure 4.48) revealed a pseudo molecular ion peak at *m/z* 193.0402 (calc. 193.0501) $[M+H]^+$, suggesting molecular ion formula $C_{10}H_9O_4$. The UV spectrum (Appendix 13) showed maximum absorption at 204, 228, 296 and 344 nm. The IR spectrum (Appendix 30) showed absorption maxima at 3383.0 cm^{-1}, indicating the presence of a hydroxyl functional group.

The ^1H NMR spectra (Figure 4.49) of **L** showed the presence of two doublets signal at δ_H 6.30 (d, *J*= 9.5 Hz) and δ_H 7.64 (d, *J*= 9.5 Hz) came from H-3 and H-4 respectively, characteristic of the pyrone ring of coumarin (Khan & Sagar, 2015). The presence of two aromatic proton singlet peaks at δ_H 7.03 and 7.12 was attributed to H-5 and H-8, respectively. In this spectrum, a three protons singlet peak at δ3.75 ppm was assigned for methoxy proton belonging to C-6. The ^{13}C NMR spectrum (Figure 4.50) of **L** exhibited ten carbons peak present in this compound, one is carbonyl peak appear at δ_c 161.3.

Finally, through analysis of all NMR spectra (^1H, ^{13}C, COSY, HSQC, HMBC) and upon comparison with the literature review the structure of compound **L** was confirmed (Table 4.16) as scopoletine **(154)** isolated from the plant *Uncaria cordata* (Abdullah et al., 2016). **154** has been shown to have pharmacological effects, such as those of an antioxidant agent, antibacterial, antituberculous, antifungal, and antihepatotoxic, in in vitro experiments. Antithyroid, , anti-proliferative, antihypertensive, anti-inflammatory, anti-adrenergic and anti-dopaminergic, anti-hyperuricemic, and antidiabetic actions are all examples of pharmacological effects that have been demonstrated *in vivo* (Firmansyah et al., 2021).

Table 4.16: ^{1}H NMR (600 MHz) and ^{13}C NMR (150 MHz) spectral data of scopoletine (154) in pyridine-d_5.

	Scopoletine (154)		Scopoletine (Abdullah et al., 2016)	
Position	δ_H (*m*, *J* in Hz)	δ_C	δ_H (*m*, *J* in Hz) in $CDCl_3$	δ_C in $CDCl_3$
2		161.3		161.5
3	6.30 (*d*, *J*=9.5)	112.2	6.30 (*d*, *J*=9.42)	113.4
4	7.67 (*d*, *J*=9.5)	143.8	7.63 (*d*, *J*=9.48)	143.3
4a		110.9		111.5
5	7.04 (*br s*)	109.3	6.87 (*br*, *s*)	107.5
6		146.0		150.3
7		152.8		144.0
8	7.12 (*br s*)	103.9	6.95 (*br*, *s*)	103.2
8a		150.3		149.7
OMe	3.75 (*s*)	55.9	3.98 (*s*)	56.4

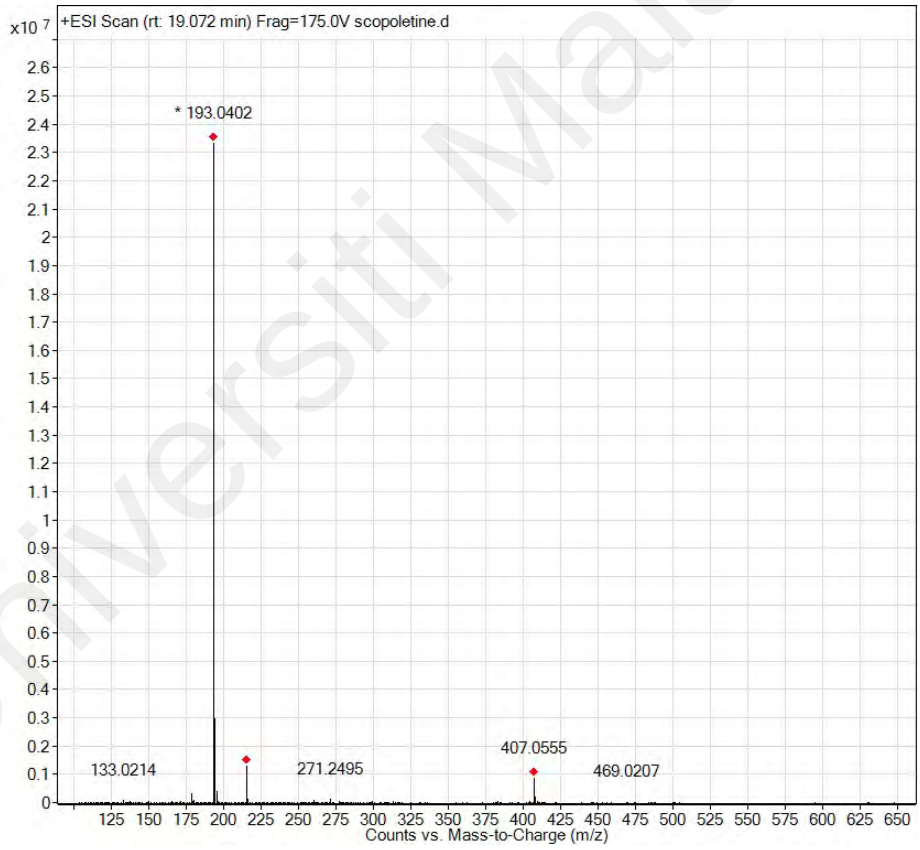

Figure 4.48: LC-ESI spectrum of scopoletine (154).

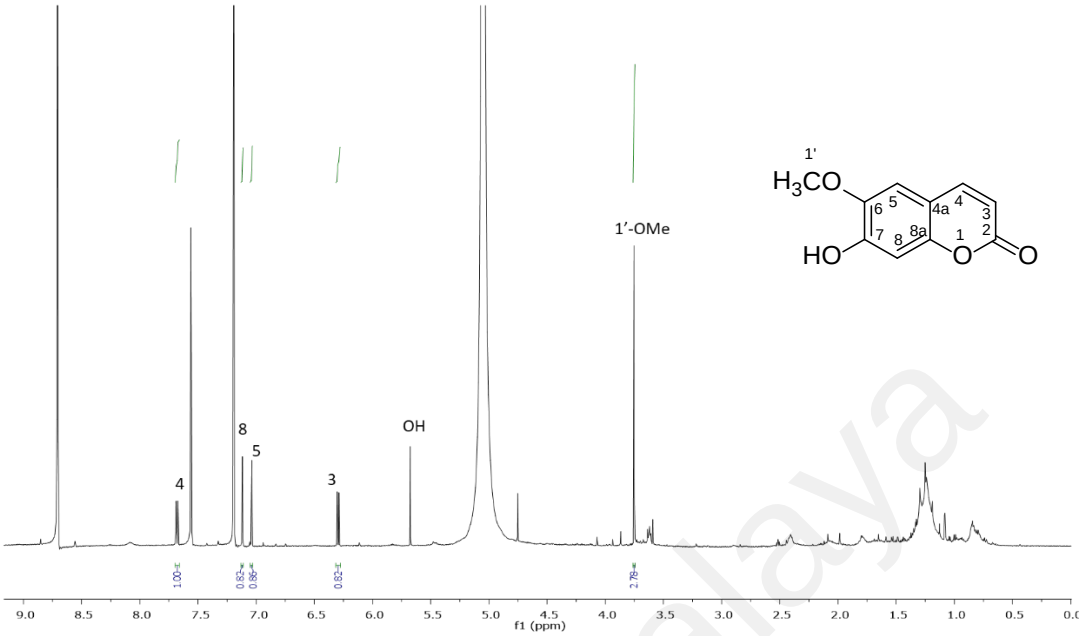

Figure 4.49: ^{1}H NMR spectrum of scopoletine (154).

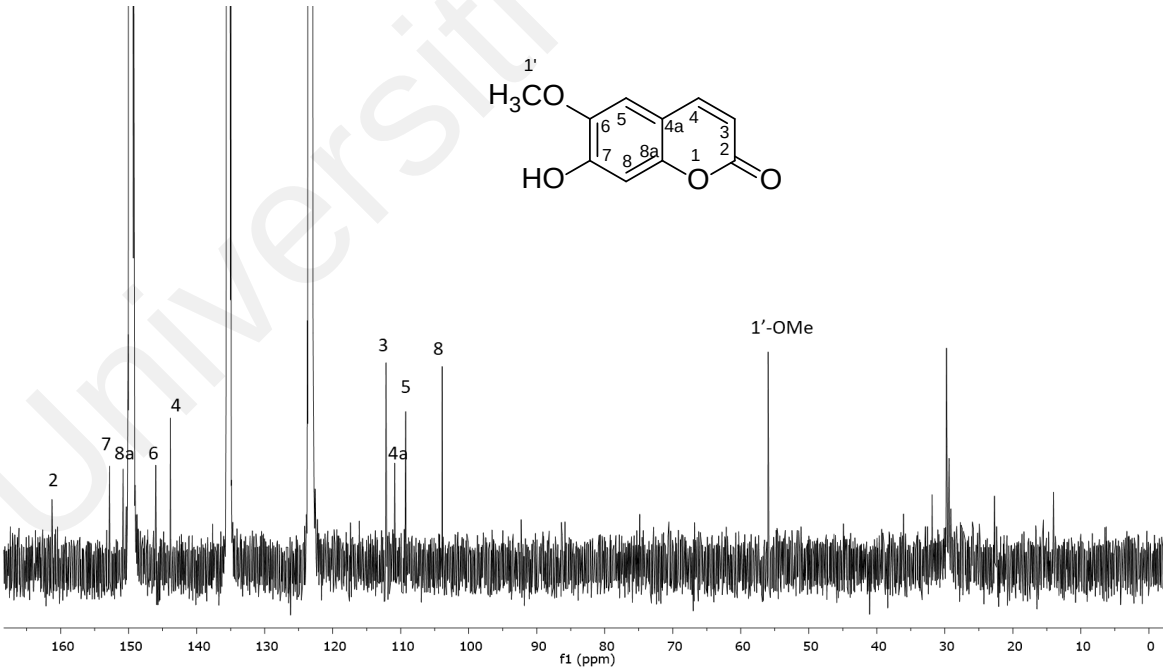

Figure 4.50: ^{13}C NMR spectrum of scopoletine (154).

4.2.13 Compound M: 4'-Hydroxyacetophenone (155)

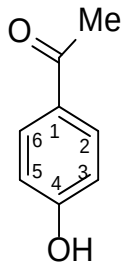

Compound **M** was found as a solid, amorphous, and light beige substance. Analysis of the LC-ESI spectrum (Figure 4.51) revealed a pseudomolecular ion with *m/z* at 137.0754 (calcd. 137.0603) $[M+H]^+$, which is due to the molecular formula of $C_8H_9O_2$. The UV spectrum (Appendix 14) showed the absorption maxima at 276, 218 and 204 nm. The IR spectrum (Appendix 31) indicated the presence of the OH group at 3351 cm^{-1} and carbonyl group at 1663 cm^{-1}.

The ^{1}H NMR spectrum (Figure 4.52) showed that compound **M** is a 1,4 -disubstituted aromatic ring attached to the OH and methoxy groups with its two typical AA'BB' doublets signals at δ_H 7.90 (*bd*, *J*=8.6); (H-2, H-6) and δ_H 6.88 (*bd*, *J*=8.6); (H-3, H-5). The ^{13}C NMR spectrum (Figure 4.53) exhibited eight carbons: three quaternary, four methine, and one methyl group.

The complete assignments of the ^{1}H NMR and ^{13}C NMR spectroscopy data of compound **M** were achieved with the aid of COSY, HMBC and HSQC experiments. All the above-mentioned NMR spectroscopic data of compound **M** and upon comparison with literature (Gatenyo et al., 2013)(Table 4.17), revealed as a 4'-hydroxyacetophenone **(155)** and has been reported as antiviral (Huang et al., 2014).

Table 4.17: ^{1}H NMR (600 MHz) and ^{13}C NMR (150 MHz) spectral data of 4' -hydroxyacetophenone (155) in $CDCl_3$.

	4'-hydroxyacetophenone (155)		4'-hydroxyacetophenone (Gatenyo et al., 2013)	
Position	δ_H (*m*, *J* in Hz)	δ_C	δ_H (*m*, *J* in Hz) in $CDCl_3$	δ_C in $CDCl_3$
1		130.6		129.6
2	7.90 (*d*, *J*=8.6)	130.9	7.91 (*d*, *J*=8.5)	131.3
3	6.88 (*d*, *J*=8.6)	115.3	6.95 (*d*, *J*=8.5)	115.6
4		160.0		161.6
5	6.88 (*d*, *J*=8.6)	115.3	6.95 (*d*, *J*=8.5)	115.6
6	7.90 (*d*, *J*=8.6)	130.9	7.91 (*d*, *J*=8.5)	131.3
1'		196.8		198.6
2'	2.55 (*s*)	26.3	2.60 (*s*)	26.4

Figure 4.51: LC-ESI spectrum of 4'-hydroxyacetophenone (155).

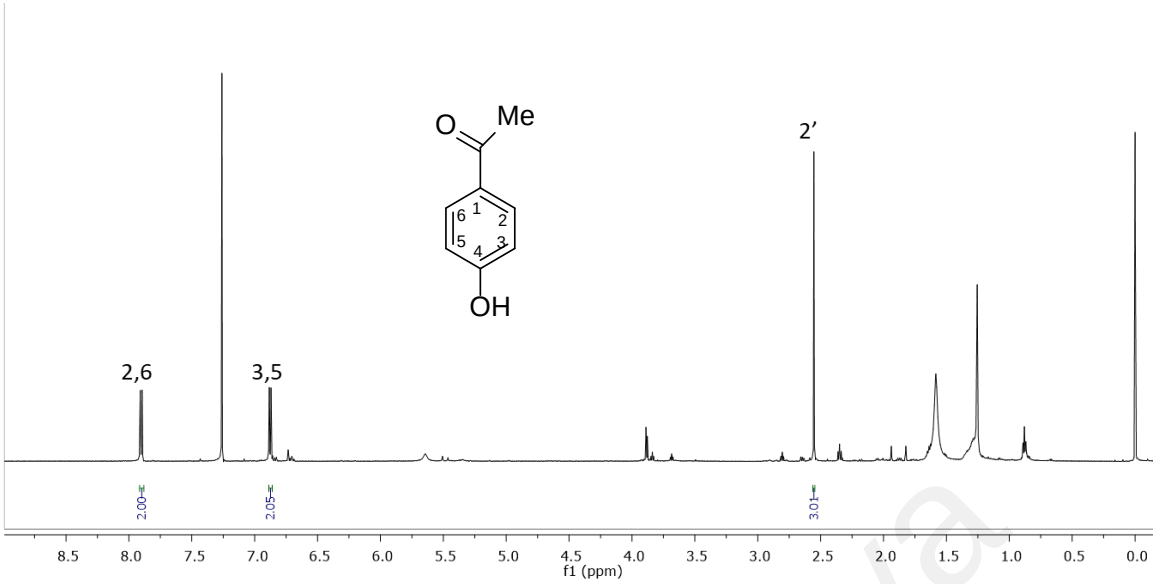

Figure 4.52: ^{1}H NMR spectrum of 4’-hydroxyacetophenone (155).

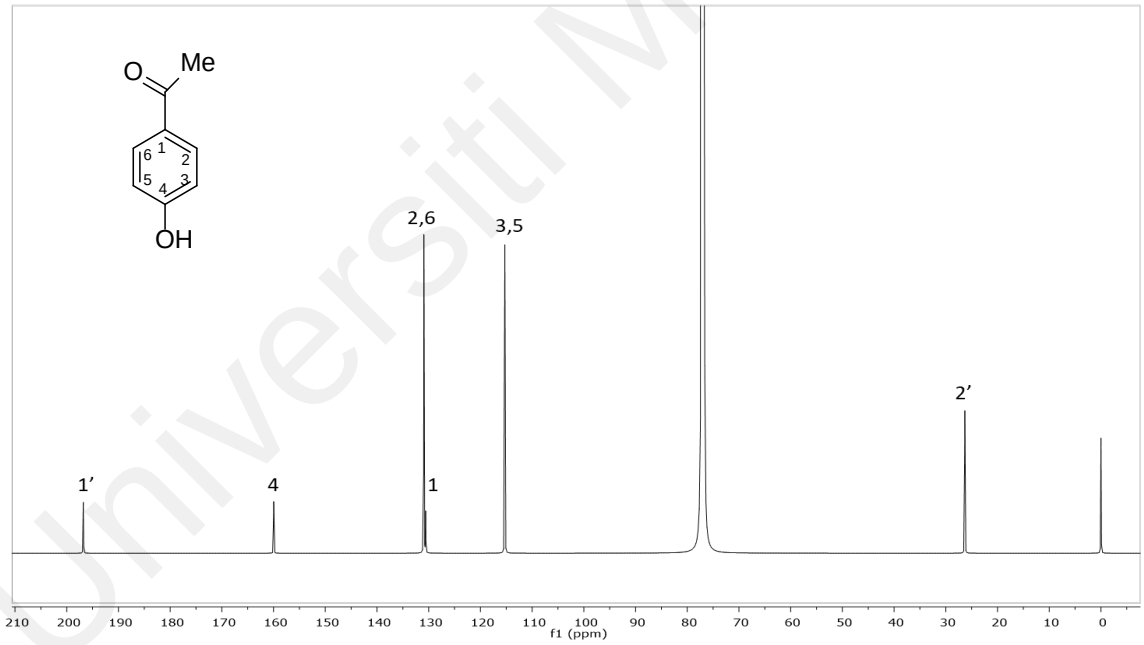

Figure 4.53: ^{13}C NMR spectrum of 4’-hydroxyacetophenone (155).

4.2.14 Compound N: Decarboxylportentol acetate (156)

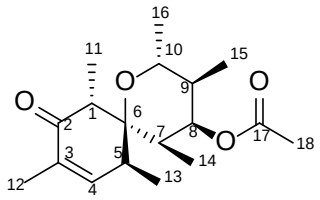

Compound **N** was obtained as a colorless amorphous solid, $[\alpha]_D^{28}$ = +97.86 (c 0.007, $CHCl_3$), showed the molecular formula $C_{18}H_{29}O_4$ determined by LC-ESI (Figure 4.54) at m/z 309.2038 (calc. 309.2067) $[M+H]^+$. The UV spectrum (Appendix 15) revealed absorption maxima at 241 nm. The IR (Appendix 32) absorptions at 1742 and 1666 cm^{-1} indicated the presence of carbonyl and 1231 cm^{-1} the ether functionalities.

^{1}H NMR displayed seven methyl group that attached to C-1, C-3, C-5, C-7, C-9, C-10 and C-17 (Figure 4.55).The proton H-4 appeared as a doublet of doublet (*J*= 6.4,1.3 Hz) at δ_H 6.60 in the uppermost field, being surrounded by H-5. In the other ring, proton H-8 appeared at upfield region due to the linkage with the ester group.

The ^{13}C NMR spectrum revealed 18 carbon signals due to one sp3 quaternary carbon, two carbonyl carbons, one olefinic, one sp2 methine, six sp3 methine, and seven methyl carbons (Figure 4.56). Among them, four carbons (δ_c 76.7, 80.7, 170.6, and 200.5) belonged to C-8, C-6, C-17 and C-2 were attributed to those bearing an oxygen atom.

All these signals are reminiscent of the polyketide decarboxylportentol acetate **(156)**. Analysis of COSY, HSQC, HMBC and NOESY and comparison with the literature review (Table 4.18) (Morita et al., 2012) confirmed the identification of **N**. It first isolated in *Laumoniera bruceadelpha* and showed significant activity toward antiplasmodium (Morita et al., 2012).

Table 4.18: ^{1}H NMR (600 MHz) and ^{13}C NMR (150 MHz) spectral data of decarboxylportentol acetate (156) in $CDCl_3$.

	Decarboxylportentol acetate (156)		Decarboxylportentol acetate (Morita et al., 2012)	
Position	δ_H (*m*, *J* in Hz)	δ_C	δ_H (*m*, *J* in Hz) in $CDCl_3$	δ_C in $CDCl_3$
1	2.76 (*q*, J= 6.8)	46.6	2.79 (*q*, *J*=6.8)	46.6
2		200.5		200.5
3		133.4		133.5
4	6.60(*dd*, *J*= 6.4,1.3)	147.4	6.62 (*d*, *J*= 6.6)	147.4
5	3.35(*dq*, *J*= 6.7,6.4)	33.9	3.37 (*dq*, *J*= 6.6, 7.0)	33.9
6		80.7		80.7
7	2.06 (*m*)	37.1	2.09 (*dq*, *J*= 2.9, 7.3)	37.1
8	5.10 (*t*, *J*= 3.1)	76.7	5.13 (*dd*, *J*=3.0, 2.9	76.9
9	1.53 (*m*)	40.5	1.56 (*m*)	40.5
10	3.54(*dq*, *J*= 6.0,12.3)	66.3	3.56 (*dq*, *J*=12.2, 6.3)	66.3
11	1.14(*d*, *J*= 6.8)	7.3	1.16 (*d*, *J*= 6.8)	7.3
12	1.70(*s*)	15.6	1.72 (*s*)	15.6
13	1.01 (*d*, *J*= 6.7)	14.6	1.13 (*d*, *J*=7.0)	14.7
14	0.60 (*d*, *J*= 7.4)	16.9	0.62 (*d*, *J*= 7.3)	17.0
15	0.76 (*d*, *J*= 6.9)	12.9	0.79 (*d*, *J*= 6.9)	12.9
16	1.01 (*d*, *J*= 6.0)	19.0	1.14 (*d*, *J*= 6.3)	19.0
17		170.6		170.6
18	2.08 (*s*)	20.9	2.10 (*s*)	20.9

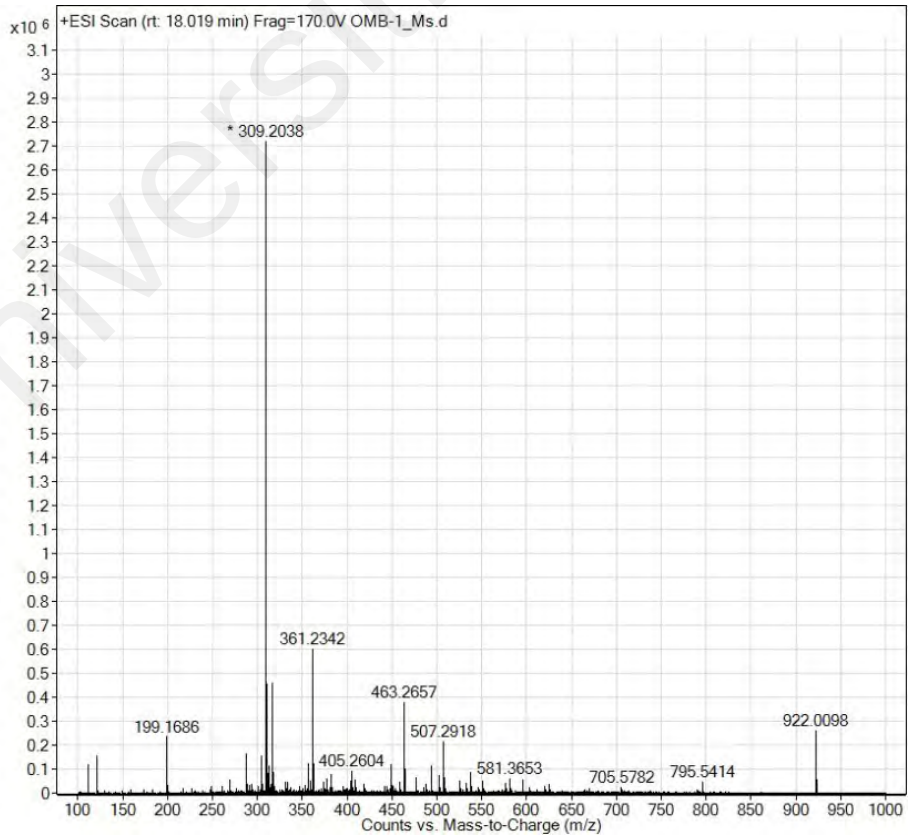

Figure 4.54: LC-ESI spectrum of decarboxylportentol acetate (156).

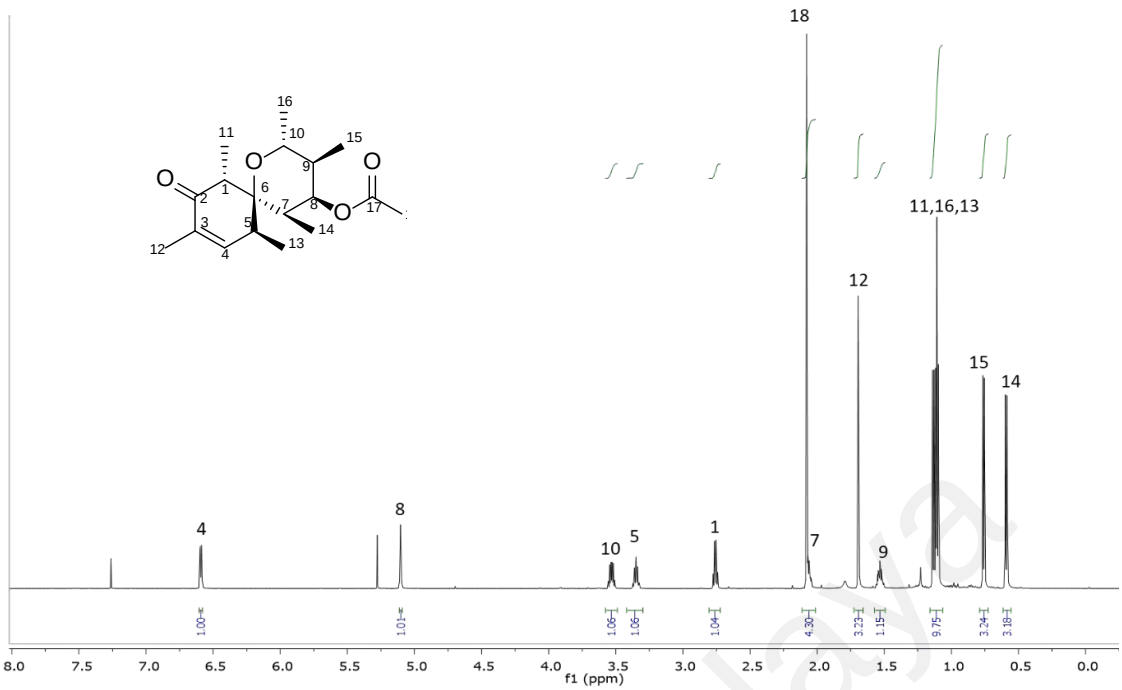

Figure 4.55: ^{1}H NMR spectrum of decarboxylportentol acetate (156).

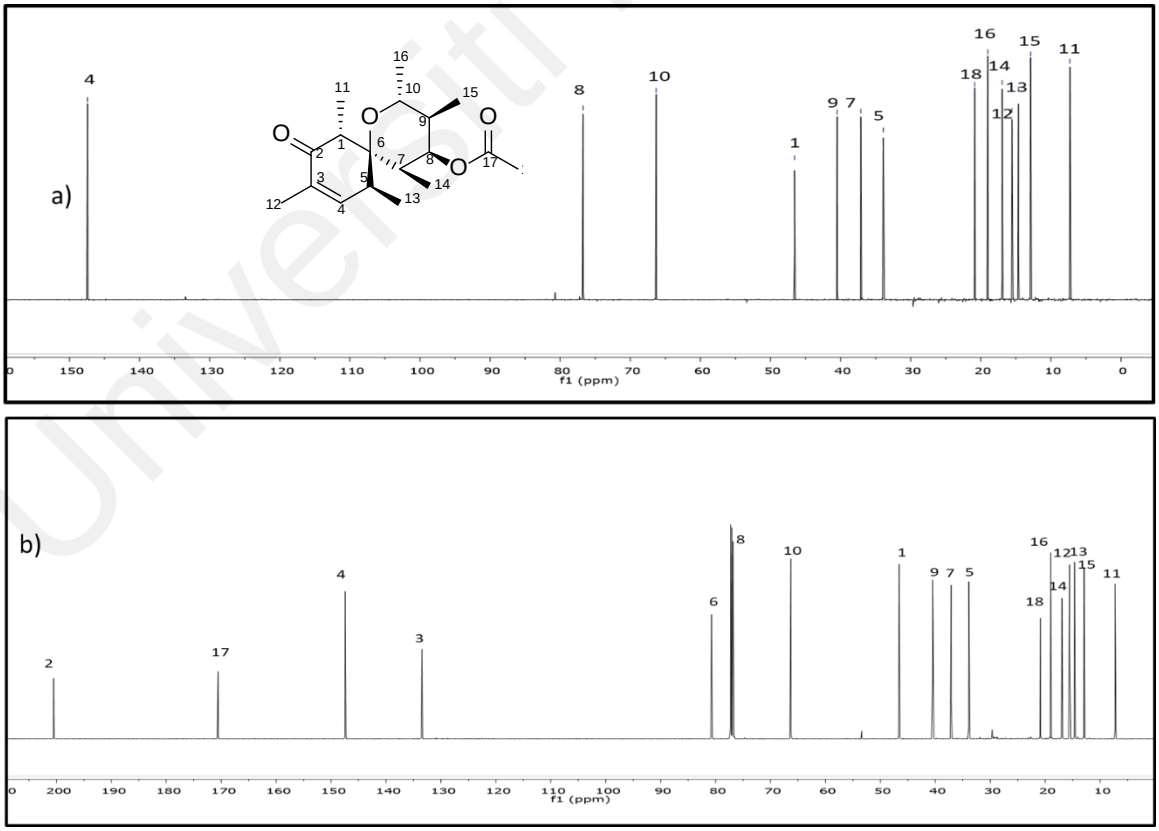

Figure 4.56: a) DEPT135 b) ^{13}C NMR spectra of decarboxylportentol acetate (156).

4.2.15 Compound O: Scoparone (157)

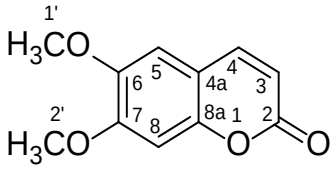

Compound **O** was found to be a white, solid, amorphous compound that also exhibits blue fluorescence when exposed to UV light, similar to scopoletine **O**. The LC-ESI spectrum (Figure 4.57) revealed a pseudomolecular ion peak at *m/z* 207.0650 (calc. 207.0657) $[M+H]^+$, signifying molecular ion formula $C_{11}H_{11}O_4$. The UV spectrum (Appendix 16) showed bands with the maximum absorption at 204, 271 and 290 nm. The IR spectrum (Appendix 33) revealed that absorption maxima at 1732 cm^{-1} due to the carbonyl group.

The spectral data showed that (Table 4.15 and 4.17) **O** were in close agreement with scopoletine **(154)**. The ^1H NMR spectrum (Figure 4.57) displayed signals characteristic of a coumarin. The lactone ring protons showed an AB pattern for H-3 (δ 6.30, *d, J* = 9.6 Hz) and H-4 (δ 7.64, *d, J* = 9.6 Hz). The two singlets at δ_H 6.*85* and δ_H 6.86 ascribed to the aromatic proton at C-5 and C-8. It was found that there were no hydroxyl groups, and that C-7 had an extra methoxy group.

The identification of the compound and its ^{13}C NMR (Figure 4.59) assignments were established unambiguously by 2D NMR studies. The ^1H NMR and ^{13}C NMR data (Table 4.19) of **O** were found to be identical to those reported for scoparone **(157)** (Intekhab & Aslam, 2009). Taking these data into consideration, **O** was identified as scoparone **(157)**. It has been reported as anti-tumour, anti-coagulant, antioxidant, anti-microbial, anti-inflammatory, and showed gastroprotective efficacy (Kim et al., 2013; Son et al., 2015).

Table 4.19: ^{1}H NMR (600 MHz) and ^{13}C NMR (150 MHz) spectral data of scoparone (157) in $CDCl_3$.

	Scoparone (157)		**Scoparone (Intekhab & Aslam, 2009)**	
position	δ_H (*m*, *J* in Hz)	δ_C	δ_H (*m*, *J* in Hz) in $CDCl_3$	δ_C in $CDCl_3$
2		161.3		164.4
3	6.30 (*d J*=9.5)	113.5	6.15 (*d J*=9.6)	116.6
4	7.64 (*d J*=9.5)	143.2	7.86 (*d J*=9.6)	139.4
4a		104.7		104.7
5	6.85 (*br s*)	108.1	6.29 (*br s*)	95.5
6		146.4		157.6
7		152.9		162.2
8	6.86 (*br s*)	100.1	6.41 (*br s*)	93.5
8a		150.1		157.5
OMe	3.92 (*s*)	56.4	3.89 (*s*)	56.5
OMe	3.95 (*s*)	56.4	3.85 (*s*)	56.6

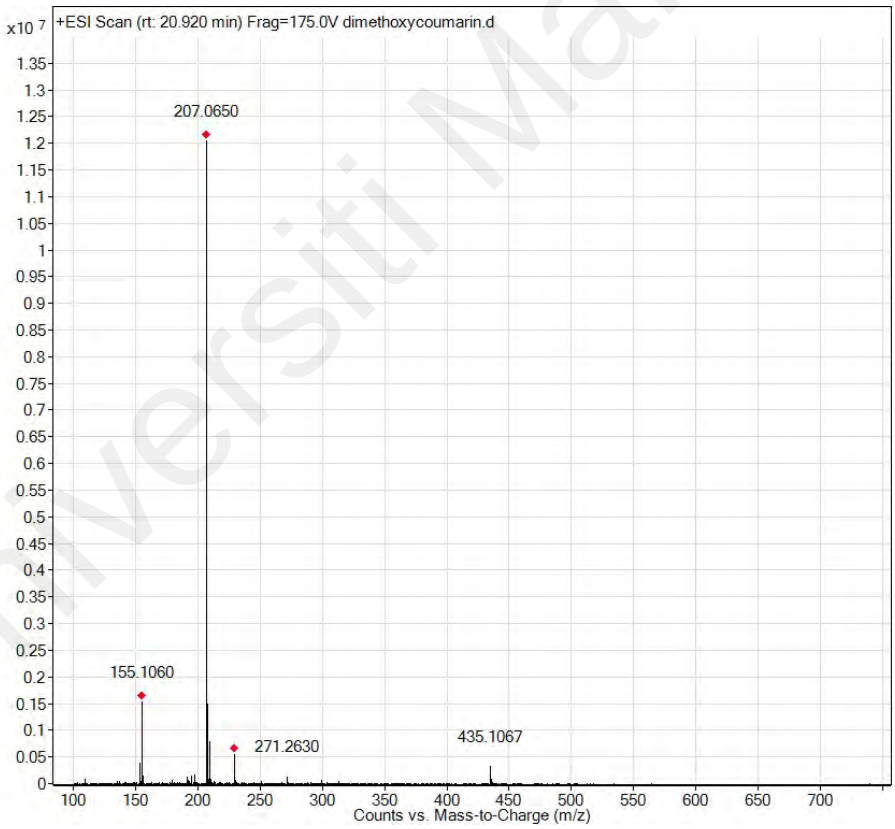

Figure 4.57: LC-ESI spectrum of scoparone (157).

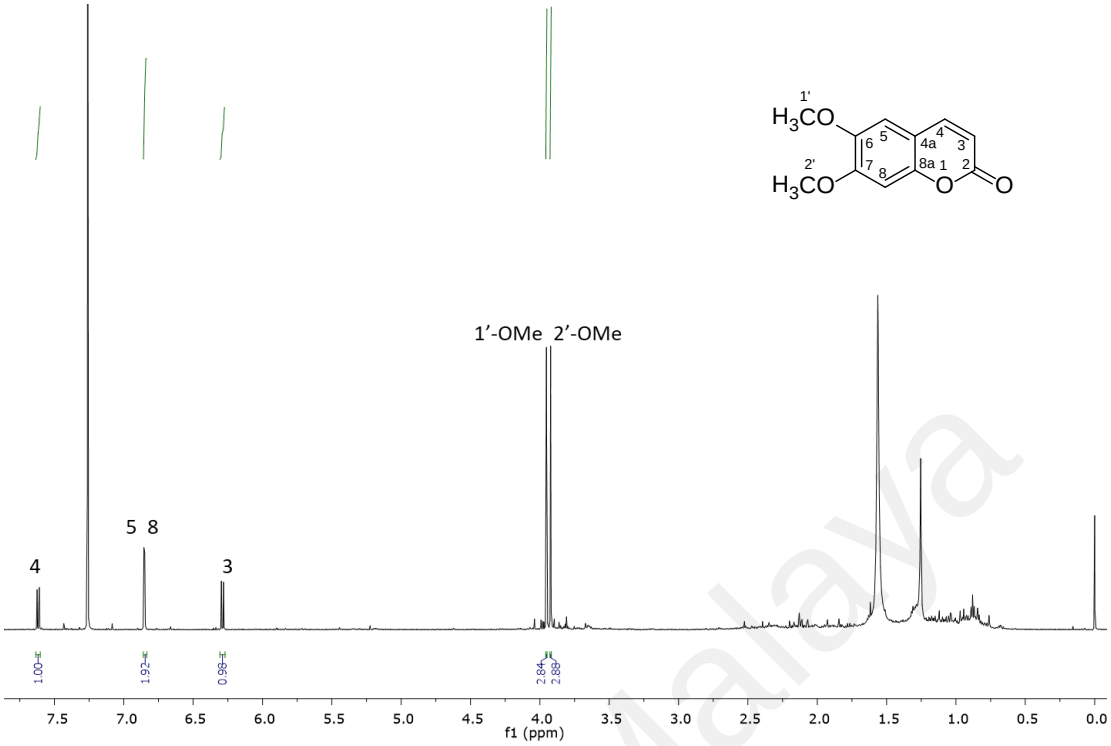

Figure 4.58: ^{1}H NMR spectrum of scoparone (157).

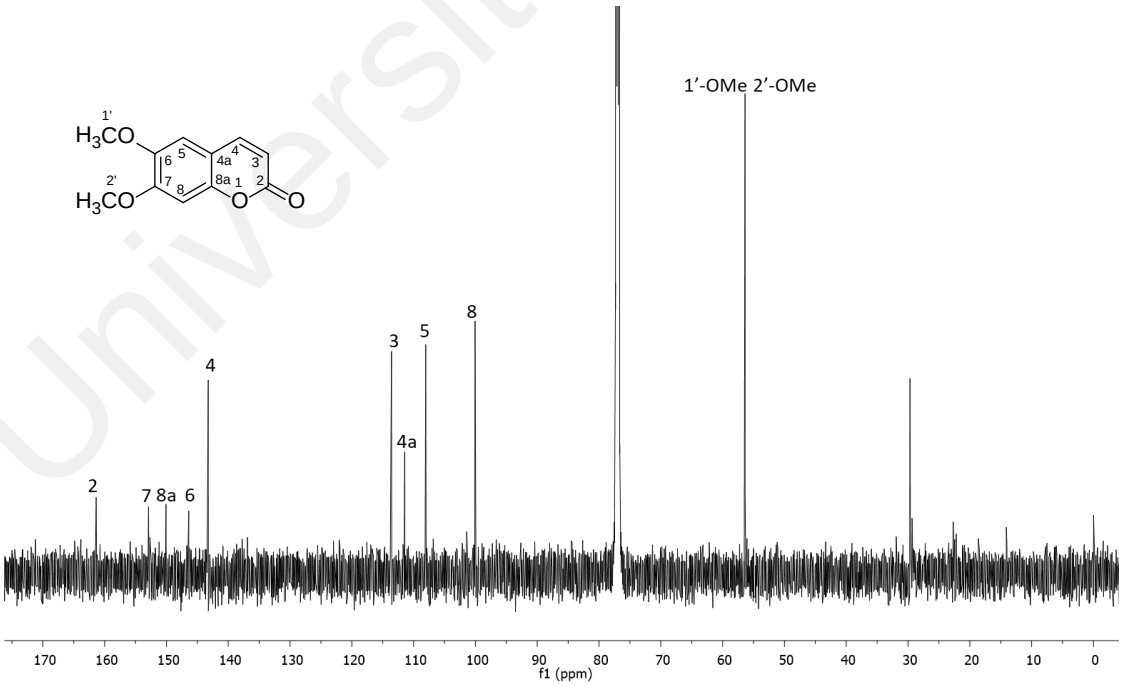

Figure 4.59: ^{13}C NMR spectrum of scoparone (157).

4.2.16 Compound P: 2'-hydroxy-3'-methoxyacetophenone (158)

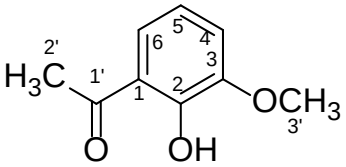

Compound **P** was isolated as pale yellow amorphous solid. The positive LC-ESI analyses (Figure 4.60) showed a pseudomolecular ion peak at *m/z* at 167.1088 $[M+H]^+$ corresponding to the molecular formula $C_9H_{11}O_3$ (calc. 167.0708). The IR spectrum (Appendix 34) showed absorption bands at 3357 and 1658 cm^{-1} due to the presence of the hydroxyl and the conjugated CO group, respectively. The UV spectrum (Appendix 17) revealed absorption maxima at 304, 275, 228 and 206 nm.

The ^1H NMR spectrum (Figure 4.61) showed three aromatic protons at δ_H 7.53 (*dd*, *J*=5.8,1.8) belonging to H-6 and H-4, and an overlapping broad doublet at δ_H 6.95 (*bd*, *J*=5.8) belonging to H-5, indicating the presence of a 1,2,3-trisubtituted benzene moiety. At H 3.96, the broad singlet methoxy peak was seen. In addition, a methyl group was attached to the carbonyl carbon (C-1') at most upfield region at δ_c 196.8. The ^{13}C NMR spectrum (Figure 4.62) showed that there were nine carbon resonances, including four quaternary, three methine, and two methyl groups.

The complete assignments of NMR (Table 4.20) spectroscopic data of compound **P** were obtained using the COSY, HMBC and HSQC experiments. The 2D NMR analysis throughout and in detail confirmed that the structure of compound **P** is paeonol or 2'-hydroxy-3'-methoxyacetophenone **(158)**. The anti-inflammatory, anti-allergic, and anti-cancer properties of this compound have been reported (Tang et al., 2016).

Table 4.20: ^{1}H NMR (600 MHz) and ^{13}C NMR (150 MHz) spectral data of 2'-hydroxy-3'-methoxyacetophenone (158) in $CDCl_3$.

	2'-hydroxy-3'-methoxyacetophenone (158)		**2'-hydroxy-3'-methoxyacetophenone (Du et al., 2010)**	
Position	δ_H (*m*, *J* in Hz)	δ_C in $CDCl_3$	δ_H (*m*, *J* in Hz) in $CDCl_3$	δ_C in $CDCl_3$
1		130.3		121.6
2		150.4		152.7
3		146.6		148.8
4	7.53 (*dd*, *J*=5.8,1.8)	109.7	7.054 (*d*, *J*=7.6)	116.9
5	6.95 (*bd*, *J*=5.8)	113.8	6.82-6.86 (*m*)	118.2
6	7.53 (*dd*, *J*=5.8,1.8)	124.0	7.32 (*d*, *J*=8.2)	119.6
1'		196.8		204.9
2'CH_3	2.56 (*bs*)	16.2	2.63 (*s*)	27.0
3'OCH_3	3.96 (*bs*)	56.0	3.89 (*s*)	56.1
OH			12.58 (*s*)	

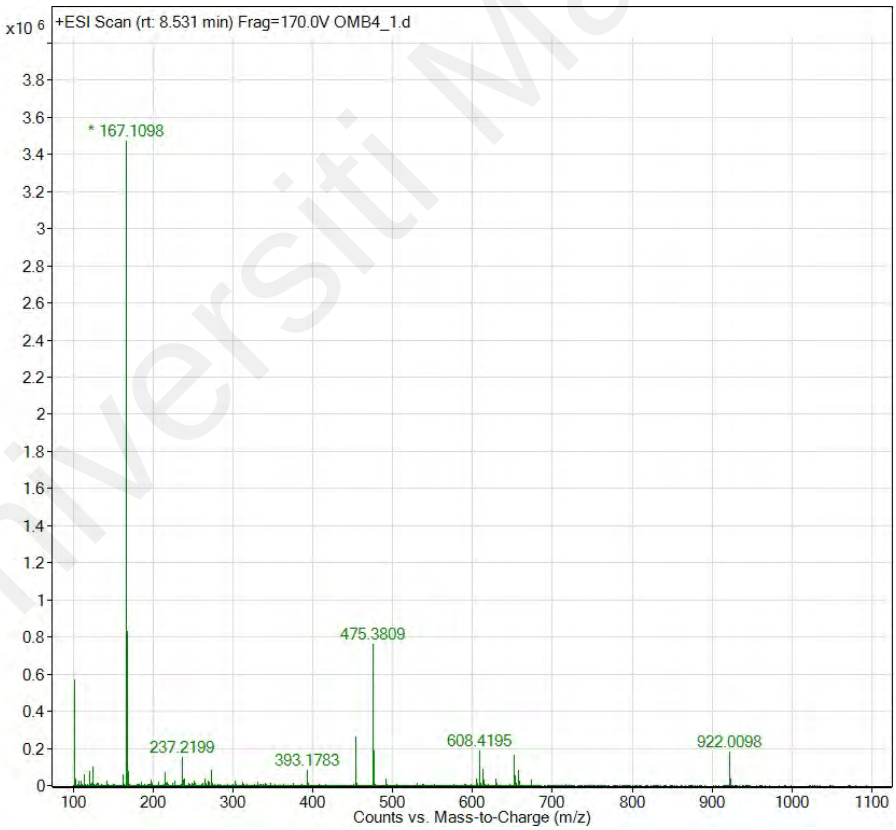

Figure 4.60: LC-ESI spectrum of 2'-hydroxy-3'-methoxyacetophenone (158).

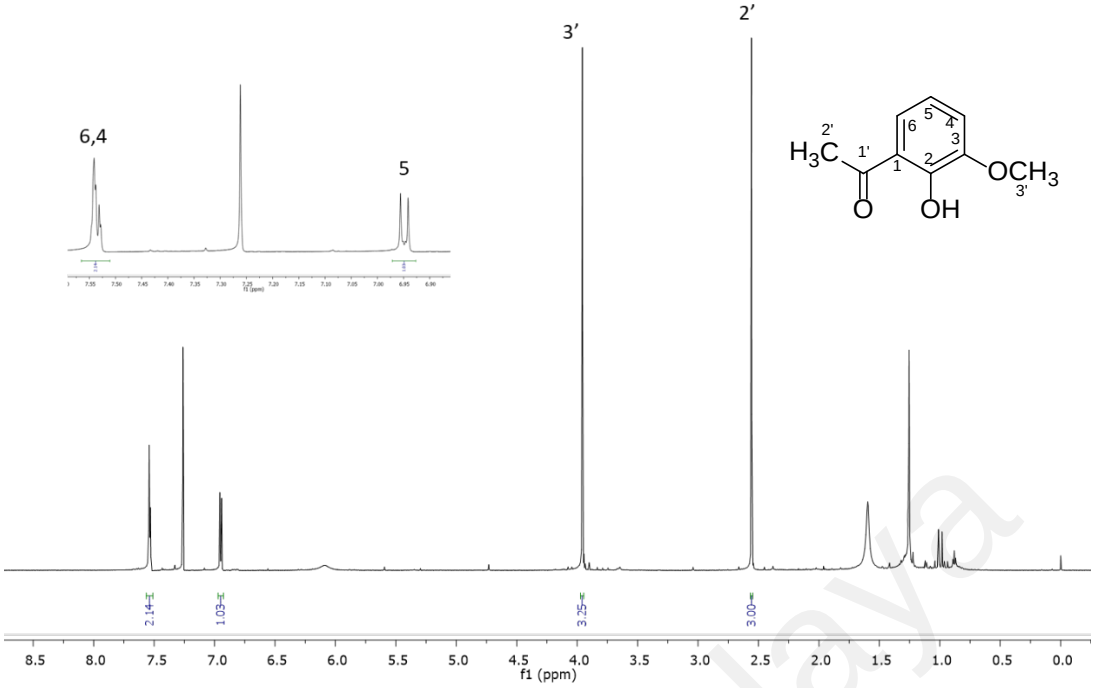

Figure 4.61: ^{1}H NMR spectrum of 2'-hydroxy-3'-methoxyacetophenone (158).

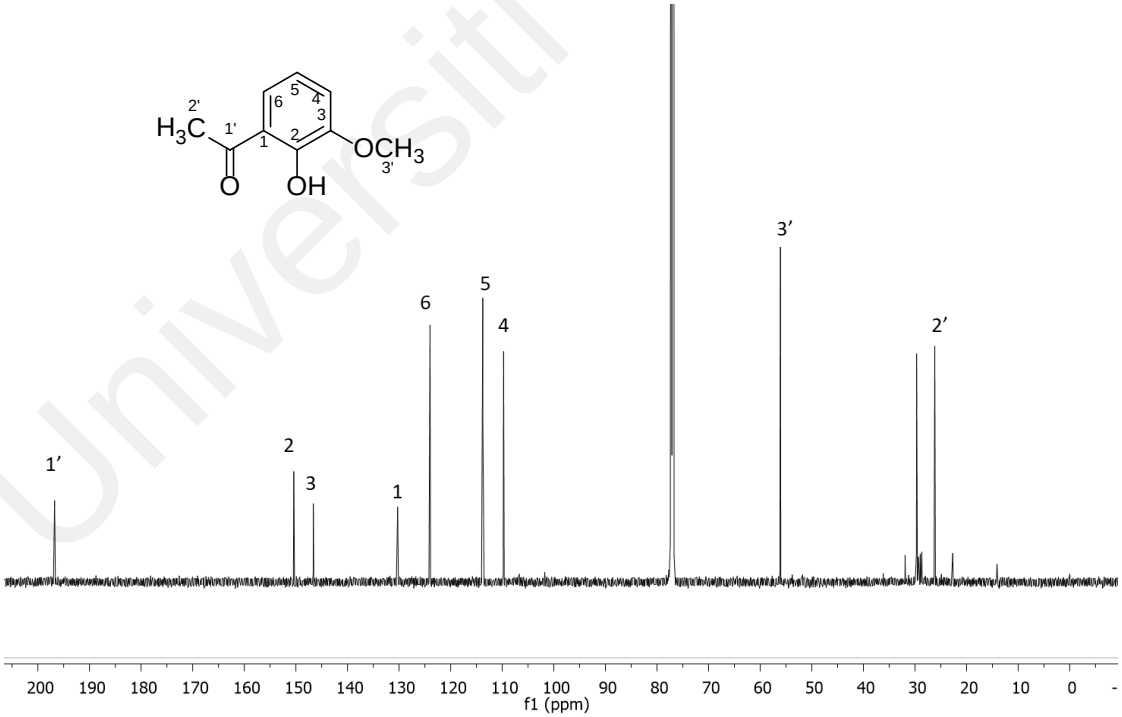

Figure 4.62: ^{13}C NMR spectrum of 2'-hydroxy-3'-methoxyacetophenone (158).

4.2.17 Compound Q: hexyl *p*-coumarate (159)

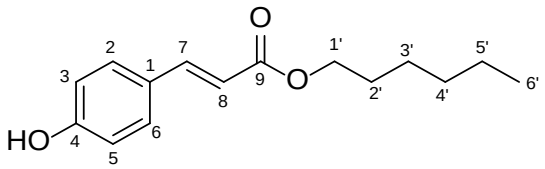

Compound **Q** was isolated as a white amorphous powder. The LC-ESI mass spectrum (Figure 4.63) showed a pseudomolecular ion peak at *m/z* 249.1574 (calc 249.1491) $[M+H]^+$, and analysis revealed that the molecular formula is $C_{15}H_{21}O_3$. The IR spectrum (Appendix 35) revealed significantly the presence of hydroxyl and carbonyl respectively at 2916.3 and 1676.0 cm^{-1}. The UV spectrum (Appendix 18) revealed absorption maxima at 374, 311, 226 and 205 nm.

In the ^{1}H NMR spectrum (Figure 4.64) of compound **Q**, the signals at δ_H 7.43 (*d*, *J*=8.2), δ_H 7.43 (*d*, *J*=8.2) and δ_H 6.97 (d, *J*=8.2), δ_H 6.97 (*d*, *J*=8.2) indicated the presence of a 1, 4 disubstituted benzene group with a pair of characteristic AA'BB', corresponding to H-2, H-6 and H-3, H-5, respectively. The signals at δ_H 7.82 (*d*, *J*=16.0) and δ_H 6.84 (*d*, *J*=16.0) indicated a trans double bond in the molecule. Two triplet signals at δ_H 4.12 and 0.88 were assigned to H-1' (*J*=6.9) and the terminal methyl proton to H-6'(*J*=6.4). The multiplex signal observed at δ_H 1.35 showed the presence of three methylene groups belonging to H3', H4' and H5'.

The assignments of the above protons were confirmed by the ^{13}C NMR spectrum (Figure 4.65), which showed three quaternary carbons, six methines, one methyl, one carbonyl and five methylene groups. Table 4.21 shows a comparison of the assignments of the ^{1}H NMR and ^{13}C NMR data. Thus, structure **Q** was identified as hexyl *p*-coumarate **(159)** based on the LCMS, NMR spectral data and comparison with literature values (Lopes et al., 2020; Nishioka et al., 1997). Some research suggests that **159** may have antiparasitic properties (Lopes et al., 2020).

Table 4.21: ^{1}H NMR (600 MHz) and ^{13}C NMR (150 MHz) spectral data of hexyl *ρ*-coumarate (159) in pyridine-d$_5$.

	Hexyl *ρ*- coumarate (159)		Hexyl *ρ*-coumarate (Lopes et al., 2020)	
Position	δ_H (*m*, *J* in Hz)	δ_C	δ_H (*m*, *J* in Hz) in $CDCl_3$	δ_C in $CDCl_3$
		124.7		127.0
2	7.43 (*d*, *J*=8.2)	129.0	7.42-7.40 (*d*, *J* =8.62)	130.1
3	6.97 (*d*, *J* =8.2)	115.2	6.88-6.86 (*d*, *J* =8.64)	116.1
4		159.8		158.4
5	6.97 (*d*, *J* =8.2)	115.2	6.88-6.86 (*d*, *J* =8.64)	116.1
6	7.43 (*d*, *J* =8.2)	129.0	7.42-7.40 (*d*, *J* =8.62)	130.1
7	7.82 (*d*, *J* =16.0)	143.5	7.63 (*d*, *J* =15.95)	145.0
8	6.84 (*d*, *J*=16.0)	113.6	6.28 (*d*, *J* =15.94)	115.4
9		165.8		168.3
1'	4.12 (*t*, *J*=6.9)	62.8	4.19 (*t*, *J*=6.74)	65.1
2'	1.50 (*q*, *J*=6.9)	27.5	1.69 (*q*, *J*=16.0)	28.8
3'	1.35 (*m*)	30.4	1.36 (*m*)	31.6
4'	1.35 (*m*)	24.6	1.36 (*m*)	25.8
5'	1.35 (*m*)	21.3	1.36 (*m*)	22.7
6'	0.88 (*t*, *J*=6.4)	12.59	0.89 (*t*, *J*=6.02)	14.1

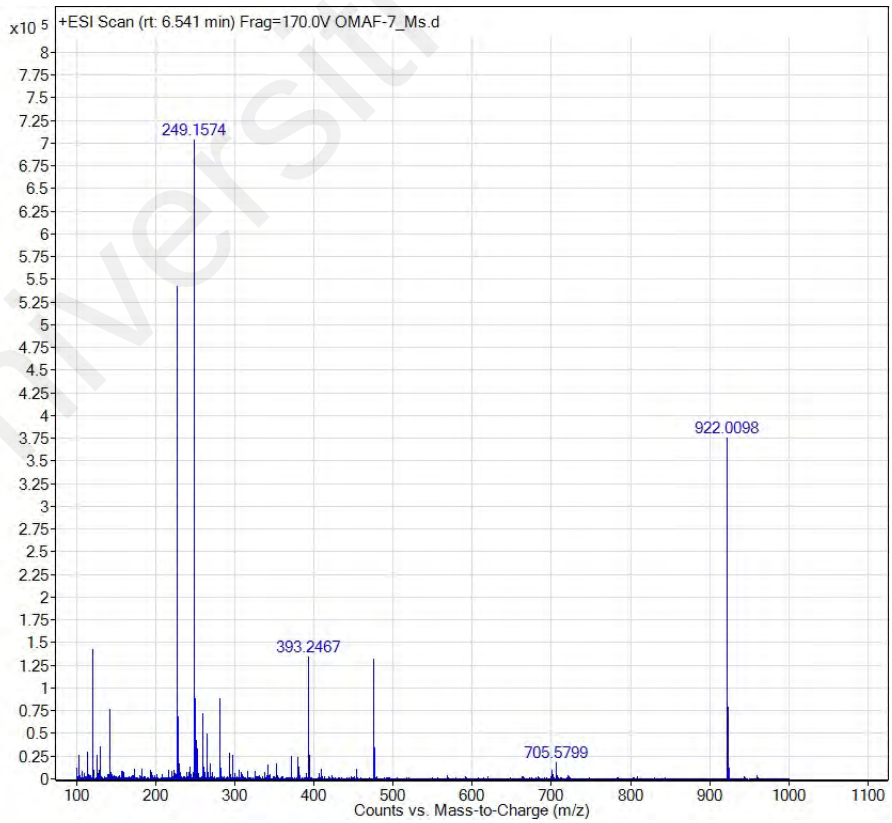

Figure 4.63: LC-ESI spectrum of hexyl *ρ*-coumarate (159).

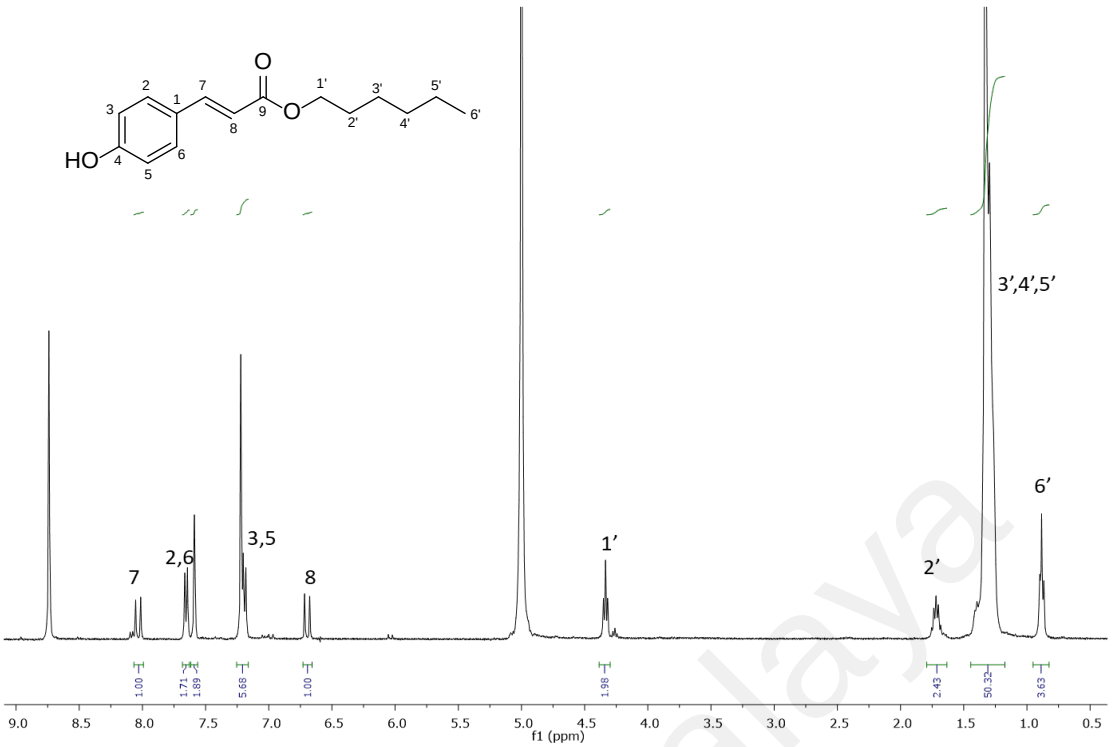

Figure 4.64: ^{1}H NMR spectrum of Hexyl *ρ*-coumarate (159).

Figure 4.65: ^{13}C NMR spectrum of Hexyl *ρ*-coumarate (159).

4.2.18 Physical data of the isolated compound

Dihydrodeglycocadambine **(149)** : light yellow amorphous solid

$[\alpha]^{25}_{D}$: +57.3 (*c* 0.0004, MeOH)

Mass Spectrum (*m/z*): 385.1754 $[M+H]^+$

Molecular formula: $C_{21}H_{23}N_2O_5$

UV λ_{max}, nm: 222 and 274

IR V_{max} (NaCl), cm^{-1}: 3339, 1731

^1H NMR: Table 4.5

^{13}C NMR: Table 4.5

Cadambine **35**: white amorphous solid

$[\alpha]^{25}_{D}$: -122.77(c=0.001, MeOH)

Mass Spectrum (*m/z*): 545.2135 $[M+H]^+$

Molecular formula: $C_{27}H_{32}N_2O_{10}$

UV λ_{max}, nm: 232 and 274

IR V_{max} (NaCl), cm^{-1}: 3295, 1683 and 1072

^1H NMR: Table 4.6

^{13}C NMR: Table 4.6

Naucledine **6**: yellow amorphous solid

Molecular formula: $C_{18}H_{15}N_3O_2$

Mass Spectrum (*m/z*): 306.1236 $[M+H]^+$

UV λ_{max}, nm: 329, 280 and 220

IR V_{max} (NaCl), cm^{-1}: 3402, 1731

^1H NMR: Table 4.7

^{13}C NMR: Table 4.7

Methyl 9*H*-*β*-carboline-4-Carboxylate **158**: dark yellow amorphous solid

Molecular formula: $C_{13}H_{10}N_2O_2$

Mass Spectrum (*m/z*): 227.1155$[M+H]^+$

UV λ_{max}, nm: 206, 298, 312, 366 and 381

IR V_{max} (NaCl), cm^{-1}: 2919 and 1723

^1H NMR: Table 4.8

^{13}C NMR: Table 4.8

*Nor*harman **124**: brownish amorphous solid

Molecular formula: $C_{11}H_9N_2$

Mass Spectrum (*m/z*): 169.0760 $[M+H]^+$

UV λ_{max}, nm: 211, 234, 288,304, 350

IR V_{max} (NaCl), cm^{-1}: 3166.5, 2923.9

^1H NMR: Table 4.9

^{13}C NMR: Table 4.9

Harmane **7**: brownish amorphous solid

Molecular formula: $C_{12}H_{10}N_2$

Mass Spectrum (*m/z*): 183.0994$[M+H]^+$

UV λ_{max}, nm: 348,335, 287, 243

IR V_{max} (NaCl), cm^{-1}: 31453

^1H NMR: Table 4.10

^{13}C NMR: Table 4.10

Naulafine **33**: reddish brown amorphous solid

Molecular formula: $C_{20}H_{13}N_3O$

Mass Spectrum (*m/z*): 312.1155 $[M+H]^+$

UV λ_{max}, nm: 205, 302, 314, 366 and 385

IR V_{max} (NaCl), cm^{-1}: 2919 and 1667

^1H NMR: Table 4.11

^{13}C NMR: Table 4.11

Neonaucline **5**: yellowish amorphous solid

Molecular formula: $C_{20}H_{15}N_3O_3$

Mass Spectrum (*m/z*): 346.0926 $[M+H]^+$

UV λ_{max}, nm: 382, 298 and 205

IR V_{max} (NaCl), cm^{-1}: 3364 and 1731

^1H NMR: Table 4.12

^{13}C NMR: Table 4.12

1,2,3,4-tetrahydronorharmane-1-one **156**: brownish amorphous solid

Molecular formula: $C_{11}H_{10}N_2O$

Mass Spectrum (*m/z*): 187.0896 $[M+H]^+$

UV λ_{max}, nm: 299 and 201

IR V_{max} (NaCl), cm^{-1}: 3233 and 1655cm

^1H NMR: Table 4.13

^{13}C NMR: Table 4.13

Cinnamamide **157**: white amorphous solid

Molecular formula: $C_9H_{10}NO$

Mass Spectrum (*m/z*): 148.0753$[M+H]^+$

UV λ_{max}, nm: 217, 272

IR V_{max} (NaCl), cm^{-1}: 3368, 1655

^1H NMR: Table 4.14

^{13}C NMR: Table 4.14

Benzamide **155**: crystalline needles

Molecular formula: C_7H_8NO

Mass Spectrum (*m/z*): 122.0598$[M+H]^+$

UV λ_{max}, nm: 294, 280

IR V_{max} (NaCl), cm^{-1}:3365, 1646

^1H NMR: Table 4.15

^{13}C NMR: Table 4.15

Scopoletine **153**: pale yellow amorphous

Molecular formula: $C_{10}H_8O_4$

Mass Spectrum (*m/z*): 193.0423$[M+H]^+$

UV λ_{max}, nm: 204, 228, 296 and 344

IR V_{max} (NaCl), cm^{-1}: 3383

^1H NMR: Table 4.16

^{13}C NMR: Table 4.16

4' hydroxyacetophenone **154**: light beige solid

Molecular formula: $C_8H_8O_2$

Mass Spectrum (*m/z*): 137.0754$[M+H]^+$

UV λ_{max}, nm: 276,218,204

IR V_{max} (NaCl), cm^{-1}: 3351, 1663

^1H NMR: Table 4.17

^{13}C NMR: Table 4.17

Decarboxylportentol acetate **158**: colourless amorphous solid

$[\alpha]^{28}_D$: +97.86 (*c* 0.007, $CHCl_3$)

Molecular formula: $C_{18}H_{28}O_4$

Mass Spectrum (*m/z*): 309.2038$[M+H]^+$

UV λ_{max}, nm: 241

IR V_{max} (NaCl), cm^{-1}: 1742, 1666, 1231

^1H NMR: Table 4.18

^{13}C NMR: Table 4.18

Scoparone **151**: white amorphous solid

Molecular formula: $C_{10}H_8O_4$

Mass Spectrum (*m/z*): 207.0650$[M+H]^+$

UV λ_{max}, nm: 204, 271

IR V_{max} (NaCl), cm^{-1}: 1732

^1H NMR: Table 4.19

^{13}C NMR: Table 4.19

2'-Hydroxy-3'-methoxyacetophenone **152**: white amorphous solid

Molecular formula: $C_9H_{11}O_3$

Mass Spectrum (*m/z*): 167.0630$[M+H]^+$

UV λ_{max}, nm: 206, 228, 275, 304

IR V_{max} (NaCl), cm^{-1}: 3357, 1658

^1H NMR: Table 4.20

^{13}C NMR: Table 4.20

Hexyl *p*-coumarate **149**: white amorphous powder

Molecular formula: $C_{15}H_{20}O_3$

Mass Spectrum (*m/z*): 249.1574$[M+H]^+$

UV λ_{max}, nm: 374, 311 ,226, 205

IR V_{max} (NaCl), cm^{-1}: 2916,1676

^1H NMR: Table 4.21

^{13}C NMR: Table 4.21

4.3 Biological activity results

The dichloromethane extract of *O. maingayi* has been tested for cholinesterase inhibitory assay. The results showed that the DCE exhibited moderate more than 54% of inhibition at 100 µg/mL on BChE. Therefore, all fractions F1-F0 tested based on inhibition against BChE were carried out. Further evaluation showed that fractions 7 and 9 were able to inhibit the BChE at more than 80% at a concentration of 100 µg/mL (Figure 4.66).

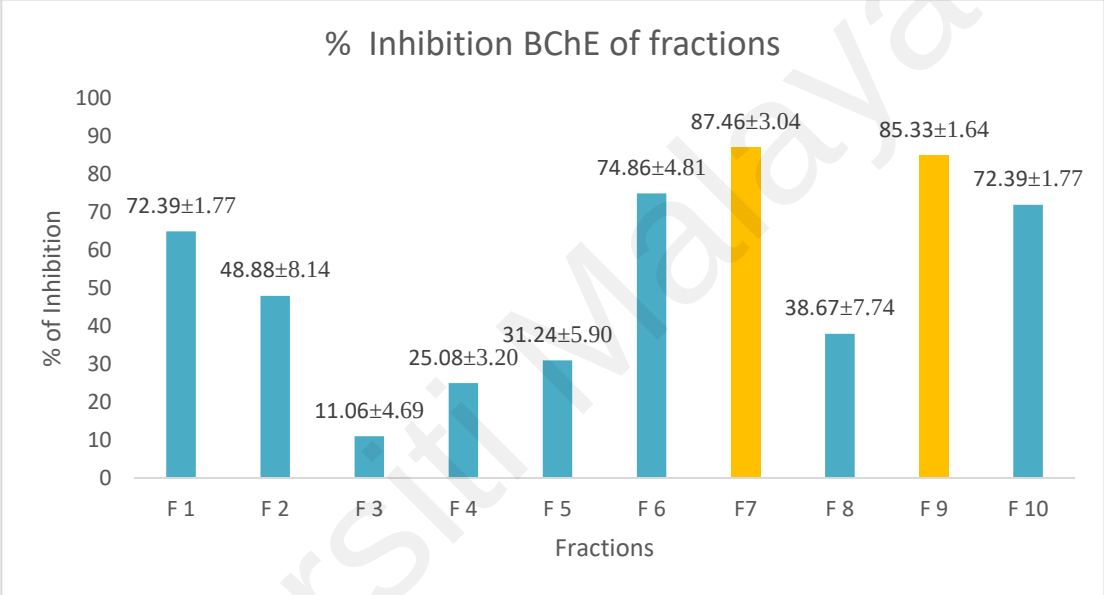

Figure 4.66: Percentage of BChE inhibitory activity of fraction from *O. maingayi*

After that, harmane **(7)** which was isolated from F7 while both naucledine **(6)** and dihydrodeglycocadamine **(149)** obtained from both F9 were tested against BChE inhibitory activity. Interestingly, all the three indole alkaloids (Table 4.22) had potent inhibition toward BChE. Naucledine **(6)** was the most potent BChE inhibitor with IC_{50} value of 22.08 ± 0.66 µM followed by harmane **(7)** and dihydrodeglycocadambine **(149)** (23.96 ± 1.67 and 30.32 ± 2.04 µM, respectively).

In addition, the potency of the indole alkaloids is comparable with the previous reported IC_{50} value of a standard, galantamine (28.29 ± 2.12 µM) (Liew et al., 2015). Galantamine **(1)** is a naturally occurring plant tertiary alkaloid drug or cholinesterase inhibitor that used to treat mild to moderate dementia related to Alzheimer's disease

(Clarke, 2007a). Compared with galantamine **(1),** naucledine **(6)** and harmane **(7)** exhibited slightly higher inhibition against BChE. Another standard/drug, donepezil **(3)**, showed higher inhibition against BChE compared with the three indole alkaloids. However, according to a comparison study of cholinesterase inhibitor safety in real-world practice, galantamine **(1)** use was associated with a lower risk of mortality, cardiovascular serious adverse events and entry into a residential care facility as compared with low-dose donepezil **(3)** (Carney et al., 2019).

Table 4.22: BChE inhibitory activities of indole alkaloids from *O. maingayi*

Compound	IC_{50} (µM)
Naucledine **(6)**	22.08 ± 0.66
Harmane **(7)**	23.96 ± 1.67
Dihydrodeglycocadambine **(149)**	30.32 ± 2.04
Donepezil **(3)** (standard)	0.73 ± 0.11
Galantamine **(1)** (standard)	28.29± 2.12 [a]

[a]IC_{50} value from reference (Liew et al., 2015)

4.3.1 Kinetic study

In order to determine the types of inhibition of the most potent compound, an enzyme kinetic study was carried out on naucledine **(6)** with BChE. The Lineweaver-Burk plot showed that the compound exhibited mixed-type inhibition (Figure 4.67). Mixed-type inhibition in which the compound (inhibitor) was able to bind to the active site (catalytic site) and the allosteric site (oxyanion hole) of the BChE (Abdul Wahab et al., 2016), where the substrate is butyrylthiocholine (Khaw et al., 2014). Furthermore, the inhibition constant, *Ki* value, of naucledine **(6)** was 6.08 µM, which was obtained from the secondary plot of the Lineweaver-Burk plot (Figure 4.68). Harmane **(7)** which also showed potent activity towards BChE has been reported as a non-competitive inhibitor in kinetic study (Torres et al., 2012).

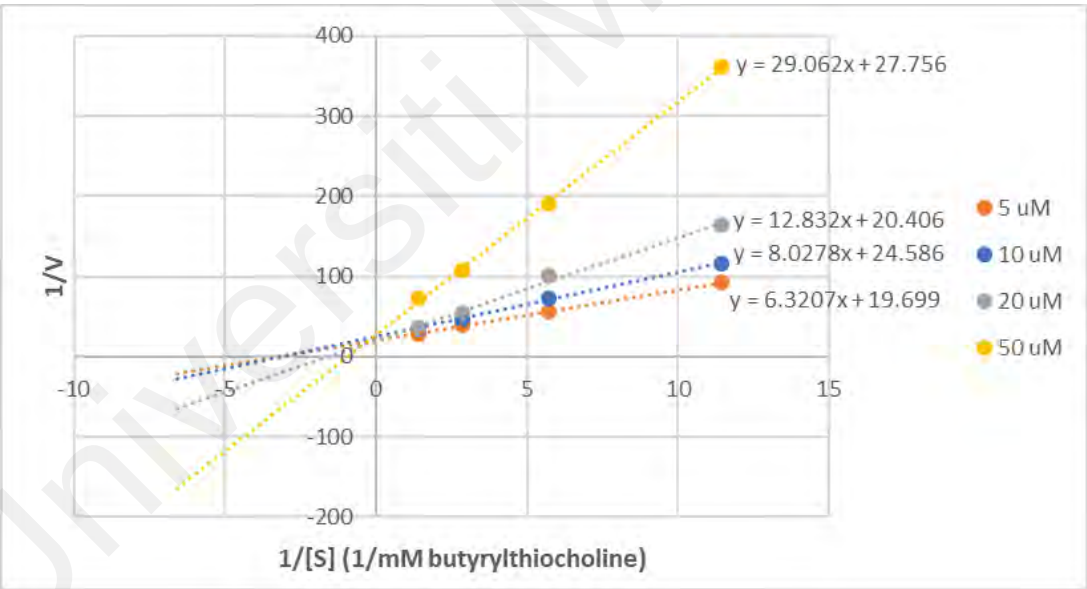

Figure 4.67: Lineweaver-Burk plots of BChE activity for naucledine (6)

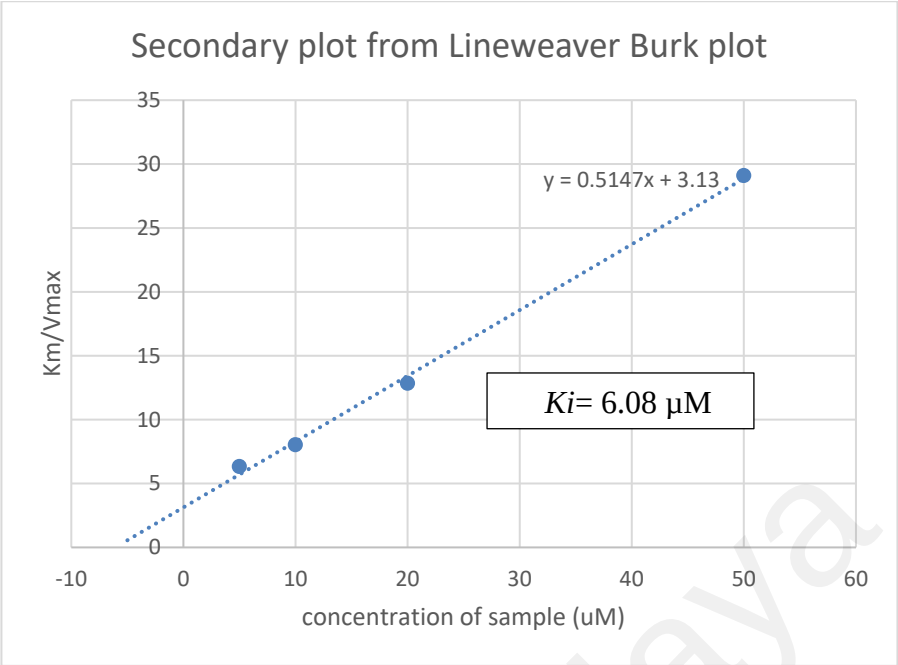

Figure 4.68: Secondary plot from Lineweaver Burk Plot of BChE activity for naucledine (6)

4.3.2 Molecular docking study

A molecular docking study was performed on the most potent compound, naucledine **(6)**, to predict the possible binding site interactions with human butyrylcholinesterase (*h*BChE). The two possible docking position based on the first two highest populated (50 and 10 out of 100 run) cluster with its respective lowest docked energy were presented in Figures 4.70A & B and 4.71A & B. Even though docking position B (-11.32 kcal/mol) (Figure 4.70B, 4.71B) has the lowest docked energy as compared to position A (-10.99 kcal/mol) (Figure 4.70A, 4.71A), the former showed that naucledine **(6)** has only interaction with Trp 82. Hence, position A with the highest populated cluster and binding energy of -10.99 kcal/mol was selected as the best docking position after thorough analysis of the binding interactions. According to the docking position A, naucledine **(6)** interacted with the oxyanion hole, which is a pocket in the active site of *h*BChE. A hydrogen bond was formed between the nitrogen atom (N-4) of naucledine **(6)** with hydrogen of the amine group in Gly 116 in oxyanion hole at a distance of 2.37 Å (Table 4.23). The amino acid residues in the oxyanion hole provide

their amide protons for the interaction (Radi & Taylor, 2006). Furthermore, naucledine **(6)** docked deep into the bottom of the catalytic site of *h*BChE, which is the enzyme's active site or catalytic triad consisting of Ser 198, Glu 325 and His 438. At the catalytic site, a hydrogen bond was formed between the N-4 of naucledine **(6)** with hydroxyl group of the side chain in Ser 198 at a distance of 3.02 Å (Figure 4.71A). Other than that, π-σ and π-cation interactions can be observed between ring A of naucledine **(6)** with hydrogen of C-δ in His 438 and between ring B of naucledine **(6)** with N-ϵ in His 438, respectively. Based on the molecular docking result, it can be suggested that the nitrogen atom (N-4) and the indole ring may contribute to the potency of naucledine **(6)** in inhibiting BChE.

In addition, based on the analysis of 2WIJ protein data structure (Carletti et al., 2009), the ligand contained within the enzyme, ethyl hydrogen ethylamidophosphate (TN7)**(169)** forms three hydrogen bonds with *h*BChE (Figure 4.70C & 4.71C). Two hydrogen bonds were formed between O-2 of TN7 with amine group of Gly116 (3.1 Å) and Ala199 (2.8 Å) which are the residues in oxyanion hole. Another one hydrogen bond was formed between O-3 of the ligand with N-ϵ of His438 (2.8 Å) which is situated at the catalytic site. Besides, a cation- π interaction can be observed between nitrogen atom of TN7**(169)** with six membered-ring of Trp 231 in acyl binding pocket. Comparing with the molecular docking result in this study, TN7**(169)** and naucledine **(6)** have similar interactions in which both also interact with the amino acid residues at oxyanion hole and catalytic site. Hence, this similarity strengthens the hypothesis in which naucledine **(6)** could inhibits BChE through these interactions. The structure with numbering of naucledine **(6)** and TN7 **(169)** were shown at Figure 4.69).

Furthermore, the finding shows that naucledine **(6)** can bind to both the active site and allosteric site of BChE, which aligns with the enzyme kinetic study that demonstrated its mixed mode inhibition of BChE.

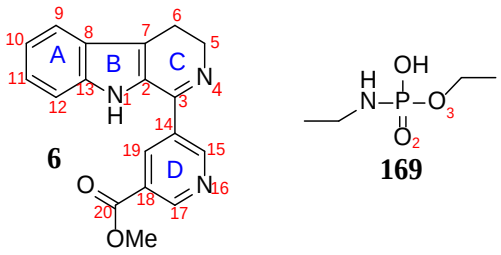

Figure 4.69: Structure of naucledine (6) and ethyl hydrogen ethylamidophosphate (TN7) (169).

Table 4.23: Binding interaction data for bioactive ligands docked into active site gorge of *h*BChE.

Ligand	Enzyme	Interacting site	Residue	Type of Interaction	Distance (Å)	Ligand Interacting
Naucledine (6)	*h*BChE	Catalytic site	Ser 198	Hydrogen	3.02	Nitrogen atom (N-4)
			His 438	Hydrophobic	-	Indole ring (ring A and B)
		Oxyanion hole	Gly 116	Hydrogen	2.37	Nitrogen atom (N-4)
Ethyl hydrogen ethylamidophosphate (TN7)	*h*BChE	Catalytic site	His 438	Hydrogen	2.8	Nitrogen atom (N-ϵ)
		Oxyanion hole	Gly 116	Hydrogen	3.1	Nitrogen atom
			Ala 199	Hydrogen	2.8	Nitrogen atom
		Acyl binding pocket	Trp 231	Hydrophobic	-	Nitrogen atom

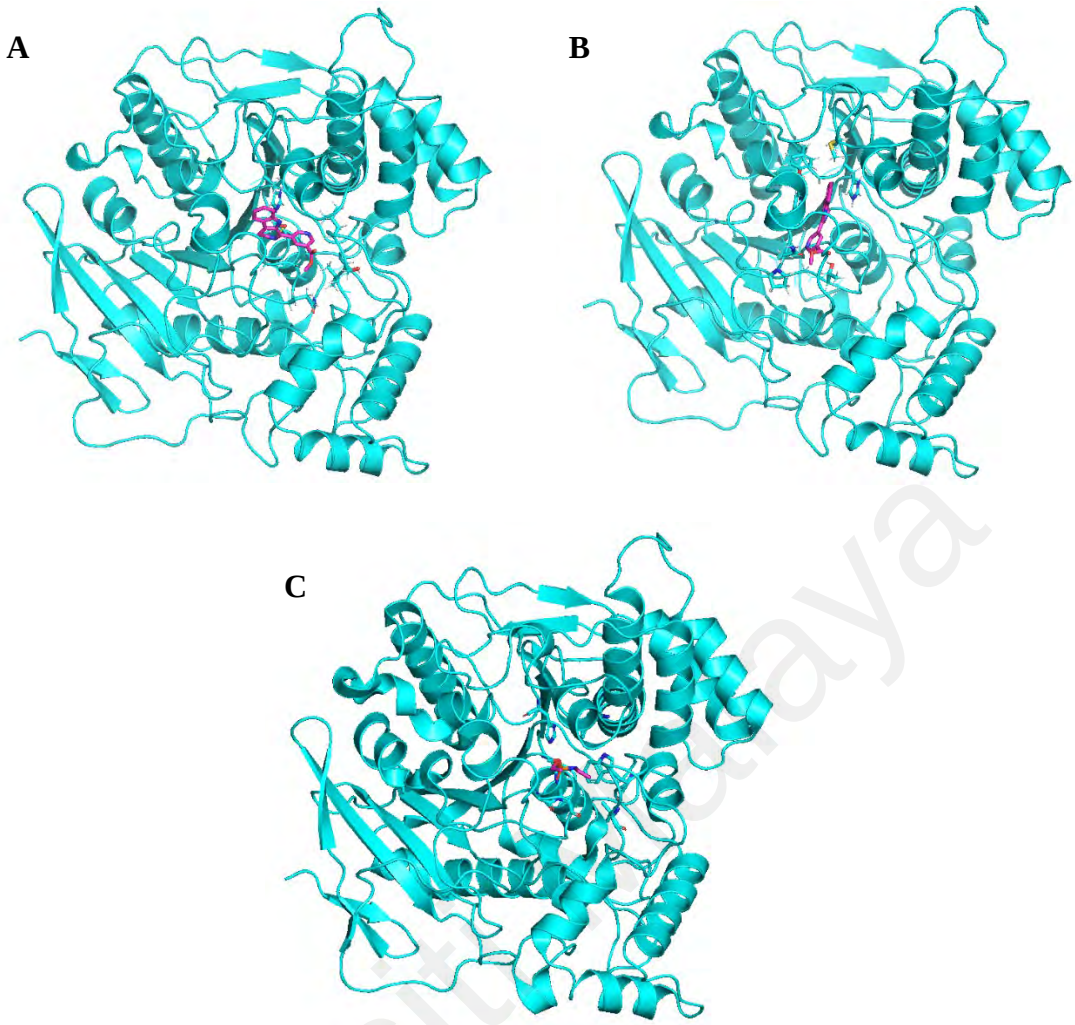

Figure 4.70: (A) Binding orientation of naucledine (6) (in stick format and magenta) at the active site of hBChE (in ribbon format) with the highest populated cluster and lowest docked energy of -10.99 kcal/mol. (B) Binding orientation of naucledine (6) (in stick format and magenta) at the active site of hBChE (in ribbon format) with the second highest populated cluster and lowest docked energy of -11.32 kcal/mol. (C) Binding orientation of ethyl hydrogen ethylamidophosphate (TN7) (in stick format and magenta) in hBChE (PDB ID: 2WIJ).

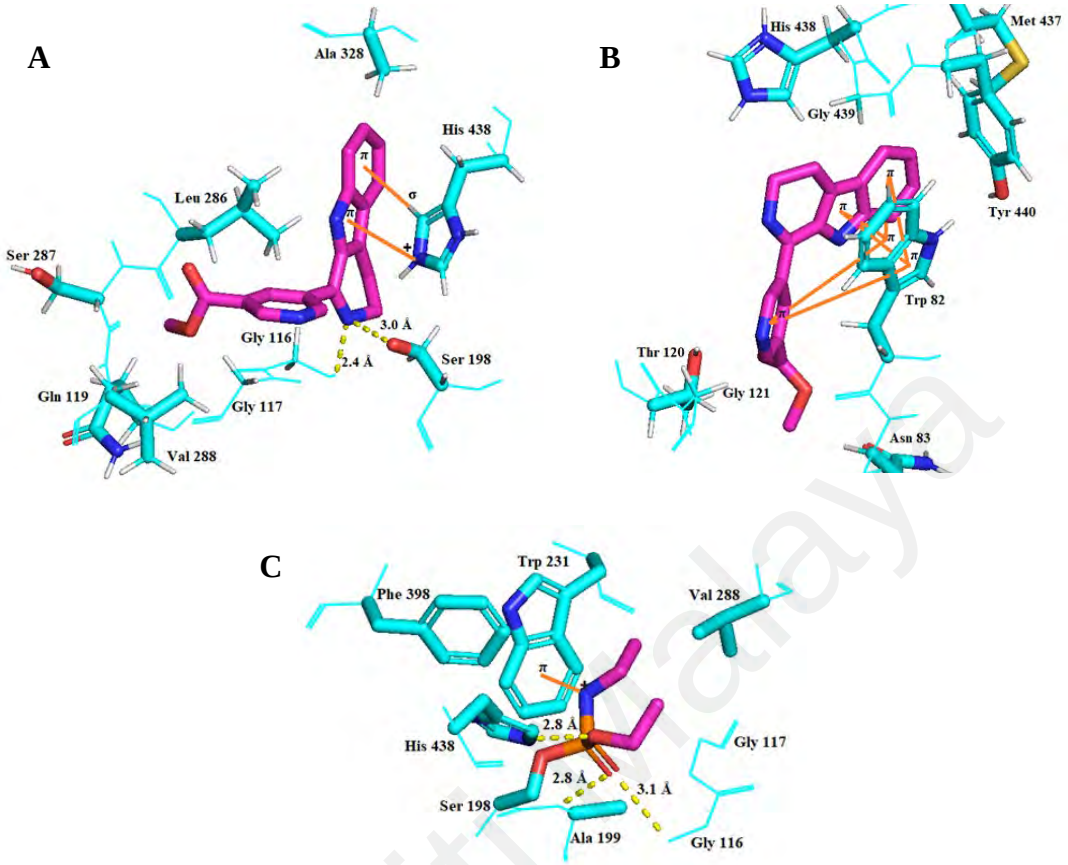

Figure 4.71 : (A) Binding interactions of naucledine (6) (in magenta) with amino acid residues of *h*BChE (with the highest populated cluster and lowest docked energy of -10.99 kcal/mol). (B) Binding interactions of naucledine (6) (in magenta) with amino acid residues of *h*BChE (with the second highest populated cluster and lowest docked energy of -11.32 kcal/mol). (C) Binding interactions of ethyl hydrogen ethylamidophosphate (TN7) (in magenta) amino acid residues of *h*BChE (PDB ID: 2WIJ). The hydrogen bond formed between the inhibitor and amino acid residues were indicated with yellow dotted line while the hydrophobic interactions were indicated with orange line. Amino acid residues of *h*BChE (in cyan) were represented by line format in which their side chain was indicated with stick format.

CHAPTER 5: CONCLUSIONS

In this study, column chromatography was used to analyse dichloromethane crude extract of the bark of *Ochreinauclea maingayi*. Ten fractions from CC were successfully gathered. To locate the targeted molecule (indole alkaloid), feature-based molecular networking (FBMN) was applied to the DCE and all fractions (F1 - F10). From MN analysis, F5 - F10 showed the presence of indole alkaloids. Twenty-two compounds were identified by MN analysis which one is new and identified as dihydrodeglycocadambine **(149).** Other compounds are cadamine **(4)**, neonaucline **(5)**, naucledine **(6)**, harmane **(7)**, cadambine **(35)**, *nor*harmane **(124)**, geissoschizine methyl ether **(148)**, 1,2,3,4 tetranorharmane-1-one **(151)**, cinnamamide **(152),** benzamide **(153),** scopoletine **(154),** scoparone **(157)**, glycrrhetic acid **(160)**, betulinic acid **(161),** oleanolic acid **(162),** ursolic acid **(163),** Di-*O*-methylfraxetin **(164)**, trans ferulic acid **(165),** 9(10)-EpOMe (leukotoxin A) **(166),** phytosphingosine **(167)**, cyclo(L-Phe-D-Pro) **(168)**. By exploiting the beneficial functions of MN, the conventional natural product isolation and identification workflow were streamlined *via* early dereplication, which saves time, effort, and cost.

The isolation and purification of DCE, afforded seventeen compounds. A new compound, dihydrodeglycocadambine **(149)** which is indole alkaloid, was identified from MN was successfully isolated from F9 and 10. Another indole alkaloids are: neonaucline **(5),** naucledine **(6)**, harmane **(7)**, naulafine **(33)**, cadambine **(35)**, *nor*harmane **(124)**, methyl 9*H*-*β*-carboline-4-carboxylate **(150),** and 1,2,3,4 tetranorharmane-1-one **(151)**.

Lastly, the BChE inhibitory activity exercised, shows that harmane **(7)**, naucledine **(6)**, and dihydrodeglycocadambine **(149)** were responsible for the BChE inhibitory activity were responsibly exhibited by the bark of *O. maingayi*. According to the kinetic study, naucledine **(6)** exhibited a mixed mode type of inhibition**.** The molecular docking analysis showed that naucledine (**6)** docked deep into the bottom gorge of BChE and interacted

with Ser 198 and His 438 at the catalytic site as well as formed hydrogen bonding with Gly 116 in oxyanion hole. It showed a higher inhibition effect than the natural drug galantamine **(1)**. Hence, this study suggests that naucledine **(6)** can be subjected to further studies in developing potential natural therapy medicine for AD. This study also demonstrated that MN analysis is useful in helping to discover known or new natural products without having to endure the time-consuming procedure of isolating and purifying them first.

REFERENCES

Aassila, H., Bourguet-Kondracki, M. L., Rifai, S., Fassouane, A., & Guyot, M. (2003). Identification of Harman as the Antibiotic Compound Produced by a Tunicate-Associated Bacterium. *Marine Biotechnology*, *5*(2), 163-166.

Abdul Wahab, S. M., Sivasothy, Y., Liew, S. Y., Litaudon, M., Mohamad, J., & Awang, K. (2016). Natural cholinesterase inhibitors from *Myristica cinnamomea* King. *Bioorganic and Medicinal Chemistry Letters*, *26*(15), 3785-3792.

Abdullah, N. H., Salim, F., & Ahmad, R. (2016). Chemical Constituents of Malaysian *U. cordata* var. ferruginea and Their *in Vitro* α-Glucosidase Inhibitory Activities. *Molecules*, *21*(5).

Abu Bakar, F. I., Abu Bakar, M. F., Abdullah, N., Endrini, S., & Rahmat, A. (2018). A Review of Malaysian Medicinal Plants with Potential Anti-Inflammatory Activity. *Advanced Pharmacological Science*, 1-13.

Aggrey, M. O., Li, H. H., Wang, W.Q., Wang, Y., & Xuan, L.J. (2019). Indole alkaloid from *Nauclea latifolia* promotes LDL uptake in HepG2 cells by inhibiting PCSK9. *Phytomedicine*, *55*, 264-268.

Agomuoh, A. A., Ata, A., Udenigwe, C. C., Aluko, R. E., & Irenus, I. (2013). Novel Indole alkaloids from *Nauclea latifolia* and their Renin-Inhibitory activities. *Chemistry & Biodiversity*, *10*(3), 401-410.

Agrawal, P. K. (1992). NMR spectroscopy in the structural elucidation of oligosaccharides and glycosides. *Phytochemistry*, *31*(10), 3307-3330.

Alam, M. M., Naeem, M., Khan, M. M. A., & Uddin, M. (2017). Vincristine and Vinblastine Anticancer Catharanthus Alkaloids: Pharmacological Applications and Strategies for Yield Improvement. In M. Naeem, T. Aftab, & M. M. A. Khan (Eds.), *Catharanthus roseus: Current Research and Future Prospects* (pp. 277-307). Springer International Publishing. https://doi.org/10.1007/978-3-319-51620-2_11

Albinsson, B., & Norden, B. (1992). Excited-state properties of the indole chromophore: electronic transition moment directions from linear dichroism measurements: effect of methyl and methoxy substituents. *The Journal of Physical Chemistry*, *96*(15), 6204-6212.

Aricioglu, F., & Altunbas, H. (2003). Harmane induces anxiolysis and antidepressant-like effects in rats. *Annals of the New York Academy of Sciences*, *1009*, 196-200.

Aron, A. T., Gentry, E. C., McPhail, K. L., Nothias, L.F., Nothias-Esposito, M., Bouslimani, A.,...Dorrestein, P. C. (2020). Reproducible molecular networking of untargeted mass spectrometry data using GNPS. *Nature Protocols*, *15*(6), 1954-1991.

Asif, M. (2016). Pharmacological Potential of Benzamide Analogues and their Uses in Medicinal Chemistry. *Modern Chemistry & Applications*, *04*.

Bartoli, G., Antonio, G., Giuli, S., Marcantoni, E., Marcolini, M., & Paoletti, M. (2008). The $CeCl_3 \cdot 7H_2O/NaI/SiO_2$ System as an Efficient Promoter for the Friedel-Crafts Reaction of Indoles to Nitroalkenes under Solvent-Free Conditions. *Synthesis-stuttgart*, *2008*, 320-324.

Bourgaud, F., Hehn, A., Larbat, R., Doerper, S., Gontier, E., Kellner, S., & Matern, U. (2006). Biosynthesis of coumarins in plants: a major pathway still to be unravelled for cytochrome P450 enzymes. *Phytochemistry Reviews*, *5*(2), 293-308.

Bouslimani, A., Sanchez, L. M., Garg, N., & Dorrestein, P. C. (2014). Mass spectrometry of natural products: current, emerging and future technologies. *Natural Product Report*, *31*(6), 718-729.

Brown, R. T., Chapple, C. L., & Lashford, A. G. (1977). Isolation of strictosidine (isovincoside) lactam from *Nauclea latifolia*. *Phytochemistry*, *16*(10), 1619-1620.

Brown, R. T., Duckworth, D. M., & Santos, C. A. M. (1991). Biogenetically patterned synthesis of cadambine. *Tetrahedron Letters*, *32*(17), 1987-1990.

Brown, R. T., & Fraser, S. B. (1974). Anthocephalus alkaloids: Cadambine and 3*α*-dihydrocadambine. *Tetrahedron Letters*, *15*(23), 1957-1959.

Cao, X. F., Wang, J. S., Wang, X. B., Luo, J., Wang, H. Y., & Kong, L. Y. (2013). Monoterpene indole alkaloids from the stem bark of *Mitragyna diversifolia* and their acetylcholine esterase inhibitory effects. *Phytochemistry*, *96*, 389-396.

Cardoso, C. L., Castro-Gamboa, I., Silva, D. H. S., Furlan, M., de Epifanio, R., Pinto, A. d. C.,...Bolzani, V. d. S. (2004). Indole Glucoalkaloids from *Chimarrhis turbinata* and Their Evaluation as Antioxidant Agents and Acetylcholinesterase Inhibitors. *Journal of Natural Product*, *67*(11), 1882-1885.

Carletti, E., Aurbek, N., Gillon, E., Loiodice, M., Nicolet, Y., Fontecilla-Camps, J.,...Worek, F. (2009). Structure-activity analysis of aging and reactivation of human butyrylcholinesterase inhibited by analogues of tabun. *The Biochemical journal*, *421*, 97-106.

Carney, G., Bassett, K., Wright, J. M., Maclure, M., McGuire, N., & Dormuth, C. R. (2019). Comparison of cholinesterase inhibitor safety in real-world practice. *Alzheimer's & Dementia: Translational Research & Clinical Interventions*, *5*(1), 732-739.

Cavdar, H., Senturk, M., Guney, M., Durdagi, S., Kayik, G., Supuran, C. T., & Ekinci, D. (2019). Inhibition of acetylcholinesterase and butyrylcholinesterase with uracil derivatives: kinetic and computational studies. *Journal of Enzyme Inhibition and Medicinal Chemistry*, *34*(1), 429-437.

Chambers, M. C., Maclean, B., Burke, R., Amodei, D., Ruderman, D. L., Neumann, S.,...Mallick, P. (2012). A cross-platform toolkit for mass spectrometry and proteomics. *Nature Biotechnology*, *30*(10), 918-920.

Chandrika, M., & Ravishankar, R. (2009). Genetic fidelity in micropropagated plantlets of *Ochreinauclea missionis* an endemic, threatened and medicinal tree using ISSR markers. *African Journal Biotechnology*, *8*.

Clarke, Z. (2007a). Galantamine. In S. J. Enna & D. B. Bylund (Eds.), *xPharm: The Comprehensive Pharmacology Reference* (pp.1-7). Elsevier. https://doi.org/https://doi.org/10.1016/B978-008055232-3.61802-1

Clarke, Z. (2007b). Ipecac. In S. J. Enna & D. B. Bylund (Eds.), *xPharm: The Comprehensive Pharmacology Reference* (pp.1-3). Elsevier. https://doi.org/https://doi.org/10.1016/B978-008055232-3.61949-X

Colović, M. B., Krstić, D. Z., Lazarević-Pašti, T. D., Bondžić, A. M., & Vasić, V. M. (2013). Acetylcholinesterase inhibitors: pharmacology and toxicology. *Current Neuropharmacology*, *11*(3), 315-335.

Crüsemann, M., O'Neill, E. C., Larson, C. B., Melnik, A. V., Floros, D. J., da Silva, R. R.,...Moore, B. S. (2017). Prioritizing Natural Product Diversity in a Collection of 146 Bacterial Strains Based on Growth and Extraction Protocols. *Journal of Natural Product*, *80*(3), 588-597.

Darvesh, S., Hopkins, D. A., & Geula, C. (2003). Neurobiology of butyrylcholinesterase. *Nature Reviews Neuroscience*, *4*(2), 131-138.

Davis, A., Govaerts, R., Bridson, D., Ruhsam, M., Moat, J., Brummitt, N.,...span. (2009). A Global Assessment of Distribution, Diversity, Endemism, and Taxonomic Effort in the Rubiaceae1. *Annals of the Missouri Botanical Garden*, *96*, 68-78.

Dmitrienko, G. I., Szakolcai, A., & McLean, S. (1974). Constituents of Nauclea diderrichii. Part VI. Naucleonine and naucleonidine. *Tetrahedron Letters*, *15*(30), 2599-2602.

Du, Z.-T., Lu, J., Yu, H.-R., Xu, Y., & Li, A.-P. (2010). A Facile Demethylation of Ortho Substituted Aryl Methyl Ethers Promoted by AlCl3. *Journal of Chemical Research*, *34*(4), 222-227.

Eastlack, S. C., Cornett, E. M., & Kaye, A. D. (2020). Kratom-Pharmacology, Clinical Implications, and Outlook: A Comprehensive Review. *Pain Therrapy*, *9*(1), 55-69.

El-Sayed, M., & Verpoorte, R. (2007). *Catharanthus* terpenoid indole alkaloids: biosynthesis and regulation. *Phytochemistry Reviews*, *6*(2), 277-305.

Ellman, G. L., Courtney, D., Andres, V., & Featherstone, R. M. (1961). A new and rapid colorimetric determination of acetylcholinesterase activity. *Biochemical Pharmacology.*, *7*, 88.

Erdogan Orhan, I., Orhan, G., & Gurkas, E. (2011). An Overview on Natural Cholinesterase Inhibitors A Multi-Targeted Drug Class and Their Mass Production. *Mini-Reviews in Medicinal Chemistry*, *11*(10), 836-842.

Ernawati, T., Mun'im, A., Hanafi, M., & Yanuar, A. (2020). Synthesis of Cinnamamide Derivatives and Their α-Glucosidase Inhibitory Activities. *Sains Malaysiana*, *49*, 315-322.

Fadaeinasab, M., Basiri, A., Kia, Y., Karimian, H., Ali, H. M., & Murugaiyah, V. (2015). New indole alkaloids from the bark of *Rauvolfia reflexa* and their cholinesterase inhibitory activity. *Cellular Physiology and Biochemistry*, *37*(5), 1997-2011.

Firmansyah, A., Winingsih, W., & Manobi, J. D. Y. (2021). Review of scopoletin: Isolation, analysis process, and pharmacological activity. *Biointerface Research in Applied Chemistry*, *11*(4), 12006-12019.

Fouotsa, H., Mkounga, P., Lannang, A. M., Vanheuverzwijn, J., Zhou, Z., Leblanc, K.,...Beniddir, M. A. (2022). Pyrrovobasine, hybrid alkylated pyrraline monoterpene indole alkaloid pseudodimer discovered using a combination of mass spectral and NMR-based machine learning annotations. *Organic & Biomolecular Chemistry*, *20*(1), 98-105.

Fox Ramos, A. E., Evanno, L., Poupon, E., Champy, P., & Beniddir, M. A. (2019). Natural products targeting strategies involving molecular networking: different manners, one goal. *Natural Product Report*, *36*(7), 960-980.

Gai, Y., Chen, H., Wu, C., Feng, F., Wang, Y., Liu, W., & Wang, S. (2013). Analysis of the traditional medicine YiGan San by the fragmentation patterns of cadambine indole alkaloids using HPLC coupled with high-resolution MS. *Journal of Separation Science*, *36*(23), 3723-3732.

Gaikwad, N., Nanduri, S., & Madhavi, Y. V. (2019). Cinnamamide: An insight into the pharmacological advances and structure–activity relationships. *European Journal of Medicinal Chemistry*, *181*, 111561.

Gatenyo, J., Vints, I., & Rozen, S. (2013). The first general route for efficient synthesis of ^{18}O labelled alcohols using the $HOF{\cdot}CH_3CN$ complex. *Chemical Communications*, *49*(67), 7379-7381.

Gauthier, S., Webster, C., Servaes, S., Morais, J.A., Rosa-Neto, P. (2022). *World Alzheimer Report 2022.Life after diagnosis:Navigating treatment, care and support.* (World Alzheimer Report 2022, Issue. A. s. D. International.

Guan, L., & Saw, L. G. (2007). *Plant conservation in Malaysia – Meeting the challenges of the twenty first century*.

Hamidah, M., Mohd Hasmadi, I., Chua, L. S. L., Lau, K. H., Faridah-Hanum, I., Yong, W. S. Y., & Pakhriazad, H. Z. (2020). Towards identification of important plant areas (IPA) for Peninsular Malaysia. Methodology and future directions. *Heliyon*, *6*(7).

Heinstein, P., Höfle, G., & Stöckigt, J. (1979). Involvement of Cathenamine in the Formation of N–Analogues of Indole Alkaloids. *Planta Medica*, *37*(12), 349,357.

Hotellier, F., Delaveau, P., & Pousset, J.-L. (1975). Nauclefine et naucletine deux nouveaux alcaloides de type indoloquinolizidine isoles du *Nauclea latifolia*. *Phytochemistry*, *14*(5), 1407-1409.

Hotellier, F., Delaveau, P., & Pousset, J.-L. (1980). Naucléidinal et epinaucléidinal, alcaloïdes du *Nauclea latifolia*. *Phytochemistry*, *19*(8), 1884-1885.

Hotellier, F., Delaveau, P., & Pousset, J. L. (1979). Alkaloids and glyco-alkaloids from leaves of *Nauclea latifolia* SM (author's transl). *Planta Medica*, *35*(3), 242-246.

Huang, T. J., Liu, S. H., Kuo, Y. C., Chen, C. W., & Chou, S. C. (2014). Antiviral activity of chemical compound isolated from *Artemisia morrisonensis* against hepatitis B virus in vitro. *Antiviral Research*, *101*, 97-104.

Iijima, S., Greig, N. H., Garofalo, P., Spangler, E. L., Heller, B., Brossi, A., & Ingram, D. K. (1992). The long-acting cholinesterase inhibitor heptyl-physostigmine attenuates the scopolamine-induced learning impairment of rats in a 14-unit T-maze. *Neuroscience Letter*, *144*(1-2), 79-83.

Intekhab, J., & Aslam, M. (2009). Constituents from *Feronia Limonia*. *Analele Universitatii Bucuresti: Chimie*, *18*(2), 95-101.

Itoh, A., Tanahashi, T., Nagakura, N., & Nishi, T. (2003). Two chromone-secoiridoid glycosides and three indole alkaloid glycosides from *Neonauclea sessilifolia*. *Phytochemistry*, *62*(3), 359-369.

Johns, S. R., Lamberton, J. A., & Sioumis, A. A. (1970). Identification of a leaf alkaloid of *Neonauclea schlechteri* (Rubiaceae) as gambirine (9-hydroxydihydrocorynantheine). *Australian Journal of Chemistry*, *23*(6), 1285.

Kam, T. S., & Choo, Y. M. (2004). Venalstonine and dioxokopsan derivatives from *Kopsia fruticosa*. *Phytochemistry*, *65*(14), 2119-2122.

Kanchanapoom, T., Sahakitpichan, P., Chimnoi, N., Petchthong, C., Thamniyom, W., Nangkoed, P., & Ruchirawat, S. (2021). Monoterpene alkaloid glycosides from the leaves of *Nauclea orientalis*. *Phytochemistry Letters*, *41*, 83-87.

Karaket, N., Supaibulwatana, K., Ounsuk, S., Bultel-Ponce, V., Pham, V. C., & Bodo, B. (2012). Chemical and bioactivity evaluation of the bark of *Neonauclea purpurea*. *Natural Product Communication*, *7*(2), 169-170.

Karayil, S., K.P, S., P.S, S., & K, V. (2014). Isolation and Structural elucidation of novel bioactive molecule Coumarin from traditionally used Medicinal Plant- *Ceropegia juncea* (Roxb.). *IOSR Journal of Pharmacy and Biological Sciences*, *9*, 19-22.

Karou, S. D., Tchacondo, T., Ilboudo, D. P., & Simpore, J. (2011). Sub-Saharan Rubiaceae: a review of their traditional uses, phytochemistry and biological activities. *Pakistan Journal of Biological Sciences*, *14*(3), 149-169.

Kaushik, N. K., Kaushik, N., Attri, P., Kumar, N., Kim, C. H., Verma, A. K., & Choi, E. H. (2013). Biomedical Importance of Indoles. *Molecules*, *18*(6), 6620-6662.

Khan, H., Patel, S., & Kamal, A. M. (2017). Pharmacological and Toxicological Profile of Harmane & *β*-Carboline Alkaloid: Friend or Foe. *Current Drug Metabolism*, *18*(9), 853-857.

Khan, N. M. M. U., & Sagar, M. (2015). Scopoletin and *β*-sitosterol glucoside from roots of *Ipomoea digitata*. *Journal of Pharmacognosy and Phytochemistry*, *4*, 5-7.

Khaw, K. Y., Choi, S. B., Tan, S. C., Wahab, H. A., Chan, K. L., & Murugaiyah, V. (2014). Prenylated xanthones from mangosteen as promising cholinesterase inhibitors and their molecular docking studies. *Phytomedicine*, *21*(11), 1303-1309.

Kim, J. K., Kim, J. Y., Kim, H. J., Park, K. G., Harris, R. A., Cho, W. J.,...Lee, I. K. (2013). Scoparone exerts anti-tumor activity against DU145 prostate cancer cells via inhibition of STAT3 activity. *Plos One*, *8*(11).

Klein-Júnior, L. C., Cretton, S., Allard, P.-M., Genta-Jouve, G., Passos, C. S., Salton, J.,...Henriques, A. T. (2017). Targeted Isolation of Monoterpene Indole Alkaloids from *Palicourea sessilis*. *Journal of Natural Products*, *80*(11), 3032-3037.

Konrath, E. L., Passos Cdos, S., Klein, L. C., Jr., & Henriques, A. T. (2013). Alkaloids as a source of potential anticholinesterase inhibitors for the treatment of Alzheimer's disease. *The Journal of Pharmacy and Pharmacology*, *65*(12), 1701-1725.

Korabecny, J., Zemek, F., Soukup, O., Spilovska, K., Musilek, K., Jun, D.,...Kuca, K. (2014). Chapter 1 - Pharmacotherapy of Alzheimer's Disease: Current State and Future Perspectives. In R. Atta ur & M. I. Choudhary (Eds.), *Drug Design and Discovery in Alzheimer's Disease* (pp. 3-39). Elsevier. https://doi.org/https://doi.org/10.1016/B978-0-12-803959-5.50001-5

Kouamé, T., Okpekon, A. T., Bony, N. F., N'Tamon, A. D., Gallard, J. F., Rharrabti, S.,...Le Pogam, P. (2020). Corynanthean-Epicatechin Flavoalkaloids from *Corynanthe pachyceras*. *Molecules*, *25*(11).

Kuang, Y. F., Yue, L., Balslev, H., & Liao, J. P. (2021). Pollen development in three selected species of Rubiaceae provides ontogenetic evidence for pollen evolution. *Review of Palaeobotany and Palynology*, *289*, 104413.

Kumar, A., Chowdhury, S. R., Jatte, K. K., Chakrabarti, T., Majumder, H. K., Jha, T., & Mukhopadhyay, S. (2015). Anthocephaline, a New Indole Alkaloid and Cadambine, a Potent Inhibitor of DNA Topoisomerase IB of *Leishmania donovani* (LdTOP1LS), Isolated from *Anthocephalus cadamba*. *Natural Product Communications*, *10*(2).

Kumar, S. (2015). Dual inhibition of acetylcholinesterase and butyrylcholinesterase enzymes by allicin. *Indian Journal of Pharmacology*, *47*(4), 444-446.

Liew, S. Y., Khaw, K. Y., Murugaiyah, V., Looi, C. Y., Wong, Y. L., Mustafa, M. R.,...Awang, K. (2015). Natural indole butyrylcholinesterase inhibitors from *Nauclea officinalis*. *Phytomedicine*, *22*(1), 45-48.

Liew, S. Y., Looi, C. Y., Paydar, M., Cheah, F. K., Leong, K. H., Wong, W. F.,...Awang, K. (2014). Subditine, a New Monoterpenoid Indole Alkaloid from Bark of *Nauclea subdita* (Korth.) Steud. Induces Apoptosis in Human Prostate Cancer Cells. *Plos One*, *9*(2).

Liew, S. Y., Mak, W. Q., Thew, H. Y., Khaw, K. Y., Hazni, H., Litaudon, M., & Awang, K. (2023). Neuroprotective Activities of New Monoterpenoid Indole Alkaloid from *Nauclea officinalis*. *Processes*, *11*(3), 646.

Liew, S. Y., Mukhtar, M. R., Hadi, A. H., Awang, K., Mustafa, M. R., Zaima, K.,...Litaudon, M. (2012). Naucline, a new indole alkaloid from the bark of *Nauclea officinalis*. *Molecules*, *17*(4), 4028-4036.

Lima, J. A., R. Costa, T. W., da Fonseca, A. C. C., do Amaral, R. F., Nascimento, M. d. D. S. B., Santos-Filho, O. A.,...Tinoco, L. W. (2020). Geissoschizoline, a promising alkaloid for Alzheimer's disease: Inhibition of human cholinesterases, anti-inflammatory effects and molecular docking. *Bioorganic Chemistry*, *104*, 104215.

Liu, B., Geng, Q., Cao, Z., Li, L., Lu, P., Lin, L.,...Lu, C. (2022). *Nauclea officinalis*: A Chinese medicinal herb with phytochemical, biological, and pharmacological effects. *Chinese Medicine*, *17*(1), 141.

Liu, Q. L., Chen, A. H., Tang, J. Y., Ma, Y. L., Jiang, Z. H., Liu, Y. P.,...Xu, W. (2017). A new indole alkaloid with anti-inflammatory activity from Nauclea officinalis. *Natural Product Research*, *31*(18), 2107-2112.

Liu, Y. P., Ju, P. K., Long, J. T., Lai, L., Zhao, W. H., Zhang, C.,...Fu, Y. H. (2018). Cytotoxic indole alkaloids from *Nauclea orientalis*. *Natural Product Research*, *32*(24), 2922-2927.

Lopes, S. P., Yepes, L. M., Pérez-Castillo, Y., Robledo, S. M., & de Sousa, D. P. (2020). Alkyl and Aryl Derivatives Based on *p*-Coumaric Acid Modification and Inhibitory Action against *Leishmania braziliensis* and *Plasmodium falciparum*. *Molecules*, *25*(14), 3178.

Lourenço, A., Marques, A. V., & Gominho, J. (2021). The Identification of New Triterpenoids in *Eucalyptus globulus* Wood. *Molecules*, *26*(12).

Maldonado, C., Barnes, C. J., Cornett, C., Holmfred, E., Hansen, S. H., Persson, C.,...Rønsted, N. (2017). Phylogeny Predicts the Quantity of Antimalarial Alkaloids within the Iconic Yellow Cinchona Bark (Rubiaceae: Cinchona calisaya) . *Frontiers in Plant Science*, *8*.

Mao, L., Xin, L., & Dequan, Y. (1984). Alkaloids of *Nauclea officinalis*. *Planta Medica*, *50*(06), 459-461.

Maria João, M., Lourdes, S., Eugenio, U., Orlando, A. A., Enrique, M., & Estela Guardado, Y. (2015). Coumarins — An Important Class of Phytochemicals. In A. V. Rao & G. R. Leticia (Eds.), *Phytochemicals* (pp. Ch. 5). IntechOpen. https://doi.org/10.5772/59982

Martins, D., & Nunez, C. V. (2015). Secondary metabolites from Rubiaceae species. *Molecules*, *20*(7), 13422-13495.

McKenzie, E., Nettleship, L., & Slaytor, M. (1975). New natural products from *Peganum harmala*. *Phytochemistry*, *14*(1), 273-275.

McLean, S., & Murray, D. (1972). The constituents of *Nauclea diderrichii*. Part IV. Miscellaneous substances; biogenetic considerations. *Canadian Journal of Chemistry*, *50*(10), 1496-1501.

Miculas, D. C., Negru, P. A., Bungau, S. G., Behl, T., Hassan, S. S. u., & Tit, D. M. (2023). Pharmacotherapy Evolution in Alzheimer & Disease: Current Framework and Relevant Directions. *Cells*, *12*(1), 131.

Morita, H., Mori, R., Deguchi, J., Oshimi, S., Hirasawa, Y., Ekasari, W.,...Hadi, A. H. (2012). Antiplasmodial decarboxyportentol acetate and 3,4-dehydrotheaspirone from *Laumoniera bruceadelpha*. *Journal of Natural Medicines* *66*(3), 571-575.

Morris, G. M., Goodsell, D. S., Halliday, R. S., Huey, R., Hart, W. E., Belew, R. K., & Olson, A. J. (1998). Automated docking using a Lamarckian genetic algorithm and an empirical binding free energy function. *Journal of Computational Chemistry*, *19*(14), 1639-1662.

Morton, J. F. (1992). The Ocean-Going Noni, or Indian Mulberry (*Morinda citrifolia*, Rubiaceae) and Some of Its "Colorful" Relatives. *Economic Botany*, *46*(3), 241-256.

Mukhtar, M. R., Martin, M.T., Domansky, M., Pais, M., Hamid, A., Hadi, A., & Awang, K. (1997). Phoebegrandines A and B, proaporphine-tryptamine dimers, from Phoebe grandis. *Phytochemistry*, *45*(7), 1543-1546.

Mukhtar, M. R., Osman, N., Awang, K., Hazni, H., Qureshi, A. K., Hadi, A. H. A.,...Litaudon, M. (2012). Neonaucline, a New Indole Alkaloid from, the Leaves of *Ochreinauclea maingayii* (Hook. f.) Ridsd. (Rubiaceae). *Molecules 17*(1), 267.

Murray, S. M. a. D. G. (1969). Isolation of indole (beta carboline), pyridine, and indole-pyridine alkaloids from *Nauclea diderrichii*. *Canadian Journal of Chemistry*, *48*, 867-868.

Mushtaq, G., Greig, N. H., Khan, J. A., & Kamal, M. A. (2014). Status of acetylcholinesterase and butyrylcholinesterase in Alzheimer's disease and type 2 diabetes mellitus. *Neurology Disorder Drug Targets*, *13*(8), 1432-1439.

Naomita, V. D., & Ravishankar, V. R. (2001). In vitro Propagation of Ochreinauclea missionis (Wall. Ex G. Don), an Ethnomedicinal Endemic and Threatened Tree. *In Vitro Cellular & Developmental Biology. Plant*, *37*(6), 820-823.

Naphen, C. N. (2019). *Targeted analogue detection from Pestalotiopsis microspora using molecular networking and mass defect filtering: towards the development of new anti-virulence leads against methicillin resistant Staphylococcus aureus.* (Doctorate thesis ,University of North Carolina). Greensboro. https://libres.uncg.edu/ir/listing.aspx?id=26577

Ngnokam, D., Ayafor, J. F., Connolly, J. D., & Nuzillard, J.-M. (2003). Nauclefolinine: A new alkaloid from the roots of *Nauclea latifolia*. *Bulletin of the Chemical Society of Ethiopia*, *17*.

Nishioka, T., Watanabe, J., Kawabata, J., & Niki, R. (1997). Isolation and Activity of N-p-Coumaroyltyramine, an α-Glucosidase Inhibitor in Welsh Onion (*Allium fistulosum*). *Bioscience, Biotechnology, and Biochemistry*, *61*(7), 1138-1141.

Nothias, L.-F., Nothias-Esposito, M., da Silva, R., Wang, M., Protsyuk, I., Zhang, Z.,...Dorrestein, P. C. (2018). Bioactivity-Based Molecular Networking for the Discovery of Drug Leads in Natural Product Bioassay-Guided Fractionation. *Journal of Natural Products*, *81*(4), 758-767.

Omar, F., Tareq, A. M., Alqahtani, A. M., Dhama, K., Sayeed, M. A., Emran, T. B., & Simal-Gandara, J. (2021). Plant-Based Indole Alkaloids: A Comprehensive Overview from a Pharmacological Perspective. *Molecules*, *26*(8).

Osman, N., Zahari, A., Hazni, H., Wan Othman, W. N. N., Rasol, N. E., Ismail, N. H.,...Awang, K. (2023). Isolation and Characterization of Compounds from *Ochreinauclea maingayi* (Hook. f.) Ridsd. (Rubiaceae) with the Aid of LCMS/MS Molecular Networking. *Separations*, *10*(2), 74.

Otasek, D., Morris, J. H., Bouças, J., Pico, A. R., & Demchak, B. (2019). Cytoscape Automation: empowering workflow-based network analysis. *Genome Biology*, *20*(1), 185.

Parameswaran, P. S., Naik, C. G., & Hegde, V. R. (1997). Secondary Metabolites from the Sponge *Tedania anhelans*: Isolation and Characterization of Two Novel Pyrazole Acids and Other Metabolites. *Journal of Natural Products*, *60*(8), 802-803.

Pavia, D. L., Lampman, G. M., Kriz, G. S., & Vyvyan, J. R. (2009). *Introduction to Spectroscopy*. Brooks/Cole.

Peri, R., & Mangipudy, R. S. (2014). Reserpine. In P. Wexler (Ed.), *Encyclopedia of Toxicology (Third Edition)* (pp. 94-96). Academic Press. https://doi.org/https://doi.org/10.1016/B978-0-12-386454-3.00779-X

Phillipson, J. D., Hemingway, S. R., & Ridsdale, C. E. (1982). The Chemotaxonomic Significance of Alkaloids in the Naucleeae S.L. (Rubiaceae). *Journal of Natural Products*, *45*(2), 145-162.

Pinho, B. R., Ferreres, F., Valentão, P., & Andrade, P. B. (2013). Nature as a source of metabolites with cholinesterase-inhibitory activity: an approach to Alzheimer's disease treatment. *Journal of Pharmacy and Pharmacology*, *65*(12), 1681-1700.

Pluskal, T., Castillo, S., Villar-Briones, A., & Orešič, M. (2010). MZmine 2: Modular framework for processing, visualizing, and analyzing mass spectrometry-based molecular profile data. *Bioinformatics*, *11*(1), 395.

Pohanka, M. (2014). Inhibitors of Acetylcholinesterase and Butyrylcholinesterase Meet Immunity. *International Journal of Molecular Sciences*, *15*(6), 9809-9825.

Pope, C. N., & Brimijoin, S. (2018). Cholinesterases and the fine line between poison and remedy. *Biochemical Pharmacology 153*, 205-216.

Portelius, E., Zetterberg, H., Andreasson, U., Brinkmalm, G., Andreasen, N., Wallin, A.,...Blennow, K. (2006). An Alzheimer's disease-specific beta-amyloid fragment signature in cerebrospinal fluid. *Neuroscience Letter*, *409*(3), 215-219.

Radi, Z., & Taylor, P. (2006). CHAPTER 12 - Structure and Function of Cholinesterases. In R. C. Gupta (Ed.), *Toxicology of Organophosphate & Carbamate Compounds* (pp. 161-186). Academic Press. https://doi.org/https://doi.org/10.1016/B978-012088523-7/50013-2

Rahman, A. U., & Basha, A. (1983). *Biosynthesis of indole alkaloids*. Clarendon Press.

Rao, A. N. (2010). How many medicinal plant species in Malay Peninsula. *Journal of Tropical Medicinal Plants*, *11*(1), 13-26.

Rao, K. V., Santarsiero, B. D., Mesecar, A. D., Schinazi, R. F., Tekwani, B. L., & Hamann, M. T. (2003). New manzamine alkaloids with activity against infectious and tropical parasitic diseases from an Indonesian sponge. *Journal of Natural Products*, *66*(6), 823-828.

Rashid, U., & Ansari, F. L. (2014). Chapter 2 - Challenges in Designing Therapeutic Agents for Treating Alzheimer's Disease-from Serendipity to Rationality. In R. Atta ur & M. I. Choudhary (Eds.), *Drug Design and Discovery in Alzheimer's Disease* (pp. 40-141). Elsevier. https://doi.org/https://doi.org/10.1016/B978-0-12-803959-5.50002-7

Razafimandimbison, S. G., & Bremer, B. (2001). Tribal Delimitation of Naucleeae (Cinchonoideae, Rubiaceae): Inference from Molecular and Morphological Data. *Systematics and Geography of Plants*, *71*(2), 515-538.

Razafimandimbison, S. G., & Bremer, B. (2002). Phylogeny and classification of Naucleeae S.L. (Rubiaceae) inferred from molecular (ITS, rBCL, and tRNT-F) and morphological data. *American Journal of Botany.*, *89*(7), 1027-1041.

Repke, D. B., Jahangir, Clark, R. D., & MacLean, D. B. (1988). Synthesis of naucléfine, angustidine, angustine, and (±)-13b, 14-dihydroangustine. *Journal of the Chemical Society, Chemical Communications*(6), 439-440.

Ridsdale, C. E. (1978). A revision of the tribe Naucleeae s.s. (Rubiaceae). *Blumea: Biodiversity, Evolution and Biogeography of Plants*, *24*(2), 307-366.

Robbrecht, E. (1988). *Tropical Woody Rubiaceae. Characteristic Features and Progressions. Contributions to a New Subfamilial Classification* (Vol. 1).

S. C. Lim, K. S. G. K. T. C. (2004). *Identification and utilisation of lesser-known commercial timbers in Peninsular Malaysia 1: Ara, Bangkal, Bebusok and Bekoi* (Vol. 29). Timber Technology Centre (TTC), FRIM.

Sahoo, C. R., Paidesetty, S. K., & Padhy, R. N. (2019). *Nor*harmane as a potential chemical entity for development of anticancer drugs. *European Journal of Medicinal Chemistry*, *162*, 752-764.

Saidi, N. (2010). Cinnamide and benzamide from species of *Cryptocarya crassivervia*. *Jurnal Natural*, *10*(2), 39-41.

Sainsbury, M., & Webb, B. (1975). Parvine, a new angustine-type alkaloid from *Nauclea parva*. *Phytochemistry*, *14*(12), 2691-2693.

Santos, C. L. G., Angolini, C. F. F., Neves, K. O. G., Costa, E. V., de Souza, A. D. L., Pinheiro, M. L. B.,...da Silva, F. M. A. (2020). Molecular networking-based dereplication of strictosidine-derived monoterpene indole alkaloids from the curare ingredient *Strychnos peckii*. *Rapid Communications in Mass Spectrometry*, *34*(S3), e8683.

Shigemori, H., Kagata, T., Ishiyama, H., Morah, F., Ohsaki, A., & Kobayashi, J. I. (2003). Naucleamides A—E, New Monoterpene Indole Alkaloids from *Nauclea latifolia*. *Chemical and Pharmaceutical Bulletin*, *51*(1), 58-61.

Sichaem, J., Surapinit, S., Siripong, P., Khumkratok, S., Jong-aramruang, J., & Tip-pyang, S. (2010). Two new cytotoxic isomeric indole alkaloids from the roots of *Nauclea orientalis*. *Fitoterapia*, *81*(7), 830-833.

Simpson, M. G. (2010). 8 - Diversity and Classification of Flowering Plants: Eudicots. In M. G. Simpson (Ed.), *Plant Systematics (Second Edition)* (pp. 275-448). Academic Press. https://doi.org/https://doi.org/10.1016/B978-0-12-374380-0.50008-7

Son, D. J., Lee, G. R., Oh, S., Lee, S. E., & Choi, W. S. (2015). Gastroprotective efficacy and safety evaluation of scoparone derivatives on experimentally induced gastric lesions in rodents. *Nutrients*, *7*(3), 1945-1964.

Song, S., Liu, P., Wang, L., Li, D., Fan, H., Chen, D., & Zhao, F. (2019). In vitro anti-inflammatory activities of naucleoffieine H as a natural alkaloid from *Nauclea officinalis* Pierrc ex Pitard, through inhibition of the iNOS pathway in LPS-activated RAW 264.7 macrophages. *Natural Product Research*, *34*(18), 2694-2697.

Stanforth, S. P. (2006). *Natural Product Chemistry at a Glance*. Blackwell Pub.

Stefan, D. L., Åsa, K., Sylvain, G. R., & Birgitta, B. (2014). Phylogeny and Generic Delimitations in the Sister Tribes Hymenodictyeae and Naucleeae (Rubiaceae). *Systematic Botany*, *39*(1), 304-315.

Tan, T. Y. C., Lee, J. C., Mohd Yusof, N. A., Teh, B. P., & Syed Mohamed, A. F. (2020). Malaysian herbal monograph development and challenges. *Journal of Herbal Medicine*, *23*, 100380.

Tang, B., Peng, C. Y., Darko, O. K., Tao, T., Huang, Y., Su, Q., & Yang, X. (2016). Paeonol, a Powerful Natural Product with Broad Biological Spectra by Inhibiting Inflammatory Pathway. *Current Traditional Medicine*, *2*(2), 72-79.

Terry, A. V., & Buccafusco, J. J. (2003). The Cholinergic Hypothesis of Age and Alzheimer Disease-Related Cognitive Deficits: Recent Challenges and Their Implications for Novel Drug Development. *Journal of Pharmacology and Experimental Therapeutics*, *306*(3), 821.

Thomsen, T., Kaden, B., Fischer, J. P., Bickel, U., Barz, H., Gusztony, G.,...Kewitz, H. (1991). Inhibition of acetylcholinesterase activity in human brain tissue and erythrocytes by galanthamine, physostigmine and tacrine. *European Journal Of Clinical Chemistry and Clinical Biochemistry*, *29*(8), 487-492.

Torres, J. M., Lira, A. F., Silva, D. R., Guzzo, L. M., Sant'Anna, C. M. R., Kümmerle, A. E., & Rumjanek, V. M. (2012). Structural insights into cholinesterases inhibition by harmane *β*-carbolinium derivatives: A kinetics – molecular modeling approach. *Phytochemistry*, *81*, 24-30.

van der Hooft, J. J., Wandy, J., Barrett, M. P., Burgess, K. E., & Rogers, S. (2016). Topic modeling for untargeted substructure exploration in metabolomics. *The Proceedings of the National Academy of Sciences*, *113*(48), 13738-13743.

Vincenti, F., Montesano, C., Di Ottavio, F., Gregori, A., Compagnone, D., Sergi, M., & Dorrestein, P. (2020). Molecular Networking: A Useful Tool for the Identification of New Psychoactive Substances in Seizures by LC–HRMS. *Frontiers in Chemistry*, *8*(1039).

Vrabec, R., Maříková, J., Ločárek, M., Korábečný, J., Hulcová, D., Hošťálková, A.,...Cahlíková, L. (2022). Monoterpene indole alkaloids from *Vinca minor* L. (Apocynaceae): Identification of new structural scaffold for treatment of Alzheimer's disease. *Phytochemistry*, *194*.

Wandy, J., Zhu, Y., van der Hooft, J. J. J., Daly, R., Barrett, M. P., & Rogers, S. (2017). Ms2lda.org: web-based topic modelling for substructure discovery in mass spectrometry. *Bioinformatics*, *34*(2), 317-318.

Wang, G., Hou, L., Wang, Y., Liu, H., Yuan, J., Hua, H., & Sun, L. (2022). Two new neolignans and an indole alkaloid from the stems of *Nauclea officinalis* and their biological activities. *Fitoterapia*, *160*.

Wang, M., Carver, J. J., Phelan, V. V., Sanchez, L. M., Garg, N., Peng, Y.,...Bandeira, N. (2016). Sharing and community curation of mass spectrometry data with Global Natural Products Social Molecular Networking. *Nature Biotechnology*, *34*(8), 828-837.

Watrous, J., Roach, P., Alexandrov, T., Heath, B. S., Yang, J. Y., Kersten, R. D.,...Dorrestein, P. C. (2012). Mass spectral molecular networking of living microbial colonies. *Proceedings of the National Academy of Sciences*, *109*(26), E1743-E1752.

Whitmore, T. C., & Ng, F. S. P. (1989). *Tree Flora of Malaya: A Manual for Foresters*. Longman.

Wu, X. F., Bheeter, C. B., Neumann, H., Dixneuf, P. H., & Beller, M. (2012). Lewis acid-catalyzed oxidation of benzylamines to benzamides. *Chemical Communications*, *48*(100), 12237-12239.

Yang, H.-D., Kim, D., Lee, S., & Young, L. (2016). History of Alzheimer's Disease. *Dementia and Neurocognitive Disorders*, *15*, 115.

Yang, J. Y., Sanchez, L. M., Rath, C. M., Liu, X., Boudreau, P. D., Bruns, N.,...Dorrestein, P. C. (2013). Molecular networking as a dereplication strategy. *Journal of Natural Product*, *76*(9), 1686-1699.

Yang, Z. D., Duan, D. Z., Du, J., Yang, M. J., Li, S., & Yao, X. J. (2012). Geissoschizine methyl ether, a corynanthean-type indole alkaloid from *Uncaria rhynchophylla* as a potential acetylcholinesterase inhibitor. *Natural Product Research*, *26*(1), 22-28.

Yu, J. S., Nothias, L.-F., Wang, M., Kim, D. H., Dorrestein, P. C., Kang, K. B., & Yoo, H. H. (2022). Tandem Mass Spectrometry Molecular Networking as a Powerful and Efficient Tool for Drug Metabolism Studies. *Analytical Chemistry*, *94*(2), 1456-1464.

Yu, J. S., Seo, H., Kim, G. B., Hong, J., & Yoo, H. H. (2019). MS-Based Molecular Networking of Designer Drugs as an Approach for the Detection of Unknown Derivatives for Forensic and Doping Applications: A Case of NBOMe Derivatives. *Analytical Chemistry*, *91*(9), 5483-5488.

Yu, P., Chen, Z., Liu, Y., Gu, Z., Wang, X., Zhang, Y.,...Tian, Z. (2022). Bioactivity-Guided Separation of Anti-Cholinesterase Alkaloids from *Uncaria rhynchophlly* (Miq.) Miq. Ex Havil Based on HSCCC Coupled with Molecular Docking. *Molecules*, *27*(6), 2013.

Yuan, H. L., Zhao, Y. L., Qin, X. J., Liu, Y. P., Yu, H. F., Zhu, P. F.,...Luo, X. D. (2020). Anti-inflammatory and analgesic activities of *Neolamarckia cadamba* and its bioactive monoterpenoid indole alkaloids. *Journal of Ethnopharmacology*, *260*.

Zhan, Z. J., Yu, Q., Wang, Z. L., & Shan, W. G. (2010). Indole alkaloids from *Ervatamia hainanensis* with potent acetylcholinesterase inhibition activities. *Bioorganic and Medicinal Chemistry Letters*, *20*(21), 6185-6187.

Zhang, J., Song, M., Ao, Y. L., Li, Y., Zou, X. Y., Xu, J.,...Ye, W. C. (2020). Alstolarines A and B, two unusual monoterpenoid indole alkaloids with an acetal moiety from *Alstonia scholaris*. *Organic Chemistry Frontiers High.*, *7*(21), 3468-3473.

Zhang, Z., ElSohly, H. N., Jacob, M. R., Pasco, D. S., Walker, L. A., & Clark, A. M. (2001). New Indole alkaloids from the bark of *Nauclea orientalis*. *Journal of Natural Products*, *64*(8), 1001-1005.

Zhao, B., Moochhala, S. M., & Tham, S.-y. (2004). Biologically active components of Physostigma venenosum. *Journal of Chromatography B*, *812*(1), 183-192.

Zhao, C., Zhang, C., He, F., Zhang, W., Leng, A., & Ying, X. (2019). Two new alkaloids from *Portulaca oleracea* L. and their bioactivities. *Fitoterapia*, *136*, 104166.

Zhou, H., He, H. P., Kong, N. C., Wang, T. J., & Hao, X. J. (2008). Indole alkaloids from the Leaves of *Anthocephalus chinensis*. *Helvetica Chimica Acta*, *91*(11), 2148-2152.